Biological and Medical Physics, Biomedical Engineering

Marek Procházka

Surface-Enhanced Raman Spectroscopy

Bioanalytical, Biomolecular and Medical Applications

Springer

Surface-Enhanced Raman Spectroscopy

BIOLOGICAL AND MEDICAL PHYSICS, BIOMEDICAL ENGINEERING

The fields of biological and medical physics and biomedical engineering are broad, multidisciplinary and dynamic. They lie at the crossroads of frontier research in physics, biology, chemistry, and medicine. The Biological and Medical Physics, Biomedical Engineering Series is intended to be comprehensive, covering a broad range of topics important to the study of the physical, chemical and biological sciences. Its goal is to provide scientists and engineers with textbooks, monographs, and reference works to address the growing need for information.

Books in the series emphasize established and emergent areas of science including molecular, membrane, and mathematical biophysics; photosynthetic energy harvesting and conversion; information processing; physical principles of genetics; sensory communications; automata networks, neural networks, and cellular automata. Equally important will be coverage of applied aspects of biological and medical physics and biomedical engineering such as molecular electronic components and devices, biosensors, medicine, imaging, physical principles of renewable energy production, advanced prostheses, and environmental control and engineering.

More information about this series at http://www.springer.com/series/3740

Marek Procházka

Surface-Enhanced Raman Spectroscopy

Bioanalytical, Biomolecular and Medical Applications

Springer

Marek Procházka
Institute of Physics
Charles University in Prague
Prague 2
Czech Republic

ISSN 1618-7210 ISSN 2197-5647 (electronic)
Biological and Medical Physics, Biomedical Engineering
ISBN 978-3-319-23990-3 ISBN 978-3-319-23992-7 (eBook)
DOI 10.1007/978-3-319-23992-7

Library of Congress Control Number: 2015950036

Springer Cham Heidelberg New York Dordrecht London

Printed on acid-free paper

Springer International Publishing AG Switzerland is part of Springer Science+Business Media (www.springer.com)

This book is dedicated to Prof. Blanka Vlčková from the Department of Physical and Macromolecular Chemistry, Faculty of Science, Charles University in Prague, on the occasion of her jubilee.

Preface

About 40 years after its discovery, surface-enhanced Raman scattering (SERS) spectroscopy has become a fully grown spectroscopic technique and the number of applications in the chemical, material, and particularly in life sciences has been rapidly expanding. Several monographs covering SERS theory and applications are available, but a compact monograph written by one author and focused on bio-related SERS applications is missing. The motivation to compile this book was to provide the best possible overview of the bioanalytical, biomolecular and medical applications of SERS. Please regard this book primarily as a review of selected bio-related SERS applications reported during the past two decades. Of course, it was impossible to include all applications from the extensive SERS literature in one book. I must apologize to all colleagues whose work is not described or cited here. I hope this book will be useful for students and newcomers with only little background in SERS spectroscopy as well as for experts who just need a quick overview of SERS applications with keyword "bio".

As an M.Sc. student at Faculty of Mathematics and Physics, Charles University in Prague, I chose SERS spectroscopy as my research topic with very little knowledge about it and even less knowledge about how complicated it could be. During the twenty plus years that I have been working on SERS spectroscopy I have discovered how mysterious it is and at the same time what a fascinating research field it is. When I was researching material for this book, the most exciting thing for me was the appreciation I got from seeing the great amount of progress that has been made in SERS spectroscopy over the past two decades.

I would like to thank two special persons/teachers: Prof. Blanka Vlčková from the Department of Physical and Macromolecular Chemistry, Faculty of Science, Charles University in Prague, a pioneer of SERS in Czech Republic and Prof. Josef Štěpánek from the Institute of Physics, Faculty of Mathematics and Physics, Charles University in Prague. I was infected with their enthusiasm for scientific work and without them I would never have come to the position where I now find myself.

I thank also my colleagues and students from Division of Biomolecular Physics, Institute of Physics, Faculty of Mathematics and Physics, Charles University in Prague for encouraging me during my work on this book. In particular, I should mention those who helped me in the completion of this book. I thank Dr. Eva Kočišová for reading the manuscript and helping with the graphics. I thank my Ph.D. students Mgr. Vlastimil Peksa for valuable comments on the manuscript and Mgr. Martin Šubr for reference database. I thank Dr. Vladimír Kopecký, Jr. for typography. Finally, I would like to thank Mr. Marshall Johnson for English editing of this book. Please note that I used British English. Financial support from the Czech Science Foundation (Project number P205/13/20110S) is also greatly appreciated.

Prague, June 2015 Marek Procházka

Contents

1 Introduction 1
References 4

2 Basics of Raman Scattering (RS) Spectroscopy 7
2.1 Short History of Raman Effect 7
2.2 Basic Theory of RS 8
2.3 Molecular Vibrations and Their Raman Activity 12
2.4 Raman Experiment 15
2.5 Raman Spectroscopy for Biomolecular Studies 17
References 18

3 Basics of Surface-Enhanced Raman Scattering (SERS) 21
3.1 SERS Mechanisms 21
3.1.1 EM Mechanism of SERS 22
3.1.2 Chemical (Molecular) Mechanism of SERS 24
3.2 SERS EFs 26
3.3 SM-SERS 28
3.4 SERS-Active Substrates 30
3.4.1 Metallic NP Hydrosols 30
3.4.2 NPs and Nanostructures on Planar Supports Prepared by Bottom-Up Techniques 34
3.4.3 Nanostructures Fabricated Using Nanolithographic (Top-Down) Techniques 37
3.4.4 Highly Ordered Metallic Nanostructures Fabricated by Template Techniques 39
3.4.5 Commercially Available Substrates 47
3.5 Practical Aspects of SERS 48
3.6 Related Enhanced Techniques 50
References 53

4 Bioanalytical SERS Applications 61
4.1 Quantitative SERS Methods. 61
4.1.1 SERS-Active Substrates for Quantitative SERS 61
4.1.2 Internal Intensity Standards for Quantitative SERS. 65
4.1.3 Sensitivity and Specificity of SERS Sensor 68
4.2 SERS Sensing of Pharmaceuticals and Drugs. 70
4.2.1 SERS Sensing of Pharmaceuticals 70
4.2.2 SERS Sensing of Drugs 72
4.3 SERS Sensing of Pollutants, Food Contaminants and Food Additives 77
4.3.1 SERS Sensing of Pollutants and Pesticides 77
4.3.2 SERS Sensing of Melamine 82
4.3.3 SERS Sensing of Food Colourants. 84
4.4 SERS Identification of Biowarfare Agent Anthrax 86
References 87

5 Biomolecular SERS Applications. 93
5.1 SERS Biomolecular Detection Schemes 93
5.2 Nucleic Acids (NAs) and Their Components 95
5.2.1 Intrinsic Detection of NAs 96
5.2.2 Intrinsic NA Detection Using Hybridization 98
5.2.3 Intrinsic NA Detection Using TERS. 100
5.2.4 Extrinsic Detection of NAs 100
5.2.5 Extrinsic NA Detection Using Hybridization 102
5.3 Proteins and Their Components 104
5.3.1 Intrinsic Detection of Proteins 104
5.3.2 Extrinsic Detection of Proteins. 108
5.3.3 Immunoassays 109
5.4 Lipids and Membranes 118
References 120

6 SERS Investigations of Cells, Viruses and Microorganisms. 127
6.1 Intracellular SERS Investigations 127
6.1.1 Intracellular SERS Detection Strategies. 127
6.1.2 Delivery of the Metallic NPs Inside the Cells 129
6.1.3 Chemical Probing in Cells by Intrinsic SERS Spectra. . . . 131
6.1.4 Chemical Probing in Cells Using SERS Tags with RRMs 134
6.1.5 Endosomal pH Monitored by SERS 137
6.1.6 Intracellular SERS Using Tip-like Substrates 139
6.1.7 Experimental Aspects of Intracellular SERS Studies 140
6.2 Detection and Identification of Viruses and Microorganisms 141
6.2.1 Detection and Identification of Viruses 141

6.2.2 Detection and Identification of Bacteria 142
6.2.3 Detection and Identification of Yeasts. 145
References 145

7 Medical Applications of SERS. 149
7.1 Glucose Sensing In Vitro 149
7.2 Pathogen Sensing In Vitro. 151
7.2.1 Pathogen Sensing Using NA Hybridization 152
7.2.2 Pathogen Sensing Using Immunoassays 157
7.2.3 Direct Bacterial Identification in Human Body Fluids. . . . 159
7.3 SERS Cancer Diagnostics In Vitro 162
7.3.1 Cancer Diagnostics Using NA Hybridization 163
7.3.2 Cancer Diagnostics Using Immunoassays 166
7.3.3 Direct Cancer Diagnostics from Blood Plasma. 169
7.3.4 Direct Cancer Diagnostics from Urine and Saliva. 173
7.4 SERS In Vitro Diagnostics of Other Diseases 175
7.5 SERS-Based Medical Therapy and Theranostics In Vitro. 179
7.6 SERS Ex Vivo: Tissue Diagnostics and Histology 185
7.7 SERS Medical Applications In Vivo. 187
7.7.1 In Vivo Glucose Sensor 187
7.7.2 In Vivo Imaging and Tumour Targeting 189
7.7.3 Clinical Utility of SERS 195
7.7.4 Intracellular SERS Monitoring of Drug Release In Vivo. 200
7.7.5 Toxicity Issue 202
References 202

8 Conclusions and Outlook 213

Index 219

Acronyms

2-AP	2-Aminopurine
4-ATP	4-Aminothiophenol
4-MBA	4-Mercaptobenzoic acid
4-NBT	4-Nitrobenzenethiol
6-MP	6-Mercaptopurine
6-TG	6-Thioguanine
AAO	Anodic alumina oxide
Ab	Antibody
AEF	Analytical enhancement factor
AFM	Atomic force microscopy
AFP	α-Fetoprotein
Arg	Arginine
BiASERS	Bianalytical SERS
BSA	Bovine serum albumin
CCD	Charged-coupled device
CEA	Carcinoembryonic antigen
CL	Colloidal lithography
COIN	Composite organic-inorganic nanoparticle
CT	Computed tomography
CTAB	Cetyltrimethylammonium bromide
CTCs	Circulating tumour cells
CuTMPyP	Copper(II) 5,10,15,20-tetrakis(1-methyl-4-pyridyl)porphyrin
CV	Crystal violet
Cy	Cyanine
Cys	Cysteine
DA	Dopamine
DFA	Discriminant function analysis
DFT	Density functional theory
DMPC	1,2-Dimyristoyl-*sn*-glycero-3-phosphocholine
DNA	Deoxyribonucleic acid
DOX	Doxorubicin

DPA	Dipicolinic acid
ds	Double strand
DSNB	5,5'-Dithiobis(succinimidyl-2-nitrobenzoate)
DT	Decanethiol
DTTC	3,3'-Diethylthiatricarbocyanine
EBL	Electron beam lithography
EDTA	Ethylenediaminetetraacetic acid
EF	Enhancement factor
EGF	Epidermal growth factor
EGFR	Epidermal growth factor receptor
ELISA	Enzyme-linked immunosorbent assay
EM	Electromagnetic
EpCAM	Epithelial cell adhesion molecule
ERLs	Extrinsic Raman labels
FON	Film over nanospheres
GLAD	Glancing angle vapour deposition
Gly	Glycine
GSH–OEt	Glutathione monoester
HBLs	Hybrid bilayers
HCA	Hierarchical cluster analysis
HCL	Hole-mask colloidal lithography
His	Histidine
HIV	Human immunodeficiency virus
HNSs	Hollow nanoshells
HOMO	Highest occupied molecular orbital
HPLC	High-performance liquid chromatography
IBL	Ion beam lithography
ICG	Indocyanine green
IgG	Immunoglobulin
IR	Infrared
LB	Langmuir-Blodgett
LC	Liquid chromatography
LDA	Linear discriminant analysis
Leu	Leucine
LOD	Limit of detection
LOQ	Limit of quantification
LS	Least-squares
LSPR	Localized surface plasmon resonance
LUMO	Lowest unoccupied molecular orbital
MELLFs	Metal-like liquid films
Met	Methionine
MG	Metallic glassy
MH	Mercaptohexanol
MNPs	Magnetic nanoparticles
MRI	Magnetic resonance imaging

MS	Molecular sentinel
MUC	Mucine-type glycoprotein
NA	Nucleic acid
NB	Nile blue
NIL	Nanoimprint lithography
NIR	Near infrared
NP	Nanoparticle
NR	Nanorod
NRS	Normal Raman scattering
NSL	Nanosphere lithography
NW	Nanowire
OAD	Oblique angle vapour deposition
Os–BA	4-Mercaptophenylboronic acid−triosmium carbonyl cluster conjugate
OxyHb	Oxyhemoglobin
PBS	Phosphate-buffer saline
PC	Pancreatic cancer
PCA	Principal component analysis
PCR	Polymerase chain reaction
PDMS	Poly-(dimethylsiloxane)
PDT	Photodynamic therapy
PEG	Polyethylenglycol
Phe	Phenylalanine
PMMA	Poly(methylmethacrylate)
PPTT	Plasmonic photothermal therapeutic
Pro	Proline
PS	Polystyrene
PSA	Prostate-specific antigen
PVP	Polyvinylpyrrolidone
RH6G	Rhodamine 6G
RIE	Reactive ion etching
RNA	Ribonucleic acid
ROC	Receiver operating characteristic
RRS	Resonance Raman scattering
RS	Raman scattering
RSD	Relative standard deviation
RRM	Raman reporter molecule
SAM	Self-assembled monolayer
SEF	Surface-enhanced fluorescence
SEHRS	Surface-enhanced hyper Raman scattering
SEIRA	Surface-enhanced infrared absorption
SEM	Scanning electron microscopy
SERS	Surface-enhanced Raman scattering
SERRS	Surface-enhanced resonance Raman scattering
SHINERS	Shell-isolated NP-enhanced Raman spectroscopy
SHINs	Shell-isolated NPs

SM	Single-molecule
SP	Surface plasmon
SPE	Surface plasmon extinction
ss	Single strand
SWNT	Single-walled carbon nanotube
TEM	Transmission electron microscopy
TERS	Tip-enhanced Raman scattering
TPL	Two-photon luminescence
Trp	Tryptophan
Tyr	Tyrosine
UTI	Urinary tract infection
UV-vis	Ultraviolet-visible

Chapter 1
Introduction

Modern analytical techniques should be highly specific and sensitive enough to identify and quantify an analyte of interest with minimum requirements for sample pretreatment. Raman spectroscopy is a highly specific technique that enables identification of molecules through their specific molecular fingerprint information as observed in their Raman spectra. However, the Raman scattering (RS) effect is intrinsically quite weak and the Raman spectra cannot be obtained from low analyte concentrations. Surface-enhanced Raman scattering (SERS) spectroscopy can overcome this problem by using certain metallic[1] nanoparticles (NPs) or nanostructures which significantly amplify the RS signals coming from analytes attached to (or at least be in close proximity to) such nanostructural surface. "S" means that SERS is a "surface" spectroscopy technique (the analytes must be on or close to the surface), "E" means signal "enhancement" (ensured by plasmon resonances in the metal) and "R" means "Raman" (providing fingerprint information about studied analyte). Last "S" can mean "scattering" or "spectroscopy".[2] Thus, the SERS technique efficiently combines the specificity of Raman signature with high sensitivity.

Surface-enhanced Raman scattering (SERS) was discovered in the seventies by the Fleischmann group who observed a surprisingly strong Raman signal of a single monolayer of pyridine on an electrochemically roughened silver electrode (Fleischmann et al. 1974). The experiment was soon confirmed and quantified by the Van Duyne group (Jeanmaire and Van Duyne 1977) and Creighton group (Albrecht and Creighton 1977), reporting that enhancement of RS of pyridine is in order of 10^5–10^6. For more details about SERS discovery see reviews of McQuillan from the Fleischmann group (McQuillan 2009), Creighton (Creighton 2010) and Van Duyne (Haynes et al. 2005). Nowadays, SERS is understood as a very large enhancement of RS effect (basically 10^4–10^6, but even 10^{11} in some special cases) coming from

[1]The term "metallic" is used in meaning of "made from metal" (e.g. metallic substrate, metallic structure, metallic NP). On the other hand, the term "metal" is used in the case of the "metal properties" will be emphasized (e.g. metal surface).

[2]In certain literature, the abbreviation RS means "Raman spectroscopy" to emphasize the technique. Here, RS for "Raman scattering" is used to emphasize the Raman scattering effect. By analogy "S" means "scattering" in RRS, SERS, SERRS, TERS, etc.

M. Procházka, *Surface-Enhanced Raman Spectroscopy*,
Biological and Medical Physics, Biomedical Engineering,
DOI 10.1007/978-3-319-23992-7_1

molecules adsorbed on metal nanostructural surfaces. The decade following the SERS discovery was a period of intense activity in theoretical aspects of SERS with special emphasis on finding the origin of this enhancement (Moskovits 1985). Because of a poor understanding of the enhancement mechanism as well as many experimental problems, SERS remained a technique only used by a limited number of research groups. The simple use of Ag hydrosols as SERS-enhancing media (Creighton et al. 1979) opened up many possible applications of SERS for biomolecular studies (Koglin and Séquaris 1986; Cotton 1988). The observation of single-molecule (SM) detection by SERS (SM-SERS) reported in 1997 (Kneipp et al. 1997; Nie and Emory 1997) also significantly stimulated the interest in SERS applications.

The improvement of Raman instrumentation and the development of nanotechnologies (notably in terms of SERS enhancing substrate design and functionalization) in the end of the 1990s dramatically extended the field of SERS applications. Nowadays, scientists from a large range of disciplines including chemistry, physics, material and life sciences are beginning to use the SERS technique and fully exploit its tremendous potential. This can be seen in the growing number of publications about SERS and its applications as illustrated in Fig. 1.1. It includes several excellent review papers namely the first SERS review by Moskovits from 1985 (Moskovits 1985) and a recent one by Schlücker (2014). I would like to highlight many themed Journal issues namely in Journal of Raman Spectroscopy (2005, Editor Z.Q. Tian), in Faraday Discussions (2006, Editor Susan Weatherby), in Chemical Society Review (2008, Editors D. Graham and R. Goodacre), in Physical Chemistry Chemical Physics (2009, Editor P.G. Etchegoin), in Analytical Bioanalytical Chemistry (2009, Editors J. Popp and T. Mayerhöfer), in Chemical Communications (2011, Editors D. Graham, Z.Q. Tian and R. Van Duyne) and in MRS Bulletin (2013, Editors N.J. Halas and M. Moskovits). Several monographs covering SERS theory and applications are also available: "Surface-Enhanced Vibrational Spectroscopy" (R. Aroca, Wiley, 2006), "Surface-Enhanced Raman Scattering: Physics and

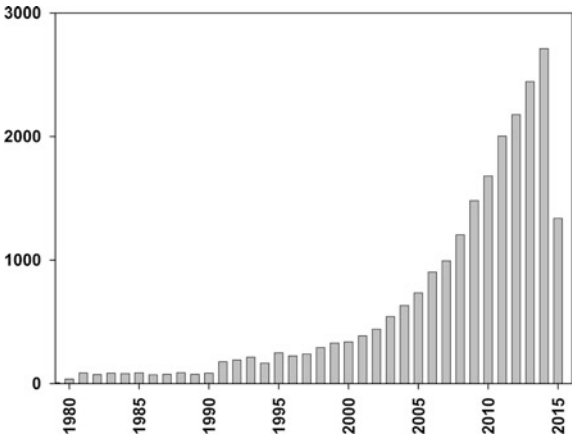

Fig. 1.1 Growing popularity of the SERS technique. This plot shows citation data in Web of Science for the term "surface enhanced Raman or SERS" (for 2015, it is incomplete, showing its value on June 30)

Applications", (Editors K. Kneipp, M. Moskovits, H. Kneipp, Springer, 2006), "Principles of Surface-Enhanced Raman Spectroscopy and Related Plasmonic Effects" (E. C. Le Ru, P. G. Etchegoin, Elsevier, 2009), "Surface-Enhanced Raman Spectroscopy: Analytical, Biophysical and Life Science Applications" (Editor S. Schlücker, Wiley, 2011) and "Frontiers of Surface-Enhanced Raman Scattering: Single Nanoparticles and Single Cells" (Editors Y. Ozaki, K. Kneipp, R. Aroca, Wiley 2014). A prestigious Faraday Discussion event about SERS spectroscopy was held at Imperial College London at September 2006. After over 40 years of SERS, hundreds of scientists are actively working in SERS field and the number of publications about SERS has exceeded 26,000 (Fig. 1.1).

SERS has many advantages over ordinary spectroscopic analytical techniques such as extremely high sensitivity, molecular selectivity, intense signals and great precision. However, the development of SERS technique so that it can become a standard analytical tool is still a big challenge and at least two main problems must be solved. First, a major issue for a routine quantitative SERS application (SERS sensing) is the requirement of a uniform SERS-enhancing substrates providing reliable and reproducible spectral signature of the studied analyte. A big effort is being made to rational designing of new SERS-enhancing substrates with aim to improve their sensitivity and spectral reproducibility (Banholzer et al. 2008). Second, SERS is a highly molecular specific technique and SERS detection is usually limited to molecules with surface-seeking groups since only molecules on or near the metal surface experience high surface enhancements. The problem to detect molecules with no surface-seeking groups or providing only weak SERS effect can be solved by chemical modification such as the labelling with highly SERS-active label (Smith 2008). With this approach the SERS spectra of labels instead of molecules are obtained leading to indirect but extremely sensitive detection. An alternative to the labelling of a target molecule is a SERS tag formed by attaching a molecule (called Raman reporter) to the metallic NPs providing a strong SERS signal (Wang et al. 2013). The surface of SERS tag can be further functionalized with a biorecognition element such as an antibody to make the tags with a specific binding feature (such as cancer biomarkers). The possibility of introducing metallic NPs or rationally designed NP tags into living cells or living organisms enables many in vitro and in vivo medical applications including diagnostics, therapy, theranostics and surgery guidance with sufficient sensitivity (Zavaleta et al. 2011; Vo-Dinh et al. 2013).

The main aim of this book is to provide a compact and full-length review of bioanalytical, biomolecular and medical applications of SERS spectroscopy reported during the last two decades. Following this introduction you will find two chapters describing basic principles of RS and SERS spectroscopy including some practical aspects related to bioapplications. The next four chapters summarized key concepts and bioanalytical (Chap. 4), biomolecular (Chap. 5), cellular (Chap. 6) and medical (Chap. 7) applications of SERS. The last chapter gives conclusions and outlook. Of course, it was impossible to include all applications from the extensive SERS literature in this book. Besides the monographs and themed Journal issues mentioned above many recent reviews covering SERS bioapplications are highly

recommended for a complete overview: Cotton (1988), Cotton et al. (1991), Dou and Ozaki (1999), Kneipp et al. (2002), Hering et al. (2008), Chourpa et al. (2008), Huh et al. (2009), Abalde-Cela et al. (2010), Alvarez-Puebla and Liz-Marzán (2010), Vo-Dinh et al. (2010), Li (2010), Procházka and Štepánek (2012), Banz et al. (2011), Aoki et al. (2013), McNay et al. (2011), Culha et al. (2012), Han et al. (2012), Larmour and Graham (2011), Faulds (2012), Ochsenkühn and Campbell (2012), Drescher and Kneipp (2012), Harper et al. (2013), Vendrell et al. (2013), Culha (2013), Xie and Schlücker (2013), Wang et al. (2013), Vo-Dinh et al. (2013), Xie and Schlücker (2014), Schlücker (2014), Nima et al. (2014), McAughtrie et al. (2014), Howes et al. (2014a, b), Cialla et al. (2014), Zheng and He (2014), Li et al. (2015), Vo-Dinh et al. (2015).

References

S. Abalde-Cela, P. Aldeanueva-Potel, C. Mateo-Mateo, L. Rodriguez-Lorenzo, R.A. Alvarez-Puebla, L.M. Liz-Marzan, Surface-enhanced Raman scattering biomedical applications of plasmonic colloidal particles. J. R. Soc. Interface **7**, S435 (2010)

M.G. Albrecht, J.A. Creighton, Anomalously intense Raman spectra of pyridine at a silver surface. J. Am. Chem. Soc. **99**, 5215 (1977)

R.A. Alvarez-Puebla, L.M. Liz-Marzán, SERS-based diagnosis and biodetection. Small **6**, 604 (2010)

P.H.B. Aoki, L.N. Furini, P. Alessio, A.E. Aliaga, C.J.L. Constantino, Surface-enhanced Raman scattering (SERS) applied to cancer diagnosis and detection of pesticides, explosives, and drugs. Rev. Anal. Chem. **32**, 55 (2013)

M.J. Banholzer, J.E. Millstone, L. Qin, C.A. Mirkin, Rationally designed nanostructures for surface-enhanced Raman spectroscopy. Chem. Soc. Rev. **37**, 885 (2008)

K.C. Bantz, A.F. Meyer, N.J. Wittenberg, H. Im, O. Kurtulus, S.H. Lee, N.C. Lindquist, S.H. Oh, C.L. Haynes, Recent progress in SERS biosensing. Phys. Chem. Chem. Phys. **13**, 11551 (2011)

I. Chourpa, F.H. Lei, P. Dubois, M. Manfait, G.D. Sockalingum, Intracellular applications of analytical SERS spectroscopy and multispectral imaging. Chem. Soc. Rev. **37**, 993 (2008)

D. Cialla, S. Pollok, C. Steinbrücker, K. Weber, J. Popp, SERS-based detection of biomolecules. Nanophotonics **3**, 383 (2014)

T.M. Cotton, The applications of SERS to biological systems, in *Spectroscopy of Surfaces*, ed. by R.J.H. Clark, R.E. Hester (Wiley, Chichester, 1988), pp. 90–153

T.M. Cotton, J.-H. Kim, G.D. Chumanov, Application of surface-enhanced Raman spectroscopy to biological systems. J. Raman Spectrosc. **22**, 729 (1991)

J.A. Creighton, Contributions to the early development of surface-enhanced Raman spectroscopy. Notes Rec. R. Soc. **64**, 175 (2010)

J.A. Creighton, C.G. Blatchford, M.G. Albrecht, Plasma resonance enhancement of Raman scattering by pyridine adsorbed on silver and gold sol particles of size comparable to the excitation wavelength. J. Chem. Soc., Faraday Trans. 2 **75**, 790 (1979)

M. Culha, Surface-enhanced Raman scattering: An emerging label-free detection and identification technique for proteins. Appl. Spectrosc. **67**, 355 (2013)

M. Culha, B. Cullum, N. Lavrik, C.K. Klutse, Surface-enhanced Raman scattering as an emerging characterization and detection technique. J. Nanotechnol. **2012**, 971380 (2012)

X.M. Dou, Y. Ozaki, Surface-enhanced Raman scattering of biological molecules on metal colloids: basic studies and applications. Rev. Anal. Chem. **18**, 285 (1999)

D. Drescher, J. Kneipp, Nanomaterials in complex biological systems: insights from Raman spectroscopy. Chem. Soc. Rev. **41**, 5780 (2012)
K. Faulds, Multiplexed SERS for DNA detection, in *Raman Spectroscopy for Nanomaterials Characterization*, ed. by C.S.S.R. Kumar (Springer, Berlin Heidelberg, 2012), pp. 353–378
M. Fleischmann, P.J. Hendra, A.J. McQuillan, Raman spectra of pyridine adsorbed at a silver electrode. Chem. Phys. Lett. **26**, 163 (1974)
X.X. Han, B. Zhao, Y. Ozaki, Label-free detection in biological applications of surface-enhanced Raman scattering. Trend. Anal. Chem. **38**, 67 (2012)
M.M. Harper, K.S. McKeating, K. Faulds, Recent developments and future directions in SERS for bioanalysis. Phys. Chem. Chem. Phys. **15**, 5312 (2013)
C.L. Haynes, C.R. Yonzon, X. Zhang, R.P. Van Duyne, Surface-enhanced Raman sensors: early history and the development of sensors for quantitative biowarfare agents and glucose detection. J. Raman Spectrosc. **36**, 471 (2005)
K. Hering, D. Cialla, K. Ackermann, T. Dörfer, R. Möller, H. Schneidewind, R. Mattheis, W. Fritzsche, P. Rösch, J. Popp, SERS: a versatile tool in chemical and biochemical diagnostics. Anal. Bioanal. Chem. **390**, 113 (2008)
P.D. Howes, R. Chandrawati, M.M. Stevens, Colloidal nanoparticle as advanced biological sensors. Science **346**, 1247390 (2014a)
P.D. Howes, S. Rana, M.M. Stevens, Plasmonic nanomaterials for biodiagnostics. Chem. Soc. Rev. **43**, 3835 (2014b)
Y.S. Huh, A.J. Chung, D. Erickson, Surface enhanced Raman spectroscopy and its applications to molecular and cellular analysis. Microfluid. Nanofluid. **6**, 285 (2009)
D.J. Jeanmaire, R.P. Van Duyne, Heterocyclic, aromatic, and aliphatic amines adsorbed on the anodized silver electrode. J. Electroanal. Chem. **84**, 1 (1977)
K. Kneipp, Y. Wang, H. Kneipp, L.T. Perelman, I. Itzkan, R.R. Dasari, M.S. Feld, Single molecule detection using surface-enhanced Raman scattering (SERS). Phys. Rev. Lett. **78**, 1667 (1997)
K. Kneipp, H. Kneipp, I. Itzkan, R.R. Dasari, M.S. Feld, Surface-enhanced Raman scattering and biophysics. J. Phys.: Condens. Matter **14**, R597 (2002)
E. Koglin, J.-M. Séquaris, Surface enhanced Raman scattering of biomolecules. Top. Curr. Chem. **134**, 1 (1986)
I.A. Larmour, D. Graham, Surface enhanced optical spectroscopies for bioanalysis. Analyst **136**, 3831 (2011)
M. Li, The applications of surface-enhanced Raman spectroscopy to identify and quantify chemical adulterants or contaminants in food, in *Applications of vibrational spectroscopy in food science* ed. by E. Li-Chan, P.R. Griffiths, J.M. Chalmers (John Wiley, Chichester, 2010), pp. 649–662
M. Li, S.K. Cushing, N. Wu, Plasmon-enhanced optical sensors: a review. Analyst **140**, 386 (2015)
S. McAughtrie, K. Faulds, D. Graham, Surface enhanced Raman spectroscopy (SERS): potential applications for disease detection and treatment. J. Photochem. Photobiol. C-Photochem. Rev. **21**, 40 (2014)
G. McNay, D. Eustace, W.E. Smith, K. Faulds, D. Graham, Surface-enhanced Raman scattering (SERS) and surface-enhanced resonance Raman scattering(SERRS): a review of applications. Appl. Spectrosc. **65**, 825 (2011)
A.J. McQuillan, The discovery of surface-enhanced Raman scattering. Notes Rec. R. Soc. **63**, 105 (2009)
M. Moskovits, Surface-enhanced spectroscopy. Rev. Modern Phys. **57**, 783 (1985)
S. Nie, S.R. Emory, Probing single molecules and single nanoparticles by surface-enhanced Raman scattering. Science **275**, 1102 (1997)
Z.A. Nima, A. Biswas, I.S. Bayer, F.D. Hardcastle, D. Perry, A. Ghosh, E. Dervishi, A.S. Biris, Applications of surface-enhanced Raman scattering in advanced bio-medical technologies and diagnostics. Drug Metab. Rev. **46**, 155 (2014)

M.A. Ochsenkühn, C.J. Campbell, Biomedical SERS studies using nanoshells, in *Raman Spectroscopy for Nanomaterials Characterization*, ed. by C.S.S.R. Kumar (Springer, Berlin Heidelberg, 2012), pp. 51–74

M. Procházka, J. Štěpánek, Surface-enhanced Raman scattering (SERS) and its application to biomolecular and cellular investigation, in *Applications of Raman Spectroscopy to Biology—from Basic Studies to Disease Diagnosis*, ed. by M. Ghomi (IOS Press, Amsterdam, 2012), pp. 1–30

S. Schlücker, Surface-enhanced Raman spectroscopy: concepts and chemical applications. Angew. Chem. Int. Ed. **53**, 4756 (2014)

W.E. Smith, Practical understanding and use of surface enhanced Raman scattering/surface enhanced resonance Raman scattering in chemical and biological analysis. Chem. Soc. Rev. **37**, 955 (2008)

M. Vendrell, K.K. Maiti, K. Dhaliwal, Y.T. Chang, Surface-enhanced Raman scattering in cancer detection and imaging. Trends. Biotechnol. **31**, 249 (2013)

T. Vo-Dinh, H.N. Wang, J. Scaffidi, Plasmonic nanoprobes for SERS biosensing and bioimaging. J. Biophoton. **3**, 89 (2010)

T. Vo-Dinh, A.M. Fales, G.D. Griffin, C.G. Khoury, Y. Liu, H. Ngo, S.J. Norton, J.K. Register, H. N. Wang, H. Yuan, Plasmonic nanoprobes: from chemical sensing to medical diagnostics and therapy. Nanoscale **5**, 10127 (2013)

T. Vo-Dinh, Y. Liu, A.M. Fales, H. Ngo, H.N. Wang, J.K. Register, H. Yuan, S.J. Norton, G.D. Griffin, SERS nanosensors and nanoreporters: golden opportunities in biomedical applications. WIREs Nanomed. Nanobiotechnol. **7**, 17 (2015)

Y. Wang, B. Yan, L. Chen, SERS tags: novel optical nanotags for bioanalysis. Chem. Rev. **113**, 1391 (2013)

W. Xie, S. Schlücker, Medical applications of surface-enhanced Raman scattering. Phys. Chem. Chem. Phys. **15**, 5329 (2013)

W. Xie, S. Schlücker, Rationally designed multifunctional plasmonic nanostructures for surface-enhanced Raman spectroscopy: a review. Rep. Prog. Phys. **77**, 116502 (2014)

C.L. Zavaleta, M.F. Kircher, S.S. Gambhir, Raman's "effect" on molecular imaging. J. Nucl. Med. **52**, 1839 (2011)

J. Zheng, L. He, Surface-enhanced Raman spectroscopy for the chemical analysis of food. Compr. Rev. Food. Sci. Food Saf. **13**, 317 (2014)

Chapter 2
Basics of Raman Scattering (RS) Spectroscopy

Abstract Raman spectroscopy is an optical spectroscopic technique based on the inelastic scattering (called Raman scattering—RS) of light by the matter (the molecule of interest for instance). RS event occurs because a molecular vibration can change the polarizability of molecule which interacts with incident light. Thus, Raman spectroscopy is a vibrational technique and Raman spectra provide specific molecular fingerprint information. RS effect was discovered by Indian physicists C.V. Raman in 1928 but only instrumental developments from 1980s brought about big progress of Raman techniques. Although RS process is intrinsically weak, Raman spectroscopy has become nowadays a routine method in many fields. This chapter gives a brief introduction to Raman spectroscopy including a short history, basics of RS theory, cross-sections, vibrations, selection rules, resonant RS, polarization properties as well as Raman experiment in macroscopic and microscopic setups. The last paragraph summarizes the advantages and disadvantages of the Raman spectroscopy for biomolecular studies and the main characteristics of Raman spectra of biomolecules.

2.1 Short History of Raman Effect

Raman spectroscopy is a vibrational optical spectroscopic technique based on the inelastic scattering of light by matter like the molecule of interest. Raman spectroscopy is a highly specific technique due to specific molecular fingerprint information as observed in the Raman spectra. This phenomenon was theoretically predicted by Smekal in 1923 (Smekal 1923). In 1928, the first experimental observation of RS effect was reported by Indian physicists C.V. Raman and K.S. Krishnan (Raman and Krishnan 1928a, b) and independently by Mandelstam and

M. Procházka, *Surface-Enhanced Raman Spectroscopy*,
Biological and Medical Physics, Biomedical Engineering,
DOI 10.1007/978-3-319-23992-7_2

Landsberg in the former Soviet Union (Mandelstam and Landsberg 1928). In the experiment of C.V. Raman sunlight was focused by a telescope onto a sample which was an organic liquid (solvents) or vapour. The scattered radiation was collected by a second lens and by a system of optical filters. In 1930, C.V. Raman earned the Nobel prize in physics for "his work on the scattering of light and for the discovery of the effect named after him". More details about history of the discovery of Raman effect can be found in the paper of Krishnan and Shankar (Krishnan and Shankar 1981).

Since the Raman effect is intrinsically quite weak, relatively high-power lasers and sophisticated optical and electronic equipment are required to detect the Raman scattered photons. This accounts for the lengthy time that elapsed in the development of Raman spectroscopy. It experienced a rebirth in the 1960s with the invention of laser and its use as a light source. However, from the 1980s the advances in optoelectronics, particularly the development of compact lasers, detectors and efficient optical filters allowed lower cost, integrated instruments to be produced commercially. Consequently, Raman spectroscopy has been adopted as a routine method in many fields because it has been shown to be simpler and faster than alternative techniques.

2.2 Basic Theory of RS

When an electromagnetic (EM) field (light) interacts with the molecule, light can be adsorbed or scattered or not interact with the molecule at all. The energy level diagram (called the Jablonski diagram) is shown in Fig. 2.1. If the energy of photons in the incident wave closely matches the energy gaps between the proper molecular levels, one photon can be absorbed and the molecule crosses to higher excited energy level (absorption). An emission process involves two photons: one is absorbed and a second one is emitted, after some time corresponding to the lifetime τ of the excited state. This corresponds to the radiative excitation energy decay of the molecule, which returns back to the ground state (fluorescence). While UV-vis absorption and fluorescence belong to electronic spectroscopies, IR absorption, involving nuclear vibrations independent from electrons (in a first approximation), is a vibrational spectroscopic method.

During light scattering process a photon crosses to a "virtual" state and immediately scatters the photon with same (elastic Rayleigh scattering) or slightly different (inelastic Raman scattering) energy. This effect mostly involves transitions between vibrational energy levels of the same electronic state of the molecule (generally the ground state), thus it belongs to vibrational spectroscopy. Figure 2.1 schematically illustrates the Rayleigh and Raman scattering processes. In this Jablonski diagram, ω_{inc} and ω_s are the frequencies of incident and scattered photons, respectively. If the E_1 is the energy of a ground vibrational level (v = 0) and E_2

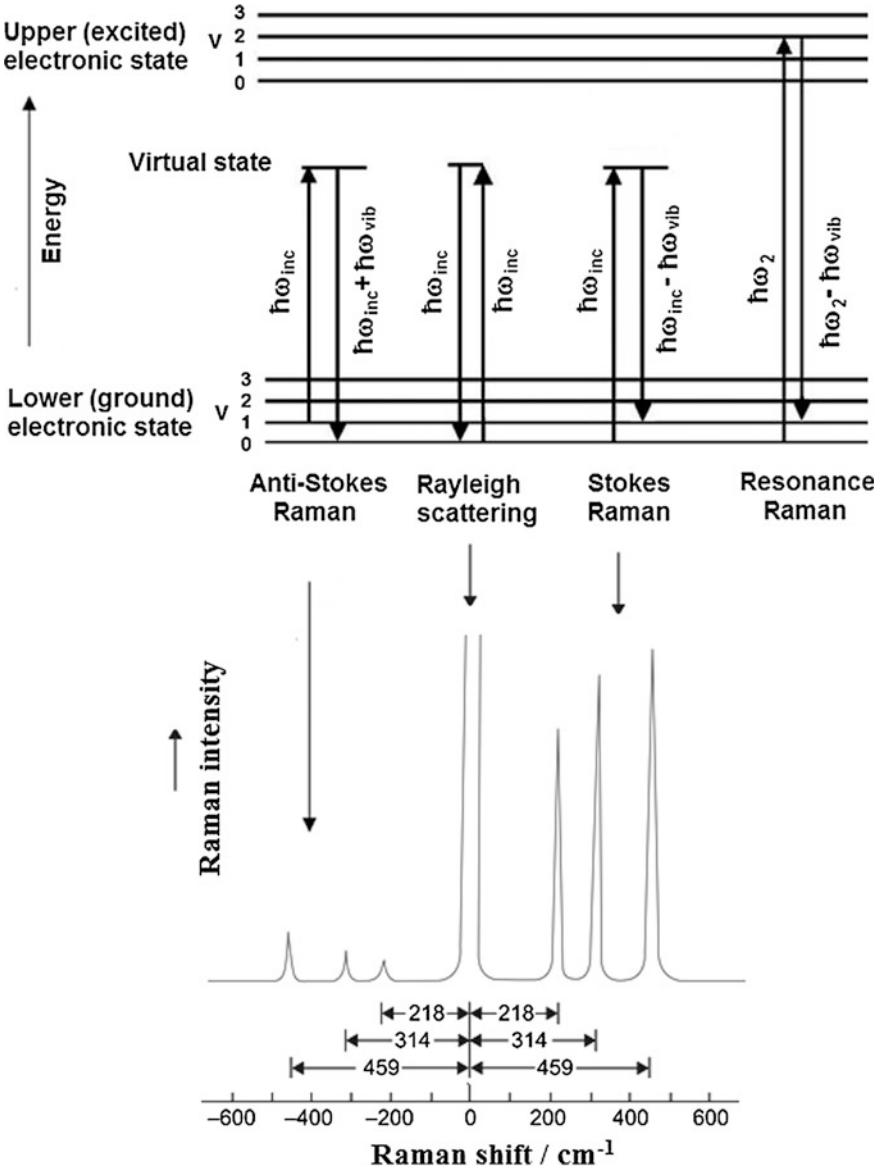

Fig. 2.1 Simplified Jablonski diagram illustrating the Rayleigh, NRS and RRS processes and corresponding Raman spectrum of CCl_4, v–the vibrational quantum numbers

that of an excited vibrational level 1 (v = 1) of the molecule electronic ground state, the scattered photon fulfils the following condition:

$$\hbar\omega_s = \hbar\omega_{inc} \pm (E_2 - E_1) \tag{2.1}$$

Rayleigh scattering arises when the energy of the molecular system both before and after the scattering process is the same ($\hbar\omega_s = \hbar\omega_{inc}$).[1] The occurrence of inelastic light scattering can be explained by classical theory in terms of a modulation of the incident radiation $E_{loc}(\omega_{inc})$ by a vibrating molecule with frequency ω_{vib}. Raman frequency can be smaller $\omega_{inc} - \omega_{vib}$ or larger $\omega_{inc} + \omega_{vib}$ than that of the incoming photon ω_{inc}. When the incident radiation is shifted to a lower frequency (lower energy), the scattered light is called Stokes shift. In this type of scattering the energy is transferred to the vibrational mode of the molecule which ends up in a higher vibrational energy state. Similarly, when the incident radiation is shifted to a higher frequency (higher energy), the scattered light is called anti-Stokes shift. In this type of scattering the energy is transferred from a vibrationally excited molecule, which ends up in a lower vibrational state after the scattering event. The scattering process when an intermediate "virtual state" does not correspond to a real energy level of the molecule is called normal Raman scattering (NRS).[2] When the energy of incident radiation $\hbar\omega_{inc}$ is close to the energy of electronic transition of the molecule ($\hbar\omega_2$ for instance, Fig. 2.1), the scattering process is taking place through an excited energy level of the molecule. This effect is called resonance Raman scattering (RRS). Since in this case the molecule crosses a "virtual" state located within its proper electronic energy levels, the fluorescence may become a competitive process. In fact, a strong fluorescence signal often makes RRS measurements difficult.

In the Raman spectrum one can observe two Raman lines located symmetrically from the Rayleigh line. Figure 2.1 shows typical NRS spectrum of carbon tetrachloride (CCl_4) as an example. At room temperature most of the molecules are in the ground vibrational state (v = 0) with a much lower population in the first vibrationally excited state (v = 1). Since there is a much higher probability (given by the Bolzmann distribution) that the molecule is in the ground vibrational state, the Stokes lines in the spectrum are more intense than the anti-Stokes lines. Therefore, the Stokes part of the spectra is mostly used in Raman spectroscopy. In vibrational spectroscopy, it is common to measure frequencies in wavenumber units (waves per unit length), which are reciprocal to wavelength.[3] The energy lost by the photons in

[1]The symbol for frequency depending on the type of spectroscopy or users is ω or ν. In fact, ω [rad s^{-1}] is an angular frequency, ν [Hz or s^{-1}] is frequency $\nu = \omega/2\pi$. Energy can be then expressed as $E = \hbar\omega = h\nu$, where h is the Planck constant and ħ the reduced Planck constant ($\hbar = h/2\pi$).

[2]The term "RS" is often used for RS under nonresonant (normal) conditions, term "normal RS" (or sometimes classical RS) is used to distinguish it from resonance RS under resonant conditions. Note that there is also the case of preresonant RS.

[3]Conversion between wavenumbers ν′ and angular frequency ω is ($\nu' = \omega/2\pi c$), c is the speed of light.

the scattering events is called the Raman shift and is expressed in wavenumbers and denoted $\Delta\nu_R$ [cm^{-1}]. It corresponds to the wavenumber of the vibrational mode that is involved in the scattering event. Raman shifts are, in contrast to luminescence, independent of the excitation wavelength. The position of Raman peaks is a property solely of the electronic ground state. The Raman intensity in NRS spectra is directly proportional to the concentration of the molecule.

Light scattering processes are related to the polarizability of the molecule which interacts with the EM field. A simple classical EM field description of Raman spectroscopy can be used to explain many of the important features of Raman band intensities. The incident EM field $E_{loc}(\omega_{inc})$, induces a dipole moment μ_{ind} in the molecule proportional to the molecular polarizability $\alpha_{molecule}$:

$$\mu_{ind} = \alpha_{molecule} \cdot E_{loc}(\omega_{inc}) \tag{2.2}$$

The induced dipole moment μ_{ind} and the incident local electric field $E_{loc}(\omega_{inc})$ have vectorial properties, while the electronic polarizability $\alpha_{molecule}$ of the molecule is a tensor of rank two with nine components. The polarizability tensor is often symmetric and only six components are relevant.

Three dipole components occur: $\mu_{ind}(\omega_{inc})$, $\mu_{ind}(\omega_{inc} - \omega_{vib})$ and $\mu_{ind}(\omega_{inc} + \omega_{vib})$, which correspond to Rayleigh, Stokes Raman and anti-Stokes Raman scattering, respectively. The molecular polarizability $\alpha_{molecule}$ is a function of the proper molecule. It is a tensor: some of its components can vary during the vibration of nuclei around their equilibrium position in the EM field of the electrons. In a quantum mechanical treatment of the polarizability and in using a simplified second-order time-dependent theory, the Raman transition between |i> and |f> states can be expressed by the tensor element:

$$\left(\alpha_{\rho\sigma}\right)_{if} = \sum_{s \neq i,f} \left[\frac{\langle i|D_\sigma|s\rangle\langle s|D_\rho|f\rangle}{E_i - E_s + \hbar\omega_{inc} + i\Gamma} + \frac{\langle i|D_\rho|s\rangle\langle s|D_\sigma|f\rangle}{E_f - E_s - \hbar\omega_{inc} + i\Gamma} \right] \tag{2.3}$$

The summation runs over all the excited states s of the molecule, operators D_ρ, D_σ are components of the electric dipole moment operator and Γ is a "damping factor" which can be related to the width of the excited state vibrational levels. In the case of RRS, the first term in (2.3) is much smaller than the second one, which becomes only limited by the Γ factor. Thus, under these conditions, RS is enhanced by factor 10^3–10^5.

RS process is intrinsically weak. Since only a very small fraction of light is inelastically scattered, the intensity ratio of Rayleigh line and Raman lines is approximately 10^5–10^{12}. The efficiency of particular molecule (with a random orientation with respect to the incident field polarization) to scatter light by RS can be determined by a differential Raman cross-section:

$$\frac{d\sigma_r}{d\Omega} \tag{2.4}$$

Differential Raman cross-section characterizes the radiation profile of the RS process taking into account the orientation of the molecule with respect to the incident light and the direction of observation of the scattered light (scattering configuration). Differential Raman cross-section can be derived from expression:

$$\frac{dP_R}{d\Omega}(\Omega) = \frac{d\sigma_r}{d\Omega}(\Omega) S_{inc} \tag{2.5}$$

where P_R is a power of the RS process (proportional to the number of photons per unit time involved in the process), S_{inc} is incident power density and $d\Omega$ is an element of the solid angle. The differential Raman cross-section depends on a given vibrational mode for a given molecule and thus it must be defined a cross-section for each vibrational mode. Moreover, the Raman cross-section depends on the excitation wavelength and the refractive index of the medium (environment). NRS cross-sections per molecule typically range between 10^{-31}–10^{-29} cm^2 sr^{-1}, while, by comparison, fluorescence spectroscopy provides effective cross-sections in order of 10^{-16} cm^2 sr^{-1} (Kneipp et al. 2002). The RRS cross-section for dyes such as rhodamine 6G (RH6G) at resonance conditions can be of the order of 10^{-23}–10^{-24} cm^2 sr^{-1} and SERS cross-sections can be even of the order of 10^{-16} cm^2 sr^{-1} (Le Ru and Etchegoin 2009).

RS is a polarized effect and the assignment of Raman bands to the vibrations in a molecule can be obtained by analysing the scattered light parallel and perpendicular to the incoming E vector. It can be done by the Raman depolarization ratio:

$$\rho = \frac{I_{II}}{I_{\perp}} \tag{2.6}$$

where $I_\perp$ is the intensity of the Raman scattered light polarized perpendicular to the plane normal to the excitation beam and I_{II} is the intensity of the scattered light polarized parallel to the plane normal to the excitation beam. Detailed calculations show that for vibrations which do not preserve molecular symmetry during the motion of nuclei (not totally symmetric modes) the vibration is unpolarized and $\rho = 0.75$. For modes which do preserve molecular symmetry (totally symmetric modes), the vibration is polarized and $\rho < 0.75$.

More details about the theory of RS can be found in (Carey 1982; Ferraro and Nakamoto 1994; Long 2002; Schrader 1995; Smith and Dent 2005).

2.3 Molecular Vibrations and Their Raman Activity

Vibrations in the molecule are small oscillations of the atoms around their equilibrium positions. In a classical mechanical model, the vibrations in the molecules can be described by the harmonic oscillator. According to this, frequency of a

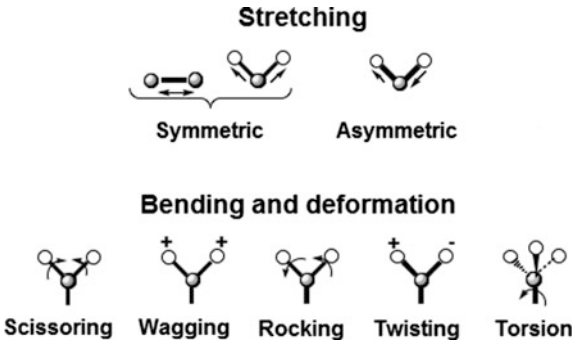

Fig. 2.2 Basic types of the normal vibrational modes. *Arrows* show directions of deflections of atoms, *plus* and *minus* signs indicate deflections of atoms above and below the plane

particular vibration ω_{vib} is related to the reduced masses of vibrating atoms m_{red} and the forces of their interactions (described by the force constants *f*):

$$\omega_{vib} = \sqrt{\frac{f}{m_{red}}} \tag{2.7}$$

This formula has very important consequence in Raman spectra: the lighter the atoms, the higher the frequencies of vibration. The force constant is related to the bond strength: the stronger the bond, the higher the frequency of vibration will be. Note that vibration frequency is independent on the energy levels between which the transitions take place.

The simplest description of vibrational degrees of freedom of a molecule with N atoms is in terms of $3N - 6$ or $3N - 5$ (for linear molecules)[4] normal vibrational modes. Vibrational analysis concerns the study of these normal vibrational modes. It is possible to define mass-weighted normal mode coordinates which provide an equivalent description of the molecular vibrations. Normal mode coordinate Q_k a given normal mode k ($k = 1, \ldots, 3N - 6$) corresponds to a specific vibrational pattern (displacements from equilibrium) on the molecule, for which all atoms oscillate at the same frequency ω_K.

There are three basic types of the normal vibrational modes (see Fig. 2.2):

1. Valence stretching vibrations (v) corresponding to the elongation and contraction of a bond between two neighbouring atoms without any change in the bonding angle.

[4]A molecule with *N* atoms has 3 *N* internal degrees of freedom; three of them can be assigned to translations and three of them to rotations. The rest corresponds to internal deformations (vibrations). For linear molecule the rotation about the axis has no physical meaning.

2. Bending or deformation vibrations (δ) often referred to as scissoring, wagging, rocking and twisting:
   - the scissoring vibration involving in plane movement of atoms changing the angle between bonds.
   - the wagging vibration is an in phase, out of plane movement of atoms while other atoms of the molecule are in the plane.
   - the rocking vibration, atoms swing back and forth in phase in the symmetry plane of the molecule.
   - the twisting vibration involves the twisting of a bond along its main axis.
3. Torsion vibration involves the twisting of a bond along its main axis.

For systems of more than two atoms, the vibrations can be symmetrical or asymmetrical about the centre. If there is no change in the angle between any of the bonds and the plane defined by the remaining atoms, they are classified as "in plane". The opposite case is known as "out of plane" vibrations. Depending on the geometric relationship between the transition moment for a specific vibrational mode and the symmetry axis for the mode, vibrational modes may be further classified as parallel or perpendicular.

The change of the polarizability by a given vibrational mode k can be expressed by the polarizability derivative (called also a Raman tensor of the normal mode k):

$$R_k(\omega_{inc}) = \left(\frac{\partial\alpha(\omega_{inc})}{\partial Q_k}\right)_{Q_K=0} \tag{2.8}$$

Each normal mode has its own Raman tensor, i.e. there is $3N - 6$ Raman tensors for a molecule with N atoms (or $3N - 5$ for linear molecule). RS intensity is then proportional to the square of the induced dipole moment that is the square of the polarizability derivative.

Selection rules tell us if a transition is allowed or forbidden. An allowed transition has a high probability of occurring and will result in a strong band. Conversely a forbidden transition's probability is so low that the transition will not be observed. The selection rule for a Raman-active vibration is that there will be a change in polarizability during the vibration:

$$\frac{\partial\alpha}{\partial Q_k} \neq 0 \tag{2.9}$$

To predict which bands will be Raman-active depend on the symmetry of the molecule. The symmetry elements of a molecule (i.e. centre, axes or planes) are associated with the symmetry operations which define all vibrational motions. For molecules with symmetry elements in its structure, the pattern of their normal vibrational modes will also have certain symmetry. Symmetry of normal vibrational modes influences a Raman tensor and consequently Raman activity of such vibrations. If we know the point group of the molecule and the symmetry labels for

the normal modes, then group theory makes it easy to predict which normal modes will be Raman-active (Cotton 1990).

At room temperature almost all molecules are in their lowest vibrational energy level with quantum number v = 0. For each normal mode, the most probable vibrational transition is from this level to the next higher level (v = 1). Such vibrational modes are called fundamental. Other transitions to higher excited states (v = 2, for instance) result in bands called overtones. Fundamental vibrational modes are strong in Raman spectra while the overtones are much weaker. When the vibrations have the same energy levels and transition frequency, they are called degenerated corresponding to the splitting of the band in Raman spectrum. Combination bands occur when some vibrations of similar frequencies are coupled and mutually interact. This effect is called Fermi resonance. Not all fundamental vibrations can be seen in Raman spectra because they have different selection rules. From group theory it is then straightforward to show that if a molecule has a centre of symmetry, vibrations which are Raman-active will not be active in the IR absorption and vice versa.

Concerning the intensity of a particular vibrational band in Raman spectrum, it depends on the degree of change of the polarizability by a particular vibrational mode. In practice, if a vibration does not greatly change the polarizability, then the polarizability derivative (and Raman tensor) will be near zero and the intensity of the Raman band will be low. On the other hand the vibrational mode which strongly changed the polarizability will be clearly seen in the Raman spectrum as a strong band. For example, the vibrations of a highly polar moiety, such as the O–H bond, are usually weak. Typical strong Raman scatterers are moieties with π-electron electron clouds, such as C=C double bonds. Even intensities of vibrational bands observed in NRS spectra of biomolecules will be summarized in Sect. 2.5.

2.4 Raman Experiment

Figure 2.3 illustrates a typical configuration of a Raman experiment. The excitation source is a laser providing monochromatic high-power light. Most Raman instruments use continuous lasers. Various kinds of lasers from UV to IR can provide the excitation lines but the intensity of RS under nonresonant conditions is proportional to $1/\lambda^4$ which caused lower intensity for higher excitation wavelengths. In the case of ion gas lasers (such as argon and krypton), the special interference filters are implemented to avoid sharp intense lines of spontaneous emission of gas in the Raman spectra.

The light is scattered in all directions. There are two basic geometries used in a Raman experiment: 90° and 180°. In 90° scattering, the laser beam is passed through the sample and the scattered light is collected at 90°. This is particularly suitable for liquid transparent samples. In the 180° (backscattering) geometry, the laser beam is delivered through the collection lens and the scattered light is collected back through it. This is a common arrangement for nontransparent solid

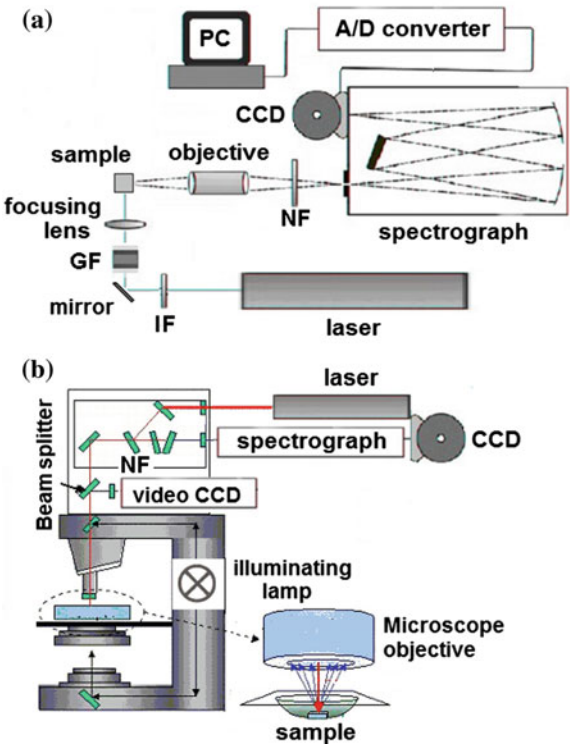

Fig. 2.3 Scheme of basic configurations of a typical Raman experiment: **a** 90° scattering geometry for macroscopic samples, **b** 180° scattering geometry for microscopic samples using an optical microscope. *GF* grey filters, *IF* interference filter, *NF* notch filter

samples and in Raman spectrometers equipped with an optical microscope. The beam splitter is used to switch between white light image of the sample and Raman measurement. A sample can be magnified by an objective and imaged by a video CCD camera. The microscope can be set up confocally. In this case, the microscope includes a pinhole in its focal plane which allows only light focused on the plane with the sample to be collected. The advantage of using a microscope is the possibility of imaging and spectral mapping in the *xy*-plane as well as of depth profiling of the sample by changing the focus in the *z*-direction. This is particularly useful for Raman studies of small biological objects such as cells. The lateral resolution about 1 μm can be reached (Kneipp et al. 2002). Another advantage of the Raman microspectrometer is that relatively low laser power can be used (about ~mW) in comparison to a macroscopic Raman instrument which typically uses laser power between ten and hundreds of mW.

Some sort of device should be used to separate the Raman scattering from the other light collected (such as elastic Rayleigh scattering). This can be done with two or three monochromators. However, filter technology has improved with the development of effective notch or edge filters. In both cases, the scattered light is focused onto the entrance slit of the spectrograph which separates spatially the scattered photons on the basis of their frequency. It is typically a dispersive

monochromator. Parameters of monochromator, such as focus length, entrance slit and spectral grating, determine a spectral resolution of the Raman experiment, which is typically 2–6 cm^{-1}. Although the photomultipliers can also be used as a detector, the multichannel CCD detectors are nowadays used providing the possibility of recording a wide spectral region in a short time. Polarization Raman spectra can be obtained if the analyser placed between a sample and entrance slit of monochromator is used to analyse the scattered light parallel and perpendicular to the incoming light from a laser (which is always polarized).

In many Raman spectrometers, the use of fibre optics and waveguides can produce a big advantage. Samples that cannot be introduced into the Raman spectrometer due to their size or hazardous nature can be investigated in situ. A lens is fixed on the end of the fibre optic probe to focus the laser beam and to function as the collecting windows in backscattering geometry. The fibre is pointed at the sample and Raman spectrum is acquired. Small sample spots (about ~ 1 μm) can be analysed this way (Smith and Dent 2005). Moreover, the portable Raman spectrometers can be used for rapid and in situ Raman analysis, which will be demonstrated in Chap. 4.

2.5 Raman Spectroscopy for Biomolecular Studies

Raman spectroscopy is a widely used technique for biomolecular studies. Any molecules that are produced by a living organism are considered as biomolecules. It includes mainly DNA and RNA, proteins, membrane structures (such as phospholipides), fatty acids and monosaccharides. From a chemical point of view all biomolecules contain some of the following atoms: carbon, hydrogen, oxygen, nitrogen, phosphor and sulphur.

It is possible to summarize some basic characteristics of Raman vibrational bands observed in NRS spectra of biomolecules (Schrader 1995; Smith and Dent 2005):

1. Stretching vibrations associated with chemical bands are more intense than deformation ones. For example, O–H deformation vibration of water at $\sim 1640\ cm^{-1}$ is weak while O–H stretching vibrations of water at 3400–3600 cm^{-1} are stronger.
2. Multiple chemical bonds often give rise to intense stretching modes, e.g. Raman bands due to a C=C vibrations (around 1640 cm^{-1}) are more intense than that due to C–C vibrations. On the other hand C=O vibrations are weak in Raman spectrum.
3. Stretching vibrations of single bands containing hydrogen (C–H, S–H, N–H, O–H, P–O–H, O–H) appear at high frequency region ($\sim$2500–4000 cm^{-1}). The 2000–2500 cm^{-1} region is referred to as the multiple bands (N=C=O, C≡C, C≡N) and 1500–2000 cm^{-1} region to as double bands (C=O, C=N, C=C, N=N).

4. Below 1500 cm^{-1} many biomolecules have spectral features of C–C and C–N vibrations (both stretching and deformation ones). This region is generally referred to as the fingerprint region.
5. Raman bands below $\sim$650 cm^{-1} usually involve atoms of large atomic mass (such as sulphurs or metal-organic groups) and give rise the stretching vibrations of high Raman intensity. It is for example S–S disulphide bonds in proteins or Fe–O in haemoglobin both with Raman bands around 500 cm^{-1}.
6. For cyclic compounds the "breathing" vibrational mode is usually the most intense. It is a case of 1005 cm^{-1} Raman band of phenylalanine (Phe) amino acid observed in NRS spectra of proteins or nucleobases at 700–900 cm^{-1}.

Main benefits of Raman spectroscopy for biomolecular applications can be summarized as follows (Carey 1982):

1. Raman spectroscopy is highly specific technique enabling identification of molecules through their specific molecular fingerprint information observed in their Raman spectra.
2. Raman spectra can be obtained from molecules in aqueous solutions since Raman spectrum of water is weak in the spectral region where Raman lines of molecules occur (200–3300 cm^{-1}).
3. The time scale of the RS effect is instantaneous. Thus, in a system where rapid chemical exchanges are occurring, each species contributes a Raman signal proportional to its concentration.
4. Only a small amount (volume) of a sample is required for obtaining Raman spectra.
5. Raman spectra may be recorded in a short time (1 s or even less).
6. RRS spectroscopy can be used to obtain Raman spectra of chromophores in low concentrations (about 10^{-4}–10^{-6} M).

There are of course also certain disadvantages that should be taken into account in any Raman applications:

1. The high laser power can induce unwanted photochemical effects in the sample (photobleaching, photodecomposition).
2. Raman spectroscopy requires high concentrations of studied molecules (about 0.1–0.01 M for NRS measurements).
3. Solutions usually require a high level of optical homogeneity.
4. In the case of RRS, the Raman spectrum is easily obscured by a competing process such as fluorescence.

References

P.R. Carey, *Biochemical applications of Raman and resonance Raman spectroscopies* (Academic Press, San Diego, 1982)

F.A. Cotton, *Chemical applications of group theory* (John Wiley & Sons, Chichester, 1990)

J.R. Ferraro, K. Nakamoto, *Introductory Raman spectroscopy* (Academic Press, San Diego, 1994)
K. Kneipp, H. Kneipp, I. Itzkan, R.R. Dasari, M.S. Feld, Surface-enhanced Raman scattering and biophysics. J. Phys.: Condens. Matter **14**, R597 (2002)
R.S. Krishnan, R.K. Shankar, Raman effect: history of the discovery. J. Raman Spectrosc. **10**, 1 (1981)
E.C. Le Ru, P.G. Etchegoin, *Principles of surface enhanced Raman spectroscopy and related plasmonic effects* (Elsevier, Amsterdam, 2009)
D. Long, *The Raman effect: a unified treatment of the theory of Raman scattering by molecules* (Wiley, Chichester, 2002)
L. Mandelstam, G. Landsberg, A novel effect of light scattering in crystals. Naturwissenschaften **16**, 557 (1928)
C.V. Raman, K.S. Krishnan, A new type of secondary radiation. Nature **121**, 501 (1928a)
C.V. Raman, K.S. Krishnan, A new class of spectra due to secondary radiation Part I. Indian J. Phys. **2**, 399 (1928b)
B. Schrader (ed.), *Infrared and Raman spectroscopy: methods and applications* (VCH Publishers, Weinheim, 1995)
A. Smekal, Zur Quantentheorie der Dispersion. Naturwissenschaften **43**, 873 (1923)
E. Smith, G. Dent, *Modern Raman spectroscopy—a practical approach* (Wiley, Chichester, 2005)

Chapter 3
Basics of Surface-Enhanced Raman Scattering (SERS)

Abstract Surface-enhanced Raman scattering (SERS) spectroscopy is based on the enormous enhancement of Raman scattering of molecules adsorbed on suitable metallic (mainly silver and gold) nanostructures. Two mechanisms contribute to the total enhancement: the electromagnetic one based on resonance excitations of surface plasmons in the metal and the chemical (or molecular) one increasing the polarizability of the molecule. Average enhancement factors are about 10^4–10^6 but even values about 10^{11} can be achieved in some cases. This chapter will briefly introduce the basics of SERS theory and some experimental aspects of SERS (choice of metal, distance dependence, selection rules, enhancement factors, "hot spots", single-molecule SERS, resonant SERS). The SERS substrate plays a key role in any SERS application. An overview of SERS-active substrates employed in bioanalytical, biomolecular and medical SERS applications and their properties will be discussed. It includes nanoparticles in suspension, nanoparticles assembled and immobilized on solid substrates (bottom-up approach) and nanostructures fabricated directly on solid substrate (top-down approach). The related enhancing techniques (tip-enhanced RS—TERS, shell-isolated nanoparticles-enhanced Raman scattering—SHINERS, surface-enhanced infrared absorption—SEIRA and surface-enhanced fluorescence—SEF) will also be presented.

3.1 SERS Mechanisms

According to (2.2), the magnitude of the induced dipole moment μ_{ind}, which characterizes the RS effect, is given by a product of the molecular polarizability $\alpha_{molecule}$ and the local electric field E_{loc} of the frequency ω_{inc} demonstrating two possible ways of enhancing RS.[1] Interaction of the molecule with a rough metal surface must enhance either E_{loc} or $\alpha_{molecule}$. Thus, the SERS enhancing mechanism is traditionally separated into two main multiplicative contributions: EM and chemical (or molecular).

[1] μ_{ind} and $E_{loc}(\omega_{inc})$ are vectors, while $\alpha_{molecule}$ is a tensor.

M. Procházka, *Surface-Enhanced Raman Spectroscopy*,
Biological and Medical Physics, Biomedical Engineering,
DOI 10.1007/978-3-319-23992-7_3

The following section will summarize the basic facts about both mechanisms, for more details see e.g. Moskovits (1985), Aroca (2006), Otto et al. (1992), Campion and Kambhampati (1998), Schatz et al. (2006), Kneipp et al. (2006), Le Ru and Etchegoin (2009), Etchegoin and Le Ru (2011), Schlücker (2011). Despite big number of papers and books about SERS theory, some confusing ideas about the origin of enhancement still persist among SERS researchers. Recently, Moskovits discussed six such misconceptions regarding SERS demonstrating that nowadays SERS is rather well understood and that the mechanism that underlies the current understanding of SERS is the plasmonic theory (Moskovits 2013).

3.1.1 EM Mechanism of SERS

The EM mechanism is schematically depicted in Fig. 3.1 for the case of Au NP. This is a main enhancement effect based on amplification of the EM field due to resonance excitations of localized conduction-electron oscillations at the metallic nanostructural surface, called surface plasmons (SPs). This type of resonance is termed dipolar localized surface plasmon resonance (LSPR) and can be derived from extinction spectrum (called surface plasmon extinction—SPE), involving both absorption and elastic scattering of a particular metallic nanostructure. The resonance frequency ω_{max} of plasmons in the metallic nanostructure depends on, among other parameters, the dielectric functions of the metal $\varepsilon_{metal}(\omega)$ and the surrounding medium $\varepsilon_m(\omega)$. Firstly, the coupled state of the photon and LSPs is accompanied by sharply enhanced amplitude of the EM field in the closest vicinity of the roughened metal surface. The molecule adsorbed at the surface is thus subjected to much stronger E_{loc}. Secondly, molecular dipole radiates RS but not in free space but in close proximity of metal. The frequency-shifted Stokes RS radiation at $\omega_s = \omega_{inc} - \omega_{vib}$ for one particular vibrational mode (Fig. 3.1b) itself can excite a LSPR of the metallic nanostructure in Fig. 3.1a. The local field enhancement and Raman radiation enhancement have the same physical origin: the EM field couples to LSPR of the metallic substrate. Although the coupling may not be identical, the resonances should at least be qualitatively similar for both enhancements.

The overall SERS intensity depends on both the "incoming" (ω_{inc}) and the "outgoing" ($\omega_s = \omega_{inc} - \omega_{vib}$) field:

$$I_{SERS} = I_{inc}(\omega_{inc}) \cdot I(\omega_s) = |E_{inc}(\omega_{inc})|^2 \, |E(\omega_s)|^2 \tag{3.1}$$

Optimal SERS enhancement therefore requires that both the incident radiation at ω_{inc} and the Stokes Raman shifted radiation at $\omega_s = \omega_{inc} - \omega_{vib}$ are in resonance with the LSPR peak of the metallic nanostructure. Generally, the nanostructures with typical dimensions $\sim$30–100 nm are necessary to fulfil the conditions of LSPR resonance with visible light. LSPR strongly depends on the size and shape of nanostructures (Schatz et al. 2006) and is also strongly modified for closely spaced

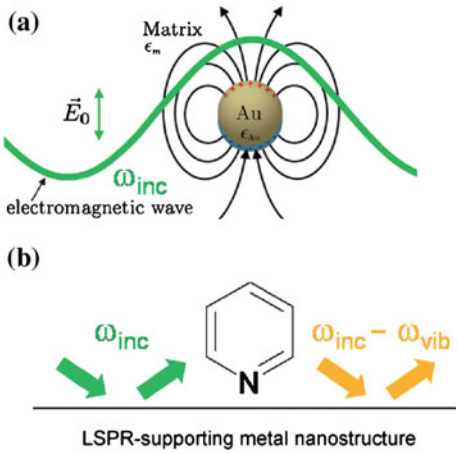

Fig. 3.1 EM enhancement in SERS. **a** A gold NP acts as a nanoantenna by excitation of a dipolar localized surface plasmon resonance (LSPR). **b** Both the "incoming" field (ω_{inc}) and the "outgoing" field ($\omega_{inc} - \omega_{vib}$) are enhanced by elastic light scattering off the LSPR-supporting metallic nanostructure (reproduced with permission from Schlücker 2014. Copyright 2014 Wiley-VCH Verlag GmbH & Co. KGaA, Weinheim)

nanostructures due to the existence of coupling which primarily comes from the interactions of the LSPR of individual nanostructures (Le Ru and Etchegoin 2009).

In the simple cases, the I_{SERS} can be reduced to $|E(\omega_{inc})|^4$ factor (Le Ru and Etchegoin 2009). Moderate increase of E_{loc}/E_{inc} leads to huge RS enhancements which is termed the SERS enhancement factor (EF). EM enhancement depends also on the properties of the metal and the distance of the molecule from the surface. The EM $EF_{em}(\omega_s)$ can be described explicitly for a small metallic sphere (its radius r is smaller than one twentieth of the incident light's wavelength) as:

$$EF_{em}(\omega_S) \cong \left|\frac{\varepsilon(\omega_{inc}) - \varepsilon_0}{\varepsilon(\omega_{inc}) + 2\varepsilon_0}\right|^2 \left|\frac{\varepsilon(\omega_S) - \varepsilon_0}{\varepsilon(\omega_S) + 2\varepsilon_0}\right|^2 \left(\frac{r}{r+d}\right)^{12} \tag{3.2}$$

where $\varepsilon(\omega)$ is the complex frequency-dependent dielectric function of the metal, ε_o is the dielectric constant of the bulk medium and d is the distance of the molecule from the surface. Index *inc* stands for the incident and *s* for the scattered light. Large SERS enhancement is obtained if, at the wavelengths of the incident and/or scattered radiation, the real part of $\varepsilon(\omega)$ is close to $-2\varepsilon_o$ and the imaginary (damping) part of $\varepsilon(\omega)$ is small. Le Ru and Etchegoin defined a "quality factor" which reflects above mentioned conditions for both real and imaginary part of dielectric function of metal (Le Ru and Etchegoin 2009). Figure 3.2 illustrates the "quality factor" for selected metal/air NP. The shaded part is the area of EF up to 10^5. It is clear that only the free-electron-like (noble) metals (Ag, Au, Cu) are proper materials for surface-enhancing substrates when the common visible or NIR excitation are applied. Ag and Au are the most widely used metals for SERS

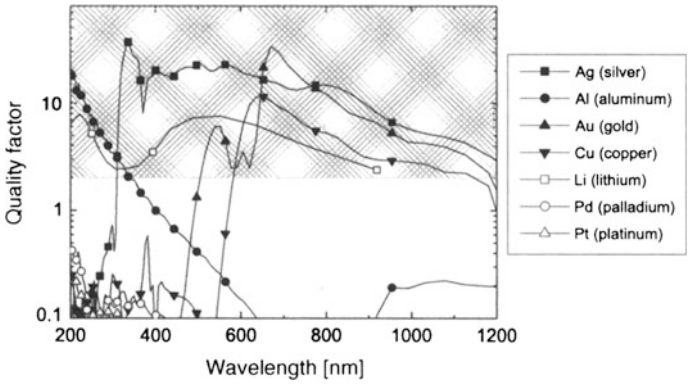

Fig. 3.2 The "quality factor" for selected metallic/air NP. The shaded part is the area of EF up to 10^5 (adapted with permission from Le Ru and Etchegoin 2009. Copyright 2009 Elsevier B.V.)

applications; Ag can be used in broad excitation range from 400 to 1200 nm, Au from 600 to 1200 nm. Copper and lithium, highly reactive metals, rarely serve for SERS (Aroca 2006). The transition metals (namely Pt, Ru, Rh, Pd, Fe, Co and Ni) are applicable when excited by UV radiation (Tian et al. 2006) but they are generally less enhancing (EF about 10^1–10^4). Recently, the SERS in deep UV on aluminium surfaces with high enhancement (about 10^6) has been reported (Sigle et al. 2013). Finally, the scattered molecule does not need to be in direct contact with the metal surface. I_{SERS} is proportional to $\sim 1/d^{12}$ and thus it is rapidly going down with the increasing distance d from the surface. It has been demonstrated that the Raman enhancing effect is detectable for $d \leq 5$–10 nm (Aroca 2006).

Nonhomogenous electric field around metallic nanostructure is responsible for the surface selection rules of SERS (Moskovits 1985). According to them, three types of vibrational modes may be found in SERS spectrum: (i) those excited by the normal component of the field and resulting in an induced dipole with a strong component perpendicular to the surface, (ii) those excited by the tangential component of the field with a strongly induced dipole tangential to the surface and (iii) mixed cases. The intensity of particular Raman bands then depends on the orientation of the molecule with respect to the surface.

3.1.2 Chemical (Molecular) Mechanism of SERS

The chemical (or molecular) mechanism reflects increased molecular polarizability tensor $\alpha_{molecule}$ and consequently Raman cross-section. This mechanism has a number of requirements, such as the existence of special "active sites", the formation of a metal-adsorbate chemical bond sometimes referred to as a first-layer effect (Otto 2005). One common model to explain this mechanism is the

charge-transfer between the molecule and the metal surface (Brolo et al. 1997; Le Ru and Etchegoin 2009). In fact, the molecule is expected to be chemisorbed on the metal, i.e. bound with the adsorption enthalpy comparable to chemical-bond energy (more negative than –40 kJ mol^{-1}) allowing formation of a charge-transfer complex between the molecule and the metal surface. The general model of charge-transfer process involves the transfer of an electron from the Fermi level of the metal to the lowest unoccupied molecular orbital (LUMO) of the molecule as illustrated in Fig. 3.3. The incident photon frequency ω_{inc} is in resonance with a charge-transfer transition of the newly formed surface-adsorbate complex. Then the electron relaxes back to the metal. If the electron resides in the molecule long enough, scattered photon ($\omega_s = \omega_{inc} - \omega_{vib}$) will carry information about a vibrational state of the molecule (ω_{vib}). The energy of the Fermi level (E_f) can be modulated by the applied potential (in the case of metallic electrode) or by excitation wavelength.

The chemical mechanism is generally weaker than the EM one. Both experimental results and theoretical calculations show EF of 10^0–10^2 depending on chemical structure, interaction with metal and particular vibration (Valley et al. 2013). On the other hand, surface roughness and the presence of localized SPs are not required for the chemical mechanism as has been demonstrated by SERS measurements on smooth copper surface with EF about 100 (Kambhampati et al. 1998). Distinction between EM and chemical mechanism is generally complicated; the existence of the charge-transfer mechanism can be experimentally proved by measurement of excitation profiles, i.e. dependence of SERS spectra on excitation wavelength (Srnová-Šloufová et al. 2000). Recently, charge difference density calculations were used to give direct evidence for charge-transfer mechanism as well as to distinguish between charge-transfer and EM mechanism (Xia et al. 2014).

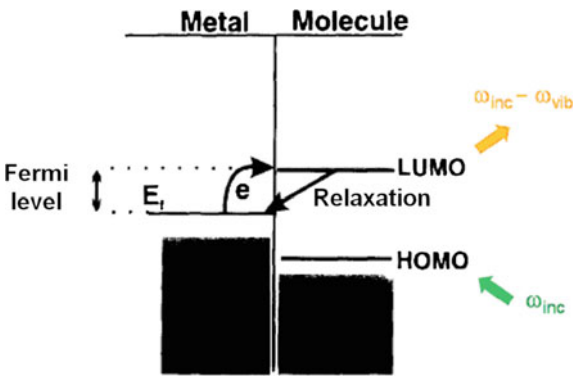

Fig. 3.3 Charge-transfer mechanism of SERS. *LUMO* the lowest unoccupied molecular orbital, *HOMO* the highest occupied molecular orbital (adapted with permission from Brolo et al. 1997. Copyright 1997 Elsevier B.V.)

3.2 SERS EFs

The SERS EF is a key characteristic of the SERS effect. Up to now, several types of SERS EFs have been proposed with the aim of finding an optimal quantity enabling the comparison of experiments across different substrates and different conditions as well as theoretical calculations (Le Ru et al. 2007; Le Ru and Etchegoin 2009).

The common definition of EF compares integral intensities of the strongest band in SERS (I_{SERS}) and conventional NRS or RRS (I_{RS}) spectrum, normalized to numbers of molecular scatters participating in respective cases, measured at the same set-up:

$$EF = \frac{I_{SERS}/N_{SERS}}{I_{RS}/N_{RS}} \tag{3.2}$$

In the case of the backscattering experiment (e.g. Raman microscopy), the value of N_{SERS}/N_{RS} is often estimated as a ratio of the effective surface density of adsorbed molecules in SERS measurement to the spatial molecular density in conventional Raman measurement multiplied by the effective high of the scattered volume.

The analytical enhancement factor (*AEF*), used in SERS analytical applications, considers ratio of molecular concentrations of measured analyte:

$$AEF = \frac{I_{SERS}/c_{SERS}}{I_{RS}/c_{RS}} \tag{3.3}$$

This parameter is suitable to display how the surface enhancement improves the analytical capability of Raman method in particular cases, but depends not only on the SERS phenomenon but also on the type of substrate and its coverage by the adsorbate.

Additional resonance enhancement can be achieved for adsorbed chromophore molecules when excitation wavelength coincides with both LSPR and an allowed molecular electronic transition of adsorbate. This phenomenon is called surface-enhanced resonance Raman scattering (SERRS). Although RRS/NRS enhancement about 10^3–10^5 can be reached, SERRS/RRS factor is only 10^2–10^3 due to additional damping of molecular resonance for chromophore molecules adsorbed on metal surface (Weitz et al. 1983).

The EF strongly depends on properties of the SERS-active system (metallic substrate and analyte) and on experimental conditions (the excitation wavelength used). Due to different dielectric functions, Ag provides higher EF than Au in excitation region ~400–600 nm. Above 600 nm Au becomes comparable to Ag and can deliver maximum EF of the order 10^{10}–10^{11} (Le Ru and Etchegoin 2009). Figure 3.4a illustrates the EF calculated for dimer of two Ag spheres and for the corresponding isolated single NP (Xu et al. 2000). It is evident that EF from single NPs is typically of the order of only 10^3. A very close spacing between particles is beneficial for the generation of extremely strong EFs (10^8–10^{11}). In this case, the

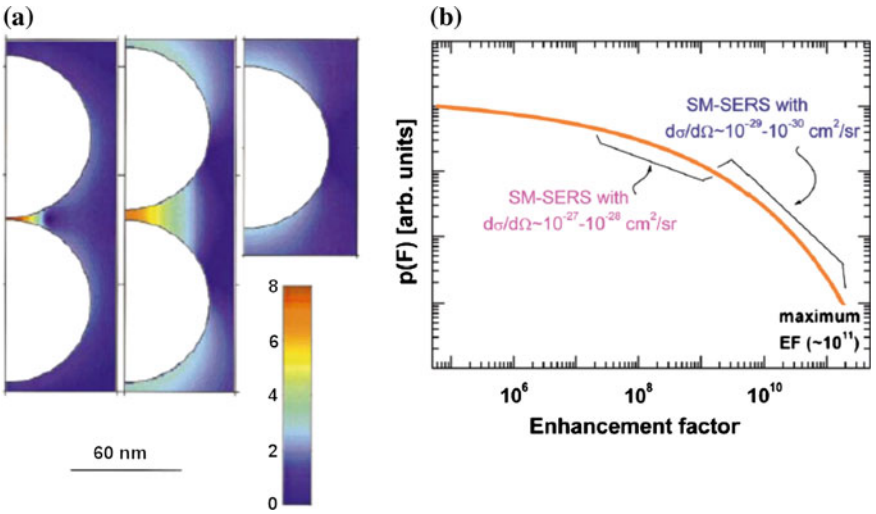

Fig. 3.4 EFs of SERS. **a** EF calculated for dimer of two spheres and for the corresponding isolated single Ag NP (90 nm diameter). The wavelength of the incident field was 514.5 nm with vertical polarization. The colour scale is logarithmic and EFs outside the range 10^0–10^8 are shown in *dark blue* and *dark red*, respectively (adapted with permission from Xu et al. 2000. Copyright 2000 The American Physical Society). **b** Long-tail probability distribution of EFs in SERS (reproduced with permission from Blackie et al. 2009. Copyright 2009 American Chemical Society)

conditions for LSPR excitation are modified due to interparticle coupling of plasmon resonances. Certain resonances in highly spatially localized regions ("hot spots"), in the junctions between two NPs (dimer) for instance, are the source of an extremely high enhanced local field (Le Ru and Etchegoin 2009). When the distance (gap) between two NPs increases from $\sim$2 to 10 nm, the maximum EF in the "hot spot" drops rapidly (Fig. 3.4a). In practice, the gap between NPs is difficult to control, TERS technique when a "hot spot" is formed between tip and metal surface allows better control.

From a practical point of view, the definition of EF falls into one of two categories:

1. Average EFs, EF value of 10^4–10^6 is obtained as an average from a few highly enhancing "hot spots" and many weak enhancing sites of the metallic substrate. These values can be considered as a standard for SERS.
2. SM EFs, which represent the EFs from "hot spots" on the substrate (Blackie et al. 2009). In the first SM-SERS experiments, EFs was estimated as large as $\sim 10^{14}$ (Kneipp et al. 2006), but it was critically reassessed later by Le Ru and Etchegoin determining that EFs were about 10^{11} (Le Ru et al. 2007). In fact, molecules with relatively high differential RS cross-sections (10^{-27}–10^{-28} cm^2 sr^{-1}) such as dyes require EFs of "only" 10^7–10^8 for SM-SERS. In contrast, extremely large EFs of 10^9–10^{11} are necessary to reach SM-SERS for molecules

with "normal" differential RS cross-sections (10^{-29}–10^{-30} cm^2 sr^{-1}), usually called "nonresonant". SM EF exhibits long-tail behaviour: the slope in the high enhancement region defines a long-tail distribution (with a cut-off at the "hot spot") that completely dominates the statistics (Fig. 3.4b). Distribution also clearly shows that moderate EFs have much higher probabilities than extreme EFs. It is directly linked to the strong spatial localization of the "hot spots" and to the fact that they represent a really small fraction of the typical area available for the molecule (Blackie et al. 2009; Etchegoin and Le Ru 2011). For example, Fang and co-workers (Fang et al. 2008) calculated that in the case of lithographically prepared metal nanosurface, only 63 out of 1 million molecules at the hottest sites (those with EFs > 10^9) contribute to 24 % to the overall SERS signal, while the coldest sites contain 61 % of the molecules but contribute just 4 % to the overall SERS signal.

3.3 SM-SERS

In 1997, SM-SERS experiments were independently reported by Nie and Emory (Nie and Emory 1997) and Kneipp and co-workers (Kneipp et al. 1997). Nie and Emory were able to selectively obtain a signal from a single RH6G molecule adsorbed on a single Ag NP by combination of AFM and SERS microscopy (Nie and Emory 1997). Kneipp and co-workers observed SM-SERS of adenine acquired from a small aggregate of Ag NPs (Kneipp et al. 1997).

SERS signal in the SM-SERS experiment depends on the existence of "hot spots". It is a necessary condition for the molecule to be located in the "hot spot" to see the spectrum of the single molecule but the "hot spot" molecule coincidence is statistically a rare event. The SM-SERS spectra often exhibit strong intensity fluctuations including both intensity and spectral changes as well as alternating on/off periods called blinking (Nie and Emory 1997), which were usually considered to be characteristic for SM event. However, these fluctuations were even observed for high dye concentrations as well as under other circumstances. Since SM-SERS experiments are carried out under large enhancement conditions, this event is highly irreproducible. Additional effects as photobleaching, photodesorption, contamination by carbonous species, substrate morphology changes, substrate heating can contribute to intensity fluctuations. Thus, SERS intensity fluctuations do not represent by themselves a proof of a SM event (Le Ru and Etchegoin 2009).

A novel approach based on the use of two analytes (bianalytical SERS—BiASERS) was proposed as a more reliable proof of SM-SERS (Le Ru et al. 2006; Dieringer et al. 2007; Le Ru and Etchegoin 2009). In this experiment, the SERS signal is measured from a mixture of two species with distinguishable SERS spectrum. If the SERS spectrum is a mixture of both analytes, it means that there are many molecules at the "hot spots". The observation of a SERS signal of only one

analyte is clear evidence that it comes from a very small number of molecules. This approach is illustrated in Fig. 3.5 for RH6G and nile blue (NB) dyes on Ag NP aggregate. Each event on the vertical axis corresponds to an individual SERS spectrum (0.05 s integration time). The apparent absolute differential cross-section of the 612 cm^{-1} mode of RH6G (dark grey) and of the 590 cm^{-1} mode of NB (light grey) are shown as cumulative bars on the *x*-axis. Examples of SERS spectra (over the full range of acquisition, from 550 to 1700 cm^{-1}) are given for pure SM-SERS events of RH6G and NB and also for a mixed event. The SM EF of the 612 cm^{-1} peak of RH6G is also given for a few selected SM-SERS RH6G events. The two large mixed events are attributed to large colloidal aggregates. This technique overcomes the problem of poor statistics: low dye concentrations, suggesting that there is on average one dye molecule per NP, do not necessarily provide satisfactory proof. In BiASERS, it is possible to work with higher concentrations and identify SM events in the large spectral set.

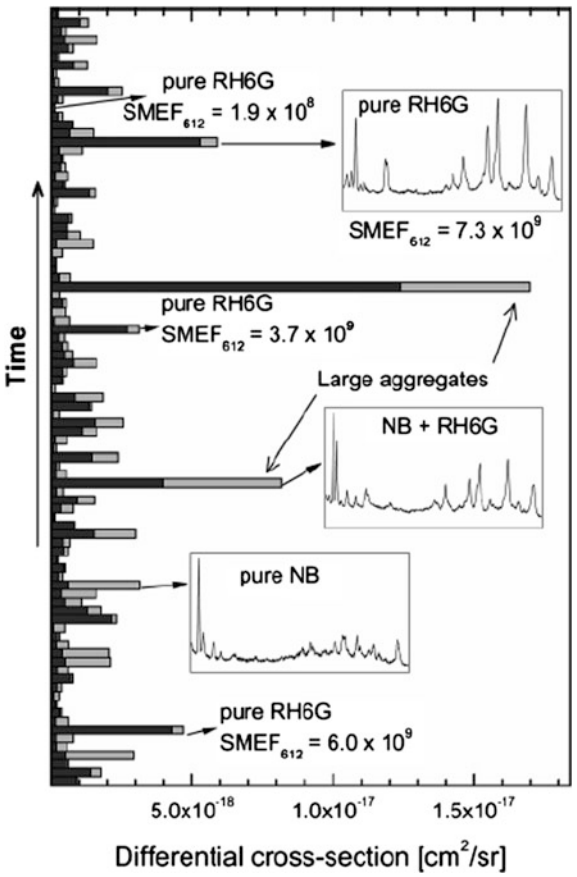

Fig. 3.5 BiASERS on Ag NP aggregate. *RH6G* rhodamine 6G, *NB* nile blue dyes, *SMEF* single-molecule enhancement factor. For more details see text (reproduced with permission from Le Ru et al. 2007. Copyright 2007 American Chemical Society)

It is evident that SM-SERS is not a universal technique because not every molecule is able to be adsorbed on the "hot spot" site to get a SM-SERS signal. Up to now, authentic SM-SERS spectra were obtained only from a few dyes and nonresonant molecules (Le Ru et al. 2007; Pieczonka and Aroca 2008; Blackie et al. 2009).

3.4 SERS-Active Substrates

The employed SERS substrate plays a key role in any application of SERS spectroscopy. Since the discovery of SERS, a broad variety of metallic substrates including electrodes, island films, well-dispersed NPs sols, NP films and highly ordered nanostructures have been prepared and tested for analytical SERS applications. Nowadays, SERS substrates can be classified in three basic categories: (i) NPs in suspension, (ii) NPs assembled and immobilized on solid substrates (bottom-up approach) and (iii) nanostructures fabricated directly on solid substrate (top-down approach). Several book chapters and reviews summarized the various types of SERS substrates, their preparation procedures and properties, e.g. Baia et al. (2008), Banholzer et al. (2008), Ko et al. (2008), Brown and Milton (2008), Lin et al. (2009), Wang and Wang (2011), Zhang et al. (2010), Fan et al. (2011), Zhang and Zhang (2012), Gopalakrishnan et al. (2012), Cao et al. (2013), Le Ru and Etchegoin (2009). The key parameters of SERS enhancing substrates are sensitivity and spectral reproducibility. Here, some examples of SERS substrates used in biomolecular and bioanalytical SERS studies will be introduced. The applications of various SERS substrates will be done in following chapters.

3.4.1 Metallic NP Hydrosols

Metallic hydrosols (colloids) are formed by suspension of metallic NPs with various shapes and diameters (about 5–200 nm). The preparation is simple, inexpensive and routine with no need for specialized equipment. On the other hand, the purity of chemicals and glass vessels is crucial for successful preparation and the colloids often suffer from poor time stability. Such Ag and Au hydrosols are prepared by "wet chemistry" (reduction of $AgNO_3$ or $HAuCl_4$ with appropriate reduction agent) or laser ablation. Widely used reduction agents include sodium borohydrate (Creighton et al. 1979), trisodium citrate (Lee and Meisel 1982), hydroxylamine hydrochloride (Leopold and Lendl 2003) and ethylenediaminetetraacetic acid (EDTA) (Heard et al. 1983). The problem of chemically prepared hydrosols is the presence of ions and surface organic contaminants as products of the chemical reduction that can superimpose SERS spectra of studied analyte (Yaffe and Blanch 2008). This problem can be overcome by using "chemically pure" hydrosols prepared with laser ablation of a metal foil in ultrapure water by a pulse

laser (Fojtik and Henglein 1993; Procházka et al. 1997a). Sizes and shapes of laser-ablated NPs are primarily influenced by the excitation wavelength, pulse duration and laser power.

Morphological and optical properties of metallic NPs can be determined by UV-vis absorption spectroscopy of hydrosol suspension and scanning or transmission electron microscopy (SEM or TEM) of dried hydrosol drops on carbon-coated Cu grid (Le Ru and Etchegoin 2009). Position and halfwidth of bands in SPE spectrum depend on type of metal (due to dielectric constant), size and shape of NP. SEM or TEM gives direct information about particle size distribution and morphology of colloidal aggregates, although some modification of aggregation state of hydrosol drop dried on microscopic grid cannot be avoided. Finally, an important property of metallic colloid in solution is its surface potential (or surface charge) which greatly affects a given analyte capability to be adsorbed into the surface. This parameter can be determined through zeta potential measurements by photon correlation spectroscopy (Le Ru and Etchegoin 2009).

SPE maxima are ranging from 380 to 440 nm and 510 to 540 nm for Ag and Au hydrosols, respectively, showing different LSPR properties for both metals (Aroca et al. 2005). The preparation of Ag/Au mixed colloids allows the combination of the SERS properties of both metals and thus a broadening of the interval of available excitations. Ag-coated Au NPs and Au-coated Ag NPs can be prepared by growing Ag or Au on citrate-reduced Au or Ag NPs with chemical reduction of the corresponding salt. The morphology of the resulting mixed NPs depends on the relative amount of the depositing metal (Freeman et al. 1996; Rivas et al. 2000). However, the colloidal suspension usually results in a broad distribution of sizes and shapes. For example, while NPs of borohydride-reduced colloid provide monodispersal distribution and a shape close to spherical, citrate-reduced colloid also contains a fraction of nonspherical NPs such as blocks and rods (Lee and Meisel 1982). Big NPs have a tendency towards sediment during storage and thus SERS activity of colloid strongly depends on their age or fraction (Freeman et al. 1999). Physical properties of Ag colloids prepared using different reduction agents are compared for example in paper of Larmour and co-workers (Larmour et al. 2012). For example, borohydride-reduced Ag NPs provide the smallest particle sizes (mean diameter about 13 nm) and the narrowest size distribution. The EDTA-reduced, citrate-reduced and hydroxylamine-reduced colloids are composed of bigger NPs (main size about 30–40 nm).

Since the mid-1990s, a large effort has been devoted to more sophisticated control of the NP shape, size and aggregation through appropriate modifications of preparation protocol (Wang and Wang 2011). Ag and Au NPs of hexagonal (Shao et al. 2004), triangular (Chen and Carroll 2002), cubic (Sun and Xia 2002; Orendorff et al. 2005), star (Kumar et al. 2008), dogbone, block, wire and rod (Orendorff et al. 2005) shapes were prepared. SEM and TEM images of such NPs immobilized on 4-mercaptobenzoic acid (4-MBA) self-assembled monolayers (SAMs) are shown in Fig. 3.6. Experimental results indicate for instance that individual nanocubes, nanotriangles, nanorods (NRs) and nanostars can provide an EF as high as 10^9 which is much higher than for individual nanospheres (Li et al.

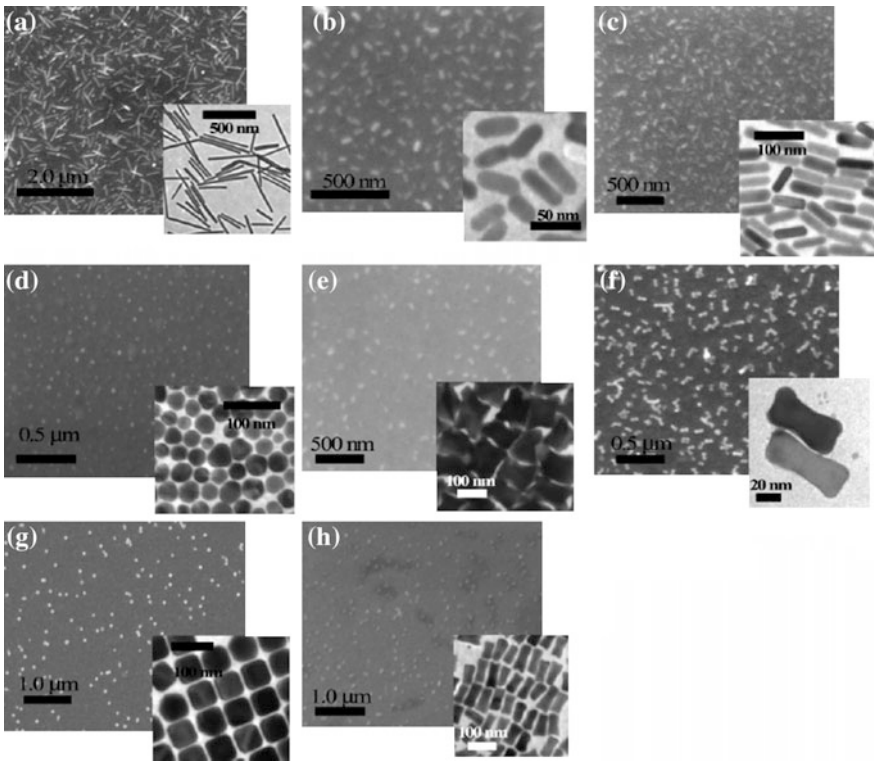

Fig. 3.6 SEM and TEM (*inset*) images of **a** aspect ratio 16 rods, **b** aspect ratio 3.2 rods, **c** aspect ratio 4.4 rods, **d** spheres, **e** tetrapods, **f** dogbones, **g** cubes and **h** blocks immobilized on 4-MBA SAMs (reproduced with permission from Orendorff et al. 2005. Copyright 2005 American Chemical Society)

2012a). Au NRs have a very unique SPE due to both transverse and longitudinal LSPR modes. Longitudinal LSPR is tunable by changing the aspect ratio and can provide efficient SERS enhancement in the NIR region (El-Sayed 2001). This has enabled Au NRs to be used like SERS probes for molecular and cell imaging, in vivo tumour detection and photothermal therapy (see Chap. 7).

Nanoshells are hybrid NPs consisting of a dielectric core (such as silica) and a metallic shell (Oldenburg et al. 1998). The LSPR behaviour of the nanoshells is sensitive to the inner and outer dimensions of the metallic shell layer. A red shift is achieved by increasing the size of the silica core while simultaneously reducing the thickness of the metallic shell (Oldenburg et al. 1999). Moreover, the hybrid resonance response can be tuned by an interaction between the LSPR supported by the inner and the outer surfaces of the metallic shell layer (Prodan and Nordlander 2003). The tunable plasmon wavelength range of Au nanoshells is from 600 nm to 2.2 μm which makes these substrates ideal for use in the biological environment as IR excitation reduces problems associated with autofluorescence of biological

media. The metallic nanoshells or NPs are the main components of SERS tags in the extrinsic detection scheme introduced in Chap. 5. The SERS tag can be further functionalized with a biorecognition element to employ it as a specific SERS probe in intracellular and medical applications described in Chaps. 6 and 7. Recently, shell-isolated NPs (SHINs) were prepared and tested for SERS (Li et al. 2010; Li and Tian 2014). The Ag or Au NP core is protected by an ultrathin shell of SiO_2, Al_2O_3, MnO_2 or Ag_2S to meet the demand of various chemical environments (Li et al. 2013). The shell must be less than 5 nm thick to ensure sufficient EM enhancement; typically 2 nm thickness is used. The advantage of SHINs is better stability than bare NPs. Also the shell isolates the metal surface from the probed molecules and therefore prevents a potentially disturbing interaction.

Freshly prepared hydrosols consist of NPs isolated due to the Coulombic repulsive barrier resulting from the double layer of charged ions on the NP surface (Weitz et al. 1985; Le Ru and Etchegoin 2009). The stability of the colloidal suspensions is shown by the zeta potential values. For a colloid to be considered stable, the value should be less than −30 mV. The borohydride-reduced Ag colloids have a less negative zeta potential and therefore are not very stable (stability is generally considered in days or weeks). Other reduction agents produce more stable Ag colloids with zeta potential less negative than −30 mV. Due to the interaction of the adsorbate with the colloidal surface the zeta potential drastically increases and NPs stick together forming aggregates of different size and shape. It can be achieved in at least two ways (Le Ru and Etchegoin 2009): (i) positively-charged analyte is attached on the surface, (ii) negatively-charged or neutral analyte replaces the negatively-charged surface species. Aggregation of metallic colloids is known to be influenced by various parameters including the surface potential of the colloid, the chemical nature and the concentration of the adsorbate, the temperature and the presence of a particular preaggregating agent (Weitz et al. 1985). Several preaggregation agents can be employed in SERS experiments; perchlorate, nitrate and chloride are the most frequent (Le Ru and Etchegoin 2009). Among them, the chloride anions are the most important due to so-called "chloride activation" of SERS signal (Otto et al. 2003). Although this effect is not fully understood, it is unquestionable that addition of Cl^- anions to the NPs enhances the SERS signal. Various effects of Cl^- anions on metallic NPs such as change of the zeta potential, aggregation and adsorption state as well as creation of analyte-surface complex necessary for chemical enhancement should be taken into account (Otto et al. 2003; Le Ru and Etchegoin 2009).

Aggregation of NPs has a significant influence on a SERS experiment. Whereas the NP resonates at a particular frequency, its random aggregate could resonate at different wavelengths within broad spectral region. Thus, the aggregation shifts the SPE to red with respect to the SPE of isolated NPs. This situation is demonstrated for borohydride-reduced Ag colloid and copper 5,10,15,20-tetrakis(1-methyl-4-pyridyl)porphyrin (CuTMPyP) adsorbate in Fig. 3.7 (adapted from Procházka et al. 1997b). Another important impact of aggregation is interparticle coupling of LSPR

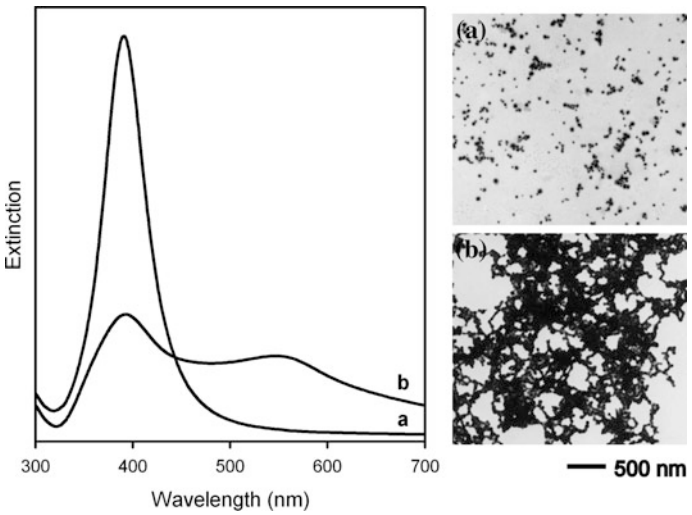

Fig. 3.7 Aggregation of borohydride-reduced Ag colloid by copper(II) 5,10,15,20-tetrakis (1-methyl-4-pyridyl) porphyrin (CuTMPyP), **a** SPE spectra and TEM image of parent Ag colloid, **b** SPE spectra and TEM image of Ag colloid/CuTMPyP (1 μM) system (adapted with permission from Procházka et al. 1997b. Copyright 1997 American Chemical Society)

of NPs being close or touching each other. This effect leads to much higher SERS enhancement in comparison to individual NPs. The most efficient SERS-active substrates often consist of a collection of aggregated NPs exhibiting fractal structure (Weitz et al. 1985; Stockman et al. 1992). Certain localized resonances generated in the nanosized gaps between NPs ("hot spots") are the source of extremely high enhancement ($\sim 10^{11}$) (Stockman et al. 1992). The big disadvantage is that the aggregation process is time-dependent, some big macroscopic aggregates have tendency to precipitate from the solution. Moreover, the distribution of LSPR of NPs aggregates of different sizes and shapes is strongly inhomogeneous which causes poor reproducibility of SERS enhancements (Wentrup-Byrne et al. 1993).

3.4.2 NPs and Nanostructures on Planar Supports Prepared by Bottom-Up Techniques

Stability and spectral reproducibility of metallic NPs can be significantly improved if rationally designed NPs are self-assembled or immobilized on planar solid supports. In colloidal science, such an approach is commonly called a bottom-up technique.

3.4.2.1 NPs Self-assembled in Planar Supports

Different techniques employed to assemble metallic NPs with various sizes and shapes are summarized in several reviews: Fan et al. (2011), Guo and Dong (2011), Romo-Herrera et al. (2011). Preparation procedures include chemical attachment of NPs via small molecules or bifunctional polymers (Freeman et al. 1995; Orendorff et al. 2005; Baia et al. 2008), inverse micelle polymer film (Jang et al. 2013), layer-by-layer assembly (Zhang et al. 2007), solvent-induced evaporation (Wang et al. 2007), electrostatic interaction between NPs and surface (Han et al. 2008), liquid-liquid interface Langmuir-Blodgett (LB) assembly (Tao et al. 2008) and external field driven assembly (Wu et al. 2010a). As an example, Fig. 3.6 shows representative SEM and TEM images of NPs of various size and shape immobilized on a glass slide via SAMs of 4-MBA (Orendorff et al. 2005).

The average EFs reported for assembled and immobilized NPs range from 10^5 to 10^7 (Olson et al. 2001; Toderas et al. 2007; Fan et al. 2011; Procházka et al. 2012). Further growth of NPs by chemical or electrochemical methods reduces the inter-particle spacing and increases the EF (Lin et al. 2009). The NPs monolayer surfaces can also be generated by simultaneous immobilization of both Au and Ag NPs (Joseph et al. 2012). Moreover, using bifunctional linker it is possible to form 3-dimensional multilayer NP structures and with a number of NP layers optimize the SERS enhancement. SERRS of NB near SM detection from multilayer assemblies of spherical Ag NPs has been reported (Fan and Brolo 2009). Both Au and Ag immobilized NPs provide excellent reproducibility (the spatial and the sample to sample variation of SERS signal less than 20 %) in micro-Raman measurements using focused $\sim$1 μm laser spot (Olson et al. 2001; Fan and Brolo 2009; Procházka et al. 2012). If defocused ($\sim$100 μm diameter) laser beam is used on spherical Au NPs assemblies, a variation of signal only about 5 % can be reached (Hajduková et al. 2007).

Recently, Yüksel and co-workers reported plasmonic arrays of enzymatically generated Ag NPs (Yüksel et al. 2015). First, a DNA strand was spotted onto the planar glass surface in an ordered array layout. Second, a streptavidin-horseradish peroxidase complex was bound to the immobilized DNA. Finally, the deposition of "desert-rose like" Ag NPs was catalyzed by horseradish peroxidase via a redox reaction. In this catalytic process, an oxygen atom was detached from hydrogen peroxide and bound to the prostethicheme group of the enzyme causing a change of the iron oxidization state. The Ag ions were electron acceptors and hydroquinone was the corresponding electron donor, which was oxidized to 4-benzoquinone. However, these SERS substrates showed a strong background signal overlapping the SERS spectra of studied analytes. Thus, the plasma enhanced atomic layer deposition was applied to cover Ag NP array with a dielectric layer of alumina (Al_2O_3). This coating insured the SERS activity and stability of Ag NPs arrays for at least 4 weeks after preparation under ambient storing conditions and weak background signal. The sensitivity of these SERS-active substrates was proved by detection of riboflavin down to 10 nM concentration.

3.4.2.2 Metallic NR Arrays Prepared by Angle Vapour Deposition

The angle deposition of Ag or Au from electron beam evaporation system is used for fabrication of NPs arrays on solid substrate (Negri and Dluhy 2013). This technique is known as oblique (or glancing) angle vapour deposition (OAD or GLAD). Scheme of OAD procedure and SEM image of such typical structure are shown in Fig. 3.8.

The deposition angle determines the length of the nanostructures growing on the substrate. For example, if the substrate is rotated to a specific angle such that the vapour from the metal source is incident on the substrate to the glancing angle, long preferentially cylindrical NRs growth on the surface. Typical parameters of such substrates are: NR lengths of ~800–900 nm, diameters ~80–90 nm, tilt angles of ~71° with respect to the surface normal, NR densities of 15–25 per μm^2, average spacing between rods ~150 nm, EF ~10^8 (Driskell et al. 2008). OAD technique led to the development of Ag NRs arrays as uniform, reproducible, large area SERS-active substrates with high SERS enhancement (Negri and Dluhy 2013). Spectral reproducibility from Ag OAD is good apart from occasional "hot spot" sites where the intensity is higher. The number of "hot spots" represents 2–6 % of SERS-active sites of mapping substrate area (Šubr et al. 2015).

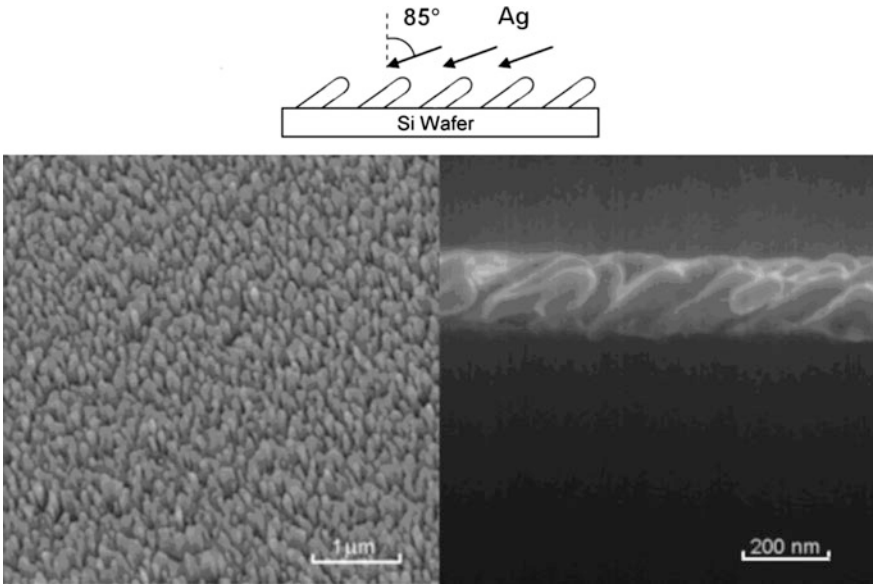

Fig. 3.8 Ag NR arrays prepared by OAD technique. Scheme of OAD procedure and SEM images of a typical Ag NR array (*top* and *side view*) (reproduced from Šubr et al. 2015. Copyright 2015 Šubr et al.)

3.4.3 *Nanostructures Fabricated Using Nanolithographic (Top-Down) Techniques*

This approach is generally classified as top-down and mainly covers the preparations of highly ordered metallic nanostructures by electron beam lithography (EBL) and chemical etching techniques.

3.4.3.1 Electron Beam Lithography (EBL) and Ion Beam Lithography (IBL)

Using EBL and IBL maskless techniques, an array of highly ordered structures is produced by a focused electron or ion beam drawing patterns over the resist wafer in a serial manner with nanometre resolution (Kahl et al. 1998). The scheme for two fabrication strategies for SERS substrates using EBL is shown in Fig. 3.9. The left

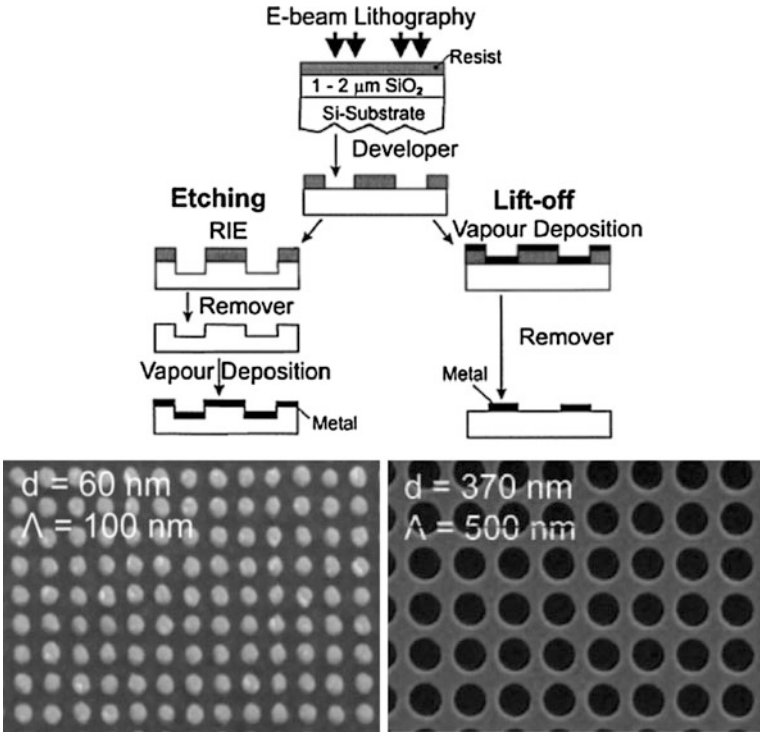

Fig. 3.9 EBL for preparation of highly ordered SERS nanostructures. *Top* Scheme of two fabrication procedures (Reproduced with permission from Kahl et al. 1998. Copyright 1998 Elsevier S.A.) *Bottom* SEM images of a gold nanodisk array with a 40 nm diameter and a 60 nm edge-to-edge (*left*) in comparison to a nanohole array with a 370 nm diameter and a 100 nm edge-to-edge distance (*right*). Λ is a grating pitch (reproduced from Yu et al. 2008. Copyright 2008 American Chemical Society)

hand side process consists of a chemical etching that follows the electron beam exposing, the dissolution of the remaining resist poly(methylmethacrylate) (PMMA) layer and deposition of metal. The substrate ends up with metal over the whole surface. The right hand side shows a metal deposition immediately after the e-beam exposition. After removal of the photoresistor layer, the substrate will present a series of isolated NPs, separated by regions where only bare Si substrate is exposed.

Important advantages of EBL are the possibility to control the NPs size, shape and interparticle distance with great accuracy. Fabrication of a nanosubstrate by means of EBL is nowadays a multistep process that starts with designing patterns using computer-assisted design software. The EBL tool provides a programmable exposure of substrates coated with a resist to a focused electron beam. Yu and co-workers compared the SERS from Au nanodisks and nanoholes fabricated by EBL as a function of the separation and dimensions of the nanostructures (Yu et al. 2008). The nanoholes array with the best SERS enhancement 4×10^5 had a diameter of 370 nm and a grating pitch of 500 nm. The best SERS EF (1×10^3) was demonstrated for nanodisks array with a diameter of 60 nm and grating pitch of 100 nm (Fig. 3.9). Moreover, when the edge-to-edge distance was maintained, enhancement increased for nanoholes but decreased for nanodisks as diameter was increased. It was explained by shifts of LSPR to the NIR regime as nanohole diameter increased.

Soft lithography relies on a patterned master to create morphologies complimentary to those present on the master in a single step, such as embossing or moulding. Various modifications of anisotropic reactive ion etching (RIE) enable formation of grooves, wells, pillars and other nonplanar structures on Si, SiO_2 and polymeric substrates with excellent control of the sidewall profile and characteristic sizes ranging from tens of nanometres (Madou 2002). Recently, the EBL technique served for example to fabricate a reproducible Au nanocuboid array (Das et al. 2013). The SERS enhancement was estimated to be 1.4×10^5. These SERS substrates were employed as biosensors for the investigation of myoglobin and wild/mutated peptides. Aouani and co-workers prepared by EBL broadband periodic nanoantennas of arbitrary shape and size generating EM enhancement from the visible to the NIR wavelength regions (Aouani et al. 2013).

Recently, metallic nanohole arrays with a high nanohole density were fabricated by EBL and tested as molecular SERS sensors (Tabatabaei et al. 2015). The 3-dimensional nanosensor consisted of a gold film containing the metallic nanohole arrays with an underlying cavity and a gold nanocone array at the bottom of the cavity. The plasmonic tunability with respect to the experimental conditions and also the wavelength of the incident light was evaluated both experimentally and theoretically. These nanosensors provided a remarkable sensitive detection of 10^{-16} M probe molecule 4-nitrobenzenethiol (4-NBT) with a short acquisition time of 1 s. Consequently, a reliable EF of $\sim 10^7$ was determined. Moreover, reproducible SERS signals have been obtained on such nanosensors with concentrations down to 100 aM of 4-NBT.

It is necessary to note that EBL and IBL methods generally suffer from high cost, long preparation times (several days) and a need for specialized equipment. The cost and preparation time can be much lower with the use of a template techniques discussed in Sect. 3.4.4.

3.4.3.2 Nanoimprint Lithography (NIL)

NIL is a perspective method to produce batches of the substrates with identical properties. A mould of desired nanostructure can be prepared by EBL, then aligned and pressed into the photoresist covering on the substrate. After curing, the mould is lifted off and the substrate is deposited with metal. After the photoresist removal, a highly ordered nanostructures such as nanodots (Li et al. 2007) or plasmonic crystals formed of precisely controlled nanostructural arrays (Yao et al. 2010) over a large area can be fabricated. NIL has a high efficiency and a low-cost, but problems such as weak coupling and low enhancement effect still exist.

3.4.4 Highly Ordered Metallic Nanostructures Fabricated by Template Techniques

Control over the morphology of the metallic nanostructures is required for the SERS sensing applications to reach sufficient uniformity and spectral reproducibility. The use of templates that allow the deposition of metals with controlled geometry is one of the most promising approaches to overcome such challenges. These techniques are generally much easier, cheaper and faster than EBL and IBL. The template directed approach can be considered as bottom-up techniques described above. Since template assisted substrates have great importance for SERS sensing applications, the principles of the most widely applied will be depicted in this section.

3.4.4.1 Nanosphere Lithography (NSL)

NSL—often called colloidal lithography (CL)—is an effective technique using self-assemblies of polystyrene (PS) micro- or nano-particles on solid surfaces as 2- or 3-dimensional masks for metal deposition (Zhang et al. 2010). The size and shapes of the close-packed nanospheres and the holes between them, in addition to the metal deposition conditions, such as evaporation angle or specific deposition technique (e.g., sputtering, thermal deposition), influence the achieved metallic patterns. A different kinds of metallic nanostructures can be obtained (Fig. 3.10):

1. Vapour deposition of 100–200 nm metal layer surface forms the “film over nanospheres” (FON) (Baia et al. 2005; Baia et al. 2008).

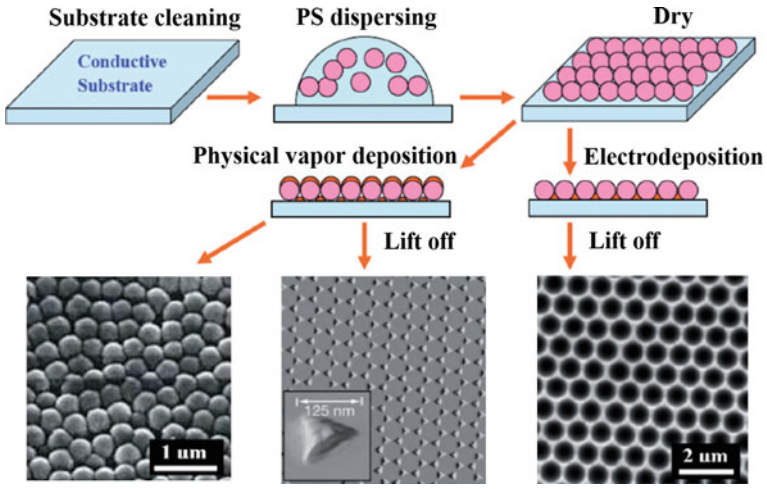

Fig. 3.10 Template methods using NL to fabricate ordered nanostructures for SERS. Scheme of preparation technique and SEM images of various nanostructures, *PS* polystyrene (reproduced with permission from Wu et al. 2008. Copyright 2008 The Royal Society of Chemistry)

2. Removing of a PS mask gives a periodical nanostructure array. In 1995, Hulteen and Van Duyne (1995) reported the preparation of periodic Ag triangle arrays with areas of 4–25 μm^2 using double layer PS sphere mask.
3. Electrochemical deposition of metal followed by removal of PS mask leaves nanostructured film containing a regular hexagonal array of metallic nanoislands, nanoholes or nanovoids depending on the thickness of the deposited film (Abdelsalam et al. 2005).

NSL is now recognized as a simple, inexpensive and repeatable nanofabrication technique used to produce highly ordered nanostructures with diverse functionalities (Zhang et al. 2010). The advantage of the NSL methods is that the shape, size and spacing of the nanostructures can be controlled by the size of NS and the thickness of deposited metal, so that LSPR can be adjusted to the particular excitation wavelength (Jensen et al. 2000). Ag and Au nanostructured arrays have an extremely high density of SERS-active sites providing EF $\sim 10^6$–10^8 as well as a high level of periodicity necessary to achieve excellent spectral reproducibility (Haynes et al. 2005). Poor chemical stability of Ag-based substrates can be overcome by coating the Ag surfaces with 1 nm alumina layer (Stiles et al. 2008). On the other hand, obtaining a large area of small (less than 200 nm diameter) without any defect is a big challenge. Štolcová and Proška were able to prepare $\sim cm^2$ Au FONs consisting of 20 nm thick gold layer sputtered on a SAM of PS spheres of 107 nm diameter (microParticles GmbH, Berlin). Although PS nanospheres do not reveal a perfect close-packed arrangement (Fig. 3.11a), packing defects are negligible with regard to measuring a laser spot with diameter about 2 μm. The

substrates are highly uniform, showing excellent reproducibility and have a shelf-lifetime in a timescale of months. Moreover, they can be prepared on a silicon wafer support, which can serve as the Raman intensity standard in case of quantitative analysis (Peksa et al. 2015).

When the FON is peeled off the glass substrate and the NS template is removed, nanobowl (semishell) structures with sharp edges providing high SERS enhancement can be formed (Xu et al. 2009). The peeling step can significantly disturb the hexagonal ordering of spheres. To obtain hexagonally ordered semishells, Štolcová and co-workers employed the monolayers of PS nanospheres of 253 nm diameter deposited onto thin Formvar® (polyvinyl formal) film (Štolcová et al. 2012). After gold deposition, the structure was placed onto glass slide by the metallized side and subsequently PS dissolved with Formvar® in 1,2-dichlorethane (Fig. 3.11b). Dissolving of both PS and Formvar® led to free-standing gold semishell arrays with undisturbed ordering. The final metallic structures are surprisingly robust and can be deposited even on surfaces with high curvature.

Although the number of structural shapes obtained by CL and NSL technique is limited, it can be significantly broadened by using template-assisted self-assembly, angled deposition or etching (Zhang et al. 2010). Recently, the arrays of corrugated anisotropic structures called nanocorals (Wu et al. 2010b) were produced by RIE of the monolayers of PS microspheres of 471 and 253 nm diameter (Štolcová et al. 2013). The RIE process resulted in anisotropic shrinking of PS microspheres and formation of prominent corrugations at their upper part. Figure 3.11c shows the side view of the ellipsoidal corrugated structure obtained from a PS sphere of 471 nm diameter. Its height and width were estimated from 270 and 320 nm, respectively. The prepared Au nanocorals array is shown in Fig. 3.11d. SERS spectra of 4-aminothiophenol (4-ATP) measured on this substrate displayed a high signal-to-noise ratio and an excellent homogeneity over the whole well-ordered domains.

A periodic array of ring-shaped nanocavities (10 nm gap size) was fabricated by combination of NSL with an atomic layer deposition and an ion milling (Im et al. 2013). The scheme of preparation procedure is shown in Fig. 3.12a. First, an Ag FON substrate (200 nm thick Ag film on PS nanospheres of 500 nm diameter) was prepared. For nanoring cavity formation, a thin Al_2O_3 layer was deposited on the Ag surface via an atomic layer deposition. It was followed by a deposition of another Ag film of 200 nm thickness, forming $Ag/Al_2O_3/Ag$ layers on the nanospheres. A subsequent anisotropic etching of the top Ag layer using blanket ion milling revealed the underlying Al_2O_3 layer as well as the bowl-shaped Ag nanostructures formed along the curvature of the Ag FON substrate, separated by a thin Al_2O_3 layer. Partially removing the Al_2O_3 using a buffered oxide etching solution with controlled etching time produced Ag-air-Ag nanoring cavities. The final nanostructure array is shown in Fig. 3.12a. The resonant coupling between NPs and the ring-shaped nanocavity in this integrated device boosts light-coupling efficiency into the ultrathin gap and increases SERS enhancements by at least one order of magnitude compared with conventional Ag FON substrates or isolated metallic nanogaps. The average EF of such Ag structures was 10^8.

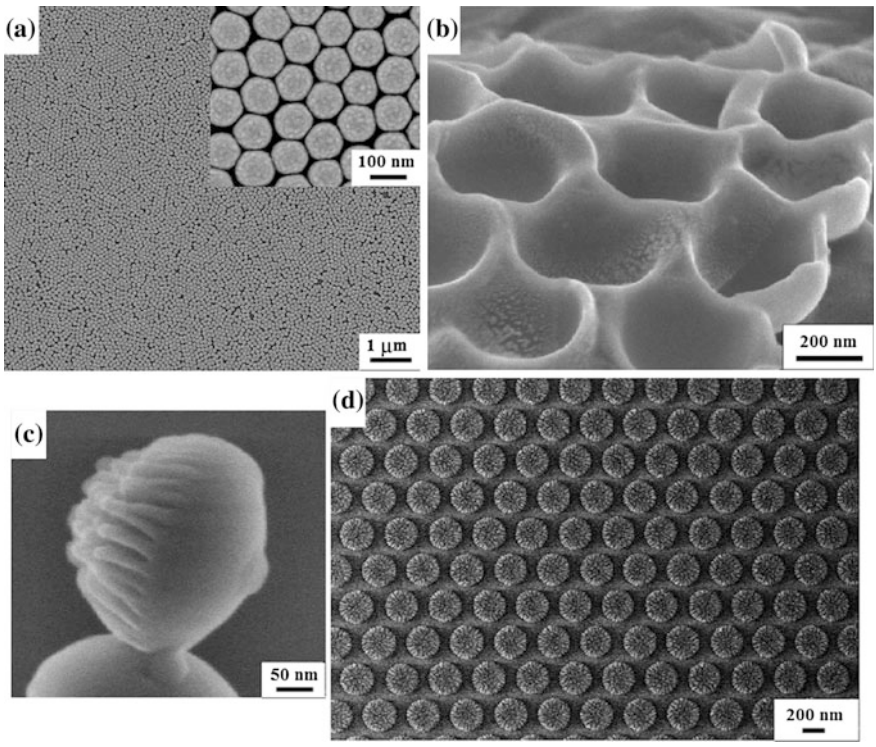

Fig. 3.11 SEM images of Au FON and related structures as SERS substrates. **a** Au FONs on a SAM of PS nanospheres of 107 nm diameter (reproduced with permission from Peksa et al. 2015. Copyright 2015 American Chemical Society). **b** Au nanobowls prepared by PS NS of 253 nm diameter (adapted from Štolcová et al. 2012). **c** *Side view* of a PS nanocoral of 471 nm diameter. **d** Au nanocorals array prepared by PS nanospheres of 471 nm diameter. (**c**, **d**–adapted from Štolcová et al. 2013)

Close-packed Ag pyramidal arrays have been fabricated by using inverted pyramidal pits on Si as a template to form homogeneous and highly reproducible SERS substrates (Wang et al. 2013). The preparation procedure and SEM image of a typical substrate are shown in Fig. 3.12b. First, a monolayer of PS nanospheres was deposited on the Si substrate. Second, the RIE process was performed to reduce the size of the PS nanospheres. The 550 nm PS nanospheres were reduced to about 160 nm after etching for 6 min. The organosilane SAM was assembled on the PS nanospheres monolayer-masked substrate by vapour phase deposition. Then, the Si wafer was ultrasonicated in ethanol to remove the PS nanospheres. Next, an inverted pyramid Si pits array was created by etching the sample with the KOH solution at a certain temperature under stirring. The size of the pyramidal pits was controlled by varying the etching duration. The sample was rinsed with deionised water to remove any residual KOH solution. Finally, the Ag pyramidal arrays were created by thermal evaporation utilizing the pyramidal pits array as a template and

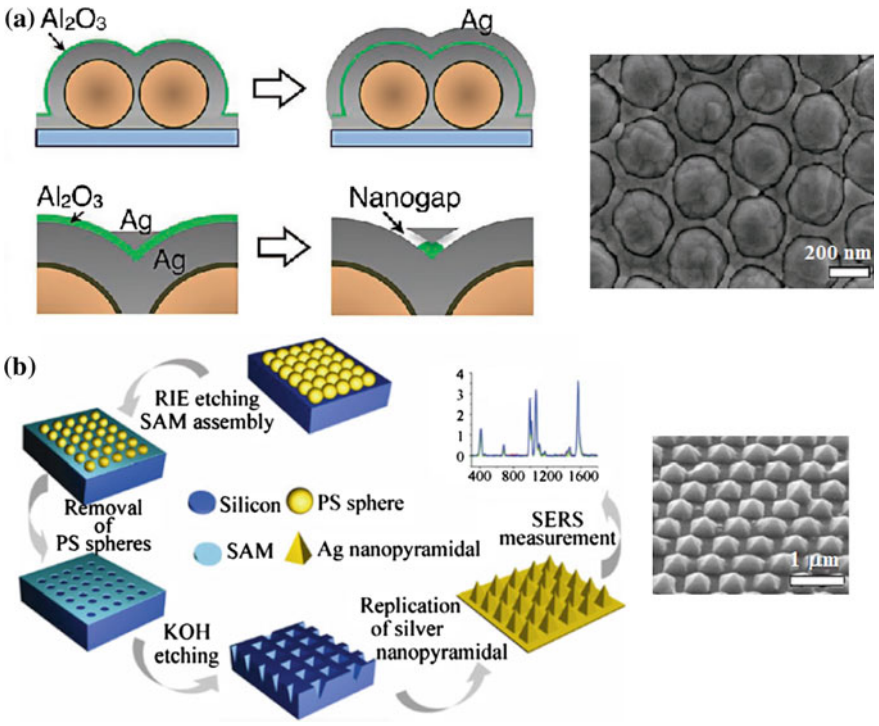

Fig. 3.12 Highly ordered SERS substrates of various shape. **a** Periodic array of Ag ring-shaped nanocavities, scheme of fabrication process and SEM image (adapted with permission from Im et al. 2013. Copyright 2013 Wiley-VCH Verlag GmbH & Co. KGaA, Weinheim). **b** Close-packed Ag pyramidal arrays, scheme of fabrication process and SEM image (adapted with permission from Wang et al. 2013. Copyright 2013 Tsinghua University Press and Springer-Verlag Berlin Heidelberg)

peeling them off with sticky tape. The sharp nanotip and the four edges of the Ag pyramids resulted in strong EM enhancement with an average EF of about 3×10^7. The variation of SERS signal obtained from 10^{-6} M benzenethiol was lower than 9 % both across a single substrate and different batches of substrates.

Van Duyne group reported a specific type of FON substrates, immobilized NR assemblies (Greeneltch et al. 2013). The surface of the 200 nm metallic film forms a forest of radial nanopillars protruding from the underlying base of 600 nm silica nanospheres (Fig. 3.13a). The described growth features are similar to those reported using the GLAD technique. The location of the nanopillars at the sphere junctions provides tunable SERS "hot spots". The pillars localize the electric field to small gap regions and their tips, increasing the overall EF (Fig. 3.13b). The Ag immobilized NR assemblies are highly robust and achieve high EFs (10^7–10^8) and uniformity on the inch scale.

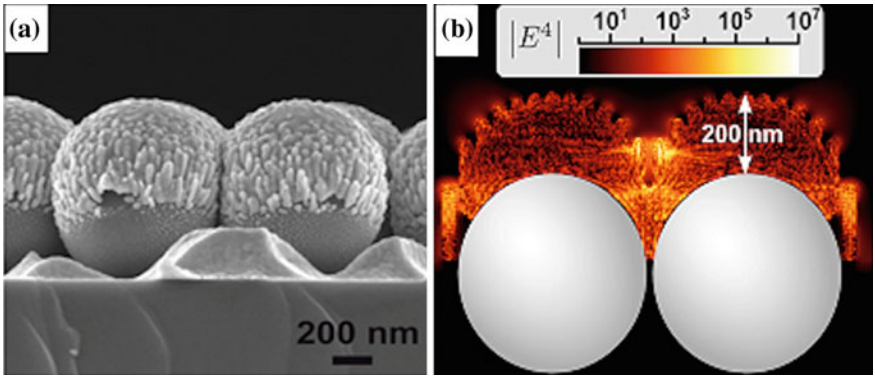

Fig. 3.13 Immobilized NR assemblies as SERS substrates. SEM image (**a**) and electric field enhancement calculation for 805 nm excitation wavelength (**b**) (reproduced with permission from Greeneltch et al. 2013. Copyright 2013 American Chemical Society)

3.4.4.2 "Hole Mask" Colloidal Lithography (HCL)

The HCL technique is based on a sacrificial layer combined with a thin film mask with nanoholes (thus the name "hole mask"). The "hole mask" in evaporation and/or etching steps defines a pattern and the sacrificial layer is used to remove the "hole mask" after processing (Fredriksson et al. 2007). The basic fabrication steps are illustrated in Fig. 3.14. A polymer film such as PMMA is spin-coated onto a glass or Si wafer surface. This is followed by deposition of a colloidal solution containing PS beads. A thin film, which is resistant to reactive oxygen plasma etching, is then deposited onto the surface. The PS beads are tape-stripped away, leaving nanoholes in the plasma-resistant film ("hole mask") resting on the sacrificial PMMA layer. The average spacing and diameters of the holes are thus determined by the separation distance and size of the removed colloidal particles. Reactive O_2 plasma etching is applied to selectively remove the PMMA exposed underneath the nanoholes in the masking film. At this stage the mask resembles the ones produced with EBL: a thin, patterned resist film covering the surface, in addition to the "hole mask" film on top. The "hole mask" can then either be used as a metal deposition mask or etching mask, or both. After metal deposition, the double-layer film ("hole mask" + polymer) is lifted off. Different kinds of large array areas (several cm^2) can be fabricated such as: (a) array of identically oriented elliptical Au nanostructures; (b) Au nanocone array; (c) binary arrays of Au–Ag nanodisc pairs, (d) embedded nanodiscs with overall sizes currently down to 20 nm and occupying 10–50 % of the total surface area (Fig. 3.14).

The HCL technique has several advantages in comparison to EBL: large area coverage, high fabrication speed (the fabrication time does not scale with area), independent control over feature size and spacing, simplicity (the nanofabrication process is reduced down to conventional material deposition and RIE) and thus economical viability. Additional advantages include substantially increased range

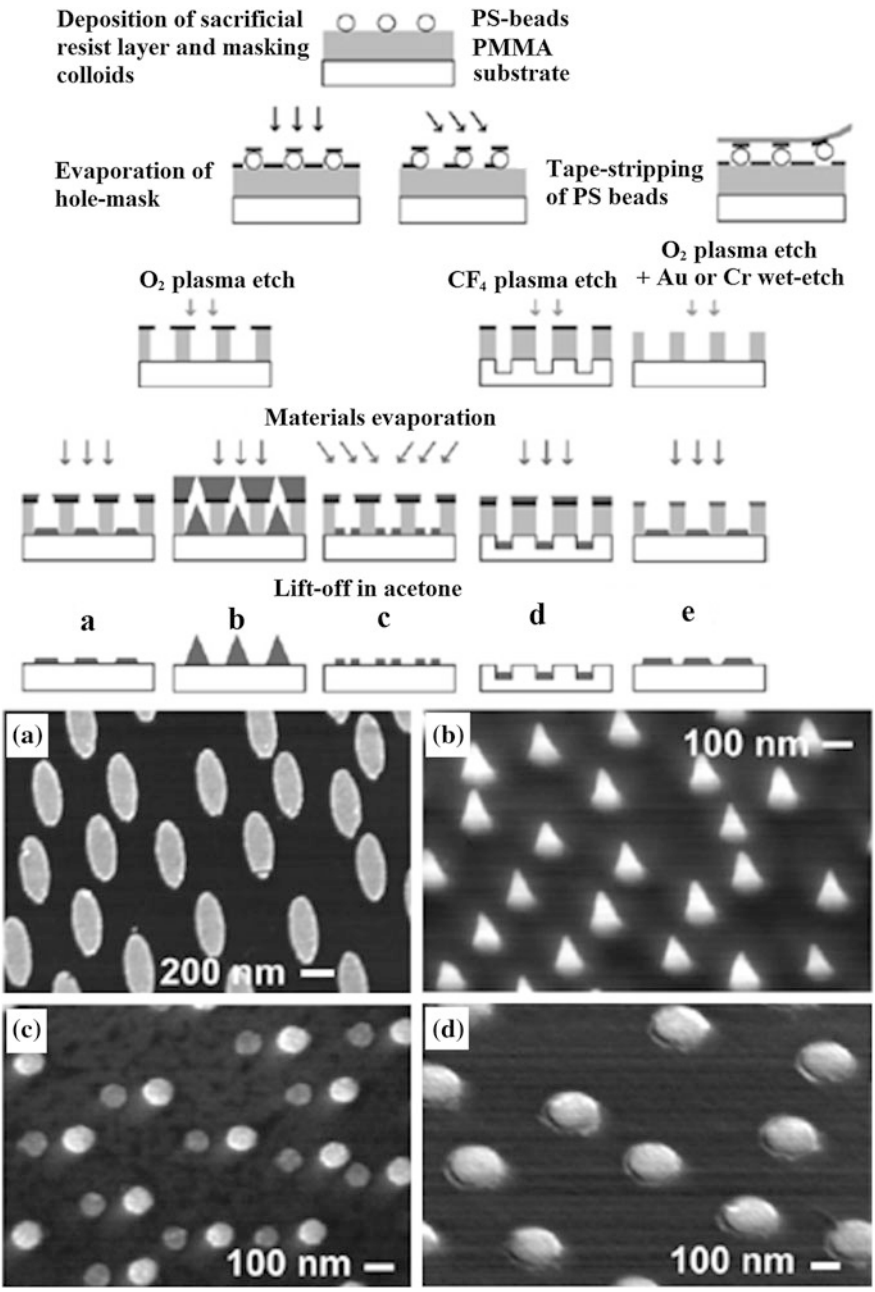

Fig. 3.14 HCL technique for fabrication of SERS substrates. Scheme of the basic process steps and SEM images of resulting structures. **a** Au elliptical array; **b** Au nanocone array; **c** binary arrays of Au–Ag nanodisc pairs; **d** embedded nanodiscs (adapted with permission from Fredriksson et al. 2007. Copyright 2007 Wiley-VCH Verlag GmbH & Co. KGaA, Weinheim)

of materials and of nanostructure geometries that can be employed. Moreover, HCL essentially relies on well-established routines like polymer film (resist) preparation and lift-off directly analogous to those in EBL.

3.4.4.3 Electrochemical Depositions

The electrodeposition of metal on anodic alumina oxide (AAO) nanopore templates has been developed for the fabrication of highly reproducible SERS substrates. The AAO template can be obtained by high-voltage dissolution of alumina in acidic solutions resulting in regular hexagonal packing of pores of tens of nanometres. The electrodeposition of metal is carried out by alternating current deposition at 10–25 V. This step is followed by dissolution of the alumina layer in a phosphoric acid which releases metallic arrays of NRs or nanowires (NWs) (Tian et al. 2002). It is also possible to find commercial AAO membranes. Polycarbonate membranes with pore diameters varying in the range of 20–500 nm can be used as templates for the electrodeposition of NWs and nanotubes. The 50 nm Au NWs provide SERS EF of 1.3×10^7 (Batista et al. 2009).

Recently, air-stable metallic $Pd_{40.5}Ni_{40.5}P_{19}$ glassy (MG) nanowire arrays were prepared by a cheap and rapid die nanoimprinting technique using a commercial AAO template (Liu et al. 2014). The scheme of the preparation procedure and SEM of a typical substrate are shown in Fig. 3.15. The steel die mould with the MG specimen and the AAO template was subsequently placed on a heating plate that had been heated to 633 K. Then the MG specimen was die nanoimprinted into the AAO template with a certain pressure and held for several minutes to make the MG fill the nanopores of the AAO template. Finally, the MG nanowire arrays with a

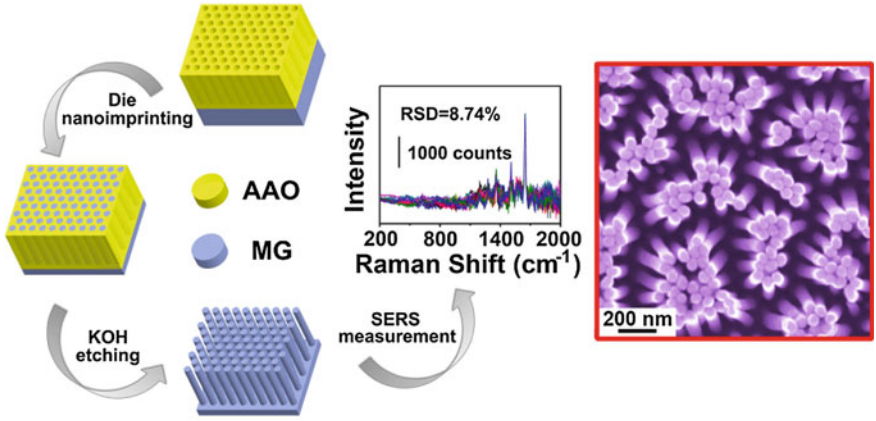

Fig. 3.15 Nanowire arrays as SERS substrate prepared by electrochemical depositions. The scheme of the preparation procedure and SEM image of a typical substrate (adapted with permission from Liu et al. 2014. Copyright 2014 Nature Publishing Group)

diameter of 6 mm were released by dissolving the AAO template in KOH solution after die nanoimprinting and then the SERS activity using RH6G was tested. Although Pd and Ni are not strong SERS-active metals, such substrates provided high SERS activity with an EF of 1×10^5 and an excellent reproducibility with signal variation only about 10 % measured from 121 points over an area of 100 μm × 100 μm.

3.4.5 Commercially Available Substrates

Some commercial substrates were/are also available for SERS but to date none of them have become universal substrates for SERS analytical applications. Klarite® substrates designed from silicon regular inverse pyramidal patterns coated with Au layer (Perney et al. 2007) are one example. This substrate had been commercially available initially by a spin-off enterprise of the University of Southampton and then marketed by the Renishaw, Inc., Renishaw Diagnostics. Although the Klarite® substrates do not provide high EF, the spectral reproducibility is sufficient for some sensing applications.

Recently, a simple fabrication method of SERS substrates with a high and uniform enhancement based on Au- or Ag-coated silicon nanopillars was reported (Schmidt et al. 2012). The fabrication process involved maskless RIE forming vertical silicon nanopillars in the range of 50–80 nm wide and of 600–1600 nm long. Then, metal was deposited by electron beam evaporation or magnetron sputtering onto the silicon nanopillars. Evaporation resulted in metal lumps at the top of the silicon pillars while sputtering yielded conformal coatings. By subsequently depositing a droplet of solvent (in this case water) onto the substrate and letting it evaporate, surface tension causes the nanopillars to lean towards their nearest neighbours thus creating self-assembled "hot spots". SEM images of the final vertical Ag nanopillars and leaning ones after deposition of adsorbate are shown in Fig. 3.16. The Ag-coated nanopillars produced across large areas (cm^2) have a

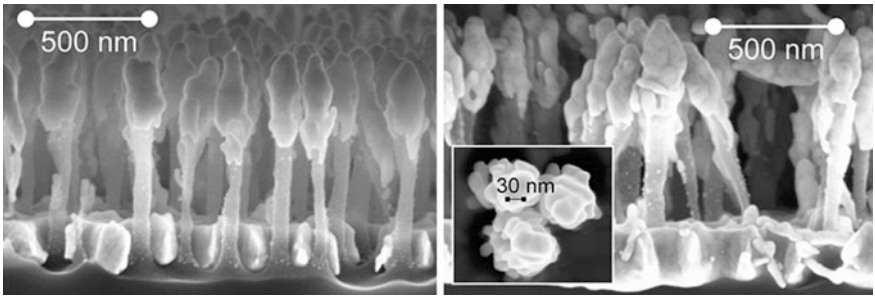

Fig. 3.16 Au-coated nanopillars as SERS-active substrates: vertical (*left*) and leaning (*right*) nanopillars (reproduced with permission from Yang et al. 2013. Copyright 2013 American Chemical Society)

uniform SERS signal intensity (8 % deviation) and can be employed for both liquid and gas phase detection in various chemical and biochemical applications. They can also be functionalized for specific detection of target molecules as was shown for TAMRA-labelled vasopressin molecules in the picomolar concentration specifically captured by Au-coated nanopillars functionalized with aptamers (Yang et al. 2013). Such Ag and Au substrates are now commercially available by Silmeco (www.silmeco.com).

3.5 Practical Aspects of SERS

SERS and SERRS have great potential for (bio)analytical and (bio)sensing applications. High sensitivity allows very low concentrations of biomolecules to be detected. Moreover, fluorescence quenching of highly fluorescent species, specificity and easy molecular recognition are the other advantages of SERS. However, SERS can be difficult to realize in some practical applications. SERS is a highly molecular specific technique and not all molecules are able to give a SERS signal. Thus, two important problems have to be solved for each SERS study: (i) the studied molecule should be attached (or getting close) to a metallic substrate, (ii) and the SERS signal should be sufficiently strong enough to be observed (especially in very low analyte concentrations). Adsorption of a particular molecule on the metallic SERS-active substrate is guided by its size, charge, water solubility, etc. The problem to detect weak SERS-active species can be overcome by their labelling or other chemical modification. Primarily labelling with SERS-active labels led to indirect but very sensitive detection of some biomolecules and opened up for SERS spectroscopy numerous biomolecular and biomedical applications. For SERS biosensing, spectral reproducibility is also a key point which will be discussed in Chap. 4.

Concerning the choice of SERS substrate, colloidal suspensions are very effective SERS substrates, but particle size distribution between batches of colloid as well as the aggregation process are difficult to control enough to obtain reproducible SERS spectra. Although Ag and Au hydrosols have become the most common SERS substrates, their use for quantitative SERS applications is difficult. Highly ordered nanostructures due to the high degree of control in geometry offer a unique opportunity to match experimental results (LSPR properties, SERS enhancement and spectral reproducibility) with theoretical calculations. To maximize SERS enhancement, the relationship between the surface nanostructure and the laser excitation wavelength must be carefully optimized. Generally, excitation wavelength determines the conditions of LSPR and consequently, EF of particular SERS-active system. The SERS excitation profile (i.e. the SERS intensity plotted as a function of the excitation wavelength) does not, in general, track the SPE spectrum of the SERS substrate (Le Ru and Etchegoin 2009). This is a direct consequence of the fact that the SERS spectrum will be dominated by the resonances involving the “hot spots” while the SPE spectrum of the SERS substrate will

include contributions from the entire nanostructure. For example, the SERS signal of molecules adsorbed on a closely spaced NP dimer will be dominated by the near fields in the interstice, while the SPE spectrum of the dimer will involve absorption and scattering events by the dimer as a whole. For more complex systems, the opportunity for significant differences between the SERS excitation profile and the SERS spectrum increases (Moskovits 2013).

Another important point to consider when using metallic nanosubstrates is that some contaminants (mainly carbonaceous species) coming from the preparation as well as from the air can be adsorbed on the surface which causes a particularly large problem for Ag solid surfaces (Lin et al. 2009; Negri and Dluhy 2013). In the case of analytes in high concentration and/or with a strong affinity to the metal surface, this problem can be negated because an analyte will probably replace the contaminants from the surface. On the other hand, when a substrate is used to detect analytes in low concentration and/or low-adsorbed analytes the signal of contaminants will greatly interfere with that of an analyte and thus in this case a clean SERS substrate is required. The simplest way is to clean the metallic substrate in a vacuum with plasma, UV light or ultrasound but this can have influence on its SERS activity (Lin et al. 2009; Negri et al. 2011). UV light was applied to clean recyclable substrates based on the ordered array of Au semishells on hollow TiO_2 spheres. UV light caused TiO_2 photocatalytic degradation of the adsorbed molecules and thus the substrate was fully recyclable (Li et al. 2012b). A different concept is to replace the surface contaminants with a strong adsorbate having less interference with an analyte spectrum such as iodide anions (Lin et al. 2009). Pure chemical stability of Ag-based substrates can be overcome by coating the Ag surfaces with 1 nm alumina layer (Stiles et al. 2008) or keep it (overnight or longer) in a vacuum after Ag deposition (Šubr et al. 2015).

In the case of successful SERS measurement, some differences between SERS and NRS spectrum of analyte should be taken into account:

1. SERS spectrum is affected by the LSPR of metallic substrates which is wavelength dependent. Thus, the peaks in the SERS spectrum can be enhanced by a different factor depending on LSPR of metallic substrate and a particular vibration frequency.
2. Surface selection rules for SERS are generally different from that for NRS, as the symmetry of the molecular nuclear and/or electron arrangement may be disturbed or even broken at the surface. Thus, the orientation of the molecule relative to the surface normal is important and can be detected: flat versus tilted versus perpendicular orientations give rise to distinct SERS signatures since the various vibrational bands of the adsorbed molecule, e.g., bands due to “in plane” and “out of plane” modes of an aromatic compound are differently enhanced according to the corresponding components of the tensor $\alpha_{molecule}$.
3. Some analytes can strongly interact with a metal surface, even forming a surface complex in some cases. Therefore, SERS spectrum can differ from that of NRS in the absence of metal. The interaction of some biomolecules, such as proteins,

with a metal surface can cause a distortion of its native conformation or structure.
4. SERS signals acquired from analytes at low concentrations can fluctuate due to changes in SERS substrate conditions, adsorption-desorption of analyte and/or photobleaching.
5. Spectral bands of contaminants (e.g. carbonous species) and/or surface ions coming from metallic substrates preparation can be observed in SERS spectrum of studied analyte. Thus, close attention should be paid to the interpretation of SERS spectra.
6. SERS spectra sometimes show a broad background which is not observed in NRS conditions.
7. Raman signal strongly depends on the amount of scattered molecules, usually controlled by added concentration, but in the SERS conditions the highest surface density do not always correlates with the highest SERS signal.
8. For large molecules, such as proteins, the distance dependence of SERS should also be considered: the molecular part close to the metal surface dominates the spectra.

3.6 Related Enhanced Techniques

Plasmon-assisted RS can operate in different modalities depicted in Fig. 3.17. The first modality is represented by bare Au NPs deposited as a film on a solid support and the molecules to be probed are in direct contact with the metal surface (Fig. 3.17a). This contact mode also applies to transition metal-coated NPs (Fig. 3.17b), which extend the SERS application to other wavelength regions and transition-metal catalyzed reactions. In contrast, tip-enhanced Raman scattering (TERS) operates in a noncontact mode: the Au tip, acting as the Raman signal amplifier and the probed molecules on the surface are separated from each other (Fig. 3.17c). With this powerful approach of chemical imaging at the nanometre scale, any substrate can be probed without additional constraints on material composition and surface topography.

TERS spectroscopy was firstly reported in 2000 (Stöckle et al. 2000). It combines atomic force microscopy (AFM) and confocal SERS microscopy (Pettinger 2006). A metal-coated nanotip scans the surface of the sample and SERS spectra are successively measured from the spots of the sample in contact with the tip, where the SERS enhancement is localized. It provides ultrahigh spatial resolution (better than $\lambda/20$). TERS shows rather moderate EFs in the range from 10^2 to 10^4, but taking advantage of the near-field coupling between the metal tip and the sample on the metallic substrate, even EFs of 10^9 allowing SM TERS detection can be achieved (Yeo et al. 2009). TERS and its methodological development recently led to the first biological applications (Yeo et al. 2009; Elfick et al. 2010).

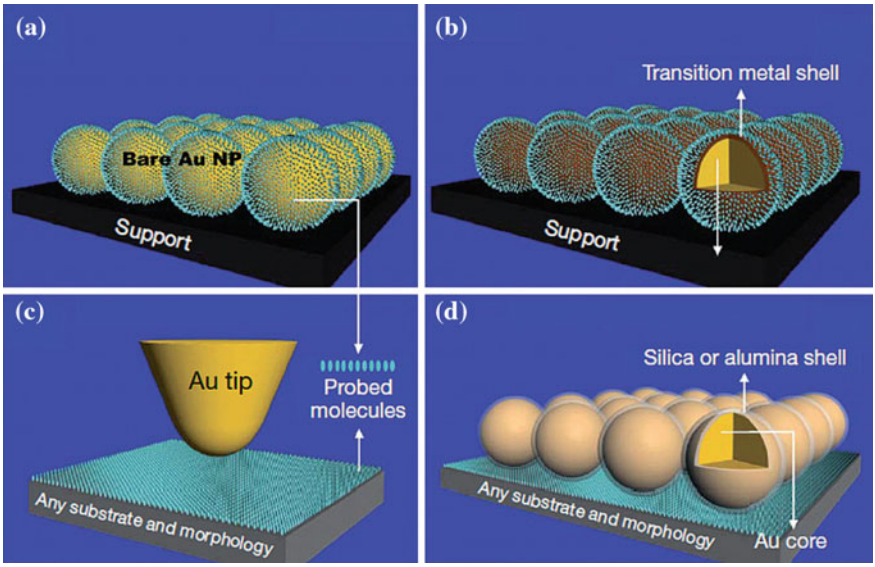

Fig. 3.17 Different modalities of SERS. Probed molecules are indicated as *blue dots*. See text for details (reproduced with permission from Li et al. 2010. Copyright 2010 Nature Publishing Group)

Shell-isolated NP-enhanced Raman scattering (SHINERS) (Li et al. 2010, Li and Tian 2014) also operates in the noncontact mode by using Au NPs protected by a 2 nm ultrathin glass shell which isolates the Au surface from the probed molecules and therefore prevents a potentially disturbing interaction (Fig. 3.17d). A very short metal-molecule separation of 2 nm still leads to a significant SERS signal compared to the contact mode. This approach is very flexible; it can be applied to virtually any surface by adapting to the surface topography as a "smart film" and therefore the simultaneous interrogation of the entire surface is possible by "spatial multiplexing". Moreover, the noncontact mode also prevents the direct metal-molecule interaction and thus it does not perturb the electronic, vibrational and/or conformational properties of the molecule due to adsorption onto the metal surface.

Interaction of an EM field with a nanostructured metal surface also strongly influences other optical phenomena, namely absorption and luminescence. Surface-enhanced infrared absorption (SEIRA) of monolayers of benzoic acids on thin Ag island films was first observed in 1980s (Hartstein et al. 1980). The EM mechanisms is attributed to a local field enhancement and, correspondingly, to an enhancement of the absorption cross-section. Absorption can be enhanced generally by a factor of 10^1–10^3 (Osawa 2001; Aroca 2006) and SEIRA is used as a complementary technique to SERS in some cases (Aroca 2006).

Fluorescence (which is a special case of luminescence) in the vicinity of plasmonic metal can be both surface-enhanced and surface-quenched (Weitz et al. 1983). The fluorescence is a stepwise process involving first absorption which is enhanced by EM mechanism. For the second step (emission), the presence of metal

modifies the decay rates (radiative and nonradiative) resulting in modified fluorescence lifetimes of the fluorophore but mainly to quantum yield or radiative efficiency (Le Ru and Etchegoin 2009). In the case of dyes with high quantum yield (~ 1), the metallic nanostructure provides channels for absorption of the emitted radiation and radiation efficiency becomes much smaller than 1 (Weitz et al. 1983; Le Ru and Etchegoin 2009). Thus, fluorescence is quenched which is considered a large advantage of SERS over the conventional RS of highly fluorescent species. On the other hand, in the case of molecules with a low quantum yield (<0.01) combination of enhanced absorption and modified quantum yield can enhance fluorescence (Weitz et al. 1983). In systems with interacting plasmonic NPs, the interplay between fluorescence enhancement and quenching becomes substantially more complicated. This is probably because both of these processes are affected by a variety of parameters, some of which appear to be related to the actual morphology of the NP assembly (Lakowicz et al. 2004). Both theoretical and experimental studies show that fluorescence can be enhanced by a factor of 10^1–10^3 (Aroca 2013) which never reaches the SERS EFs. Surface-enhanced fluorescence (SEF) was first observed in the 1980s in Ag island films (Weitz et al. 1983). EF of fluorescence strongly depends on distance of fluorophore from the metal surface. This is illustrated in Fig. 3.18. In the case of short distance (~ 1 nm), fluorescence is quenched (Fig. 3.18a). In longer distance (a few nm), both SERS and SEF can be

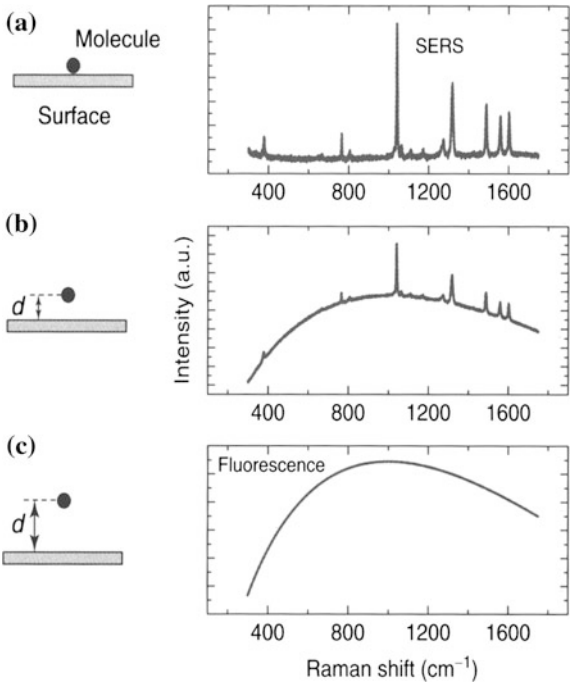

Fig. 3.18 Scheme of the relative intensities of fluorescence and SERS for fluorophore molecule at different distance *d* from the metal surface. See text for details (adapted from Etchegoin and Le Ru 2011. Copyright 2011 Wiley-VCH Verlag GmbH & Co. KGaA, Weinheim)

observed (Fig. 3.18b). For long distance (~5–20 nm) the optimal EF is obtained for fluorescence which dominates the spectrum (Fig. 3.18c). Optimal distance is established by spacer layers of defined thickness (e.g. LB, layer-by-layer films, SiO_x, Al_2O_3) between the fluorophore and the metal surface (Aroca 2013).

References

M.E. Abdelsalam, P.N. Bartlett, J.J. Baumberg, S. Cintra, T.A. Kelf, A.E. Russell, Electrochemical SERS at a structured gold surface. Electrochem. Comm. **7**, 740 (2005)

H. Aouani, M. Rahmani, H. Šípová, V. Torres, K. Hegnerová, M. Beruete, J. Homola, M. Hong, M. Navarro-Cía, S.A. Maier, Plasmonic nanoantennas for multispectral surface-enhanced spectroscopies. J. Phys. Chem. C **117**, 18620 (2013)

R. Aroca, *Surface-enhanced vibrational spectroscopy* (Wiley, Chichester, 2006)

R. Aroca, Plasmon enhanced spectroscopy. Phys. Chem. Chem. Phys. **15**, 5355 (2013)

R.F. Aroca, R.A. Alvarez-Puebla, N. Pieczonka, S. Sánchez-Cortés, J.V. García-Ramos, Surface-enhanced Raman scattering on colloidal nanostructures. Adv. Colloid Interface Sci. **116**, 45 (2005)

M. Baia, L. Baia, S. Astilean, Gold nanostructured films deposited on PS colloidal crystal templates for surface-enhanced Raman spectroscopy. Chem. Phys. Lett. **404**, 3 (2005)

M. Baia, S. Astilean, T. Iliesku, New developments in SERS-active substrates, in *Raman and SERS Investigations of Pharmaceuticals* (Springer, Berlin, 2008), pp. 187–205

M.J. Banholzer, J.E. Millstone, L. Qin, C.A. Mirkin, Rationally designed nanostructures for surface-enhanced Raman spectroscopy. Chem. Soc. Rev. **37**, 885 (2008)

E.A. Batista, D.P. dos Santos, G.F.S. Andrade, A.C. Sant'Ana, A.G. Brolo, M.L.A. Temperini, Using polycarbonate membranes as templates for the preparation of Au nanostructures for surface-enhanced Raman scattering. J. Nanosci. Nanotechnol. **9**, 3233 (2009)

E.J. Blackie, E.C. Le Ru, P.G. Etchegoin, Single-molecule surface-enhanced Raman spectroscopy of nonresonant molecules. J. Am. Chem. Soc. **131**, 14466 (2009)

A.G. Brolo, D.E. Irish, B.D. Smith, Applications of surface enhanced Raman scattering to the study of metal-adsorbate intractions. J. Mol. Struct. **405**, 29 (1997)

R.J.C. Brown, M.J.T. Milton, Nanostructures and nanostructured substrates for surface-enhanced Raman scattering (SERS). J. Raman Spectrosc. **39**, 1313 (2008)

A. Campion, P. Kambhampati, Surface-enhanced Raman scattering. Chem. Soc. Rev. **27**, 241 (1998)

Y. Cao, D. Li, F. Jiang, Y. Yang, Z. Huang, Engineering metal nanostructures for SERS applications. J. Nanomater. **2013**, 123812 (2013)

S. Chen, D.L. Carroll, Synthesis and characterization of truncated triangular silver nanoplates. Nano Lett. **2**, 1003 (2002)

J.A. Creighton, C.G. Blatchford, M.G. Albrecht, Plasma resonance enhancement of Raman scattering by pyridine adsorbed on silver and gold sol particles of size comparable to the excitation wavelength. J. Chem. Soc. Faraday Trans. 2 **75**, 790 (1979)

G. Das, M. Chirumamilla, A. Toma, A. Gopalakrishnan, R.P. Zaccaria, A. Alabastri, M. Leoncini, E. Di Fabrizio, Plasmon based biosensor for distinguishing different peptides mutation states. Sci. Rep. **3**, 1792 (2013)

J.A. Dieringer, R.B. Lettan II, K.A. Scheidt, R.P. Van Duyne, A frequency domain existence proof of single-molecule surface-enhanced Raman spectroscopy. J. Am. Chem. Soc. **129**, 16249 (2007)

J.D. Driskell, S. Shanmukh, Y. Liu, S.B. Chaney, X.J. Tang, P. Zhao, R.A. Dluhy, The use of aligned silver nanorod arrays prepared by oblique angle deposition as surface enhanced Raman scattering substrates. J. Phys. Chem. C **112**, 895 (2008)

A.P.D. Elfick, A.R. Downes, R. Mouras, Development of tip-enhanced optical spectroscopy for biological applications: a review. Anal. Bioanal. Chem. **396**, 45 (2010)

M.A. El-Sayed, Some interesting properties of metals confined in time and nanometer space of different shapes. Acc. Chem. Res. **34**, 257 (2001)

P.G. Etchegoin, E.C. Le Ru, Basic electromagnetic theory of SERS, in *Surface Enhanced Raman Spectroscopy: Analytical, Biophysical and Life Science Applications,* ed. by S. Schlücker (Wiley-WCH, Weinheim, 2011), pp. 1–38

M. Fan, A.G. Brolo, Silver nanoparticles self assembly as SERS substrates with near single molecule detection limit. Phys. Chem. Chem. Phys. **11**, 7381 (2009)

M. Fan, G.F.S. Andrade, A.G. Brolo, A review on the fabrication of substrates for surface enhanced Raman spectroscopy and their applications in analytical chemistry. Anal. Chim. Acta **693**, 7 (2011)

Y. Fang, N.-H. Seong, D.D. Dlott, Measurement of the distribution of site enhancements in surface-enhanced Raman scattering. Science **321**, 388 (2008)

A. Fojtik, A. Henglein, Laser ablation of films and suspended particles in a solvent: formation of cluster and colloid solutions. Ber. Bunsenges. Phys. Chem. **97**, 252 (1993)

H. Fredriksson, Y. Alaverdyan, A. Dmitriev, C. Langhammer, D. Sutherland, M. Zäch, B. Kasemo, "Hole mask"colloidal lithography. Adv. Mater. **19**, 4297 (2007)

R.G. Freeman, K.C. Grabar, K.J. Allison, R.M. Bright, J.A. Davis, A.P. Guthrie, M.B. Hommer, M.A. Jackson, P.C. Smith, D.G. Walter, M.J. Natan, Self-assembled metal colloid monolayers-an approach to SERS substrates. Science **267**, 1629 (1995)

R.G. Freeman, M.B. Hommer, K.C. Grabar, M.A. Jackson, M.J. Natan, Ag-Clad Au nanoparticles: Novel aggregation, optical and surface-enhanced Raman scattering properties. J. Phys. Chem. **100**, 718 (1996)

R.G. Freeman, R.M. Bright, M.B. Hommer, M.J. Natan, Size selection of colloidal gold aggregates by filtration: effect on surface-enhanced Raman scattering intensities. J. Raman Spectrosc. **30**, 733 (1999)

A. Gopalakrishnan, M. Malerba, S. Tuccio, S. Panaro, E. Miele, M. Chirumamilla, S. Santoriello, C. Dorigoni, A. Giugni, R. Proietti Zaccaria, C. Liberale, F. De Angelis, L. Razzari, R. Krahne, A. Toma, G. Das, E. Di Fabrizio, Nanoplasmonic structures for biophotonic applications: SERS overview. Ann. Phys. **524**, 620 (2012) (Berlin)

N.G. Greeneltch, M.G. Blaber, A.I. Henry, G.C. Schatz, R.P. Van Duyne, Immobilized NR assemblies: fabrication and understanding of large area surface-enhanced Raman spectroscopy substrates. Anal. Chem. **85**, 2297 (2013)

S. Guo, S. Dong, Metal nanomaterial-based self-assembly: development, electrochemical sensing and SERS applications. J. Mat. Chem. **21**, 16704 (2011)

N. Hajduková, M. Procházka, J. Štěpánek, M. Špírková, Chemically reduced and laser-ablated gold nanoparticles immobilized to silanized glass plates: preparation, characterization and SERS spectral testing. Colloid Surf. A-Physicochem. Eng. Asp. **301**, 264 (2007)

Y. Han, S. Sukhishvili, H. Du, J. Cefaloni, B. Smolinsko, Layer-by-Layer self-assembly of oppositely charged Ag nanoparticles on silica microspheres for trace analysis of aqueous solutions using surface-enhanced Raman scattering. J. Nanosci. Nanotechnol. **8**, 5791 (2008)

A. Hartstein, J.R. Kirtley, J.C. Tsang, Enhancement of the infrared absorption from molecular monolayers with thin metal overlayers. Phys. Rev. Lett. **45**, 201 (1980)

C.L. Haynes, C.R. Yonzon, X. Zhang, R.P. Van Duyne, Surface-enhanced Raman sensors: early history and the development of sensors for quantitative biowarfare agents and glucose detection. J. Raman Spectrosc. **36**, 471 (2005)

S.M. Heard, F. Grieser, C.G. Barraclough, J.V. Sanders, The characterization of Ag sols by electron-microscopy, optical-absorption and electrophoresis. J. Colloid Interf. Sci. **93**, 545 (1983)

J.C. Hulteen, R.P. Van Duyne, Nanosphere lithography—a materials general fabrication process for periodic particle array surfaces. J. Vac. Sci. Technol. A **13**, 1553 (1995)

H. Im, K.C. Bantz, S.H. Lee, T.W. Johnson, C.L. Haynes, S.-H. Oh, Self-assembled plasmonic nanoring cavity arrays for SERS and LSPR biosensing. Adv. Mater. **25**, 2678 (2013)

Y.H. Jang, K. Chung, L.N. Quan, B. Špačková, H. Šípová, S. Moon, W.J. Cho, H.Y. Shin, Y. J. Jang, J.E. Lee, S.T. Kochuveedu, M.J. Yoon, J. Kim, S. Yoon, J.K. Kim, D. Kim, J. Homola, D.H. Kim, Configuration-controlled Au nanocluster arrays on inverse micelle nano patterns: versatile platforms for SERS and LSPR sensors. Nanoscale **5**, 12261 (2013)

T.R. Jensen, M.D. Malinsky, C.L. Haynes, R.P. Van Duyne, Nanosphere lithography: tunable localized surface plasmon resonance spectra of silver nanoparticles. J. Phys. Chem. B **104**, 10549 (2000)

V. Joseph, M. Gensler, S. Seifert, U. Gernert, J.P. Rabe, J. Kneipp, Nanoscopic properties and application of mix-and-match plasmonic surfaces for microscopic SERS. J. Phys. Chem. C **116**, 6859 (2012)

M. Kahl, E. Voges, S. Kostrewa, C. Viets, W. Hill, Periodically structured metallic substrates for SERS. Sens. Actuator B-Chem. **51**, 285 (1998)

P. Kambhampati, C.M. Child, M.C. Foster, A. Campion, On the chemical mechanism of surface enhanced Raman scattering: experiment and theory. J. Chem. Phys. **108**, 5013 (1998)

K. Kneipp, Y. Wang, H. Kneipp, L.T. Perelman, I. Itzkan, R.R. Dasari, M.S. Feld, Single molecule detection using surface-enhanced Raman scattering (SERS). Phys. Rev. Lett. **78**, 1667 (1997)

K. Kneipp, H. Kneipp, H.G. Bohr, Single-molecule SERS spectroscopy, in *Surface-Enhanced Raman Scattering: Physics and Applications*, vol. **103**, ed. by K. Kneipp, M. Moskovits, H. Kneipp (Springer-Verlag, Berlin Heidelberg, 2006), pp. 261–277 (Top. Appl. Phys.)

H. Ko, S. Singamaneni, V.V. Tsukruk, Nanostructured surfaces and assemblies as SERS media. Small **4**, 1576 (2008)

P.S. Kumar, I. Pastoriza-Santos, B. Rodriguez-Gonzalez, F.J. Garcia de Abajo, L.M. Liz-Marzan, High-yield synthesis and optical response of gold nanostars. Nanotechnology **19**, 015606 (2008)

J.R. Lakowicz, C.D. Geddes, I. Gryczynski, J. Malicka, Z. Gryczynski, K. Aslan, J. Lukomska, E. Matveeva, J. Zhang, R. Badugu, J. Huang, Advances in surface-enhanced fluorescence. J. Fluoresc. **14**, 425 (2004)

I.A. Larmour, K. Faulds, D. Graham, SERS activity and stability of the most frequently used silver colloids. J. Raman Spectrosc. **43**, 202 (2012)

P.C. Lee, D. Meisel, Adsorption and surface-enhanced Raman of dyes on silver and gold sols. J. Phys. Chem. **86**, 3391 (1982)

N. Leopold, B. Lendl, A new method for fast preparation of highly surface-enhanced Raman scattering (SERS) active silver colloids at room temperature by reduction of silver nitrate with hydroxylamine hydrochloride. J. Phys. Chem. B **107**, 5723 (2003)

E.C. Le Ru, P.G. Etchegoin, *Principles of Surface Enhanced Raman Spectroscopy and Related Plasmonic Effects* (Elsevier, Amsterdam, 2009)

E.C. Le Ru, M. Meyer, P.G. Etchegoin, Proof of single-molecule sensitivity in surface enhanced Raman scattering (SERS) by means of a two-analyte technique. J. Phys. Chem. B **110**, 1944 (2006)

E.C. Le Ru, E. Blackie, M. Meyer, P.G. Etchegoin, Surface enhanced Raman scattering enhancement factors: a comprehensive study. J. Phys. Chem. C **111**, 13794 (2007)

J.F. Li, Z.Q. Tian, Shell-isolated nanoparticle-enhanced Raman spectroscopy (SHINERS), in *Frontiers of Surface-Enhanced Raman Scattering: Single Nanoparticles and Single Cells*, ed. by Y. Ozaki, K. Kneipp, R. Aroca (Wiley, Chichester, 2014), pp. 163–192

Z. Li, W.M. Tong, W.F. Stickle, D.L. Neiman, R.S. Williams, L.L. Hunter, A.A. Talin, D. Li, S.R.J. Brueck, Plasma-induced formation of Ag nanodots for ultra-high-enhancement surface-enhanced Raman scattering substrates. Langmuir **23**, 5135 (2007)

J.F. Li, Y.F. Huang, Y. Ding, Z.L. Yang, S.B. Li, X.S. Zhou, F.R. Fan, W. Zhang, Z.Y. Zhou, D.Y. Wu, B. Ren, Z.L. Wang, Z.Q. Tian, Shell-isolated nanoparticle-enhanced Raman spectroscopy. Nature **464**, 392 (2010)

M. Li, S.K. Cushing, J.M. Zhang, J. Lankford, Z.P. Aguilar, D.L. Ma, N.Q. Wu, Shape-dependent surface-enhanced Raman scattering in gold–Raman probe–silica sandwiched nanoparticles for biocompatible applications. Nanotechnology **23**, 115501 (2012a)

X. Li, H. Hu, D. Li, Z. Shen, Q. Xiong, S. Li, H.J. Fan, Ordered array of gold semishells on TiO_2 spheres: an ultrasensitive and recyclable SERS substrate. ACS Appl. Mater. Interfaces **4**, 2180 (2012b)

J.F. Li, X.D. Tian, S.B Li, J.R. Anema, Z.L. Yang, Y. Ding, Y.F. Wu, Y.M. Zheng, Q.Z. Chen, B. Ren, Z.L. Wang, Z.Q. Tian, Surface analysis using shell-isolated nanoparticle-enhanced Raman spectroscopy. Nat. Protoc. **8**, 52 (2013)

X.M. Lin, Y. Cui, Y.H. Xu, B. Ren, Z.Q. Tian, Surface-enhanced Raman spectroscopy: substrate-related issues. Anal. Bional. Chem. **394**, 1729 (2009)

X. Liu, Y. Shao, Y. Tang, K.-F. Yao, Highly uniform and reproducible Surface enhanced Raman scattering on air-stable metallic glassy nanowire array. Sci. Rep. **4**, 5835 (2014)

M.J. Madou, *Fundamentals of Microfabrication: The Science of Miniaturization* (CRC Press, Boca Raton, 2002)

M. Moskovits, Surface-enhanced spectroscopy. Rev. Modern Phys. **57**, 783 (1985)

M. Moskovits, Persistent misconceptions regarding SERS. Phys. Chem. Chem. Phys. **15**, 5301 (2013)

P. Negri, R.A. Dluhy, Ag nanorod based surface-enhanced Raman spectroscopy applied to bioanalytical sensing, J. Biophotonics **6**, 20 (2013)

P. Negri, N.E. Marotta, L.A. Bottomley, R.A. Dluhy, Removal of surface contamination and self-assembled monolayers (SAMs) from silver (Ag) nanorod substrates by plasma cleaning with argon. Appl. Spectrosc. **65**, 66 (2011)

S. Nie, S.R. Emory, Probing single molecules and single nanoparticles by surface-enhanced Raman scattering. Science **275**, 1102 (1997)

S.J. Oldenburg, R.D. Averitt, S.L. Westcott, N.J. Halas, Nanoengineering of optical resonances. Chem. Phys. Lett. **288**, 243 (1998)

S.J. Oldenburg, J.B. Jackson, S.L. Westcott, N.J. Halas, Infrared extinction properties of gold nanoshells. Appl. Phys. Lett. **75**, 2897 (1999)

L.G. Olson, Y.S. Lo, T.P. Beebe, J.M. Harris, Characterization of silane-modified immobilized gold colloids as a substrate for surface-enhanced Raman spectroscopy. Anal. Chem. **73**, 4268 (2001)

C.J. Orendorff, A. Gole, T.K. Sau, C.J. Murphy, Surface-enhanced Raman spectroscopy of self-assembled monolayers: sandwich architecture and nanoparticles shape dependence. Anal. Chem. **77**, 3261 (2005)

M. Osawa, Surface-enhanced infrared absorption. Top. Appl. Phys. **81**, 163 (2001)

A. Otto, The 'chemical' (electronic) contribution to surface-enhanced Raman scattering. J. Raman Spectrosc. **36**, 497 (2005)

A. Otto, I. Mrozek, H. Grabhorn, W. Akemann, Surface-ehnanced Raman scattering. J. Phys.: Condens. Matter **4**, 1143 (1992)

A. Otto, A. Bruckbauer, Y.X. Chen, On the chloride activation in SERS and single molecule SERS. J. Mol. Struct. **661–662**, 501 (2003)

V. Peksa, M. Jahn, L. Štolcová, V. Schulz, J. Proška, M. Procházka, K. Weber, D. Cialla-May, J. Popp, Quantitative SERS analysis of azorubine (E 122) in sweet drinks. Anal. Chem. **87**, 2840 (2015)

N.M.B. Perney, F.J.G. de Abajo, J.J. Baumberg, A. Tang, M.C. Netti, M.D.B. Charlton, M.E. Zoorob, Tuning localized plasmon cavities for optimized surface-enhanced Raman scattering. Phys. Rev. B **76**, 035426 (2007)

B. Pettinger, Tip-enhanced Raman spectroscopy (TERS), in *Surface-Enhanced Raman Scattering: Physics and Applications*, vol. **103**, ed. by K. Kneipp, M. Moskovits, H. Kneipp (Springer-Verlag, Berlin Heidelberg, 2006), pp. 217–240 (Top. Appl. Phys.)

N.P.W. Pieczonka, R.F. Aroca, Single molecule analysis by surface-enhanced Raman scattering. Chem. Soc. Rev. **37**, 946 (2008)

M. Procházka, P. Mojzeš, J. Štěpánek, B. Vlčková, P.-Y. Turpin, Probing applications of laser ablated Ag colloids in SERS spectroscopy: Improvement of ablation procedure and SERS spectral testing. Anal. Chem. **69**, 5103 (1997a)

M. Procházka, P. Mojzeš, B. Vlčková, P.-Y. Turpin, Surface-enhanced resonance Raman scattering from copper(II) 5,10,15,20-tetrakis(1-methyl-4-pyridyl)porphyrin adsorbed on aggregated and nonaggregated silver colloids. J. Phys. Chem. B **101**, 3161 (1997b)

M. Procházka, P. Šimáková, N. Hajduková-Šmídová, SE(R)RS microspectroscopy of porphyrins on immobilized Au nanoparticles: testing spectral sensitivity and reproducibility. Colloid Surf. A-Physicochem. Eng. Asp. **402**, 24 (2012)

E. Prodan, P. Nordlander, Structural tunability of the plasmon resonances in metallic nanoshells. Nano Lett. **3**, 543 (2003)

L. Rivas, S. Sánchez-Cortés, J.V. García-Ramos, G. Morcillo, Mixed silver/gold colloids: a study of their formation, morphology, and surface-enhanced Raman activity. Langmuir **16**, 9722 (2000)

J.M. Romo-Herrera, R.A. Alvarez-Puebla, L.M. Liz-Marzan, Controlled assembly of plasmonic colloidal nanoparticle clusters. Nanoscale **3**, 1304 (2011)

G.C. Schatz, M.A. Young, R. P. Van Duyne, Electromagnetic mechanism of SERS, in *Surface-Enhanced Raman Scattering: Physics and Applications*, vol. **103**, ed. by K. Kneipp, M. Moskovits, H. Kneipp (Springer-Verlag, Berlin Heidelberg, 2006), pp. 19–46 (Top. Appl. Phys.)

S. Schlücker (ed.), *Surface enhanced Raman spectroscopy: Analytical, biophysical and life science applications* (Wiley-WCH, Weinheim, 2011)

S. Schlücker, Surface-enhanced Raman spectroscopy: concepts and chemical applications. Angew. Chem. Int. Ed. **53**, 4756 (2014)

M.S. Schmidt, J. Hübner, A. Boisen, Large area fabrication of leaning silicon nanopillars for surface-enhanced Raman spectroscopy, Adv. Mater. **24**, OP11 (2012)

Y. Shao, Y. Jin, S. Dong, Synthesis of gold nanoplates by aspartate reduction of gold chloride. Chem. Commun. **9**, 1104 (2004)

D.O. Sigle, E. Perkins, J.J. Baumberg, S. Mahajan, Reproducible deep-UV SERRS on aluminium nanovoids. J. Phys. Chem. Lett. **4**, 1449 (2013)

I. Srnová-Šloufová, B. Vlčková, T.L. Snoeck, D.J. Stufkens, P. Matějka, Surface-enhanced Raman scattering and Surface-enhanced resonance Raman scattering excitation profiles of Ag-2,2′-bipyridine surface complexes and of $[Ru(bpy)3]^{2+}$ on Ag colloidal surfaces: manifestations of the charge-transfer resonance contributions to the overall surface enhancement of Raman scattering. Inorg. Chem. **39**, 3551 (2000)

P.L. Stiles, J.A. Dieringer, N.C. Shah, R.P. Van Duyne, Surface-enhanced Raman spectroscopy. Annu. Rev. Anal. Chem. **1**, 601 (2008)

R.L. Stöckle, Y.D. Suh, V. Deckert, R. Zenobi, Nanoscale chemical analysis by tip-enhance Raman spectroscopy. Chem. Phys. Lett. **318**, 131 (2000)

M.I. Stockman, V.M. Shalaev, M. Moskovits, R. Botet, T.F. George, Enhanced Raman scattering by fractal clusters: scale-invariant theory. Phys. Rev. B **46**, 2821 (1992)

L. Štolcová, J. Proška, M. Procházka, Hexagonally ordered gold semishells as tunable SERS substrates, in *Proceedings of Nanocon* (Czech Republic, Brno, 2012), pp. 225–229

L. Štolcová, M. Domonkos, T. Ižák, J. Proška, M. Procházka, A. Kromka, Plasma treatment as a versatile technique for preparation of plasmonic nanoantenna arrays, in *Electromagnetics Research Symposium (PIERS) Proceedings*, pp. 426–430. Stockholm, Sweden, 12–15 Aug 2013

M. Šubr, M. Petr, V. Peksa, O. Kylián, J. Hanuš, M. Procházka, Ag NR arrays for SERS: aspects of spectral reproducibility, surface contamination, and spectral sensitivity. J. Nanomater. **2015**, 729231 (2015)

Y. Sun, Y. Xia, Shape-controlled synthesis of gold and silver nanoparticles. Science **298**, 2176 (2002)

A.R. Tao, J. Huang, A.P. Yang, Langmuir–blodgettry of nanocrystals and nanowires. Acc. Chem. Res. **41**, 1662 (2008)

M. Tabatabaei, M. Najiminaini, K. Davieau, B. Kaminska, M.R. Singh, J.J.L. Carson, F. Lagugné-Labarthet, Tunable 3D plasmonic cavity nanosensors for surface-enhanced Raman spectroscopy with sub-femtomolar limit of detection. ACS Photonics **2**, 752 (2015)

Z.Q. Tian, B. Ren, D.Y. Wu, Surface-enhanced Raman scattering: from noble to transition metals and from rough surfaces to ordered nanostructures. J. Phys. Chem. B **106**, 9463 (2002)

Z.Q. Tian, Z.L. Yang, B. Ren, D.Y. Wu, SERS from transition metals and excited by ultraviolet light, in *Surface-Enhanced Raman Scattering: Physics and Applications* vol. **103**, ed. by K. Kneipp, M. Moskovits, H. Kneipp (Springer-Verlag, Berlin Heidelberg, 2006), pp. 125–146 (Top. Appl. Phys.)

F. Toderas, M. Baia, L. Baia, S. Astilean, Controlling gold nanoparticle assemblies for efficient surface-enhanced Raman scattering and localized surface plasmon resonance sensors. Nanotechnology **18**, 255702 (2007)

N. Valley, N. Greeneltch, R.P. Van Duyne, G.C. Schatz, A look at the origin and magnitude of the chemical contribution to the enhancement mechanism of surface-enhanced Raman spectroscopy (SERS): theory and experiment. J. Phys. Chem. Lett. **4**, 2599 (2013)

H. Wang, J. Kundu, N.J. Halas, Plasmonic nanoshell arrays combine surface-enhanced vibrational spectroscopies on a single substrate. Angew. Chem. Int. Ed. **46**, 9040 (2007)

Y. Wang, E. Wang, Nanoparticle SERS substrates, in *Surface enhanced Raman spectroscopy: analytical, biophysical and life science applications*, ed. by S. Schlücker (Wiley-WCH, Weinheim, 2011), pp. 39–70

Y. Wang, N. Lu, W. Wang, L. Liu, L. Feng, Z. Zeng, H. Li, W. Xu, Z. Wu, W. Hu, Y. Lu, L. Chi, Highly effective and reproducible surface-enhanced Raman scattering substrates based on Ag pyramidal arrays. Nano Res. **6**, 159 (2013)

D.A. Weitz, S. Garoff, J.I. Gersten, A. Nitzan, The enhancement of Raman scattering, resonance Raman scattering, and fluorescence from molecules adsorbed on a rough silver surface. J. Chem. Phys. **78**, 5324 (1983)

D.A. Weitz, M.Y. Lin, C.J. Sandroff, Colloidal aggregation revisited: new insights based on fractal structure and surface-enhanced Raman scattering. Surf. Sci. **158**, 147 (1985)

E. Wentrup-Byrne, S. Sarinas, P.M. Fredericks, Analytical potential of surface-enhanced Fourier transform Raman spectroscopy on silver colloids. Appl. Spectrosc. **47**, 1192 (1993)

D.Y. Wu, J.F. Li, B. Ren, Z.Q. Tian, Electrochemical surface-enhanced Raman spectroscopy of nanostructures. Chem. Soc. Rev. **37**, 1025 (2008)

H. Wu, F. Bai, Z. Sun, R.E. Haddad, D.M. Boye, Z. Wang, J.Y. Huang, H. Fan, Nanostructured gold architectures formed through high pressure-driven sintering of spherical nanoparticle arrays. J. Am. Chem. Soc. **132**, 12826 (2010a)

L.Y. Wu, B.M. Ross, S. Hong, L.P. Lee, Bioinspired nanocorals with decoupled cellular targeting and sensing functionality. Small **6**, 503 (2010b)

L. Xia, M. Chen, X. Zhao, Z. Zhang, J. Xia, H. Xu, M. Sun, Visualized method of chemical enhancement mechanism on SERS and TERS. J. Raman Spectrosc. **45**, 533 (2014)

H. Xu, J. Aizpurua, M. Käll, P. Apell, Electromagnetic contributions to single-molecule sensitivity in surface-enhanced Raman. Phys. Rev. E **62**, 4318 (2000)

M.J. Xu, N. Lu, H.B. Xu, D.P. Qi, Y.D. Wang, L.F. Chi, Fabrication of functional silver nanobowl arrays via sphere lithography. Langmuir **25**, 11216 (2009)

N.R. Yaffe, E.W. Blanch, Effects and anomalies that can occur in SERS spectra of biological molecules when using a wide range of aggregating agents for hydroxylamine-reduced and citrate-reduced silver colloids. Vib. Spectrosc. **48**, 196 (2008)

J. Yang, M. Palla, F.G. Bosco, T. Rindzevicius, T.S. Alstrøm, M.S. Schmidt, A. Boisen, J. Ju, Q. Lin, Surface-enhanced Raman spectroscopy based quantitative bioassay on aptamer-functionalized nanopillars using large-area Raman mapping. ACS Nano **7**, 5350 (2013)

J. Yao, A.P. Le, S.K. Gray, J.S. Moore, J.A. Rogers, R.G. Nuzzo, Functional nanostructured plasmonic materials. Adv. Mat. **22**, 1102 (2010)

B.S. Yeo, J. Stadler, T. Schmid, R. Zenobi, W. Zhang, Tip-enhanced Raman spectroscopy—its status, challenges and future directions. Chem. Phys. Lett. **472**, 1 (2009)

Q. Yu, P. Guan, D. Qin, G. Golden, P.M. Wallace, Inverted size-dependence of surface-enhanced Raman scattering on gold nanohole and nanodisk arrays. Nano Lett. **8**, 1923 (2008)
S. Yüksel, M. Ziegler, S. Goerke, U. Hübner, K. Pollok, F. Langenhorst, K. Weber, D. Cialla-May, J. Popp, Background-free bottom-up plasmonic arrays with increased sensitivity, specificity and shelf life for SERS detection schemes. J. Phys. Chem. C **119**, 13791 (2015)
J. Zhang, L. Zhang, Nanostructures for surface plasmons. Adv. Opt. Photonics **4**, 157 (2012)
X. Zhang, H. Chen, H. Zhang, Layer-by-layer assembly: from conventional to unconventional methods. Chem. Commun. **14**, 1395 (2007)
J. Zhang, Y. Li, X. Zhang, B. Yang, Colloidal self-assembly meets nanofabrication: from two-dimensional colloidal crystals to nanostructure arrays. Adv. Mater. **22**, 4249 (2010)

Chapter 4
Bioanalytical SERS Applications

Abstract SERS spectroscopy can be applied for the detection of biologically relevant molecules in real complex matrix (e.g. human body fluids, drinks, food). The quantitative SERS measurements are, in practice, the result of considerable effort in optimizing an enhancing substrate and experimental conditions. This chapter will explain the basic principles of quantitative bioanalytical SERS measurements from the point of view of SERS-active substrates, internal intensity standards, sensitivity (limit of detection) and specificity. The successful SERS sensing of analytes with very low affinity for SERS-enhancing surface is possible due to suitable chemical modification of a metal surface to promote the capture of particular analytes. The results of some SERS bioanalytical applications on pharmaceuticals, drugs (including nicotine and cocaine), pollutants and pesticides, food contaminants and food additives (melamine, food colourants) and biowarfare agents (anthrax) will be summarized. The limits of detection as well as accuracy of SERS analysis are comparable and in some cases even better than these provided by standard analytic techniques (such as HPLC).

4.1 Quantitative SERS Methods

4.1.1 SERS-Active Substrates for Quantitative SERS

Reproducibility and sensitivity represent a major preoccupation of researchers interested in developing practical quantitative SERS methods (Bell and Sirimuthu 2008; Bell and Stewart 2011). In the case of quantitative analysis and sensing, the prerequisites to SERS substrates were postulated by Natan in his concluding remark at Faraday Discussion 132 (Natan 2006). According to it, we can summarize the main features of SERS enhancing metallic substrate for sensing:

1. SERS sensitivity: The substrate should provide high SERS sensitivity, which is generally considered as SERS enhancement better than 10^5.
2. Spot-to-spot reproducibility: The substrate should be uniform so that the SERS signal shows variation less than 20 % over a 10 mm^2 area.

M. Procházka, *Surface-Enhanced Raman Spectroscopy*,
Biological and Medical Physics, Biomedical Engineering,
DOI 10.1007/978-3-319-23992-7_4

3. Substrate-to-substrate (batch-to-batch) reproducibility: The SERS signal variation for different batches of substrate prepared by the same method should be less than 20 %.
4. Stability: The substrate should provide good stability even after a longer shelf time (signal variation less than 20 % measured over one month). It particularly means that the substrate should be long-term stable without any destabilization or destruction by environmental conditions, like oxidation.
   Tian and co-workers added a following criterion (Lin et al. 2009):
5. The substrate should be clean enough so that it can be applied to study even weakly adsorbated analytes. It particularly means that the signals from the SERS substrate itself involving Raman spectrum of possible surface contaminants as well as background of the substrate such as autofluorescence of metal should be as low as possible. In practice, the obtained SERS spectrum should be good enough to distinguish the Raman features of the analyte present in low concentrations from the background signal of the SERS substrate.
   Brown and Milton (Brown and Milton 2008) added a following criterion:
6. Ease and low-cost of preparation and use of the substrate.

Brown and Milton (Brown and Milton 2008) reported a table summarizing the general performance of basic types of metallic structures suitable for SERS in terms of the above criteria (Table 4.1). Significant differences between particular substrates from the point of view of sensitivity, reproducibility and ease/cost of preparation can be clearly seen. The difficulty to obtain SERS-active substrates that simultaneously meet all above criteria is evident. The aggregates of Ag NPs, for instance, can provide extremely high SERS enhancement enabling even SM detection but spectral reproducibility is poor. On the other hand, highly ordered nanostructures reduce the maximal enhancement for the sake of gaining

Table 4.1 Comparison of the relative performance of the different types of nanostructures used in SERS applications

	Sensitivity	Spot-to-spot/batch-to-batch reproducibility	Ease/cost of preparation
Free NPs	1	5/3	1/1
Clusters of NPs	2	5/3	2/1
Templated NPs	2	4/2	2/1
Structured arrays of NPs	2	3/2	3/2
Unstructured surfaces	4	5/5	1/1
Chemically roughened surfaces	3	3/3	1/1
Lithographically produced surfaces	1	1/1	4/4
3D structured surfaces	1	2/1	4/3

Decrease in order from 1 to 5 (1 is the best, 5 is the worst). All the columns are the relevance with respect to the utility of nanostructures in industrial applications (adapted with permission from Brown and Milton 2008. Copyright 2008 John Wiley & Sons, Ltd)

reproducibility. One can suppose that SERS will be applied to real analytical problems when the balance between reproducibility and enhancement is optimized. It has been referred to as the "SERS uncertainty principle" which means that higher substrate reproducibility leads to lower EFs and vice versa (Brown and Milton 2008). Moreover, some trade-offs are possible in the case of specific purposes. In quantitative analysis, for example, uniformity and reproducibility are crucial, however, in trace analysis, maximized enhancement is needed. In bio-related applications, a clean, highly enhancing and biocompatible substrate is required, which is fulfilled by gold-based substrates. From a practical point of view, the cost, ease of preparation and use should also be taken into account. For example, free NPs are generally easier and cheaper to fabricate, while preparation of large structure areas by lithography is expensive and time-consuming.

Quantitative SERS measurements are, in practice, the result of considerable effort in optimizing an enhancing substrate and experimental conditions. This may involve standard colloidal NPs as well as the premeditated design of uniform solid nanostructural substrates (Bell and Sirimuthu 2008; Bell and Stewart 2011). It was explained in Chap. 3 and also shown in Table 4.1 that the metallic colloids are difficult to prepare with high reproducibility and to control the aggregation stage during the SERS experiment. This problem can be partly solved by a lab-on-a-chip device that integrates several laboratory functions (such as mixing of samples and spectral detection) in a single chip of size of only a few square centimetres or milimetres. A standardized flow injection and microfluidic systems in a lab-on-a-chip device reduce mechanical and optical variations between runs to a considerable extent and in some cases can produce quantitative intensity data directly from measurements (Henkel et al. 2011). A successful system design to integrate SERS with microfluidics platforms needs to take into account three important factors: (i) mixing of analyte and SERS-active nanostructures, (ii) synthesis or implementation of SERS-active substrate inside microfluidic devices and (iii) target trapping in microfluidic channels for better SERS detection. The integration of microfluidic devices and SERS has been widely investigated in different bioanalytical applications. Microfluidic-SERS devices improve the detection sensitivity and reduce the time-cost as well as the reaction volume of the assay. On the other hand, memory effects caused by the precipitation of NP aggregates have been reported in a single-phase flow channel devices and multi-phase channels should be used to avoid this problem. Additionally, microfluidic devices combined with the immunoassay platforms can serve to efficient and highly selective capture specific antigens on a well defined spot in flow (Wang and Yu 2015).

A typical experiment on SERS microfluidic lab-on-a-chip is illustrated in Fig. 4.1 (Gao et al. 2010). A chip is formed by four different microfluidic channels fabricated from poly-(dimethylsiloxane) (PDMS). It enabled a simultaneous pumping and mixing the aqueous sample of analyte (herbicide paraquat), Ag NPs as SERS-active medium, NaCl as the aggregation agent and oil (Fig. 4.1a) inside a channel from which the SERS spectra were acquired. A continuous oil phase was introduced to encapsulate the other solutions, forming a microdroplet. This

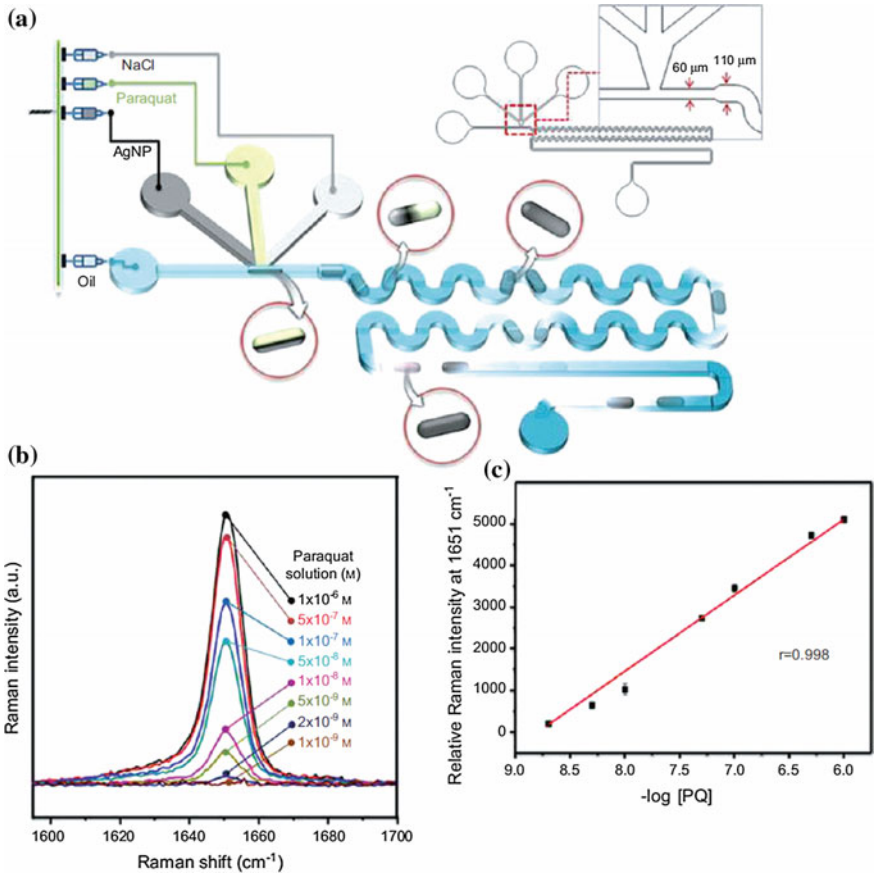

Fig. 4.1 Microfluidic (lab-on-a-chip) device for SERS detection. **a** Schematic illustration of a microdroplet channel for SERS detection. **b** SERS spectra of paraquat at different concentrations. **c** Plot of SERS intensity at 1651 cm^{-1} versus the paraquat concentration (reproduced with permission from Gao et al. 2010. Copyright 2010 Elsevier B.V.)

two-phase liquid/liquid segmented flow system prevented memory effects on channel walls since the Ag NPs did not directly contact the wall surface. Consequently, the SERS measurement conditions were consistently maintained and contamination from the surrounding environment was also avoided. SERS signals from 125 droplets at every concentration were measured and averaged for the quantitative analysis. SERS spectra of paraquat in a microdroplet channel at different concentrations are shown in Fig. 4.1b. The detection limit of paraquat in water determined by the intensity of the peak at ~ 1651 cm^{-1} was found to be about 2×10^{-9} M (Fig. 4.1c).

For solid substrates the problem is slightly different because here any heterogeneity in the enhancing nanostructural surface will increase the uncertainty in the

absolute signal intensity. The simplest way to reduce this error is to acquire spectra from multiple spots on the surface. For example, when vapour deposited film was used to detect amphetamine the batch-to-batch relative standard deviation (RSD) in the intensity of the most intense peak was reduced from 31.6 to 5.8 % by acquiring several spectra (Faulds et al. 2002). Moreover, two ways of deposition of analyte on a solid substrate are typically performed: (i) deposition of a small drop of analyte on the metallic substrate with a pipette and allowed to dry, (ii) incubation of the substrate in the analyte solution for a certain period of time and then removal and drying. In the former case, a drop often dried by "coffee-ring"effect (Deegan et al. 1997) leading to a highly inhomogeneous distribution of analyte on the metal surface. The latter case led to uniform adsorption of the analyte from solution but the concentration of analyte adsorbed on the metal surface is difficult to quantify. Recently, Deng and co-workers combined both advantages of a microfluidic device and solid substrates by integrated PDMS chip with quasi-3-dimensional gold plasmonic nanostructure arrays which served as SERS-active substrates, into an optofluidic microsystem for online sensitive and reproducible SERS detections (Deng et al. 2015). The real-time monitoring capability of the SERS-based optofluidic microsystem was investigated by kinetic on/off experiments through alternatively flowing RH6G and ethanol in the microfluidic channel. High signal reproducibility was demonstrated with a RSD less than 5 % for low concentration of pesticide malathion.

4.1.2 Internal Intensity Standards for Quantitative SERS

Another important issue of quantitative Raman detection is an internal intensity standard introduced into the experiment. The Raman signal of standard can be used to normalize intensity in Raman spectrum of studied analyte. This can eliminate problems connected with experimental factors, such as laser power fluctuations, focusing, drift in the optical alignment and positioning of the sample (Bell and Sirimuthu 2008; Bell and Stewart 2011).

In case of SERS, EF of the metallic substrate is another factor affecting SERS intensities. Since EFs are very large, the potential variations of SERS signal are also high. It is possible to use an unenhanced component that is present in the sample, such as stretching bands of water, as the internal standard (Palacký et al. 2011). Another way is to add a molecule which is not SERS-active to the SERS-active system. In this case, high concentration of the standard molecule is needed to make its unenhanced signal sufficiently strong so that it can be detected in the presence of the SERS signal of analyte. For example, ethanol was added to (Ag hydrosol)/bipyridine system and served to normalize SERS excitation profiles of bipyridine species (Srnová-Šloufová et al. 2000). This approach is particularly successful when combined with a microfluidic device. Lee and co-workers reported acetonitrile as the internal standard in microfluidic SERS-active system because it gives a strong band in a noninterfering spectral region with studied analyte—malachite

green (Lee et al. 2007). The calibration plot of the intensity of the strongest dye band at 1615 cm^{-1} normalized to the acetonitrile peak at 2258 cm^{-1} was linear over the range 0–100 ppm and had a correlation coefficient R = 0.993 (Lee et al. 2007). In the case of solid substrates, the support can serve as the internal standard which was the case of Au FONs prepared on silicon support providing distinguishable Raman peak at ~520 cm^{-1} (Peksa et al. 2015).

The disadvantage of using the internal standard which does not provide SERS spectrum is that it cannot correct for any changes in the enhancing efficiency of the substrate itself. Loren and co-workers tested several thiol derivatives as potential SERS-active internal standards for Au colloidal NPs dried onto glass slides (Loren et al. 2004). The spectra of standards contained a distinct peak at ~2300 cm^{-1}, i.e. out of a spectrum of the studied analyte (RH6G). It was found that, despite of very large variation in enhancement of SERS substrate when spectra were taken from different spots, normalization against the enhanced standard enabled an acceptable calibration over the range 0–5 mM with a prediction error of 0.5 mM.

Nevertheless, the best internal standard can be one which is chemically similar to the analyte. Such standard will be sensitive to changes in the enhancing surface which can alter its ability to enhance specific types of molecules. One example is illustrated in Fig. 4.2. Here, pyridine was used as the internal standard in the analysis of nicotine (a pyridine derivative) using polymer-stabilized Ag colloidal NPs (Bell and Sirimuthu 2004). Since both compounds attach to the surface through their pyridyl ring, any perturbation to the Ag NPs which affects the spectrum of one will affect the other in a similar way. The only problem was that their strongest Raman band lies at similar positions ~1030 cm^{-1}. Thus, the authors introduced d5-pyridine, which has the appropriate chemical properties but its strongest Raman band is shifted to 974 cm^{-1}. The intensity ratio of these two bands versus concentration was highly linear with R^2 ~ 0.998 over a 0–10 ppm range (Bell and Sirimuthu 2004). Probably the best choice of the internal standard is the case where it is an isotopically substituted form of the target analyte itself and thus, any perturbations in the experimental conditions would be expected to be effectively identical. Use of RH6G and its d4 isotopomer provided very impressive results, the reproducibility better than 3 % in very large concentration range (Zhang et al. 2005a). The only disadvantage of this approach is that isotopically substituted analogues of the analyte are costly or not readily available.

Recently, Zhou and co-workers introduced a new strategy to quantitatively measure the SERS signals of analytes based on Au-core/Ag-shell NPs with embedded molecule (4-ATP) serving as the intensity standard (Zhou et al. 2015). In this approach, a molecular layer of 4-ATP is sandwiched between the core and shell of two metals. They chose Au nanospheres to obtain a highly uniform core and silver as the shell to achieve the highest possible enhancement. Since the 4-ATP was embedded inside the shell and the analyte was adsorbed on the shell surface, they did not compete for the surface sites. Thus, the 4-ATP signal was not influenced by the detection environment. Successful detection of two analytes, toluidine blue O in aqueous solution (detection limit of 0.1 μM) and melamine in milk (see Sect. 4.3.2) was demonstrated. Shen and co-workers proved this concept using

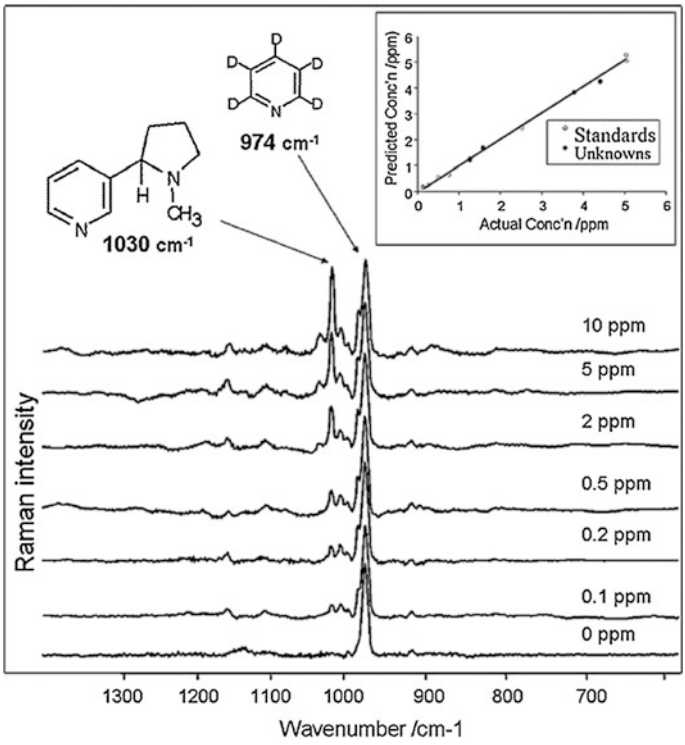

Fig. 4.2 Internal standard in SERS quantitative analysis: SERS assay for nicotine (structure shown *top left*) using polymer-stabilized Ag colloid. Spectra are normalized to the intensity of the 974 cm^{-1} band of the d5-pyridine internal standard. Linearized calibration data from the spectra are shown in the *inset* (adapted with permission from Bell and Sirimuthu 2004. Copyright 2004 The Royal Society of Chemistry)

different concentrations of 1,4-phenylene diisocyanide as a target analyte and 4-MBA as an intensity standard (Shen et al. 2015). The results clearly demonstrated that the SERS signal of the embedded 4-MBA can effectively correct the signal fluctuation as a result of the different aggregation states and measuring conditions. Moreover, the quantitative analysis of target molecule over a large concentration range was shown with a linear response of the relative SERS intensity versus the surface coverage. It enabled a reliable quantitative SERS analysis of targets with different affinities to the surface (Shen et al. 2015). The flexibility in choosing the Raman probe, the core and shell (materials, size and shape), can make this method applicable for the quantitative SERS detection of a wide variety of targets. Such core-molecule-shell NPs exhibited stable and strong SERS signals and can be used as SERS tags for SERS analysis and imaging.

In the case of microfluidic devices, the implementation of the SERS-active internal standard can compensate for the influence of the properties of the colloidal NPs on the SERS signal of analyte. März and co-workers showed that the

integration of an isotopically labelled internal standard for studied analytes (nicotine and pyridine) in the liquid-liquid two phase segmented flow led to reproducible and comparable SERS spectra independent from the introduced colloid (März et al. 2009). Later, the same group demonstrated a new concept of calibrating SERS spectra of the model analyte adenine measured by using of a lab-on-a-chip device without using an internal standard (Kämmer et al. 2014). In order to simulate varying measuring conditions, two batches of Ag colloids and two different laser powers (25 or 55 mW) were utilized. A concentration gradient was generated allowing using the analyte itself for the correction of the resulting SERS spectra regarding intensity deviations caused by different ambient conditions. The designed gradient contained three different steps: analyte, control and zero steps. The gradient scheme consisted of four control steps (of 10 min) with constant concentrations and four steps (of 16 min) with varying concentrations of adenine. Zero steps were short steps without any analyte in the droplet and they were placed between analyte and control steps for better separation. Control steps were used to calibrate the SERS intensity. The introduction of the control steps as normalization factors ensured comparability between measurements on different days and accomplished a noticeable improvement under varying parameters such as the laser power.

4.1.3 Sensitivity and Specificity of SERS Sensor

To characterize sensor systems as an analytical tool, the key parameters to be determined are related to the sensitivity and specificity (or selectivity). The following characteristics would usually be considered in the process of validation: specificity, linearity, accuracy, precision, range, limit of detection (LOD) and limit of quantification (LOQ). In the case of SERS spectroscopy, detection of an analyte can be explored qualitatively by concentration series measurements and obtained dependence fitted by Langmuir adsorption isotherm for instance. A relationship of SERS intensity versus concentration would permit useful information to be extracted. An output fit parameter, the inverse of Langmuir constant, was found to roughly scale with LOD. A plot of SERS intensity versus concentration of dipicolinic acid (DPA) analyte adsorbed on (Au NP)/Au substrate is shown in Fig. 4.3 as an example. There, are two linear regions (a, c) with a transition region (b) (Cheng et al. 2009). It is worth pointing out that in general the resulting data and limits are not universal but are strongly associated with applied instrumental and experimental conditions. Thus, one should focus attention on the methodology procedures that determine LOD and LOQ rather than specific data. To be able to compare SERS capabilities between substrates and also between data obtained in different laboratories, an objective evaluation procedure is needed.

Massarini and co-workers presented four different statistical methodologies to estimate LOD (Massarini et al. 2015) for ten common narcotic drug analytes. First is a general formula to calculate a one-sided prediction interval for the mean value of blanks (LOD_B). LOD_B is determined by extrapolation to the concentration for

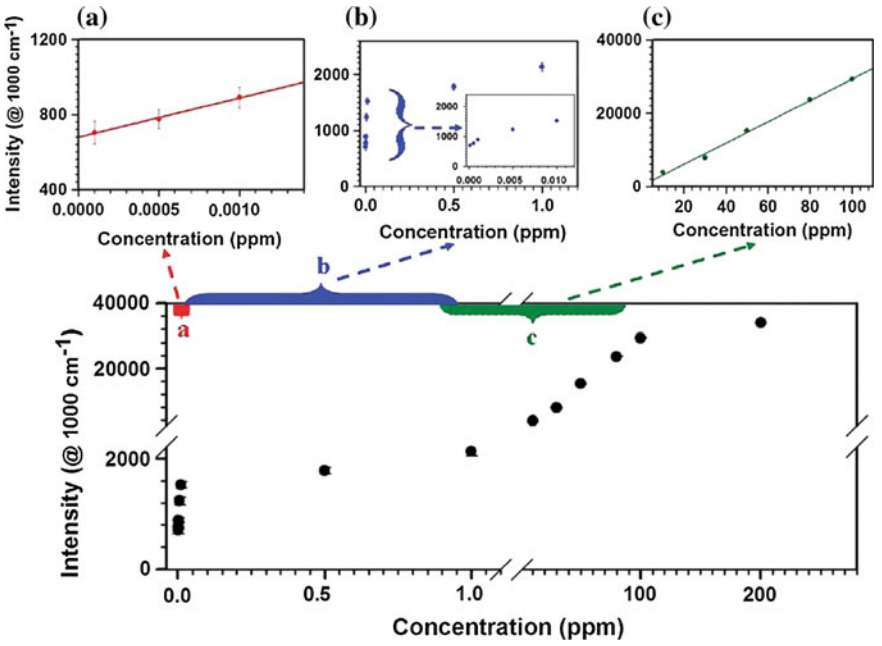

Fig. 4.3 A plot of SERS intensity versus concentration of DPA obtained from (Au NP)/Au substrate with zoomed views of the plot in three concentration regions, **a** $c < 0.01$ ppm, **b** $c < 1$ ppm and **c** $c > 1$ ppm (adapted with permission from Cheng et al. 2009. Copyright 2009 American Chemical Society)

which the SERS intensity of the analyte drops below the triple of the blank signal standard deviation (Thomsen et al. 2003). Second and third methods use a one-sided prediction interval (at significance level 0.05) of a linear regression line, where the obtained LOD in the signal domain was sometimes outside the linear concentration range. Then the corresponding concentration was calculated from a linear calibration curve (LOD_{LR}) or a nonlinear calibration curve (LOD_{NR}). The last one applied receiver operating characteristic (ROC) curves to estimate LOD_{ROC}. ROC analyses enabled determining LOD with only a few data points covering a large concentration range. Two normal probability density functions were computed from a limited set of data. The statistical significance in the signal standard deviation was increased by estimating it as an average over the standard deviation at each analytical concentration. The location of the distribution of analytical signals was interpolated until the area under the curve was larger than a threshold (an arbitrarily limit). When the optimization criterion was obtained, the mean value of the analytical signal was found and a ROC curve was plotted. LOD_{ROC} was then determined at the point in the ROC curve closest to an ideal ROC curve, passing the point [0, 1]. The corresponding concentration was calculated using a calibration curve obtained by fitting Langmuir adsorption isotherm to the data. LOD_{ROC} was always larger than LOD_B but since ROC analysis takes into account signals from

both distributions of blanks and analyte LOD_{ROC} was concluded to be the most reliable one.

Finally, the big challenge of SERS biosensing is how to ensure specificity for an analyte of interest and avoid possible adsorption of another analytes from complex matrix. It can be solved by modifying the metal surface with bifunctional chemical anchors to promote the capture of particular analytes. The anchor molecules bind to the metal surface with one functional group and can then selectively, or even specifically, bind certain analytes on the base of mutual complementarity of their chemical groups. The anchor molecules can control the secondary saturation of the surface by the analyte and, what is more, prevent nonspecific binding at the SERS-active substrate. The compounds which have seen most extensive use as surface modifying agents are various types of thiols. Thiols have a particular advantage in forming a strong covalent bond to Ag and Au surfaces, while SAM can be applied to surfaces by simple immersion in appropriate thiol solutions. This approach was employed to modify both colloids and roughened surfaces. An appropriate mixture of various thiols can even prevent nonspecific adsorption and thus ensure high specificity of the biosensor. To obtain SERS spectrum of target analyte, some multivariate data analysis such as principal component analysis (PCA) should often be applied. The PCA enables an identification of SERS spectra containing different chemical information and separation of the spectral contribution of target analyte from the complex matrix. Suitable functionalization of SERS-active substrate can also help to SERS-inactive analytes without any or with possibly low chemical affinity for the substrate to be detected. Some examples of such approach will be shown later and in Chap. 7 (glucose sensor). Another possibility to the sensing of SERS-inactive analytes is to use an extrinsic SERS detection scheme. In this case, the analyte or interaction of interest is associated with a molecule with an intense and distinguishable Raman signature (Raman reporter molecule—RRM) and its SERS spectrum and not of the analyte is acquired. This detection scheme is mostly applied for biomolecules (see Chap. 5) but some applications for sensing of small molecules were recently reported (see dopamine sensing in next section).

4.2 SERS Sensing of Pharmaceuticals and Drugs

4.2.1 SERS Sensing of Pharmaceuticals

Pharmaceuticals represent an important group of biologically important molecules. SERS is a highly suitable technique for the quality control processes of pharmaceuticals such as identification, final goods, trace impurity detection and in-line process control (Cinta Pinzaru and Pavel 2011).

Various pharmaceuticals including aspirin, paracetamol, antibiotics, antimalarials and anticarcinogenics were studied by SERS on the colloidal NPs (Wang et al.

2003; Cinta Pinzaru et al. 2004; Baia et al. 2008; Cinta Pinzaru et al. 2006; Cinta Pinzaru and Pavel 2011; Aoki et al. 2013). The LODs are between 10^{-3} and 10^{-6} M but the results are not always quantitative (Cinta Pinzaru and Pavel 2011). Water-insoluble pharmaceuticals were studied on solid SERS-active substrates (Smith et al. 2009) or SERS nanotip formed by plastic optical fibre covered by Au NPs (Taguenang et al. 2007). The latter case was used to detect aspirin and paracetamol down to 0.1 pg. Cinta Pinzaru and co-workers introduced Ag NPs to SERS study of antimalarial drugs quinine, chlorquine and mefloquine with the haematin which is a product of degradation of the haemoglobin caused by the malarial parasite (Cinta Pinzaru et al. 2006). Farquharson and co-workers (Farquharson et al. 2005) reported detection of several classes of anticancer drugs extracted from saliva using SERS. This can serve to evaluate the dosage of chemotherapy drugs. The collected saliva was first treated to separate the drugs of interest from the interfering chemical present. Ag NPs and Au NPs in a porous gel structure immobilized in glass capillaries were used as SERS-active substrate. A porous gel structure allowed for the detection of drugs even insoluble in water. This approach needed only 0.5 ml of saliva and took 5 min and the LOD was 150 ng ml^{-1} for anticarcinogenics drug 5-fluorouracil.

Wu and Cunningham developed a new SERS approach for in-line detection, identification and kinetic monitoring of drugs flowing within tubing through the SERS-active surface (Wu and Cunningham 2014). A plasmonic nanodome array surface fabricated using a nanoreplica moulding process upon a flexible plastic substrate served for SERS detection. It was subsequently integrated with a flow cell connecting with ordinary intravenous drug delivery tubing. The authors performed SERS detection of 10 pharmaceutical compounds (hydrocodone, levorphanol, morphine, oxycodone, methadone, phenobarbital, dopamine-DA, diltiazem, promethazine and mitoxantrone). The sensor provided an excellent reproducibility and stability of SERS measurements for periods extending at least 5 days. The dose-dependent SERS signal magnitude resulted in LOD of ng ml^{-1} well below typically administered dosages (mg ml^{-1}). This approach was capable of the continuous monitoring of drug delivery as materials flow through intravenous tubing that was connected in series with the sensor. Moreover, simultaneous detection of multiple drugs from the mixture was possible (Wu and Cunningham 2014). Tang and co-workers introduced a highly sensitive SERS detection of neurotransmitter DA using Au@Ag NRs aptamer-mediated dimers (Tang et al. 2015a). The detection scheme is illustrated in Fig. 4.4a. The DNA-aptamer with specific affinity to DA was used. With the addition of aptamer, the Au NR dimer probe was formed following DNA hybridization. When DA molecules were presented in the solution, the high specific recognition of aptamer and DA caused the dimer to dehybridize and to form single Au NRs. The SERS intensity was proportional to the yield of Au NR dimers in the sensor. Thus, the higher DA concentration, the weaker was the SERS signal. Sensitivity of the sensor was further improved by Ag shell-coating Au NR dimer. A standard RRM (4-ATP) was attached to the Ag shell-coated Au NR dimers and its characteristic peak at 1075 cm^{-1} was used to quantify the DA concentration. The

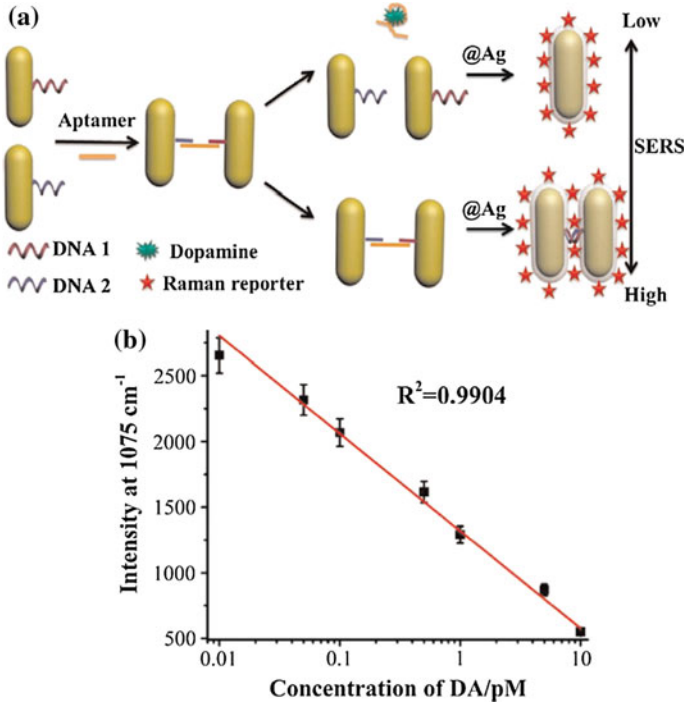

Fig. 4.4 SERS method for dopamine (DA) detection using Au@Ag NR dimers building by aptamer. **a** Detection scheme. **b** The standard curve for the DA detection, where the SERS intensities were calculated at the wavenumber 1075 cm^{-1} of Raman reporter (adapted with permission from Tang et al. 2015a. Copyright 2015 Elsevier B.V.)

linear concentration dependence over the 0.01–10 pM DA concentration range (Fig. 4.4b) and the LOD of 0.006 pM were achieved.

4.2.2 SERS Sensing of Drugs

SERS sensitive detection, identification and quantification of trace amounts of drugs and their uptake in the human body have importance in medical, forensic and criminal investigations. SERS analysis is fast, nondestructive and can be done in situ using a portable Raman spectrometer which is a big advantage when compared with separation and chemical analytical procedures.

SERS using colloidal NPs was successfully applied to the highly sensitive analysis of narcotics (Ryder 2005) as well as of other controlled substances: amphetamines (Sagmuller et al. 2001), cocaine and nicotine (Cinta Pinzaru et al. 2004), codeine, morphine and hydrocodone (Rana et al. 2011). The approach based on Au- and Ag-doped sol-gels immobilized in glass capillaries (Farquharson et al.

2005) was used by the same group to detect eighty drugs of abuse and metabolites including those insoluble in water (Inscore et al. 2011). It was also applied to a number of additional drugs such as amphetamine, diazepam, methadone and cocaine in saliva achieving LOD down to 50 ppb (Inscore et al. 2011). Izquierdo-Lorenzo and co-workers reported the SERS detection of clenbuterol, salbutamol and terbutaline, which can serve to improve performance or induce anabolic effects (Izquierdo-Lorenzo et al. 2010). The purpose of the work was to find the best experimental conditions for SERS detection as an alternative method for antidoping analysis. The adsorption of drug molecules on Ag and Au NPs was more effective at acidic pH owing to the interaction of the aromatic moieties with the metal, leading to LOD down to 10^{-4} M (Izquierdo-Lorenzo et al. 2010). In the work of Mamián-López and Poppi, urinary nicotine was determined in the presence of its metabolite cotinine and the alkaloid on Au NPs (Mamián-López and Poppi 2013). The urine samples were spiked with known amounts of the analyte and added to suspension of Au NPs for SERS analysis. SERS spectra were decomposed using the multivariate curve resolution-alternating least squares (LS) method and pure contributions were recovered. The determination of the alkaloid nicotine was successfully accomplished at concentrations 0.10, 0.20 and 0.30 μg ml^{-1} with a total error values less than 10 %.

The SERS detection sensitivity of drugs on colloidal NPs can be significantly improved by hybrid Au and magnetic NPs (MNPs). Fe_3O_4 magnetic nanocomposites dotted with Au NPs (11 nm diameter) and stabilized with inositol hexakisphosphate were used to rapidly detect trace drug-related biomarkers in saliva and fingerprints (Yang et al. 2015). Scheme of the procedure and SERS spectra of drug-related biomarkers benzoylecgonine (the major metabolite of cocaine) and cotinine (the main human metabolite of nicotine) in saliva with magnetically optimized SERS protocol are shown in Fig. 4.5. 50 μl of saliva containing drug was mixed with NPs, centrifuged and transferred onto aluminium foil (Fig. 4.5a). The MNPs were accumulated in a small spot using a magnet (Fig. 4.5b). SERS spectra from the spot were acquired using a commercial portable Raman spectrometer. The SERS spectra showed a significant increasing of SERS intensity when a magnet was applied (Fig. 4.5c). Through a magnetic field inducing effect, SERS detection of nicotine in aqueous solution was 5 nM. LOD values for magnetically optimized SERS assay, for benzoylecgonine and cotinine in saliva were 29 and 8.8 ppb, respectively. For imaging of latent fingerprint with drug by SERS, fingerprints with drugs were prepared by a clean finger touching a series of concentrations of the drug and then the spiked finger was pressed onto cleaned aluminium foil. The magnetic powder was evenly cast onto the doped fingerprint. A latent fingerprint appeared via moving the magnet under the foil. The fingerprint was then detected by a portable Raman spectrometer. LOD of cotinine in fingerprints was 100 nM (17.6 ng ml^{-1}). In future, it can serve to differentiating drug addicts from casual smokers.

An extraordinarily simple and low-cost analytical technique for SERS drug detection using Ag NPs printed onto paper by a commercial inkjet printer is illustrated in Fig. 4.6 (Yu and White 2013). Ink was formed by standard

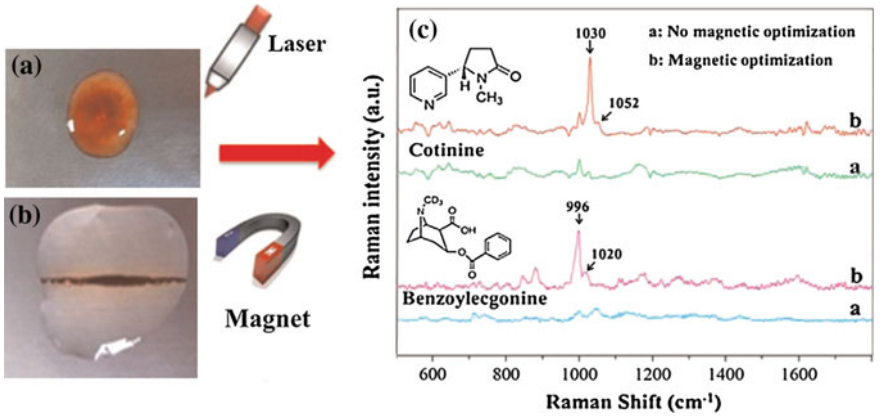

Fig. 4.5 Scheme for the procedure of detection of drug-related biomarkers in saliva with magnetically optimized SERS protocol. **a** Saliva containing drug mixed with MNPs onto aluminium foil. **b** MNPs were accumulated in small spot using a magnet. **c** SERS spectra of cotinine and benzoylecgonine obtained with and without magnetic optimization. *Inset* chemical structures of both compounds (adapted with permission from Yang et al. 2015. Copyright 2015 Elsevier B.V.)

citrate-reduced Ag NPs concentrated 100× by centrifugation and mixed with glycerol and ethanol to optimize the surface tension and viscosity for optimal printing. The ink was added into reusable cartridges and printed 10× onto the desired regions of the paper. In the printing process, NPs in the ink aggregate, formed clusters in the cellulose matrix. After printing Ag NPs onto the paper, individual dipsticks were cut out of the sheet. The entire paper strip can be utilized for sample collection, while the end of the dipstick or swab containing the Ag NPs acts as the SERS-active medium (Fig. 4.6a). For the dipstick experiments, 5 µl of sample (heroin and cocaine dissolved in methanol) was added to the collection zone in a controlled approach to mimic the uptake of analyte onto the paper. For the surface swab experiments, 5 µl of sample was spotted arbitrarily over the surface of a microscope glass slide. After the sample had dried, the SERS-active paper was soaked with methanol and wiped gently but firmly over the glass slide (Fig. 4.6b), while ensuring that the entire swab was in contact with the surface during the swab. In both cases, after the dipstick or swab had dried, it was placed into a vial (Fig. 4.6c) containing 2 ml of methanol which is quickly wicked up into the dipstick or swab toward the detection tip. After 20 min of run time, the dipstick or swab was allowed to dry and the detection zone was scanned to determine the strongest SERS signal. This was repeated for five separate trials, giving a total of five SERS measurements for each analyte concentration. A portable spectrometer (785 nm excitation) with a fibre optic Raman probe was used for SERS detection (Fig. 4.6d). By use of the lateral flow concentration, the authors achieved LOD as low as 15 ng of cocaine and 9 ng of heroin. Although these detection limits are already comparable to many rigid SERS substrates, their approach is much simpler when compared to conventional SERS substrates and traditional microfuidic devices.

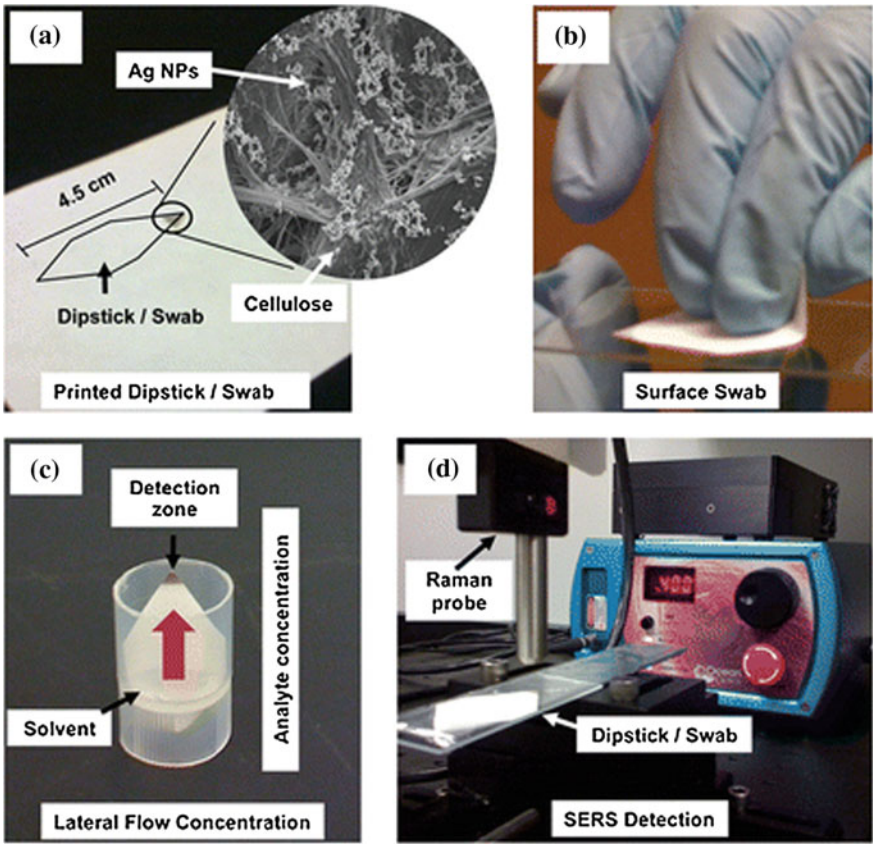

Fig. 4.6 Inkjet-printed paper-based SERS dipsticks and swabs for trace chemical detection. **a** Ag NPs printed onto paper to form a dipstick or swab (*inset* SEM of Ag NPs on paper). **b** Swabbing a surface with the SERS-active swab. **c** Lateral flow concentration by placing the dipstick or swab in a volatile solvent. **d** SERS detection with a portable spectrometer using a fibre optic Raman probe (reproduced with permission from Yu and White 2013. Copyright 2013 The Royal Society of Chemistry)

Au NRs represent other widely used substrates for SERS detection of drugs. Osberg and co-workers reported designing of a new nanosheet material consisting of micrometre-sized, ultrathin and flexible silica sheets with discrete, highly monodisperse 35 nm-diameter Au NRs dimers synthesized by on-wire lithography physically attached to it (Osberg et al. 2012). They are solution-dispersible and can be easily dispensed onto various surfaces while maintaining the geometry of the NR dimers and generate an intense SERS signal. To proof-of-concept experiment designed to illustrate the detection of illicit drugs on a dollar bill they deposited the SERS nanosheets onto the bill to enhance trace detection of benzocaine which is chemically similar to cocaine. The SERS signal was macroscopically addressable, reproducible and strong.

A new rapid method of detection and a direct readout of drugs in human urine was developed using Au NRs and a portable Raman spectrometer (Dong et al. 2015). This method was successfully applied to the detection of the drug methamphetamine in human urine. A classification algorithm called support vector machines model was built for fast identification and visualization of the results. In support vector machines algorithm, an optimal linear classifier is constructed from given set of data with different classes. The form of the classifier is a hyper plane with the maximum margin (the simultaneous minimization of the empirical classification error and maximization of the geometric margin). In the case of data sets that are not linearly separable, also a linear classifier is constructed in the high dimension space by use of the radial basis function. This procedure is equivalent to constructing a nonlinear classifier in the original input space. Furthermore, for those samples (outliers) that are linearly not separated in the high dimension space, the insensitive zone is introduced to make support vector machines less sensitive to the outliers. Since the SERS spectra are of high dimensionality and include invalid information, the PCA was employed to preprocess data with the accumulating contribution rate up 95 %. Prior to construction of support vector machines models, the SERS spectra were linearly scaled such that the intensity values were distributed between 0 and 1. The results indicated that the average classification accuracy of 50, 2.5 and 1 ppm methamphetamine and 3,4-methylenedioxy-methamphetamine in urine was 96.1 and 95.9 %, 95.3 and 95.3 %, 94.2 and 94.0 %, respectively. The detection results were displayed directly without analysis of their SERS spectra manually. Compared with the conventional method in lab, the method only needs a 2 μl sample volume and takes no more than 2 min on the portable Raman spectrometer. It seems that this method will enable rapid, convenient detection of drugs on site for the police.

Forensic analysis of hair evidence is invaluable to criminal investigations. Recently, Korouski and Van Duyne showed that SERS can be applied to detect artificial dyes on hair with a single molecule resolution (Korouski and Van Duyne 2015). A strand of hair coloured with a permanent colourant "Ion Jet Black" was immersed into a solution of Au NRs. SERS spectra were acquired by the 785 nm excitation wavelength. This study reveals that SERS can (i) identify whether hair was artificially dyed or not, (ii) determine if permanent or semipermanent colourants were used and (iii) distinguish the commercial brands that were utilized to dye the hair. Such analysis is rapid, minimally destructive and can be performed directly at the crime scene. They utilized a commercial portable Raman spectrometer to demonstrate that information about hair dye content can be determined in the field.

Yang and co-workers introduced the controlled fabrication of an Ag nanoneedle (of diameter about around 200 nm) and its application in rapid detection of narcotics (Yang et al. 2012). It was found that a SERS EF > 10^{10} could be reproducibly achieved by the nanoneedle array. The nanoneedle array was able to detect ketamine down to 27 ppb through SERS.

4.3 SERS Sensing of Pollutants, Food Contaminants and Food Additives

The monitoring of food contaminants and additives in water and/or in food/drink samples is nowadays another wide SERS bioanalytical application. The most common targets in the foods that are studied using SERS include pesticides, antibiotics and illegal drugs as well as food colourants, foreign allergenic or toxic proteins and heavy metals. Chemical contaminants involve mainly agricultural and environmental, chemical adulterants, mycotoxins and foreign food components. Food additives are substances that become part of a food product when added during the processing or preparation of that food. They include preservatives, colourants, flavours and flavour enhancers, texture modifiers, nutrients and others. Several techniques, such as chromatography, spectrophotometry and electrochemical methods, are commonly used but most of them are expensive and require sophisticated instruments and time-consuming complex sampling processes. SERS spectroscopy can provide cheap, fast and sufficiently specific and sensitive detection technique. The SERS sensing of pollutants and food contaminants and additives is summarized in recent reviews (Zheng and He 2014; Li et al. 2014) and only some examples will be introduced in this section.

4.3.1 SERS Sensing of Pollutants and Pesticides

SERS molecular sensing from a complex matrix can be hampered by poor efficiency and selectivity of the SERS surface to capture the target analyte and functionalization of the metal surface with selective coatings should often be applied. It is the case for instance of extremely hazardous pollutants, strongly carcinogenic polyaromatic hydrocarbons, which are mainly formed during the incomplete combustion of coal, oil and gas as well as tobacco. Polyaromatic hydrocarbons (such as coronene, pyrene or triphenylene) contain condensed benzene rings without any functional groups and thus they have a very low affinity for Ag or Au surfaces. Employment of host-guest interaction was found to be a successful concept for their SERS detection (Guerrini et al. 2009; Guerrini et al. 2011). The surface of hydroxylamine-reduced Ag NPs was functionalized with a dithiocarbamate calixarene host conjugate. It allowed not only the capturing of a guest molecule but also the formation of a "hot spot" in the interparticle junction when two host-functionalized Ag NPs provided high SERS response. Thus, this approach was both highly specific as well as highly sensitive. Figure 4.7 shows a host-guest complex formation in the case of a coronene molecule as a guest. The LOD ranged from 10^{-8} M (2 ppb) in the case of pyrene and triphenylene to 10^{-10} M (30 ppt) for coronene. Although these LODs were similar to those obtained by standard chromatography and fluorometry, no preconcentration step was necessary in the case of SERS analysis. Thus, the advantage of SERS using the calixarene-functionalized

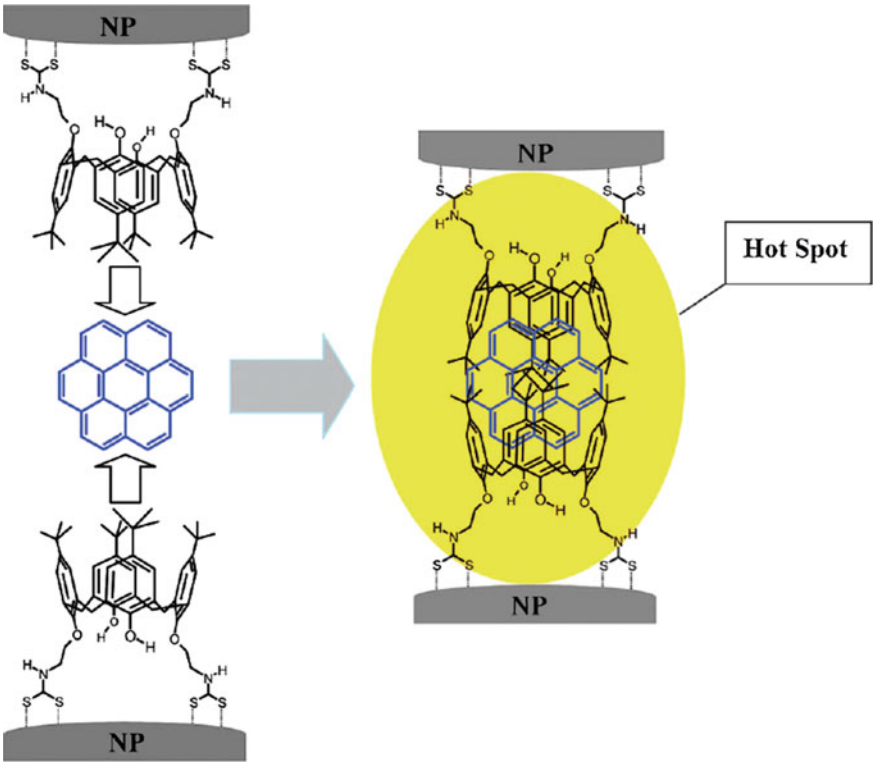

Fig. 4.7 Sensing polycyclic hydrocarbons ("guests"; coronene) by SERS in a "hot spot" by using Ag NPs functionalized with dithiocarbamate calixarene "host" conjugate (reproduced with permission from Guerrini et al. 2009. Copyright 2011 American Chemical Society)

Ag NPs was the possibility of detecting the polyaromatic hydrocarbons mixtures or multicomplex system without any pretreatment (Guerrini et al. 2011).

Recently, another host-guest approach was applied to detection of the poisoned organochlorine pesticides aldrin, dieldrin, lindane and α-endosulfan—often water contaminants (Kubackova et al. 2015). In order to overcome the inherent problem of the low affinity of these molecules, the authors developed a strategy consisting of functionalization of the metal NP surface with alkyl dithiols. This process again induced the NP linkage between metallic NPs to obtain high SERS enhancement from "hot spot" sites and to create a specific environment in the nanogaps making them suitable for the assembly of the analysed pesticides. An optimization of this approach was performed by varying the type of metallic NPs, molecular linker (aromatic versus aliphatic dithiols and the length of the intermediate chain), surface coverage, laser excitation wavelength, etc. The LOD of the organochlorine pesticides obtained by this approach down to 10^{-8} M were comparable to those determined by other techniques. However, the SERS detection offers the advantage

of a direct analysis of samples which does not necessitate the sample pretreatment required by other techniques.

The toxicity of pesticides is in the order of 50 mg kg^{-1} in the case of oral exposure according to the United States Environmental Protection Agency. Thus, the detection of such substances in food or drinks is necessary. Many examples of successful SERS detection of pesticides in concentration as little as nM can be found in literature (Aoki et al. 2013; Craig et al. 2013; Zheng and He 2014; Li 2010; Li et al. 2014). Detection of pesticides in real-food matrices involved more studies on sample extraction and optimization for SERS analysis. In the case of liquid food matrices, the analyte is extracted, mixed with metallic NPs or deposited on solid nanostructural substrate for SERS detection. Gao and co-workers reported rapid and highly sensitive trace analysis of the herbicide paraquat in water using a SERS-based microdroplet sensor with LOD about 2×10^{-9} M (Fig. 4.1) (Gao et al. 2010). A recyclable SERS-active substrate based on TiO_2 nanotube arrays coated with Au NPs was applied for the detection of herbicide 4-chlorophenol and the pesticide methyl-parathion (Li et al. 2010b). The substrates were cleaned by means of a photodegradation of the target molecules under UV irradiation. The possibility of repeated use of the same substrate for further analysis is very important because it can solve the problem of spectral irreproducibility of various batches of substrates and thus improve reliability of SERS analysis (Li et al. 2010b). Yu and White reported a new SERS substrate—Ag NPs entrapped in filter membranes—for sensitive pesticide detection (Yu and White 2012). First, the Ag NPs and next, the solution containing the target analyte were passed through the membrane. This procedure enabled the detection of the pesticide malathion in a concentration of ~60 ppb (Yu and White 2012). Recently, Deng and co-workers employed opto-fluidic microsystem with SERS-active quasi-3-dimensional gold plasmonic nanostructure arrays for sensitive and reproducible detection of malathion (Deng et al. 2015). Highly reproducible SERS signals (RSD less than 5 %) were obtained at low concentrations from 0.01 to 10 ppm. By increasing the flow rate, SERS signals increased rapidly which greatly enhanced the detection efficiency. In addition, the detection sensitivity was improved one order of magnitude to 0.001 ppm when the flow rate was increased tenfold to 0.3 ml min^{-1}.

For solid matrices like apples, homogenization of the peel or surface swab methods were used to recover pesticides on the surface. For example, homogenization extracted 3 types of pesticides (carbaryl, phosmet and azinphos-methyl) from apple and tomato peels and then their SERS spectra were obtained using a commercial SERS substrate (Liu et al. 2013). A widely used way to extract target pesticide from real matrix is pretreatment by an organic solvent. Zhang and co-workers detected carbaryl pesticide from a cabbage (Zhang et al. 2015). Here, the cabbage sample was spiked with a series of concentrations of carbaryl. Carbaryl was extracted from the cabbage by mixing with an organic solvent (acetonitrile). The mixture was then vigorously shaken and centrifuged. A drop of supernatant was placed on the SERS-active substrate formed by assembled Au NRs on Au-coated silicon slide and the SERS spectrum was measured. Results demonstrated that the actual concentrations of carbaryl in the cabbage were linearly

correlated with the concentrations predicted by the multiple linear regression models ($R > 0.97$). The LOD of carbaryl was about 2.5 ppm, meeting the maximum residue limits set by the United States Environmental Protection Agency (Zhang et al. 2015). Fang and co-workers developed a rapid, low-cost and nondestructive method to achieve the quantitative detection of the pesticide residues on fruit skins (Fang et al. 2015). A slice of pear or apple skin was first cut and cleaned using ethanol and deionized water. Then a paraquat solution with a certain concentration was sprayed onto the cleaned peels until the liquid got together and ran down. This piece of peel was spread onto a slide glass, followed by spraying the Ag colloidal NPs to cover its surface after the paraquat solution completely evaporated at room temperature. When the colloid nearly dried, the Ag NPs were located at the surface and SERS spectrum of the paraquat was acquired. The LOD of paraquat on the peels of pears and apples was in the order of 10^{-9} M, much lower than the maximum residue limit of 0.05 mg kg^{-1} ($\sim 10^{-4}$ M) in a large number of countries including the USA and China.

In situ detection of pesticides on the surface (such as fruit peel) was also reported. An additional advantage of SERS is that fluorescence from the molecules present in matrix is efficiently quenched in the proximity of metallic NPs. For example, Li and co-workers used the Au SHINs dispersed onto the clean and contaminated spot of an orange (Li et al. 2010a). Then, SERS spectra were acquired clearly showing two bands assigned to the pesticide parathion. The same result was obtained using a portable Raman instrument, suggesting that this technique could be simple to use, field portable and cost-effective for this type of analysis. Liu and co-workers detected sulphur-containing pesticides in apple, grape, pear, mango and peach peels (Liu et al. 2012). They prepared Au NPs coated with Ag shell of various thicknesses (Au@Ag NPs). The Au@Ag NPs were directly spread onto the fruit peels, taking advantage of the fact that pesticide residues either adsorb on the surface of the fruit peel or permeate into the peel. The first step was using ethanol droplet, which is a simple extraction procedure to increase the analyte concentration at the peel surface. Then, the Au@Ag NPs were deposited on the same spot and the SERS signal recorded. LODs depending on fruits were found to be in the order of ng cm^{-2} for thiram and mg cm^{-2} for chlorpyrifos and methyl parathion pesticides.

Recently, Au NRs coated Fe_3O_4 (Fe_3O_4@NRs) were used for SERS detection of pesticide thiram (Tang et al. 2015b). The procedure is illustrated in Fig. 4.8. A thiram solution was sprayed on the apple peel (a) and then Fe_3O_4@NRs suspension was spread on the peel (b). Fe_3O_4@NRs were transferred from the contaminated apple peel to a glass slide with the aid of the external magnetic field (c) and SERS spectra were measured using portable Raman spectrometer and 785 nm excitation (d). Thiram pesticide was detected in concentration as low as 1×10^{-7} M. However, the SERS spectrum of thiram collected by the different spectrometers showed a slight deviation and the authors declared their approach is more qualitative than quantitative (Tang et al. 2015b). A semiquantification procedure was established based on 4 reference concentrations in a layman's format: "No risk" (0 ppm), "Low risk" (4 ppm), "Risk" (7 ppm) and "High risk" (14 ppm) according to the United States Environmental Protection Agency tolerance levels

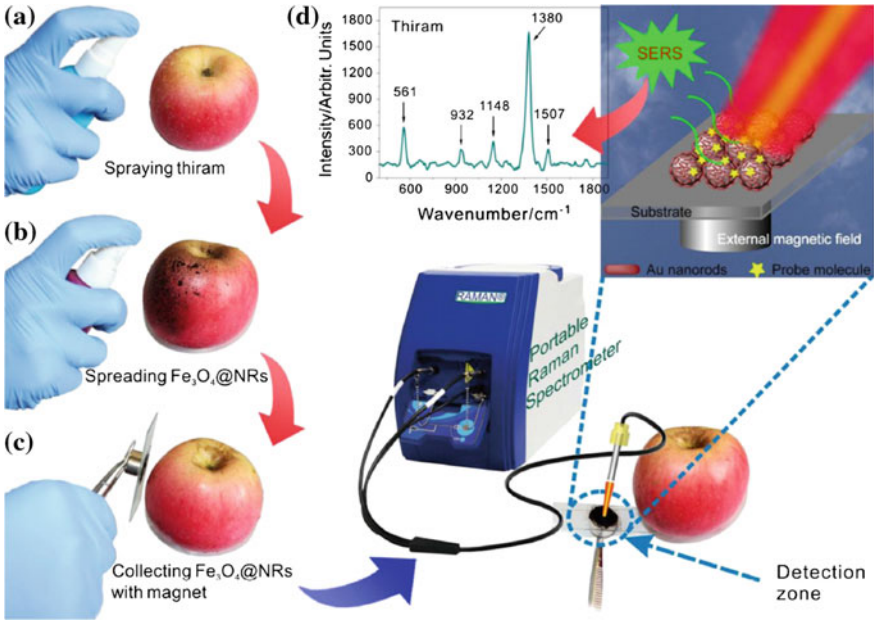

Fig. 4.8 In situ SERS detection of pesticide thiram using (Fe_3O_4@NRs). **a** Thiram solution was sprayed on apple peel. **b** Fe_3O_4@NR suspension was spread on apple peel. **c** Fe_3O_4@NR microspheres were transferred from contaminated apple peel to glass slide with the aid of the external magnetic field. **d** The spectrum of thiram was collected by portable Raman spectrometer (reproduced with permission from Tang et al. 2015b. Copyright 2015 John Wiley & Sons, Ltd)

for ferbam on fresh produce (Zheng et al. 2013). SERS spectra acquired using Ag dendrites and hand-held Raman spectrometer had good reproducibility and sensitivity. This built-in selectivity method was able to accurately semiquantify the results without showing the spectrum.

Some authors reported the combination of SERS with the separation methods (Hobro and Lendl 2011). For example, Carrillo-Carrión and co-workers reported a combination of liquid chromatography (LC) and SERS on Ag-quantum dots sponge shaped structures for pesticide identification (Carrillo-Carrión et al. 2012). A microdispenser was used as a method for the separation, identification and quantification of various pesticides, such as chlortoluron, atrazine, diuron and terbuthylazine. SERS spectra were collected from spots at different amounts injected in the LC column. Very low LODs between ~10 and 20 pg were achieved.

Peng and co-workers developed a facile strategy to assemble the vertically aligned monolayer of cetyltrimethylammonium bromide (CTAB) coated Au NRs with a 0.8 nm gaps and demonstrated their applications in the rapid trace detection of plasticizers in drinks (Peng et al. 2013). Plasticizers are carcinogen phthalate compounds presented in plastic containers or piping and can easily contaminate drinks. In the testing experiment, a commercial orange juice sample was mixed with

two phthalate plasticizers benzylbutylphthalate and bis(2-ethylhexyl)phthalate ethanol solution so their actual concentration was ~0.9 fM. 10 μl mixture solution was dropped on vertical Au NR arrays Si substrate. After ethanol totally evaporated, the SERS signal was recorded. The highly organized vertical arrays provided reproducible SERS signal of the benzylbutylphthalate and bis(2-ethylhexyl)phthalate. Moreover, both compounds can be distinguished unambiguously, although they provided some similar Raman fingerprints with vitamin C and carotene from orange juice. The LOD ~0.9 fM of plasticizers is the lowest LOD reported to date, which is 7 orders of magnitude lower than the standard of United States.

4.3.2 SERS Sensing of Melamine

Melamine (2,4,6-triamino-1,3,5-triazine) is added to the food to elevate the measured protein content. A tolerance level for melamine is 1 ppm for infant formula and 2.5 ppm (2500 ppb, equivalent of 0.02 mmol l^{-1} or 2.5 mg l^{-1}) for milk and other food products. Melamine was found as an adulterant in pet foods in 2007 in North America and in milk products in 2008 in China. The melamine is one of the most common food additives studied by SERS because of its distinct sharp peaks and emerging safety concern.

Various SERS substrates demonstrated their sensitivity and quantification ability for melamine analysis including Ag and Au NPs and commercial Klarite® substrate. Most of the substrates have exhibited great sensitivity at 10^{-7}–10^{-8} M for melamine detection, even in food products in some cases (Zheng and He 2014). Lin and co-workers detected the added melamine content in chicken, wheat gluten, home-baked cakes and noodles (Lin et al. 2008). Melamine was extracted from the matrix and deposited on a commercial Klarite® SERS-active substrate. PCA was performed and a high prediction capability was obtained. LOD ranged between 50–100 μg g^{-1} (Lin et al. 2008). Using Au NPs and a portable Raman spectrometer, Mecker and co-workers detected melamine content in a wide variety of solid matrices, including milk powder, infant formula, lactose, povidone, whey protein, wheat bran and wheat gluten. Detectable concentrations of melamine ranged from 100–200 μg l^{-1} (100–200 ppb) depending on the sample matrix (Mecker et al. 2012). Concerning liquid milk, Giovannozzi and co-workers achieved limits of 0.17 mg l^{-1} (LOD) and 0.57 mg l^{-1} (LOQ) using standard Au NPs (Giovannozzi et al. 2014). Ag NPs provided even lower values, for example, Zhang and co-workers obtained LOD = 0.01 mg l^{-1} (10 ppb) and LOQ = 0.5 mg l^{-1} (500 ppb) of melamine in liquid milk with the RSD of ≤10 % (Zhang et al. 2010). These methods did not require a long extraction procedure (total analysis time can be less than 30 min). Kim and co-workers reported LOD of the melamine about 100 ppb in infant formula (Kim et al. 2012). It was achieved with a portable sensor system equipped with a high-performance gold nanofinger SERS sensor chips and a custom-built prototype portable Raman spectrometer. Recently, Hua and co-workers developed a novel biosensor of melamine in whole milk combining

molecularly imprinted polymers and SERS (Hu et al. 2015). Molecularly imprinted polymers were synthesized by bulk polymerization of melamine (template), methacrylic acid (functional monomer), ethylenglycol dimethacrylate (cross-linking agent) and 2,2'-azobisisobutyronitrile (initiator). The efficient separation and extraction of melamine from whole milk can be achieved this way. Ag dendrite nanostructure served as SERS-active substrate for SERS detection. PCA was applied to segregated Raman spectrum of whole milk samples with different melamine concentrations. The LOD and LOQ were 0.012 and 0.039 mmol l^{-1}, respectively. Full analysis time to determine melamine in whole milk was less than 20 min.

Most of the previous SERS analysis required some pretreatment methods to extract melamine from real matrix. Betz and co-workers developed the fast SERS approach for detecting melamine in infant formula without the need for purification or additional equipment (Betz et al. 2012). For this purpose, a galvanic displacement of Cu by Ag was used to create Ag nanostructures on low-cost surfaces of Cu tape and coin and excellent SERS enhancement was obtained. A strong peak between 676 and 690 cm^{-1} was observed and served to identify melamine contamination of the formula. Both the tape and coin enabled the detection of contamination down to the 5 ppb level which is up to 200× better than that using commercial Klarite® substrates.

It is necessary to mention that the majority of SERS detection of melamine are more associated with qualitative than quantitative analysis. This is caused by poor spectral reproducibility of the SERS substrates, variation in the adsorption of analyte to the substrate (especially in the case of a dried drop) and the lack of internal standard to eliminate variation of experimental conditions. A new droplet detection configuration was developed to simplify and optimize the detection of melamine in milk using Ag NPs (Lin et al. 2014). A hydrophobic aluminium tape was employed as the supporting platform for a droplet of (Ag NPs)/milk sample. Under this configuration, melamine in milk can be quantitatively detected without any sample pretreatment. The SERS signal was distributed regularly over the wet droplet area and provided better reproducibility compared with the dried droplet configurations. The characteristic peak at 925 cm^{-1} in blank spectrum (milk without Ag NPs) was selected as an internal standard. The LOQ using this approach was 0.05 ppm with a RSD of 7.5 % (Lin et al. 2014). Guo and co-workers designed a SERS chip fabricated with self-assembled hollow Au NPs on the poly(diallyldimethylammoniumchloride)-coated glass wafers through electrostatic interaction (Fig. 4.9a) for quantitative detection of melamine in milk (Guo et al. 2014). This simple detection procedure did not need pretreatment or separation steps except of centrifugation. Here, the chip was immersed in milk with different percentage of melamine for 2 min. Then, the chip was rinsed with water and dried with nitrogen gas. Then SERS spectra were recorded (Fig. 4.9b). The position of the characteristic SERS peak at 712 cm^{-1} of melamine was used to distinguish it from other kinds of proteins or amino acids and its intensity served to monitor the percentage of melamine in milk (Fig. 4.9c). A LOD was 1 ppm and the deviation of melamine detection by this chip was 2.85 %.

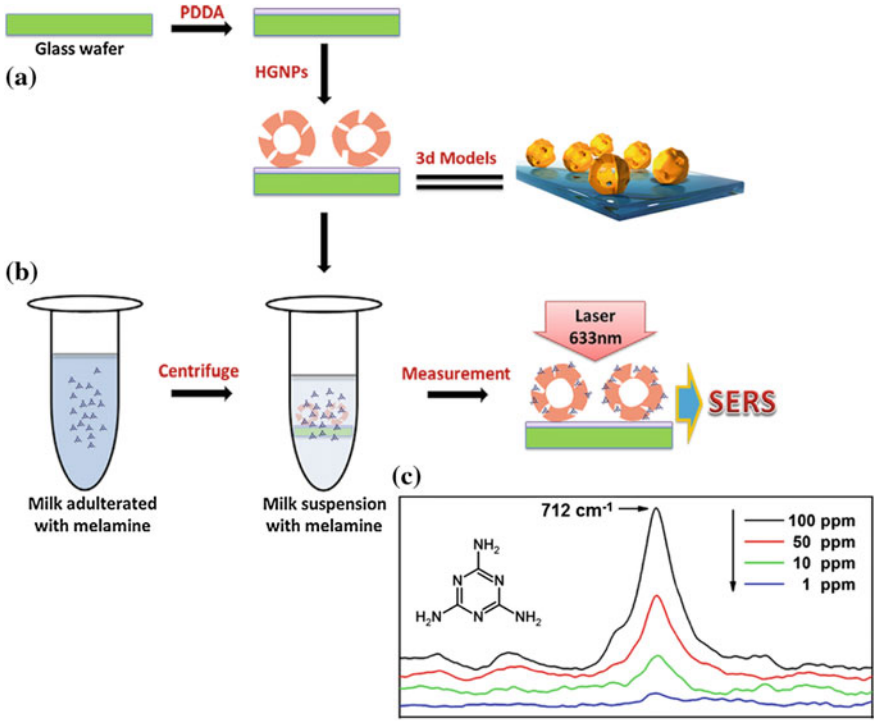

Fig. 4.9 SERS detection of melamine from milk. **a** Fabrication of hollow Au NPs chip. **b** Detection of melamine from real milk sample. **c** SERS spectra of melamine obtained using the chip. *Inset* chemical structure of melamine (adapted with permission from Guo et al. 2014. Copyright 2014 Elsevier B.V.)

Zhou and co-workers developed a new strategy for quantitative detection of melamine in milk based on Au@Ag NPs with 4-ATP as the internal reference (Zhou et al. 2015). The internal reference is embedded between Au core and Ag shell while the target analyte is outside of the Ag shell. For melamine detection, the milk samples containing different amounts of melamine were mixed with Au@4-ATP@Ag NPs and SERS spectra were taken. Two distinct peaks, 1075 and 700 cm^{-1}, associated with 4-ATP and melamine, respectively, were chosen for quantitative analysis. A strong correlation between their intensity ratio and the melamine concentration was observed. This allowed an amount of melamine in milk to be determined down to 5 μM concentration.

4.3.3 SERS Sensing of Food Colourants

Food colourants (synthetic or natural) are added to food and drinks to increase their visual attractiveness to consumers and to restore their original appearance when it

has been lost during production processes. However, some of the additive colourants are toxic or carcinogenous and represent a potential risk to human health, especially in the case of excessive consumption. For that reason, the presence of synthetic colourants in foods and drinks is rigidly controlled by legislation in many countries. Widely used food colourants are Sudan dyes, Ponceau 4R, tartrazine and azorubine.

Sudan I dye was extracted from chilli powder and detected using Au NPs in concentration as low as 48 ng in 1 g of powder (Cheung et al. 2010). Recently, Jahn and co-workers employed enzymatically generated Ag NPs prepared by a bottom-up and self-organizing procedure (see Sect. 3.4.2.1), in combination with a lipophilic sensor layer for the detection of water-insoluble azo-dye Sudan III in real food matrix, paprika products (Jahn et al. 2015). The surface modification consisted of self-assembled aliphatic hydrocarbons with a thiol moiety forming hydrophobic monolayer on the SERS substrate. The resulting layer repelled unwanted water-soluble analytes from the surface whereas water-insoluble ones were adsorbed and detected by SERS. The riboflavin was introduced as a water-soluble competitor, which is part of the relevant food matrices. Sudan III dye was detected down to 9 μmol l^{-1} concentration from paprika powder extract in the methanol. Beside this, lipophilic sensor layer can also be applied for further analytical tasks for which it is beneficial to discriminate water-soluble from insoluble substances.

Azorubine (known as E 122) is a permitted red food colourant with a maximum use level up to 50–500 mg kg^{-1} in the EU. Specifically, it is tolerated in nonalcoholic flavoured drinks at levels up to 50 mg l^{-1} and in alcoholic drinks up to 200 mg l^{-1}. Recently, we developed in collaboration with Popp group a fast and simple quantitative analysis of the azorubine in different types of beverages using SERS (Peksa et al. 2015). Seven commercially available sweet drinks with high levels of complexity (sugar/artificial sweetener, ethanol content, etc.) were tested: five with expected positive azorubine contents (energy drink, grenadine, raspberry lemonade, strawberry vodka and passion fruit vodka) and two red-coloured negative controls without azorubine (blood orange lemonade and raspberry syrup). The procedure is schematically illustrated in Fig. 4.10. Highly uniform Au FON substrates together with the use of Raman signal from silicon support as internal intensity standard enabled to determine quantitatively the concentration of azorubine in each sample. The treatment of the drink samples for SERS measurement included only 1:5 dilution with distilled water. The Au substrates were then incubated in the samples for 30 min before the SERS spectra were measured. Thus, this SERS approach is a simple and rapid (35 min) prescan method, which can be easily implemented for a field application and for preliminary testing of food samples. SERS spectra of all five positive samples clearly showed the azorubine Raman bands without any spectral interference from other additives in the drink. SERS spectral analysis provided sufficient sensitivity (0.5–500 mg l^{-1}) and determined azorubine concentration in positive samples closely correlated with those obtained by standard HPLC technique.

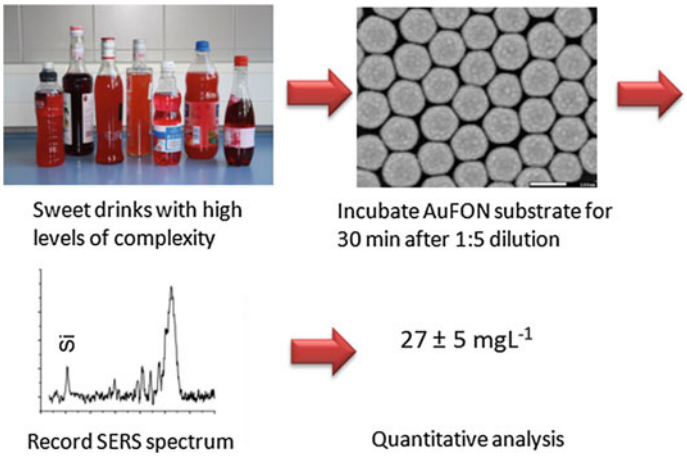

Fig. 4.10 Quantitative analysis of the azorubine in different types of beverages using SERS. Si-silicon peak used for intensity normalization (reproduced with permission from Peksa et al. 2015. Copyright 2015 American Chemical Society)

4.4 SERS Identification of Biowarfare Agent Anthrax

The detection of DPA, a biomarker for bacterial spores such as *Bacillus anthracis*, a biowarfare agent, is another interesting example of SERS sensing. A pioneer work by Van Duyne and co-workers was reported using Ag FON as SERS-active substrates (Haynes et al. 2005; Zhang et al. 2005a). The diameter of nanospheres and the thickness of the metal layer were optimized for particular excitation in SERS experiment. In this case, Ag FON substrates were optimized for 750 nm Ti:sapphire laser excitation and combined with a battery-powered portable Raman spectrometer. Calcium dipicolinate, a biomarker for *Bacillus* spores, was detected by SERS over the spore concentration range of 10^{-14}–10^{-12} M. Overall, using an 11 min procedure with a 1 min data acquisition time, their platform was capable of detecting $\sim$2600 anthrax spores, well below the anthrax infectious dose of $\sim$10,000 spores. Importantly, the shelf life of prefabricated Ag FON substrates in air exceeded 40 days. Their next step was to chemically functionalize the Ag surface to enhance the analyte binding affinity as well as the stability of substrates (Zhang et al. 2005b). The Ag FON substrates were coated with a 1 nm alumina layer deposited by atomic layer deposition, which serves to stabilize the Ag surfaces of Ag FON. DPA displays strong binding to the alumina-modified Ag FON surface and this strong affinity for carboxylate groups makes the alumina-coated Ag FON substrate an ideal candidate for *Bacillus* spores detection. The LOD was further improved to 1400 spores with a 10 s data collection time. More importantly, the alumina overlayer dramatically increased the shelf life of prefabricated substrates to at least 9 months. Although the controlled deposition of 1 nm thick alumina films is

not a trivial task, atomic layer deposition facilitates fabrication of functionalized SERS substrates while simultaneously protecting the metal surface against unwanted oxidation or environmental contamination.

Later, different kinds of SERS substrates were used in DPA detection such as (Au NP)/polyvinylpyrrolidone(PVP)/Au nanostructures (Cheng et al. 2009). The correlation between the SERS intensity and the DPA concentration (0.1 ppb to 100 ppm) was shown to exhibit two linear regions, i.e., the low (<0.01 ppm) and high concentration (>1 ppm) regions, with an intermediate region in between (see Fig. 4.3). The presence of a linear relationship in the low-concentration region was observed for the first time in SERS detection of DPA. LOD was 0.1 ppb (Cheng et al. 2009). Konrad and co-workers prepared metal-like liquid films (MELLFs) when Ag colloid was shaken with CH_2Cl_2 in the presence of a "promoter" such as 10^{-4} M tetrabutylammonium nitrate (Konrad et al. 2013). If MELLF is formed in the presence of analyte (DPA), SERS spectra of DPA can be obtained with LOD < 8 ppm and excellent reproducibility (RSD was 1.1 %).

References

P.H.B. Aoki, L.N. Furini, P. Alessio, A.E. Aliaga, C.J.L. Constantino, Surface-enhanced Raman scattering (SERS) applied to cancer diagnosis and detection of pesticides, explosives, and drugs. Rev. Anal. Chem. **32**, 55 (2013)

M. Baia, S. Astilean, T. Iliescu, *Raman and SERS Investigations of Pharmaceuticals* (Springer, Berlin, 2008)

S.E.J. Bell, N.M.S. Sirimuthu, Rapid, quantitative analysis of ppm/ppb nicotine using surface-enhanced Raman scattering from polymer-encapsulated Ag nanoparticles (gel-colls). Analyst **129**, 1032 (2004)

S.E.J. Bell, N.M.S. Sirimuthu, Quantitative surface-enhanced Raman spectroscopy. Chem. Soc. Rev. **37**, 1012 (2008)

S.E.J. Bell, A. Stewart, Quantitative SERS methods, in *Surface Enhanced Raman Spectroscopy: Analytical, Biophysical and Life Science Applications*, ed. by S. Schlücker (Wiley, Weinheim, 2011), pp. 71–86

J.F. Betz, Y. Cheng, G.W. Rubloff, Direct SERS detection of contaminants in a complex mixture: rapid, single step screening for melamine in liquid infant formula. Analyst **137**, 826 (2012)

R.J.C. Brown, M.J.T. Milton, Nanostructures and nanostructured substrates for surface-enhanced Raman scattering (SERS). J. Raman Spectrosc. **39**, 1313 (2008)

C. Carrillo-Carrión, B.M. Simonet, M. Valcárcel, B. Lendl, Determination of pesticides by capillary chromatography and SERS detection using a novel silver-quantum dots "sponge" nanocomposite. J. Chromatogr. A **1225**, 55 (2012)

H.W. Cheng, S.Y. Huan, H.L. Wu, G.L. Shen, R.Q. Yu, Surface-enhanced Raman spectroscopic detection of a bacteria biomarker using gold nanoparticle immobilized substrates. Anal. Chem. **81**, 9902 (2009)

W. Cheung, I.T. Shadi, Y. Xu, R. Goodacre, Quantitative analysis of the banned food dye Sudan-1 using surface enhanced Raman scattering with multivariate chemometrics. J. Phys. Chem. C **114**, 7285 (2010)

S. Cinta Pinzaru, I.E. Pavel, in *Surface Enhanced Raman Spectroscopy*, ed. by S. Schlücker. SERS and Pharmaceuticals (Wiley, Weinheim, 2011), pp. 129–154

S. Cinta Pinzaru, I. Pavel, N. Leopold, W. Kiefer, Identification and characterization of pharmaceuticals using Raman and surface-enhanced Raman scattering. J. Raman Spectrosc. **35**, 338 (2004)

S. Cinta Pinzaru, N. Peica, B. Küstner, S. Schlücker, M. Schmitt, T. Frosch, J.H. Faber, G. Bringmann, J. Popp, FT-Raman and NIR-SERS characterization of the antimalarial drugs chloroquine and mefloquine and their interaction with hematin. J. Raman Spectrosc. **37**, 326 (2006)

A.P. Craig, A.A. Franca, J. Irudayaraj, Surface-enhanced Raman spectroscopy applied to food safety. Annu. Rev. Food Sci. Technol. **4**, 369 (2013)

R.D. Deegan, O. Bakajin, T.F. Dupont, G. Huber, S.R. Nagel, T.A. Witten, Capillary flow as the cause of ring stains from dried liquid drops. Nature **389**, 827 (1997)

Y. Deng, M.N. Idso, D.D. Galvan, Q.M. Yu, Optofluidic microsystem with quasi-3 dimensional gold plasmonic nanostructure arrays for online sensitive and reproducible SERS detection. Anal. Chim. Acta **863**, 41 (2015)

R.L. Dong, S.Z. Weng, L.B. Yang, J.H. Liu, Detection and direct readout of drugs in human urine using dynamic surface-enhanced Raman spectroscopy and support vector machines. Anal. Chem. **87**, 2937 (2015)

H. Fang, X. Zhang, S.J. Zhang, L. Liu, Y.M. Zhao, H.J. Xu, Ultrasensitive and quantitative detection of paraquat on fruits skins via surface-enhanced Raman spectroscopy. Sens. Actuators B **213**, 452 (2015)

S. Farquharson, C. Shende, F.E. Inscore, P. Maksymiuk, A. Gift, Analysis of 5-fluorouracil in saliva using surface-enhanced Raman spectroscopy. J. Raman Spectrosc. **36**, 208 (2005)

K. Faulds, W.E. Smith, D. Graham, R.J. Lacey, Assessment of silver and gold substrates for the detection of amphetamine sulfate by surface enhanced Raman scattering (SERS). Analyst **127**, 282 (2002)

R. Gao, N. Choi, S.I. Chang, S.H. Kang, J.M. Song, S.I. Cho, D.W. Lim, J. Choo, Highly sensitive trace analysis of paraquat using a surface-enhanced Raman scattering microdroplet sensor. Anal. Chim. Acta **681**, 87 (2010)

A. Gift, C. Shende, F.E. Inscore, P. Maksymiuk, S. Farquharson, Five-minute analysis of chemotherapy drugs and metabolites in saliva: evaluation dosage. Proc. SPIE **5261**, 135 (2004)

A.M. Giovannozzi, F. Rolle, M. Sega, M.C. Abete, D. Marchis, A.M. Rossi, Rapid and sensitive detection of melamine in milk with gold nanoparticles by surface enhanced Raman scattering. Food Chem. **159**, 250 (2014)

L. Guerrini, J.V. Garcia-Ramos, C. Domingo, S. Sanchez-Cortes, Sensing polycyclic aromatic hydrocarbons with dithiocarbamate-functionalized Ag nanoparticles by surface-enhanced Raman scattering. Anal. Chem. **81**, 953 (2009)

L. Guerrini, P. Leyton, M. Campos-Vallette, C. Domingo, J.V. Garcia-Ramos, S. Sanchez-Cortes, Detection of persistent organic pollutants by using SERS sensors based on organically functionalized Ag nanoparticles, in *Surface Enhanced Raman Spectroscopy: Analytical, Biophysical and Life Science Applications*, ed. by S. Schlücker (Wiley, Weinheim, 2011), pp. 103–128

Z. Guo, Z.Y. Cheng, R. Li, L. Chen, H.M. Lv, B. Zhao, J. Choo, One-step detection of melamine in milk by hollow gold chip based on surface-enhanced Raman scattering. Talanta **122**, 80 (2014)

C.L. Haynes, C.R. Yonzon, X. Zhang, R.P. Van Duyne, Surface-enhanced Raman sensors: early history and the development of sensors for quantitative biowarfare agents and glucose detection. J. Raman Spectrosc. **36**, 471 (2005)

T. Henkel, A. März, J. Popp, SERS and Microfluidics, in *Surface Enhanced Raman Spectroscopy: Analytical, Biophysical and Life Science Applications*, ed. by S. Schlücker (Wiley, Weinheim, 2011), pp. 173–190

A.J. Hobro, B. Lendl, SERS and separation science, in *Surface Enhanced Raman Spectroscopy: Analytical, Biophysical and Life Science Applications*, ed. by S. Schlücker (Wiley, Weinheim, 2011), pp. 155–171

Y.X. Hu, S.L. Feng, F. Gao, E.C.Y. Li-Chan, E. Grant, X.N. Lu, Detection of melamine in milk using molecularly imprinted polymers–surface enhanced Raman spectroscopy. Food Chem. **176**, 123 (2015)

F. Inscore, C. Shende, A. Sengupta, H. Huang, S. Farquharson, Detection of drugs of abuse in saliva by surface-enhanced Raman spectroscopy (SERS). Appl. Spectrosc. **65**, 1004 (2011)

I. Izquierdo-Lorenzo, S. Sanchez-Cortes, J.V. Garcia-Ramos, Adsorption of beta-adrenergic agonists used in sport doping on metal nanoparticles: a detection study based on surface-enhanced Raman scattering. Langmuir **26**, 14663 (2010)

M. Jahn, S. Patze, T. Bocklitz, K. Weber, D. Cialla-May, J. Popp, Towards SERS based applications in food analytics: Lipophilic sensor layers for the detection of Sudan III in food matrices. Anal. Chim. Acta **860**, 43 (2015)

E. Kämmer, K. Olschewski, T. Bocklitz, P. Rösch, K. Weber, D. Cialla-May, J. Popp, A new calibration concept for a reproducible quantitative detection based on SERS measurements in a microfluidic device demonstrated on the model analyte adenine. Phys. Chem. Chem. Phys. **16**, 9056 (2014)

A. Kim, S.J. Barcelo, R.S. Williams, Z. Li, Melamine sensing in milk products by using surface enhanced Raman scattering. Anal. Chem. **84**, 9303 (2012)

M.P. Konrad, A.P. Doherty, S.E.J. Bell, Stable and uniform SERS signals from self-assembled two-dimensional interfacial arrays of optically coupled Ag nanoparticles. Anal. Chem. **85**, 6783 (2013)

J. Kubackova, G. Fabriciova, P. Miskovsky, D. Jancura, S. Sanchez-Cortes, Sensitive surface-enhanced Raman spectroscopy (SERS) detection of organochlorine pesticides by Alkyl Dithiol-functionalized metal nanoparticles-induced plasmonic hot spots. Anal. Chem. **87**, 663 (2015)

D. Kurouski, R.P. Van Duyne, In Situ detection and identification of hair dyes using surface-enhanced Raman spectroscopy (SERS). Anal. Chem. **87**, 2901 (2015)

S. Lee, J. Choi, L. Chen, B. Park, J.B. Kyong, G.H. Seong, J. Choo, Y. Lee, K.H. Shin, E.K. Lee, S.W. Joo, K.H. Lee, Anal. Chim. Acta **590**, 139 (2007)

M. Li, in *Applications of Vibrational Spectroscopy in Food Science* ed. by E. Li-Chan, P.R. Griffiths, J.M. Chalmers. The applications of surface-enhanced Raman spectroscopy to identify and quantify chemical adulterants or contaminants in food (Wiley, Chichester, 2010), pp. 649–662

J.F. Li, Y.F. Huang, Y. Ding, Z.L. Yang, S.B. Li, X.S. Zhou, F.R. Fan, W. Zhang, Z.Y. Zhou, D. Y. Wu, B. Ren, Z.L. Wang, Z.Q. Tian, Shell-isolated nanoparticle-enhanced Raman spectroscopy. Nature **464**, 392 (2010a)

X. Li, G. Chen, L. Yang, Z. Jin, J. Liu, Multifunctional Au-coated TiO_2 nanotube arrays as recyclable SERS substrates for multifold organic pollutants detection. Adv. Funct. Mater. **20**, 2815 (2010b)

D.W. Li, W.L. Zhai, Y.T. Li, Y.T. Long, Recent progress in surface enhanced Raman spectroscopy for the detection of environmental pollutants. Microchim. Acta **181**, 23 (2014)

M. Lin, L. He, J. Awika, L. Yang, D.R. Ledoux, H. Li, A. Mustapha, Detection of melamine in gluten, chicken feed, and processed foods using surface enhanced Raman spectroscopy and HPLC. J. Food Sci. **73**, T129 (2008)

X.M. Lin, Y. Cui, Y.H. Xu, B. Ren, Z.Q. Tian, Surface-enhanced Raman spectroscopy: substrate-related issues. Anal. Bional. Chem. **394**, 1729 (2009)

X. Lin, W.L.J. Hasi, X.T. Lou, S. Lin, F. Yang, B.S. Jia, D.Y. Lin, Z.W. Lu, Droplet detection: simplification and optimization of detecting conditions towards high sensitivity quantitative determination of melamine in milk without any pretreatment. RSC Adv. **4**, 51315 (2014)

B.H. Liu, G.M. Han, Z.P. Zhang, R.Y. Liu, C.L. Jiang, S.H. Wang, M.Y. Han, Shell thickness-dependent Raman enhancement for rapid identification and detection of pesticide residues at fruit peels. Anal. Chem. **84**, 255 (2012)

B. Liu, P. Zhou, X. Liu, X. Sun, H. Li, M.S. Lin, Detection of pesticides in fruits by surface-enhanced Raman spectroscopy coupled with gold nanostructures. Food Bioprocess. Technol. **6**, 710 (2013)

A. Loren, J. Engelbrektsson, C. Eliasson, M. Josefson, J. Abrahamsson, M. Johansson, K. Abrahamsson, Internal standard in surface-enhanced Raman spectroscopy. Anal. Chem. **76**, 7391 (2004)

M.B. Mamián-López, R.J. Poppi, Standard addition method applied to the urinary quantification of nicotine in the presence of cotinine and anabasine using surface enhanced Raman spectroscopy and multivariate curve resolution. Anal. Chim. Acta **760**, 53 (2013)

A. März, K.R. Ackermann, D. Malsch, T. Bocklitz, T. Henkel, J. Popp, Towards a quantitative SERS approach - online monitoring of analytes in a microfluidic system with isotope-edited internal standards. J. Biophotonics **2**, 232 (2009)

E. Massarini, P. Wasterby, L. Landstrom, C. Lejon, O. Beck, P.O. Andersson, Methodologies for assessment of limit of detection and limit of identification using surface-enhanced Raman spectroscopy. Sens. Actuators B Chem. **207**, 437 (2015)

L.C. Mecker, K.M. Tyner, J.F. Kauffman, S. Arzhantsev, D.J. Mans, C.M. Gryniewicz-Ruzicka, Selective melamine detection in multiple sample matrices with a portable Raman instrument using SERS-active gold nanoparticles. Anal. Chim. Acta **733**, 48 (2012)

M.J. Natan, Concluding remarks-surface enhanced Raman scattering. Faraday Discuss. **132**, 321 (2006)

K.D. Osberg, M. Rycenga, G.R. Bourret, K.A. Brown, C.A. Mirkin, Dispersible surface-enhanced Raman scattering nanosheets. Adv. Mat. **24**, 6065 (2012)

J. Palacký, P. Mojzeš, J. Bok, SVD-based method for intensity normalization, background correction and solvent subtraction in Raman spectroscopy exploiting the properties of water stretching vibrations, J. Raman Spectrosc. **42**, 1528 (2011)

V. Peksa, M. Jahn, L. Štolcová, V. Schulz, J. Proška, M. Procházka, K. Weber, D. Cialla-May, J. Popp, Quantitative SERS analysis of azorubine (E 122) in sweet drinks. Anal. Chem. **87**, 2840 (2015)

B. Peng, G.Y. Li, D.H. Li, S. Dodson, Q. Zhang, J. Zhang, Y.H. Lee, H.V. Demir, X.Y. Ling, Q. H. Xiong, Vertically aligned gold nanorod monolayer on arbitrary substrates: self-assembly and femtomolar detection of food contaminants. ACS Nano **7**, 5993 (2013)

V. Rana, M.V. Canamares, T. Kubic, M. Leona, J.R. Lombardi, Surface-enhanced Raman spectroscopy for trace identification of controlled substances: morphine, codeine, and hydrocodone. J. Forensic Sci. **56**, 200 (2011)

A.G. Ryder, Surface enhanced Raman scattering for narcotic detection and applications to chemical biology. Curr. Opin. Chem. Biol. **9**, 489 (2005)

B. Sagmuller, B. Schwarze, G. Brehm, S. Schneider, Application of SERS spectroscopy to the identificationof (3, 4-methylenedioxy)amphetamine in forensic samples utilizing matrixstabilized silver halides. Analyst **126**, 2066 (2001)

W. Shen, X. Lin, C. Jiang, C. Li, H. Lin, J. Huang, S. Wang, G. Liu, X. Yan, Q. Zhong, B. Ren, Reliable quantitative SERS qnalysis facilitated by core–shell nanoparticles with embedded internal standards. Angew. Chem. Int. Ed. **54**, 7308 (2015)

M. Smith, K. Stambaugh, L. Smith, H.J. Son, A. Gardner, S. Cordova, K. Posey, D. Perry, A.S. Biris, Surface-enhanced vibrational investigation of adsorbed analgesics. Vib. Spectrosc. **49**, 288 (2009)

I. Srnová-Šloufová, B. Vlčková, T.L. Snoeck, D.J. Stufkens, P. Matějka, Surface-enhanced Raman scattering and Surface-enhanced resonance Raman scattering excitation profiles of Ag-2,2'-bipyridine surface complexes and of $[Ru(bpy)3]^{2+}$ on Ag colloidal surfaces: manifestations of the charge-transfer resonance contributions to the overall surface enhancement of Raman scattering. Inorg. Chem. **39**, 3551 (2000)

J.M. Taguenang, A. Kassu, A. Sharma, D. Diggs, Surface enhanced Raman spectroscopy on the tip of a plastic optical fiber. Proc. SPIE **6641**, 66411X (2007)

L. Tang, S. Li, F. Han, L. Liu, L. Xu, W. Ma, H. Kuang, A. Li, L. Wang, C. Xu, SERS-active Au@Ag nanorod dimers for ultrasensitive dopamine detection. Biosens. Bioelectron. **71**, 7 (2015a)

X. Tang, R. Dong, L. Yang, J. Liu, Fabrication of Au nanorod-coated Fe_3O_4 microspheres as SERS substrate for pesticide analysis by near-infrared excitation. J. Raman Spectrosc. **46**, 470 (2015b)
V. Thomsen, D. Schatzlein, D. Mercuro, Limits of detection in spectroscopy. Spectroscopy **18**, 112 (2003)
C. Wang, C. Yu, Analytical characterization using surface-enhanced Raman scattering (SERS) and microfluidic sampling. Nanotechnology **26**, 092001 (2015)
Y. Wang, Y.S. Li, Z.X. Zhang, D.Q. An, Surface-enhanced Raman scattering of some water insoluble drugs in silver hydrosols. Spectrochim. Acta A **59**, 589 (2003)
H.Y. Wu, B.T. Cunningham, Point-of-care detection and real-time monitoring of intravenously delivered drugs via tubing with an integrated SERS sensor. Nanoscale **6**, 5162 (2014)
Y. Yang, Z.Y. Li, K. Yamaguchi, M. Tanemura, Z. Huang, D. Jiang, Y. Chen, F. Zhou, M. Nogami, Controlled fabrication of silver nanoneedles array for SERS and their application in rapid detection of narcotics. Nanoscale **4**, 2663 (2012)
T. Yang, X. Guo, H. Wang, S. Fu, Y. Wen, H. Yang, Magnetically optimized SERS assay for rapid detection of trace drug-related biomarkers in saliva and fingerprints. Biosens. Bioelectron. **68**, 350 (2015)
W.W. Yu, I.M. White, A simple filter-based approach to surface enhanced Raman spectroscopy for trace chemical detection. Analyst **137**, 1168 (2012)
W.W. Yu, I.M. White, Inkjet-printed paper-based SERS dipsticks and swabs for trace chemical detection. Analyst **138**, 1020 (2013)
D.M. Zhang, Y. Xie, S.K. Deb, V.J. Davison, D. Ben-Amotz, Isotope edited internal standard method for quantitative surface-enhanced Raman spectroscopy. Anal. Chem. **77**, 3563 (2005a)
X. Zhang, M.A. Young, O. Lyandres, R.P. Van Duyne, Rapid detection of an anthrax biomarker by surface-enhanced Raman spectroscopy. J. Am. Chem. Soc. **127**, 4484 (2005b)
X. Zhang, M. Zou, X. Qi, F. Liu, X. Zhu, B.H. Zhao, Detection of melamine in liquid milk using surface-enhanced Raman scattering spectroscopy. J. Raman Spectrosc. **41**, 1655 (2010)
Z. Zhang, Q.S. Yu, H. Li, A. Mustapha, M.S. Lin, Standing gold nanorod arrays as reproducible SERS substrates for measurement of pesticides in apple juice and vegetables. J. Food Sci. **80**, N450 (2015)
J. Zheng, S. Pang, T.P. Labuza, L. He, Semi-quantification of surface-enhanced Raman scattering using a handheld Raman spectrometer: a feasibility study. Analyst **138**, 7075 (2013)
J. Zheng, L. He, Surface-enhanced Raman spectroscopy for the chemical analysis of food. Compr. Rev. Food. Sci. Food Saf. **13**, 317 (2014)
Y. Zhou, R. Ding, P. Joshi, P. Zhang, Quantitative surface-enhanced Raman measurements with embedded internal reference. Anal. Chim. Acta **874**, 49 (2015)

Chapter 5
Biomolecular SERS Applications

Abstract SERS spectroscopy is currently undergoing rapid development as an ultra-sensitive and highly specific analytical technique for biomolecular detection. This chapter gives an overview of SERS study of biomolecules primarily of nucleic acids, proteins, membranes and their components. Both detection schemes—intrinsic and extrinsic—will be introduced. Direct spectral signature of the biomolecule can be obtained by an intrinsic scheme. An extrinsic approach using labelling of target biomolecule or SERS tag consisting of metallic NPs and Raman reporter molecule brings indirect information but much better sensitivity. For example, SERS detection limits for labelled oligonucleotides can be about 10^{-11}–10^{-12} M, which is about three orders of magnitude better than those provided by standard fluorescence technique. Hybridization of a nucleic acid to its complementary target serves to its unambiguous molecular recognizability. For protein detection, immunoassay platforms are employed to detect the target antigens or antibodies (typically small proteins) through specific antibody-antigen binding. SERS tags formed by metallic nanoparticles with attached Raman reporter molecules (and biorecognition element such as an antibody in the case of immunoassays) are used in SERS extrinsic hybridization and immunoassay experiments, thus increasing their sensitivity.

5.1 SERS Biomolecular Detection Schemes

Generally, SERS detection of biomolecules can be accomplished by two independent ways: (i) direct—intrinsic—(often called label-free) and (ii) indirect—extrinsic—using labels. The scheme of different approaches is illustrated in Fig. 5.1.

The intrinsic SERS detection is possible in case that the biomolecule provides a sufficiently good intrinsic SERS spectrum (Fig. 5.1a). This spectrum can serve for biomolecule identification, quantification and/or determination of its state, such as conformation or complex formation. This method is more reliable than extrinsic SERS labelling as it shows the direct spectral signature of the biomolecule. On the

M. Procházka, *Surface-Enhanced Raman Spectroscopy*,
Biological and Medical Physics, Biomedical Engineering,
DOI 10.1007/978-3-319-23992-7_5

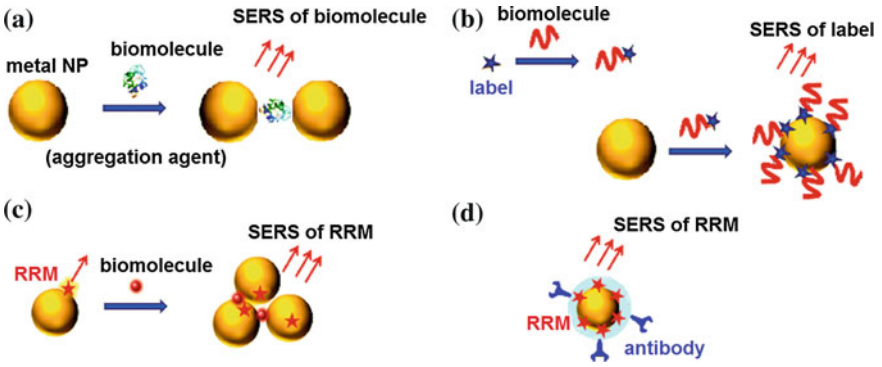

Fig. 5.1 Schematic illustration of different approaches for SERS biomolecular detection. **a** Intrinsic detection of biomolecule (protein). **b** Extrinsic detection of labelled biomolecule (DNA). **c** Extrinsic detection of biomolecule using SERS tag (metallic NP with RRM). **d** SERS tag (metallic NP with RRMs, protective shell and antibody) for immunoassay (adapted from Wang et al. 2013. Copyright 2012 American Chemical Society)

other hand, SERS is a surface-selective technique, which has an important analytical consequence: the analyte must be placed very close to the metal surface for efficient SERS detection. Therefore, intrinsic SERS detection schemes are usually limited to molecules with surface seeking groups. If it is not the case, the strategies for capturing the analyte on the surface of the SERS substrate should be applied. The metal surface can be functionalized to selectively capture particular analyte or the analyte is chemically modified with a chemical anchor (i.e. thiol group) which effectively attaches to the metal surface. Latter approach requires that enough of the target molecule structure is left during chemical modification to identify it by its Raman spectrum (Smith 2008). In the case of metallic NPs, various ions can be used to encourage adsorption of analyte and to aggregate NPs to obtain high SERS enhancement. On the other hand, if the particular biomolecule shows the SERS signal it can be so poor that it could not be detected at very low (physiological) concentrations. Other major limitations are poor selectivity and poor sensitivity. Raman bands of other species presented in complex mixture can overlap the Raman signal of target biomolecule, making its identification impossible. Despite the above mentioned limitations, due to the development of highly sensitive, biocompatible and reproducible SERS-active substrates and their premeditated treatments as well as methods for chemical modifications of target biomolecules, the intrinsic biosensing protocol becomes powerful and promising.

In extrinsic SERS biosensing, the biomolecule is labelled with a molecule (label) providing an intense and distinguishable Raman signal. In this detection scheme, the SERS or SERRS spectrum of the label adsorbed on metal surface, not of the target biomolecule, is acquired (Fig. 5.1b). The most important advantage is that each label has SERS fingerprint spectrum consisting of a set of sharp and molecularly specific Raman lines. The possibility to use a wide range of various fluorescent and nonfluorescent labels enables specific and highly sensitive

detection. Labelling with the fluorescent dyes brings additional sensitivity: when the excitation wavelength matches with the electronic absorption of the fluorescent label an additional resonance enhancement is achieved and SERRS rather than SERS is obtained (Smith 2008). Another attribute of SERRS is that fluorescence from fluorophore label close to the metal surface is quenched and thus even strongly fluorescent dyes can be used. Over 50 compounds suitable as SERRS labels and providing more sensitive detection than the fluorescence technique are listed in literature (Graham and Faulds 2008; Stevenson et al. 2011). Moreover, multiple SERRS labels can be easily individually recognized by using only a single excitation source, which brings a high potential for simultaneous detection of multiple analytes without the necessity of any separation procedure. The multiplex capacity of fluorescence is limited to ~1–3, while 10–30 seems to be realistic (and 100 is considered to be a theoretical upper limit) for SERRS using labels (Schlücker 2011). Thus, SERRS biomolecular detection using dye labels has a number of advantages over the current techniques (i.e. fluorescence) including higher sensitivity, molecule-specific Raman fingerprints, higher multiplex capabilities and the lack of necessity for a separation step.

An alternative to the labelling of the target biomolecule is a SERS tag.[1] A SERS tag is formed by attaching intrinsically strong Raman scattering molecules (RRMs) to the surface of metallic NPs or small NP aggregate (Pazos-Perez and Álvarez-Puebla 2012; Wang et al. 2013). In this extrinsic detection scheme, SERS or SERRS spectrum of RRM is used (Fig. 5.1c). Moreover, SERS tag can also be encapsulated in a polymer, glass or silica shell to ensure better mechanical and chemical stability (Schlücker 2011; Wang et al. 2013). The NP surface or its protective shell can be further functionalized with a biorecognition element such as an antibody to render the tags with a specific binding feature (Fig. 5.1d). Such SERS tags are called extrinsic Raman labels (ERLs) in some papers (Wang et al. 2009). Thus, SERS tags are nowadays employed as sensitive SERS probes in immunoassay platforms as well as in vitro and in vivo SERS diagnostics. Their medical applications will be described in detail in Chap. 7.

5.2 Nucleic Acids (NAs) and Their Components

NAs—deoxyribonucleic acid (DNA) and ribonucleic acid (RNA) are the prime biomolecules bearing genetic information and having an important function in gene expression. They form single strand (ss) composed of the sugars (D-ribose or 2-deoxy-D-ribose), the phosphates and the purine or pyrimidine bases. At physiologic conditions, DNA forms double strand (ds) helix with a negatively charged phosphate envelope. The ability to detect NAs or their specific sequences by SERS

[1]Various terms for "SERS tag" can be found in literature, e.g. SERS nanotag, SERS probe, SERS-encoded NP, SERS label, extrinsic Raman labels (ERLs).

is fundamental in molecular diagnostics including study of viruses, bacteria and early disease states or forensic identifications of criminal suspects. This chapter summarizes the basic principles of intrinsic and extrinsic NA detection including hybridization experiments; the medical applications based on NA sensing will be discussed in Chap. 7.

5.2.1 *Intrinsic Detection of NAs*

First SERS spectra of NAs and their components have been obtained on the Ag electrodes and Ag NPs (Koglin and Séquaris 1986; Cotton 1988; Cotton et al. 1991). A limitation of SERS technique for NAs detection using the colloidal NPs is related to low affinity of the negatively charged phosphates to the metallic NPs. It was found that electrolytes such as NaCl, $MgSO_4$ or $MgCl_2$ which do not strongly bind to the surface of the Ag NPs, lead to very high NPs aggregation. In these "Mg^{2+}-aggregated" Ag NPs, anionic analytes such as oligonucleotides may bind and provide a SERS signal. SERS spectra of mononucleotides (Bell and Sirimuthu 2006), oligonucleotides and ssDNA in nucleobase concentrations between 10^{-5} and 10^{-8} M (Grajcar et al. 2001) have been obtained this way. The effect of $MgCl_2$ on SERS spectra of poly(dA) is illustrated in Fig. 5.2. Addition of 5×10^{-3} M $MgCl_2$ to Ag NPs led to their aggregation (Fig. 5.2a) and strong SERS signal of poly(dA) was observed while no aggregation and no SERS signal appeared in the absence of $MgCl_2$ (Fig. 5.2b). Moreover, in such systems it was also possible to compare the local reactivity of the adenyl residues in various DNA/RNA structures (hairpins and loops) with excellent precision (Grajcar et al. 2006). $MgSO_4$ was also used to

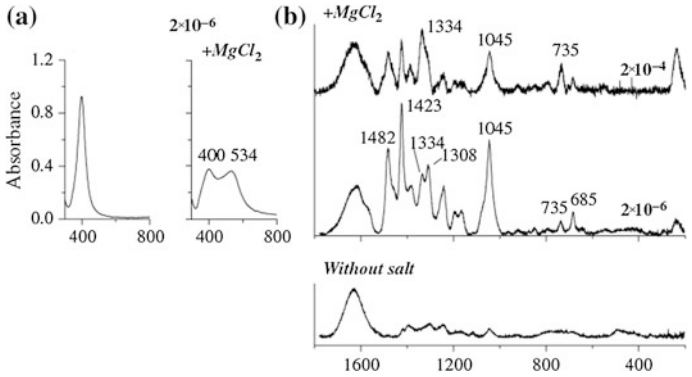

Fig. 5.2 The effect of $MgCl_2$ on SERS spectra of poly(dA). **a** Visible absorption and SERS spectra of poly(dA) in Ag colloidal NPs without and with $MgCl_2$. **b** SERS intensities are normalized on the water Raman band at $\sim$1640 cm^{-1}, concentrations are in moles of adenine residues per litre (adapted with permission from Grajcar et al. 2001. Copyright 2001 John Wiley & Sons, Ltd)

aggregate metallic NPs and to obtain SERS spectra of unmodified ssDNA and dsDNA in nM concentration (Papadopoulou and Bell 2012). Ag NRs have also been successfully employed for quantitative DNA detection (Driskell et al. 2008).

Mediated surface agents or chemical modifications can also improve the binding of NAs to the metal surface. Positively charged spermine besides the mediation of NA adsorption may also control aggregation of (Ag colloid)/DNA. LOQ of 8×10^{-13} M was reached by using this agent (Graham et al. 1997). Chemical modification of NA (by thiol group) is applied to easily attach NA chains on the metal surface. Development of Au nanoshells with attached thiolated NA chains resulted in a dramatic increase in the reproducibility of the intrinsic SERS spectra of DNA and RNA. Reproducible SERS spectra of thiolated polyadenine ssDNA (polyA) (Kundu et al. 2009a) and thiolated dsDNA oligomers (70 bases) on Au nanoshells immobilized on the glass substrate have been obtained (Barhoumi et al. 2008). Spectra are dominated by the adenine vibrational modes, they are reproducible and correspond well with NRS spectra of the same oligomers (Fig. 5.3). It seems that a critical step for obtaining highly reproducible DNA spectra was a thermal pretreatment of DNA oligomer that promoted their extended linear conformation on the Au shell substrate. Au nanoshells immobilized on glass substrate were also employed to detect spectral changes in DNA conformation upon interaction with small molecules.

A dsDNA undergoes structural changes such as denaturation after adsorption on metal surface (Cotton 1988). Intrinsic SERS of DNA has been shown to be highly sensitive to detect and distinguish the individual nucleotides and the various DNA structures. For example, SERS has been applied to detect DNA sequences as single base mismatches (mutation generating during DNA replications) of 209 base pairs

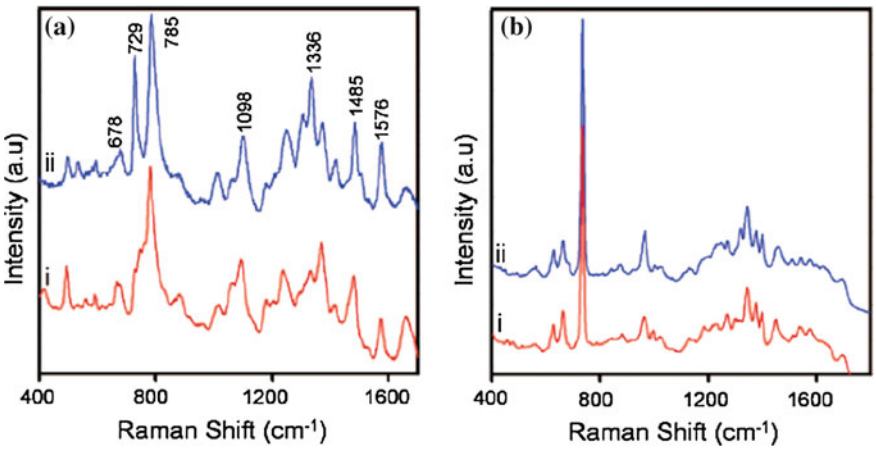

Fig. 5.3 NRS (**a**) and SERS (**b**) spectra of two different (*i*, *ii*) ds thiolated DNA oligomers (70 bases). SERS spectra were measured using Au nanoshells covered silicon NPs (adapted with permission from Barhoumi et al. 2008. Copyright 2008 American Chemical Society)

DNA fragment adsorbed on Ag electrodes (Chumanov and Cotton 1999). Prado and co-workers were able to not only distinguish four bases in ssRNA but also to estimate the percentage of each base in the mixture using decomposition procedure of the SERS spectra of ssRNA obtained from aggregated Ag NPs (Prado et al. 2011). Papadopoulou and Bell induced DNA strands to spontaneously adsorb on the Ag NPs through their nucleotide side chains. The SERS spectra were sufficiently reproducible so that they can serve to identify single-base mismatches in short (25-mer and 23-mer) strands although only nonsequence specific information was obtained (Papadopoulou and Bell 2011b). Recently, Guerrini and co-workers presented a simple strategy for ultrasensitive direct label-free analysis of unmodified dsDNA (Guerrini et al. 2015). DNA sequences were selectively sandwiched between interparticle junctions ("hot spots") to maximize SERS signal. They presented Ag NPs coated with spermine molecules which produced positive charge on Ag surface. An electrostatic adhesion of DNA promoted NPs aggregation into stable clusters, yielding intense and reproducible SERS spectra at nanogram level. As potential applications, they reported first examples of SERS recognition of single base mismatches and base methylations (5-methylated-cytosine and N6-methylated-adenine) in duplexes. Importantly, owing to the low amount of DNA required (comparable to only 10–100 cells), the analysis can be performed without the necessity of amplification, thus providing realistic direct information of the DNA in its native state (Guerrini et al. 2015). Ag NPs were used to investigate the formation and to analyse the relative strength of guanine quadruplexes (Rusciano et al. 2011). Despite these successful results, for large biomolecules such as DNA and RNA, reproducible acquisition of intrinsic SERS spectra of DNA and RNA is difficult and some discrepancies among spectra published in literature can be found.

SERS spectra of NAs are generally dominated by spectral features of bases which are better Raman scatterers than sugar and phosphate parts. Adenine is the best (Barhoumi et al. 2008) and even its SM-SERS detection on Ag NP aggregates has been reported (Kneipp et al. 1997). Adenine was also analysed in SERS investigation of possible extraterrestrial life traces. The authors depict easy experimental procedure adapted for in situ detection of adenine (10^{-12}–10^{-13} g) in Martian meteorite (Caporali et al. 2012). Vitol and co-workers reported a glass substrate coated with Ag NPs for SERS detection of nicotinic acid adenine dinucleotide phosphate, a calcium secondary messenger that plays a crucial role for intracellular Ca^{2+} release. The adenine bands dominate the spectrum and SERS detection of 100 μM nicotinic acid adenine dinucleotide phosphate from a sample volume of 1 μl was demonstrated (Vitol et al. 2010).

5.2.2 Intrinsic NA Detection Using Hybridization

One of the most unambiguous molecular recognition events is the hybridization of a NA to its complementary target. The SERS biosensors for DNA hybridization with

synthetic DNA were also successfully constructed. For example, Papadopoulou and Bell detected the closed or opened beacon conformation through hybridization of a target sequence which changed the oligonucleotide orientation. It was possible due to the fact that 24-mer thiolated polyA bound to Au NPs showed preferential enhancement of the adenine breathing vibration at 736 cm^{-1} depending on the orientation of the sequence to the surface. The oligonucleotide concentrations were 10^{-4}–10^{-8} M (Papadopoulou and Bell 2011a).

On the other hand, intrinsic (label-free) SERS detection of DNA hybridization is obstructed by poor spectral reproducibility plus the fact that the spectral signatures of hybridized and unhybridized sequences are highly similar. To overcome these issues, two approaches were applied. First, the idea was to remove adenine from the captured strand by replacing it with isomer (2-aminopurine—2-AP) which had different spectrum but preserved the same hybridization efficiency (Barhoumi and Halas 2010). This concept is depicted in Fig. 5.4. Spectrum a shows the SERS spectrum of thermally pretreated DNA on Au nanoshells dominated by the adenine peak at 736 cm^{-1}. Spectrum b represents the SERS spectrum of DNA having 2-AP substitution attached to the Au nanoshells through a thiol moiety on its 5′-end. In this spectrum, a peak at 807 cm^{-1} of the 2-AP instead of an adenine peak at 736 cm^{-1} was observed. The 736 cm^{-1} peak was a marker for hybridization between the native/unlabelled DNA target strand (left in the inset; with A—adenine) and the

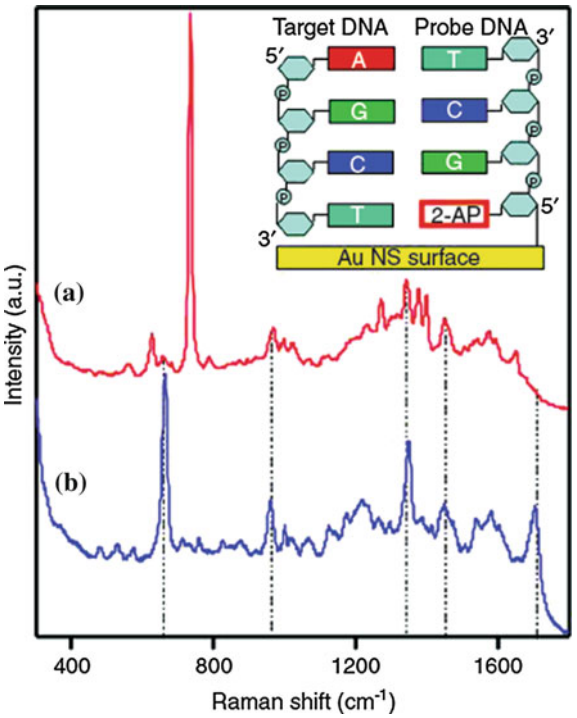

Fig. 5.4 Intrinsic SERS detection of DNA. Recorded SERS spectra of (**a**) adenine containing and (**b**) adenine noncontaining DNA sequences. Hybridization model between probe DNA having 2-AP substituted for adenine and unlabelled target DNA is shown in *inset*. *A* Adenine, *C* cytosine, *G* guanine, *T* thymine (adapted with permission from Barhoumi and Halas 2010. Copyright 2010 American Chemical Society)

modified DNA capture strand (right in the inset; with 2-AP). The intensity of the 2-AP peak was constant and depended only on the packing density of the probe DNA on the Au surface. Therefore, the intensity ratio of adenine versus 2-AP peak was a quantitative marker for the degree of hybridization. Second, a straightforward LS analysis has been employed for the quantitative determination of the relative ratios of the four nucleotide components adenine, cytosine, guanine, thymine and uracyl before and after hybridization (Abell et al. 2012). Generally, the intrinsic DNA hybridization was still problematic due to the fact that an evaporated solution caused salt crystals to deposit within the SERS substrate which decreased their selectivity and sensitivity. Moreover, the effective SERS detection limit was less than 5 nm from the surface, indicating that the hybridization assay was sensitive to only the less than first 9 nucleotides (Marotta et al. 2013). Thus, the extrinsic scheme using Raman label seems to be much more suitable for DNA hybridization studies.

5.2.3 *Intrinsic NA Detection Using TERS*

In comparison to SERS, TERS provides high reproducibility of NA spectral information with high lateral resolution and single molecule sensitivity (Treffer et al. 2012). TERS enabled a sensitive study of hydrogen bonding at single crystalline surfaces as has been illustrated for adenine and thymine on gold(III) (Zhang et al. 2010). A ssRNA cytosine homopolymer was directly detected by TERS (Bailo and Deckert 2008). The method allowed the estimation of the interaction geometry of both bases with respect to the metal surface as well as the respective strength of the bonds. Lipiec and co-workers demonstrated the potential of TERS to investigate the susceptibility of DNA bonds to radiation damage and in particular have shown that O–C cleavage is the most likely form of DNA damage since this accounted for more than half of the cleavages detected (Lipiec et al. 2014).

5.2.4 *Extrinsic Detection of NAs*

In the case of DNA analysis, both nonfluorescent and fluorescent labels can be employed. Nonfluorescent labels such as DABCYL, phtalocyanines and black hole quenchers can be easily adsorbed on NP surface. Alternatively, dyes can be adsorbed directly to the metal surface through the formation of bonds between the metal and a completing group which is part of the dye, as opposed to simple electrostatic interactions. This is very efficient for simple azo dyes which contain the benzentriazole group. Positively charged commercially available fluorescent dyes (such as BODIPY, RH6G, ROX, TAMRA, FAM, TET, yakima yellow, cyanines Cy3 and Cy5, etc.) can easily be attached to oligonucleotide probes and then detected by SERRS. Negatively charged dyes as HEX require propargylamine modification to

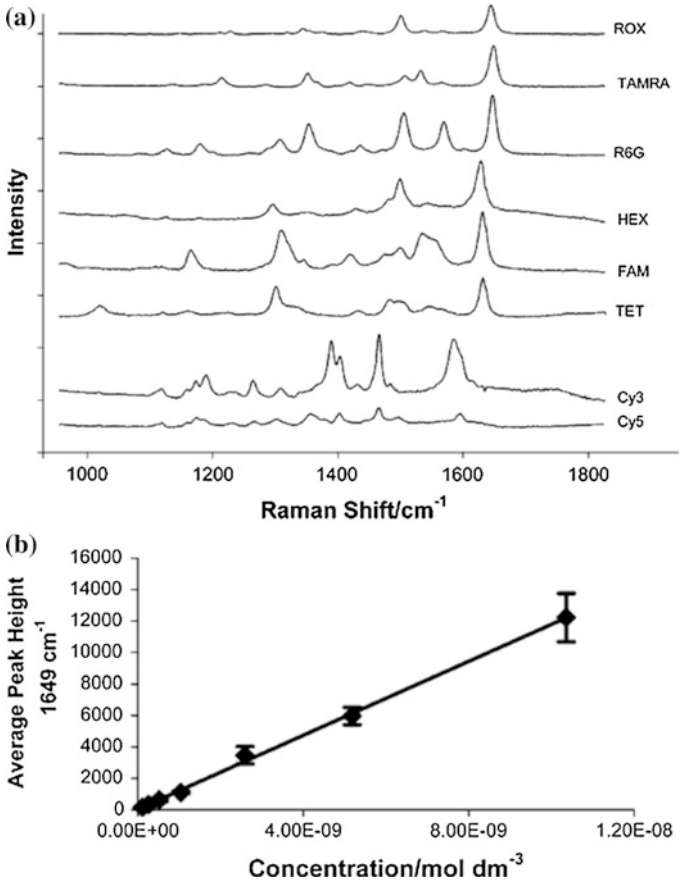

Fig. 5.5 Extrinsic SERS detection of DNA. SERRS spectra of the eight dye-labelled oligonucleotides (**a**) and plot of SERRS intensity versus concentration for 1649 cm^{-1} peak of RH6G (**b**) (adapted with permission from Faulds et al. 2004. Copyright 2004 American Chemical Society)

give a positive charge to the molecule and allow it to be easily adsorbed. The majority of the labels are attached to the 5′-position of the oligonucleotides. SERRS spectra of the eight dye-labelled oligonucleotides, obtained using 514.5 nm excitation wavelength and at 1×10^{-8} M concentration are shown in Fig. 5.5a. Dye-labelled oligonucleotides that readily adsorb onto the silver surface give a linear response at submonolayer concentrations. SERRS intensity versus concentration for 1649 cm^{-1} peak of RH6G is shown in Fig. 5.5b as an example. This enabled determining accurate LOD for SERRS detection of labelled oligonucleotides. LODs for oligonucleotides labelled with different dyes varied from 2×10^{-9} to 7.5×10^{-13} M for Ag NPs and from 1.7×10^{-9} to 7.3×10^{-11} M for Au NPs, while fluorescence LODs were only between 6.5×10^{-8} and 3.1×10^{-9} M (Faulds et al. 2004; Graham and Faulds 2008; Stevenson et al. 2011; Faulds 2012).

Multiplex detection is possible if various labels providing particular fingerprint SERRS spectrum are used allowing specific oligonucleotide sequences to be distinguished (Docherty et al. 2004). To exploit the maximum multiplicity by SERRS it is necessary to use more complex chemometric algorithms such as multivariate analysis to clearly distinguish a SERRS spectrum for each dye label (Faulds et al. 2008). The LOD for the dye-labelled oligonucleotides was in the 3–30 ppm range for the multiplexed SERRS assay (Schlücker 2014).

5.2.5 *Extrinsic NA Detection Using Hybridization*

The extrinsic DNA hybridization scheme (Vo-Dinh et al. 1999, 2006) is depicted in Fig. 5.6. It consists of several steps: (a) selection of a suitable label providing high SERS signal, (b) DNA probe sequence is labelled with label providing high SERS signal, (c) the oligonucleotide with a complementary base sequence is immobilized at the SERS-active substrate and (d) the hybridization of the labelled DNA probe

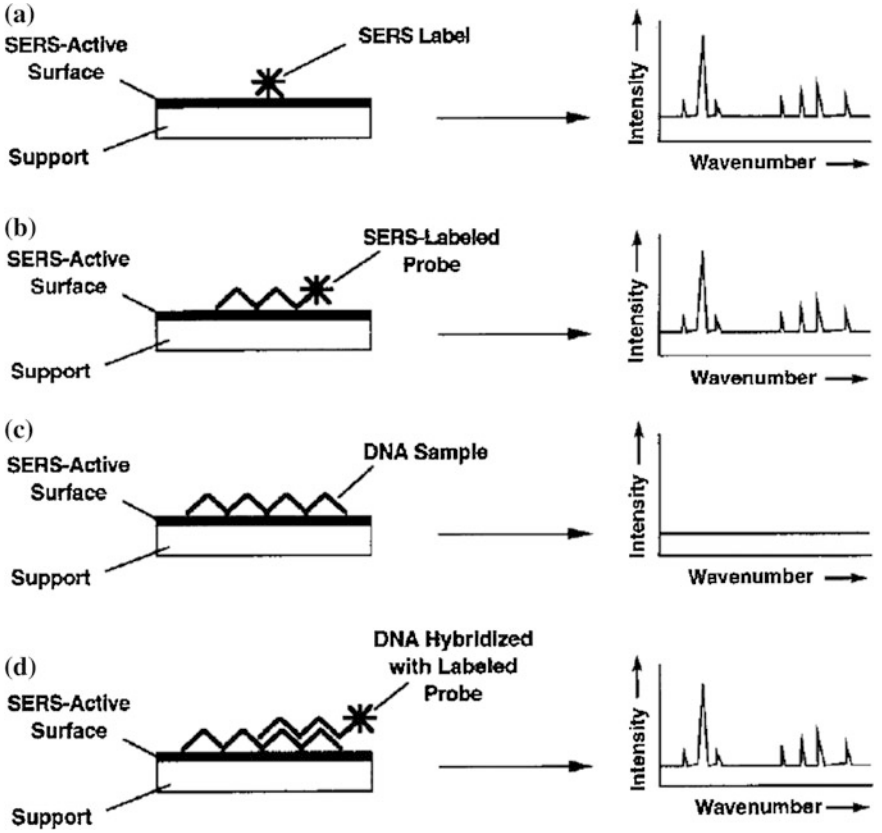

Fig. 5.6 The extrinsic DNA hybridization scheme. See text for details (adapted from Vo-Dinh et al. 1999. Copyright 1999 John Wiley & Sons, Ltd)

sequence is indicated by SE(R)RS signal of the label. SE(R)RS signal can be enhanced by heating or cooling the analyte solution to influence the extent of DNA hybridization as well as by functionalization of the metal surface.

To increase sensitivity of SERS hybridization assay, the polymerase chain reaction (PCR) can be introduced to the hybridization experiment. PCR is a well known technology in molecular biology used to amplify a single copy of DNA fragment generating thousands to millions of copies of a particular DNA sequence. In SERS hybridization approach, PCR can simultaneously amplify the specific target DNA sequences enabling enough sensitive levels of detection (Isola et al. 1998). However, PCR suffers from problems such as contamination and nonspecific amplification, the avoidance of which requires strict laboratory controls and highly trained personnel. Another concept is to use a SERS tag consisting of metallic NP with both DNA target sequence and RRMs attached to it. Hybridization of this probe with a complementary target on a DNA microarray platform is then monitored as SERS signal of RRM. Cao and co-workers reported small Au NPs with a diameter of ~13 nm functionalized with Cy3-labelled, alkylthiol-capped oligonucleotide strands (Cao et al. 2002). For hybridization, the target DNA and the small Au SERS probes were sequentially added to the chip functionalized with the corresponding capture sequence. Next, silver enhancement was performed by the reduction of silver ions with hydroquinone for the sensitive SERRS detection of the hybridization event. This concept is shown in Fig. 5.7. It allowed SERS detection of specific sequences of six viruses in multiplexed assay (see Chap. 7).

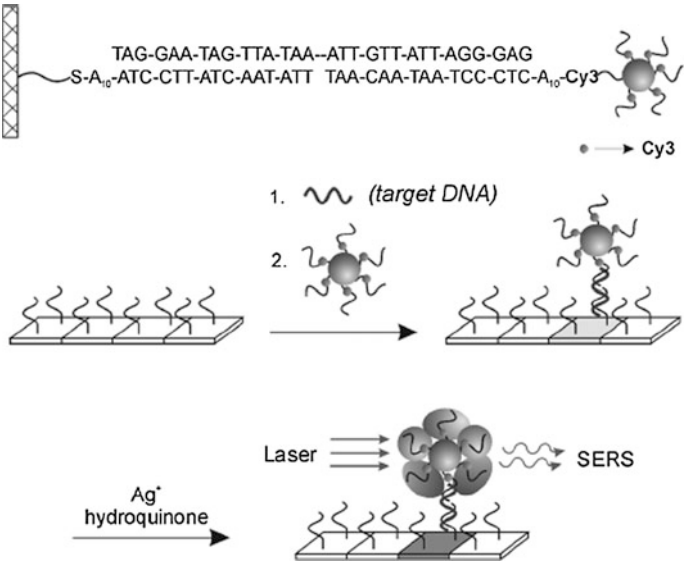

Fig. 5.7 The extrinsic DNA hybridization scheme using a SERS tag. See text for details (adapted from Cao et al. 2002. Copyright 2002 The American Association for the Advancement of Science)

One possibility to enhance the sensitivity of SERRS probes for DNA detection is a controlled DNA-based self-assembly of dye-labelled oligonucleotide-functionalized Ag NPs (Graham et al. 2008). The Ag NP coated with a monolayer of benzotriazoles is incubated with two different, noncomplementary 5′-thiol-functionalized oligonucleotide sequences. Hybridization occurs when a target sequence complementary to both sequences is added to the dye-functionalized DNA/(Ag NP) conjugates.

5.3 Proteins and Their Components

Proteins are large macromolecules consisting of one or more long chains of amino acid residues; short chains of amino acids are called peptides. Proteins perform very important biological functions within living organisms, including structural and storage functions, catalytic metabolite reactions, replicating DNA, molecular transport and immune system function. The main goal of SERS study of the amino acids and peptides is to assign Raman bands to particular amino acids and then to detect big proteins such as particular biomarkers in clinical diagnostics of various diseases including cancer. This chapter summarizes basic principles of intrinsic and extrinsic protein detection as well as immunoassays. The medical applications based on protein sensing will be discussed in Chap. 7.

5.3.1 Intrinsic Detection of Proteins

Intrinsic SERS spectra of amino acids and short peptides have been obtained using roughened electrodes or NPs. Experimental conditions such as type of the metallic substrate, pH, peptide concentration and applied electrode should be controlled for each particular SERS study. The SERS spectra vary with the orientation of the molecule on the metal surface as well as with the amino acid sequence of the peptide. In combination with density functional theory (DFT) calculations, it is possible to determine adsorption orientation of the peptides on the surface. A limitation of SERS detection using metallic NPs is done by amphiphilic character of these molecules and consequently, their lower affinity to the metal surface. This can be overcome by varying the pH or by using Ag NPs pretreated with aggregation agents containing Cl^-, SO_4^- or NO_3^- anions. The analysis of SERS spectra of some amino acids and peptides can be complicated by the presence of the anomalous bands from the particular colloid or aggregating agents (Yaffe and Blanch 2008).

Detectable concentrations of amino acids using Ag surfaces vary between 10^{-4} and 10^{-6} M. Amino acids possessing aromatic rings (such us tryptophan—Trp) or SH group (cysteine—Cys) provide even better detection limits. For example, Fedosejev and co-workers were able to detect Trp even in 1.46×10^{-8} M concentration on borohydride-reduced Ag NPs activated by a mixture of $NaHCO_3$ and

NaCl (Kandakkathara et al. 2011). The authors also found out that SERS spectra at low (below $\sim 10^{-5}$ M) and at high (above $\sim 10^{-4}$ M) concentrations differed in several features showing that at low concentrations Trp molecules bind to the surface through the indole ring, which remained flat on the surface. Campos-Vallette and co-workers measured SERS spectra of arginine (Arg) on Ag NPs in different pH values (Garrido et al. 2013). SERS spectra at pH = 7 indicated that the Arg molecules interact with the Ag surface only through the guanidinium fragment. By increasing the pH to 9, the molecule adopted a new conformation on the surface, interacting with Ag surface through the guanidinium, carboxylate and the aliphatic moieties. In addition, theoretical calculations performed by using the extended Hückel method for a model of Arg interacting with Ag surface supported the observed results. The SERS spectra of short peptides have also been obtained using Ag NPs. For instance, Podstawka and co-workers studied the series of homodipeptides consisting of Cys, glycine (Gly), leucine (Leu), methionine (Met), Phe and proline (Pro) amino acids adsorbed on Ag colloidal NPs (Podstawka et al. 2004a). They found that Gly–Gly was initially adsorbed through its C-terminus and in time rearranged to be adsorbed through its N-terminus.

The first SERS studies of big proteins were reported at 1980s using Ag electrodes. Good spectra of haemoproteins (proteins that contain a haem group), cytochrome c and myoglobin were published (Cotton et al. 1980). Later, SERS spectra of bovine serum albumin (BSA) or lysozyme (Koglin and Séquaris 1986), glucose-oxidase (Holt and Cotton 1989) and membrane proteins in bacterial and photosystem II reaction centrum (Picorel et al. 1991) were obtained. Systems prepared by the protein immobilization to Ag electrodes profited from electrochemistry for identification and monitoring of redox reactions of studied enzymes. For instance, it has been shown that a high electric field shifted the equilibrium between the native and oxidized form of cytochrome c (Murgida and Hildebrandt 2008; Hildebrandt et al. 2011). On the other hand, dense immobilization at an electrode surface increased the danger of local heating and photodecomposition of studied proteins. Thus, it was often necessary to use low laser powers or rotation electrodes to obtain SERS spectra of studied proteins. Ag NPs were applied to SERS study of flavoproteins (containing riboflavin) (Copeland et al. 1984), cytochrome c (Macdonald and Smith 1996), haemoglobin (Xu et al. 1999; Smulevich and Spiro 1985), myoglobin (Bizzarri and Cannistraro 2002), lysozyme, insulin, oxytocin, trypsin (Podstawka et al. 2004b) and enzymes (Larmour et al. 2010; Han et al. 2009b, c). It was found that in the case of Ag NPs, acidified sulphate as an aggregation agent highly enhanced the detection limit. SERS spectra of lysozyme, ribonuclease B, avidin and catalase with low LOD ($\sim$ µg ml^{-1}–ng ml^{-1}) have been obtained this way (Han et al. 2009a, c). On the other hand, SERS spectroscopy of proteins on Ag NPs suffered from poor reproducibility and the changing of protein structure due to interaction with the Ag surface.

In intrinsic peptide/protein SERS spectra, the most intensive Raman bands belong to amino acids containing aromatic or S–S groups. Halas and co-workers prepared Au nanoshells to compare SERS spectra of three dipeptides containing Cys and one aromatic amino acid Phe, tyrosine (Tyr) or Trp (Wei et al. 2008). They

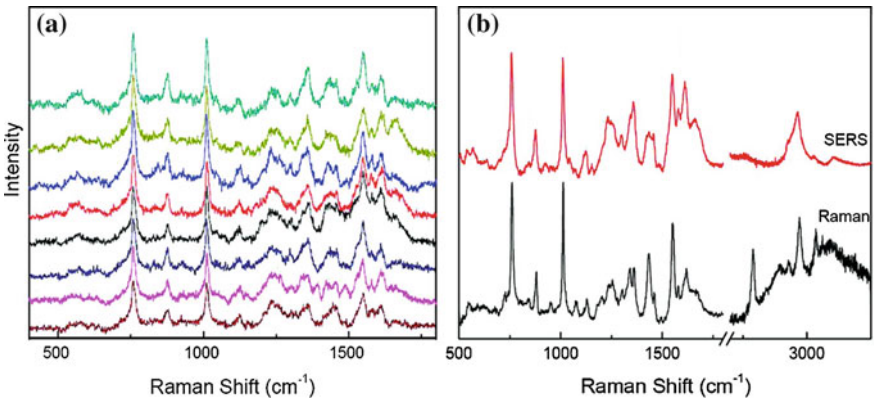

Fig. 5.8 Intrinsic SERS spectra of peptides. **a** SERS spectra of Try–Cys from eight different measurements, **b** a comparison of SERS with NRS spectra (adapted with permission from Wei et al. 2008. Copyright 2008 American Chemical Society)

found that SERS spectra were dominated by protein backbone groups and aromatic amino acid residues, which greatly simplified spectral interpretation. Moreover, SERS spectra from Au nanoshell substrate provided excellent reproducibility and close similarity to their respective NRS spectra. Figure 5.8 shows SERS spectra of Trp–Cys from eight different measurements (Fig. 5.8a) and a comparison of SERS with NRS spectra (Fig. 5.8b) as an example. Such a simple interpretation can also be used in the cases of basic proteins BSA and lysozyme. SERS spectra of BSA obtained from Au NPs showed mostly the S–S stretching vibration bands of the disulfide bridges and bands of aromatic Trp. Therefore, the authors suggested that interaction with the metal surface was realized mainly via the Trp residue (Iosin et al. 2009). SERS spectrum of lysozyme contained only spectral features of the Trp, Tyr, Phe and histidine (His) indicating their close vicinity to the metal surface (Das et al. 2009). In the case of proteins with a chromophoric group like haemoproteins, SERRS spectrum of this group dominates because the haem part is preferentially adsorbed on Ag surface. LOD is low enough for such proteins and even SM detection of haemoglobin (Xu et al. 1999), cytochrome c (Delfino et al. 2005), myoglobin (Bizzarri and Cannistraro 2002), allophycocyanin fluorescent protein (McGuinness et al. 2007) and green fluorescent proteins (Habuchi et al. 2003) on Ag NPs has been reported.

The main problem of protein SERS study is that the protein native structure can be disturbed by its interaction with a metal surface. SERS spectra of oxy- and deoxy- haemoglobin indicated a partial denaturation of haemoglobin when adsorbed on Ag colloidal NPs (Smulevich and Spiro 1985). Biocompatible coating of the metal surface by SAMs of alkanethiols terminated with NH_2– or COOH– groups mediating protein immobilization was used to preserve its native structure (Murgida and Hildebrandt 2006). Another way to keep the natural protein structure is the preparation of a specific SERS-active substrate where the protein molecule is more

or less regularly surrounded by metal. The protein then remains in its native state and the distance of a few nanometres between the two nanostructured metal creates a small gap providing large SERS enhancement. In adoptive silver films prepared by evaporation and protein deposition, proteins naturally fill cavity sites enclosed by two or more NPs. This approach also ensures a large SERS enhancement and allows protein sensing at monolayer protein surface densities without significant changes in their conformational state as was demonstrated in studies of human insulin and Ebola virus (Drachev et al. 2004; Drachev and Shalaev 2006). Another way is to employ two Ag NPs bridged by a protein molecule. SERS spectra of the Cys-mutants of the small protein FynSH3 were obtained from a single or a small number of protein molecules placed in a "hot spot" between two NPs (Pavel et al. 2008). On the other hand, spectral reproducibility is poor in this case. Ozaki and co-workers employed a different sandwich strategy for sensitive SERS detection of proteins (Han et al. 2009a, b). The sandwich structure is created by the interaction (bridge) between proteins in the middle layer and the metallic (Ag or Au) NPs in two metal layers. Intrinsic SERS spectra of cytochrome c, BSA and human immunoglobulin (IgG) were obtained with good sensitivity and reproducibility (Han et al. 2009b). The same scheme was applied when studied proteins (catalase, cytochrome c, avidin and lysozyme) were placed in the middle layer of the sandwich architecture formed by bowl-shaped silver cavity arrays and Ag NPs. The SERS spectra of catalase and cytochrome c were reported even at 5 μg ml^{-1} concentration (Gu et al. 2014).

Recently, the Ren group proposed iodide-modified Ag NPs where coated iodide layer offers a barrier to prevent the direct interaction between the proteins and the metal surface, helping to keep the native structures of proteins (Xu et al. 2014). With this method, good and highly reproducible SERS spectra of five common proteins (lysozyme, avidin, BSA, cytochrome c and haemoglobin) have been obtained. Moreover, the SERS features of the proteins without chromophore were almost identical to the respective NRS spectra. This allowed the qualitative identification of them by simply taking the intensity ratio of the Raman peaks of Trp to Phe residues. Figure 5.9A shows SERS spectra of (a) lysozyme, (b) avidin, (c) BSA, (d) Phe and (e) Trp. Figure 5.9B shows comparison between the experimental and theoretical values. The relative SERS intensity of 752/1000 cm^{-1} to the ratio of Trp/(Trp and Phe) for the three proteins is plotted. The inset table in panel B is the known number of Trp and Phe residues in each protein molecule. One can see that the relative intensities of 752/1000 cm^{-1} were in a surprisingly good agreement with the ratio of Trp/(Trp and Phe). It seems that proposed Ag iodide-modified Ag NPs can be used as a very simple way to perform intrinsic identification of proteins with a much better reliability and specificity than traditional spectroscopic methods.

A silver staining can significantly increase the sensitivity of label-free protein SERS detection. It is available for detection of proteins separated by gel electrophoresis. The basic mechanism underlying silver staining of proteins is that silver ions bound to amino acid side-chains (primary COO−, −SH) are reduced to free silver by a reductant (citric acid, formaldehyde, or photoreduction). The

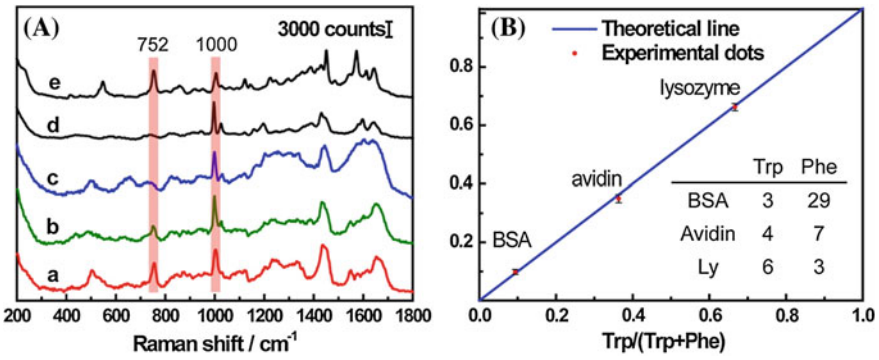

Fig. 5.9 SERS spectra of amino acids and proteins obtained using iodide-modified Ag NPs. **A** SERS spectra of (**a**) lysozyme, (**b**) avidin, (**c**) BSA, (**d**) Phe and (**e**) Trp. **B** Plot of the relative SERS intensity of 752/1000 cm^{-1} to the ratio of Trp/(Trp and Phe) for the three proteins (reproduced with permission from Xu et al. 2014. Copyright 2014 American Chemical Society)

so-called "Western-SERS" strategy is shown in Fig. 5.10a (Han et al. 2009a). It involves (i) electrophoresis, (ii) protein blotting, (iii) colloidal silver staining and (iv) SERS detection, all on a nitrocellulose membrane. Ag NPs were adsorbed along with the membrane where proteins were already adhered resulting in formation of aggregates. SERRS of myoglobin and SERS of BSA obtained by this method are shown in Fig. 5.10b. This "Western-SERS" method offers the dual advantages of simplicity and high sensitivity. It allows detection of label-free proteins directly on a nitrocellulose membrane without time and reagent-consuming procedures. Moreover, the LOD is very low, ~ 2 ng ml^{-1} due to silver staining.

The intrinsic detection of proteins is generally limited by the spectral similarity of many proteins. Moreover, the sensitivity of detection of proteins without a chromophore part is not high enough. Thus, the labelling of protein or using SERS tag with RRM providing strong SERS is promising. This approach will be introduced in Sect. 5.3.2.

5.3.2 Extrinsic Detection of Proteins

Labelling techniques have been developed to increase the sensitivity of protein detection as well as the number of proteins detectable by SERS. As for NAs, labelling is ensured by attachment of a SERRS dye to the studied protein molecule, such as benzotriazole dye used as the label to detect haem protein (Douglas et al. 2007). The employed RRMs include 5,5′-dithiobis(succinimidyl-2-nitrobenzoate) (DSNB), NBTs, methoxybenzenethiols, naphtalenethiols, (amino)thiophenols, MBAs, bipyridine and fluorescent dyes malachite green isothiocyanate and fluorescein isothiocyanate (Banz et al. 2011).

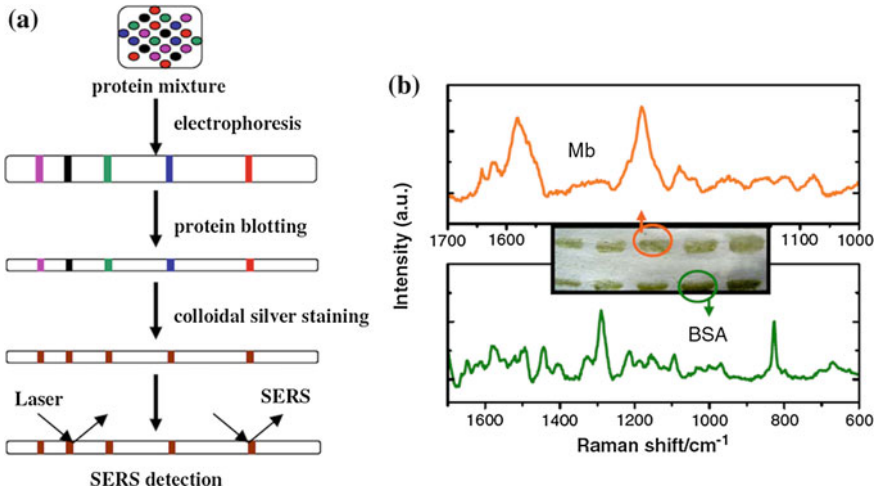

Fig. 5.10 "Western-SERS" strategy for label-free protein detection. **a** Basic scheme. **b** SERRS spectrum of myoglobin (*Mb*) and SERS spectrum of bovine serum albumin (*BSA*) (adapted with permission from Han et al. 2009a. Copyright 2009 Springer)

SERS tags containing RRMs were also applied for sensitive SERS detection of proteins. For example, Cao and co-workers reported the sensitive probe based on Ag NPs (13 nm diameter) coated with hydrophilic alkylthiol-capped oligonucleotides for the detection of small proteins (Cao et al. 2003). Each oligonucleotide contains a small molecule-recognition element such as biotin at one end and a Raman dye modification at the other end. When the corresponding target molecules are specifically bound through their recognition elements, the SERRS spectrum of dye is obtained (Cao et al. 2003). Han and co-workers developed a protein concentration assay using the SERS signal of RRM (coomassie brilliant blue dye) adsorbed nonspecifically to Ag NPs to monitor the total protein concentration (Han et al. 2010). The SERS signal of RRM displayed a linear and inverse relationship to protein concentration over a BSA concentration range from 10^{-5} to 10^{-9} g ml^{-1}. Extrinsic detection scheme is widely employed in immunoassay platforms as will be described in Sect. 5.3.3.

5.3.3 Immunoassays

Immunoassay platforms are employed to detect the target antigens or antibodies (typically small proteins) through specific antibody-antigen binding which is the main reaction of the human immune system. Immunoassays play an important role in the fields of drug identification, food safety, environmental monitoring and importantly also in clinical diagnostics. At present, the enzyme-linked

immunosorbent assay (ELISA) is the most widely used immunoassay technique for detecting the presence of antigen or its complementary antibody.

SERS is a promising technique to detect antibody-antigen binding due to its sensitivity and selectivity. Intrinsic label-free immuno-detection provides low sensitivity and specificity because in the absence of purification and separation steps the results are affected by the composition and the amount of other proteins and salts in the solution. In spite of this, Ozaki and co-workers (Dou et al. 1998) applied an intrinsic scheme to detect an antigen-antibody complex using Ag NPs. This method enabled the direct detection of mouse anti-IgG antibody (LOD $\sim 2 \times 10^{-8}$ M) via its amide and aromatic amino acid residues seen in the SERS spectrum. Later, SERS-active adoptive silver films were employed as the immunoassay capturing surface (Drachev and Shalaev 2006). The specific proteins used in these studies included the anti-FLAG M2 monoclonal antibody (fAb) and the bacterial alkaline phosphatase/C-terminal FLAG-peptide fusion (fBAP). The antigen (fBAP at 0.5 μM in tris-buffered saline solution) was first deposited on an adoptive silver films substrate followed by antibody (fAb at 4 nM) incubation. SERS signal associated with the antigen-antibody binding was strong enough to monitor this interaction.

To overcome the problem with low sensitivity and specificity, an extrinsic immunoassay scheme comprising dye labels or RRMs was employed (Ni et al. 1999, Grubisha et al. 2003). In the first application, a silver film was coated with anti-TSH (human thyroid-stimulating hormone) antibodies and then incubated with TSH (Rohr et al. 1989). A second anti-TSH antibody labelled with 4-dimethylaminoazobenzene was then added to bind to the attached THS. SERRS signal of the label served for THS quantification. Later, SERS immunoassays were constructed by using NPs as substrates which offered better reproducibility, versatility and possibility for multiplexing. Primary part of NP-based immunoassays is SERS tag consisting of metallic NP modified with RRM and an antibody. In immunoassay experiment, the antigen is selectively sandwiched between Au surface and Au NPs by the capture and labelling antibodies. Therefore, antigen is detected indirectly via SERS response of RRM (Porter et al. 2008). Figure 5.11 shows basic scheme of extrinsic immunoassays (Grubisha et al. 2003): (a) preparation of RRM- and antibody- functionalized Au NPs, (b) capture of functionalized Au NPs within a specific protein recognition on a gold coated glass slide, (c) SERS spectrum produced from captured RRM- functionalized NPs. Porter and co-workers (Porter et al. 2008) developed the immunoassay platform for SERS detection of a prostate-specific antigen (PSA). Their immunoassay platform has several advantages: (i) enhancements are reproducibly and quantitatively controlled by the size and shape of the NP, reproducible roughened capture surface is not needed, (ii) the use of RRM on NPs probe minimizes the distance between the NP surface and reporters and thus enhanced the sensitivity, (iii) multiplex analysis can be realized simply by changing the recognition elements on the capture substrate and RRM and forming multiple response on the capture substrate.

Multiplex immunoassays platform requires several RRMs to detect multiple agents. Immobilization of different antibodies and use of different reporters allow

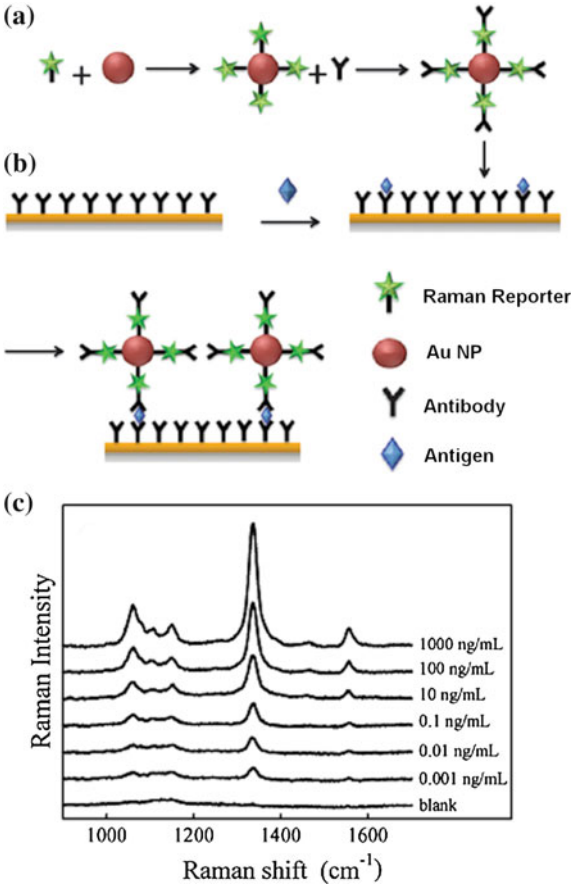

Fig. 5.11 Scheme of extrinsic immunoassays. **a** Preparation of RRM- and antibody- functionalized Au NPs. **b** Capture of functionalized Au NPs within a specific protein recognition on a gold coated glass slide. **c** SERS spectrum produced from captured RRM-functionalized NP (adapted from Grubisha et al. 2003. Copyright 2003 American Chemical Society)

various antigens to be simultaneously detected via characteristic SERS spectra of particular RRMs (Ni et al. 1999). Tian and co-workers introduced two approaches to multiplex sandwich-format SERS immunoassay. First, immobilized antibodies were exposed to the target molecule (mouse or human immunoglobulin IgG). Next, immobilized antibodies were exposed to (i) Au NPs with antibodies and two RRMs attached or (ii) Au and Au/Ag bimetallic NPs with antibodies and one RRM attached (Cui et al. 2007). First detection scheme allowed 50 μg ml^{-1} mouse and human IgG to be detected simultaneously. With second detection scheme, mouse and human IgG were detected individually at 100 μg ml^{-1} but the multianalyte assay was not successful due to overlapping peaks of the RRMs. Porter and co-workers (Wang et al. 2009) reported a tetraplexed assay to detect IgG from four species using four RRMs by employing their mixed monolayers on Au NPs.

Aptamers—short functional oligonucleotides (or proteins in some cases) that recognize target antigen protein—can be used in an immunoassay platform. Compared with traditional antibodies, aptamers have many specific advantages

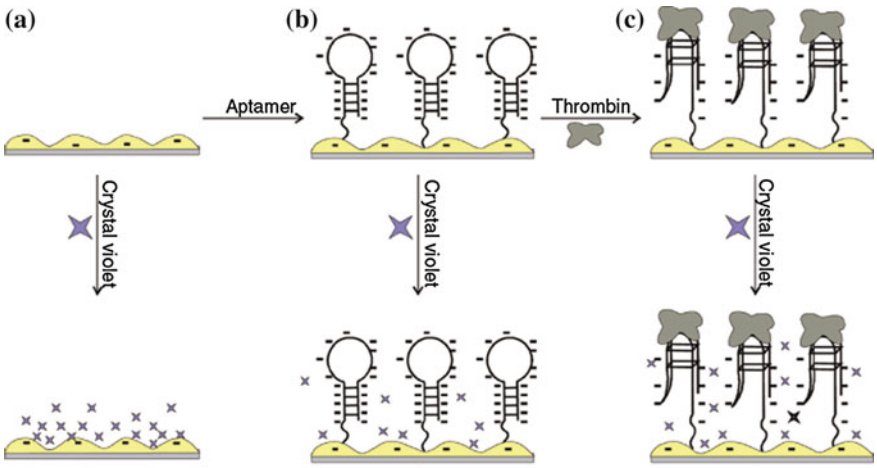

Fig. 5.12 Aptamer-based immuno-SERS detection of thrombin using crystal violet as RRM. See text for details (adapted with permission from Hu et al. 2009. Copyright 2009 American Chemical Society)

such as low molecular weight, easy and reproducible synthesis, high specificity and affinity for specific target proteins. As an example, an aptamer-based detection of thrombin applying positively charged crystal violet (CV) as RRM is shown in Fig. 5.12 (Hu et al. 2009). The thrombin detection was performed according to the different amount of the CV contributing to the overall SERS signal, based on electrostatic effects due to the changed structure of the thrombin-binding aptamer. When unmodified metallic nanostructure was employed (Fig. 5.12a), a strong SERS signal of the CV was detected. When binding to monolayer of aptamers (Fig. 5.12b), the amount of CV molecules on the metal surface was decreased due to electrostatic effects. This resulted in a lower SERS signal. In the case of thrombin binding to the aptamer structure (Fig. 5.12c), more CV molecules were bound to the surface.

Silver enhanced step can be applied to increase the sensitivity of immunoassay. Cao and co-workers (Cao et al. 2003) used the approach similar to DNA hybridization depicted in Sect. 5.2.5. Figure 5.13a, b shows two different types of probes developed for screening small molecule-protein (a: type I) and protein-protein (b: type II) interactions. Type I probes were formed by 13 nm Au NPs coated with hydrophilic alkylthiol-capped oligonucleotides (A20). Each oligonucleotide contained a small molecule-recognition element such as biotin at one end and modification with a Raman dye at the other end. Type II probes comprised 13 nm Au NPs equipped with an antibody for target (antigen) recognition, Raman-dye-modified alkylthiol-capped oligonucleotides for identification by the characteristic SERRS signature and BSA to further passivate the metal surface.

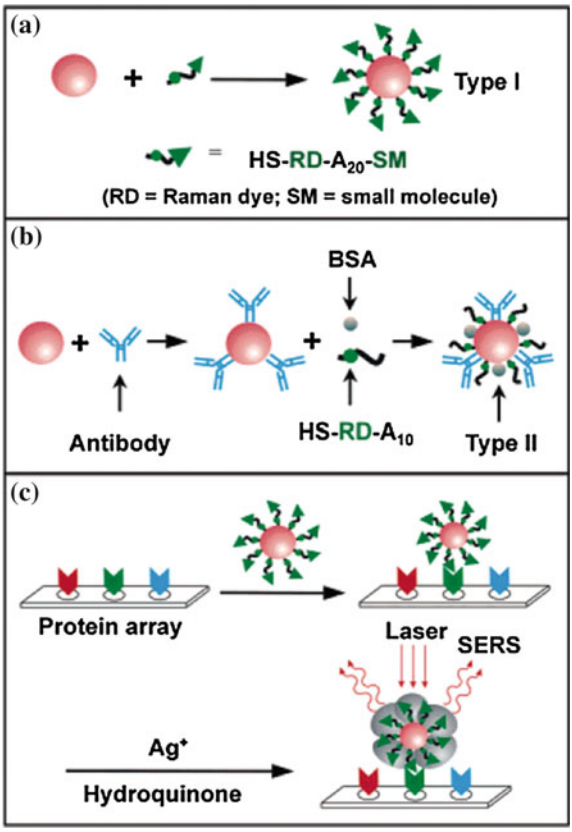

Fig. 5.13 Scheme of extrinsic immunoassays using Ag enhanced step. **a**, **b** Two NP probes. **c** SERS detection of **a** probes after immobilization on a chip and silver enhanced step with hydroquinone (reproduced with permission from Cao et al. 2003. Copyright 2003 American Chemical Society)

Figure 5.13c shows the protein chip produced by spotting the protein solution onto a functionalized glass slide. The chip was exposed to a suspension of the Raman-dye-labelled NP probes. After washing and Ag enhancement performed by the reduction of silver ions with hydroquinone, corresponding SERRS spectrum of the dye was obtained by Raman fibre optic probe. In aptamer-based thrombin assay, one thrombin molecule bound two 15-mer thrombin-binding aptamers simultaneously; thus, a sensing interface with a sandwich type aptamer/thrombin/aptamer/Au SERS tag could be fabricated. Then, higher SERS enhancement was achieved by deposition of Ag NPs on the Au SERS tags. LOD of this assay was $\sim$0.5 nM (Wang et al. 2007).

Single-walled carbon nanotubes (SWNTs) have been designed by Chen and co-workers to achieve lower LODs (Chen et al. 2008). A sandwich-assay scheme where an analyte (antibody) from a serum sample was captured by immobilized proteins in a microarray, was completed by incubation of SWNTs conjugated to goat anti-mouse antibody that specifically bind to the capture analyte. The strong SERS signal produced by the SWNT tag enabled protein detection sensitivity down

to 1 fM. Through differential conjugation of minimally cross-reactive secondary antibodies, the SWNTs were able to detect two types of target proteins simultaneously.

A novel sandwich-type immunoassay method using liposomes has been designed to detect human IgG (Liu et al. 2008). The method is based on the SERS-derived signal from RRMs (CV) encapsulated in antibody-modified liposome particles. The antigen was firstly captured by the primary antibody immobilized in microwell plates and then sandwiched by secondary antibody-modified liposome. The CV molecules were released from the liposome and transferred to specially designed substrate of Au nanosphere arrays with 10 nm gaps. SERS signal of CV showed excellent sensitivity with LOD 8 ng ml^{-1}.

The sensitivity can be further improved using anisotropic NPs, such as NRs, nanocubes or nanostars. For example, the nanocubes with RRM were 200 times more sensitive for IgG detection than spherical Au NPs (Narayanan et al. 2008). Nanostars served as a plasmonic nanosensor with inverse sensitivity (Rodríguez-Lorenzo et al. 2012). Au nanostars were modified with glucose oxidase. Hydrogen peroxide was generated due to reduction of oxygen in biocatalytic cycle of glucose oxidase. It served as reduction agent for Ag^{+} and Ag crystals were formed on the surface of Au nanostars providing SERS. The inverse sensitivity phenomenon was possible by controlling the kinetics of crystal growth with enzyme, the magnitude of the SERS signal registered by nanosensor depended on the rate of crystallization of Ag nanocrystal. When it grew slowly at low concentration of glucose oxidase, the growth of Ag coating on Au nanostars was favoured and LSPR of the nanosensors was blue-shifted providing higher SERS. The blue shift was larger at lower concentration of glucose oxidase. When Ag crystals grew fast at high concentration of glucose oxidase, the nucleation of free-standing small particles was favoured with no change of LSPR. In immunoassay scheme, Au nanostars were modified with anti-PSA antibody. PSA was captured between the Au nanostars and glucose oxidase via antibodies. The concentration of PSA was the same as the concentration of glucose oxidase. LOD of PSA was $\sim 10^{-18}$ g ml^{-1} (4×10^{-20} M = 24,000 molecules/l) in whole serum which was one order of magnitude lower than using standard ELISA.

A SERS tag-based immunoanalysis technique using magnetic separation has been developed. This method does not need an immobilization procedure on a solid substrate; instead, it applies MNPs as antibody-supporting materials. Furthermore, it overcomes the slow immunoreaction problems caused by the diffusion-limited kinetics on a solid substrate because the reaction occurs in a solution. Gong and co-workers reported such first immunoassay for α-fetoprotein (AFP). However, when Ag NPs were used, their aggregation led to their precipitation with time which reduced the SERS reproducibility (Gong et al. 2007). To solve this problem, hollow gold nanospheres were later applied as a base of SERS tags (Chon et al. 2009). This assay served for carcinoembryonic antigen (CEA) immunoanalysis. Figure 5.14a shows formation of the sandwich immunocomplex between monoclonal antibody (mAb)-conjugated hollow gold nanospheres and magnetic beads

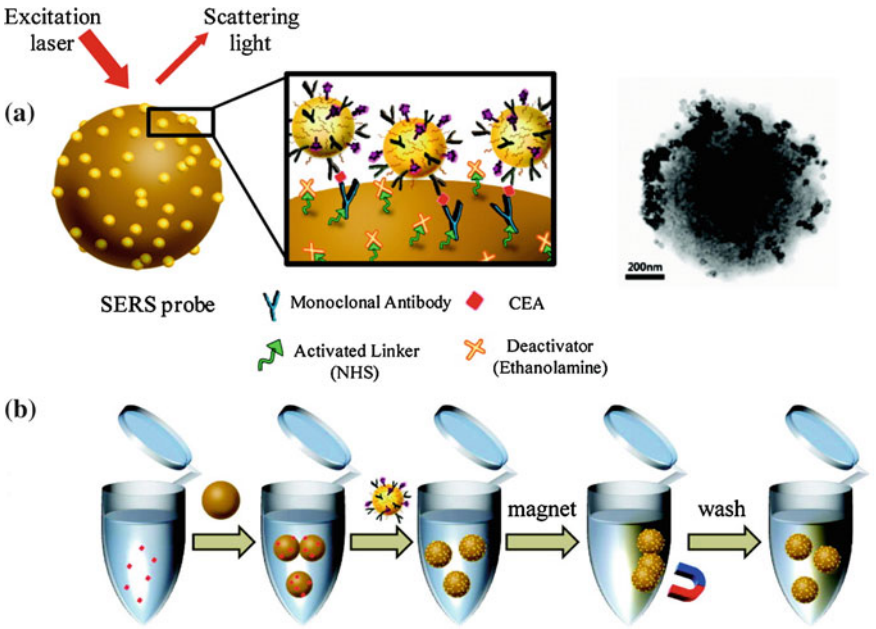

Fig. 5.14 Scheme of SERS immunoassay using MNPs. **a** Formation of the sandwich immunocomplex between antibody-conjugated hollow gold nanospheres and magnetic beads, TEM images of a single magnetic bead with carcinoembryonic (*CEA*) antigens. **b** Immunoassay process (adapted with permission from Chon et al. 2009. Copyright 2009 American Chemical Society)

together with TEM image of a single magnetic bead with CEA antigens. Figure 5.14b illustrates two steps of the sandwich immunoassy process. In the first step, mAb-conjugated magnetic beads were added in a phosphate-buffer saline (PBS) solution containing CEA. Next, the CEA-captured magnetic beads were isolated by a magnetic bar and then the solution was washed. In the second step, the obtained particles were further reacted with mAb-conjugated SERS tags in a shaker. The sandwich immunocomplexes were isolated by using a magnetic bar. The residual solution was washed and the immunocomplexes were redispersed in the PBS buffer before SERS measurements. The method was highly reproducible with LOD of 1–10 pg ml^{-1} which is approximately 100–1000 times lower than that of enzyme-linked immunosorbent assays and took less than 1 h.

Conventional SERS immunoassays involve multiple incubations and washing steps. Therefore, they are usually time-consuming and labour-intensive. The speed at which an immunoassay can be performed is limited by the rate of antigen delivery to the immobilized antibody for binding to occur. Typically heterogeneous assays rely on diffusion transport, which often leads to long incubation times for large biological molecules, particularly at low antigen concentrations. This diffusion limitation can be even more severe for NP-enabled assays, because of the

exceedingly small diffusion coefficient for SERS tags. This was evidenced by most SERS assays which reported 2–12 h incubations for each step, e.g. antigen binding and labelling (Wang et al. 2011). A rapid and automated SERS immunoassay has been designed using optoelectrofluidics based on the electrokinetic motion of particles or fluids (Hwang et al. 2010). In this study, PS microspheres as the capture substrate were utilized for the sandwich immunoassay of AFP. The PS microspheres were functionalized with monoclonal AFP antibodies to capture the AFP antigens. Ag NPs (40 nm diameter) were conjugated with a Raman active dye and polyclonal AFP antibody. The immunoassay was performed by mixing the functionalized PS microspheres, Ag NP suspension and the AFP solution in the sample chamber of the optoelectrofluidic device. After the sample injection, all the steps were automatically controlled and SERS signals were recorded from the locally concentrated immunocomplexes. Immunoreaction on this substrate was significantly faster than the conventional immunoassays on solid substrates, because all the reactions occured in solution and overcame the diffusion-limited kinetics. The assay required only 500 nl of AFP solution and $\sim$5 min analysis after sample injection with a LOD of 98 pg ml^{-1}.

The problem of any immunoassay is also the nonspecific binding along with antibody specificity which determines the LOD. Since nonspecific binding tends to be slower than a specific one, shorter assay times can suppress its interference in results. For example, Driskell and co-workers reported an approach to make the rate-limiting step of antigen capture more effective by using a rotating rod (Driskell et al. 2007). The two steps of the assay are illustrated in Fig. 5.15a. One end of a rotating rod was coated with gold and modified with dithiobis(succinimidylpropionate). Next, an antibody (anti-rabbit IgG) was coupled to this modified surface via succinimidylester chemistry, with the resulting capture substrate lowered into the sample. The rod was then rotated at a controlled rate (800 rpm), which extracted IgG onto the capture substrate. ERL (SERS tag) was constructed by Au NPs (60 nm diameter) functionalized with DSNB as RRM and IgG antibody. After rinsing, the capture substrate was immersed in an ERL solution and again rotated at a controlled rate. This step labelled the captured antigen, which was subsequently quantified by the SERS spectral intensity of the ERL. This approach reduced the assay time from 24 h (12 h capture step and 12 h labelling step) to 25 min (10 min capture step and 15 min labelling step) and resulted in a 10× improved LOD (Fig. 5.15b). Later, the same group developed an antibody-modified membrane as a flow-through capture substrate for a NPs-enabled SERS immunoassay to enhance the antibody-antigen binding kinetics (Penn et al. 2013). Such assay includes three steps: (i) antigen capture, (ii) ERL labelling and (iii) SERS detection (Fig. 5.15c). In this experiment, the RRM in ERL was 4-NBT. A thin layer of Au was plated onto polycarbonate track-etched nanoporous membranes via electroless deposition. The capture antibody was immobilized onto the surface of a gold-plated membrane via thiolate coupling chemistry to serve as a capture substrate. A syringe was then used to actively transport the analyte and ERLs to the capture substrate. It was demonstrated that the assay time for mouse IgG was reduced from 24 h to 10 min and LOD was 10× better.

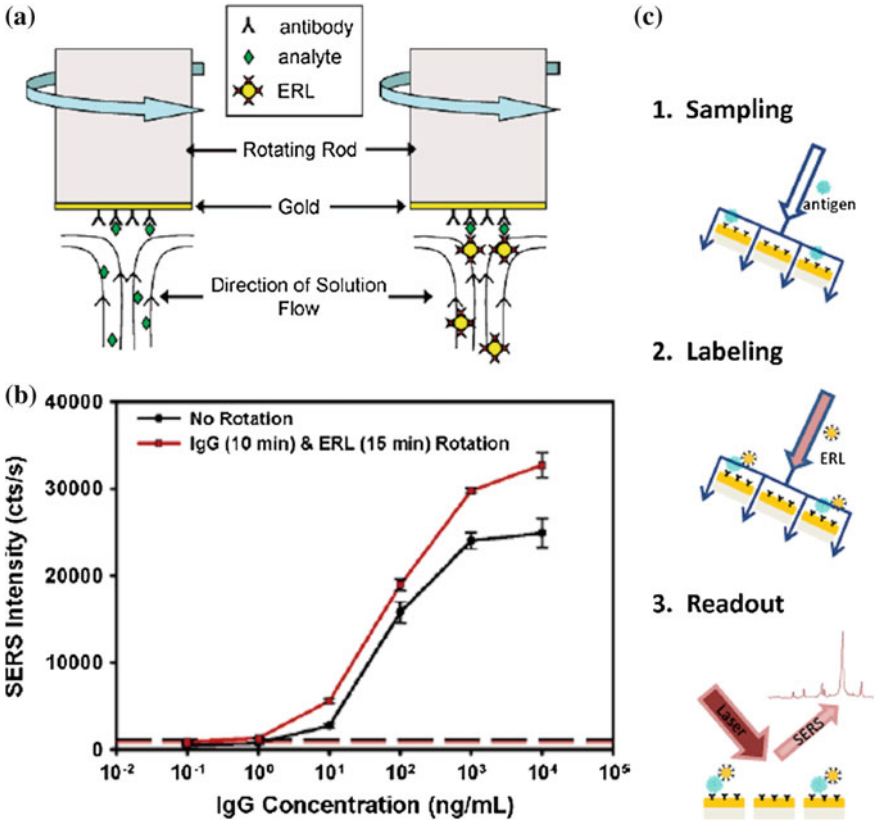

Fig. 5.15 Two approaches to increase a speed and specificity of immunoassays. **a** Scheme of rotating assay. **b** Dose-response curves for the SERS-based detection of rabbit IgG in PBS with and without rotation. The *dashed lines* represent the lowest detectable signal for assay. **c** Scheme of three-step assay using Au-plated membrane as the capture substrate and a syringe for active transport (adapted with permission from Driskell et al. 2007 (a, b) and Penn et al. 2013 (c). Copyright 2007, 2013 American Chemical Society)

Recently, Wang and co-workers demonstrated a new immunoassay platform to remove/avoid nonspecific adsorption and reduce assay time (Wang et al. 2015). This approach involved rationally designed fluorophore-integrated Au/Ag nanoshells as SERS tags and electrohydrodynamic-induced nanoscaled surface shear forces to enhance the capture kinetics of breast cancer biomarker. These forces act within nanometre distances from the electrode surface and possess the capability to induce fluid flow that can increase the number of antigen-antibody collisions while simultaneously shear away nonspecific molecules. The assay performance was validated in comparison with hydrodynamic flow and conventional immunoassay-based devices. SERS tags with Au/Ag nanoshells as the plasmonic enhancer and malachite green isothiocyanate was applied as the RRM. Detection

time using such novel immunoassay was shortened from 24 h to 40 min and the nonspecific binding was 10× lower than that of the conventional SERS immunoassay. The sensitivity was 10 fg ml^{-1} for human EGF receptor in case of patient breast cancer samples.

Nowadays, immunoassays are routinely used for detection of antigens in clinical testing, disease progression and diagnostic treatment including cancer (see Chap. 7). However, the success of immunoassays varies case-by-case depending on the particular target antigen and the biologically relevant concentration range that the assay must be able to detect.

5.4 Lipids and Membranes

Lipids are crucial structural elements of cell membranes. They store energy as fats in adipose tissue and they are important signalling molecules as well. Lipids display a large structural diversity, from amphiphilic structures with glycerol backbones like phospholipids to multiple ring structures like steroids. SERS of lipids is a developing field and expanding types of lipids that are studied could have impacts on membrane and lipid biology. Most applications of SERS of lipids and membranes involve intrinsic detection of lipid, investigations of phospholipid bilayers and their properties, as well as their interactions with various molecules of interest and the passage of molecules through them.

Lipids belong to poorly SERS-active species. Presence of both a positive and a negative charge on the molecule (which is the case of many phospholipids) makes adsorption of lipids on a metal surface difficult. Moreover, in SERS spectroscopy using metallic NPs, long fatty acid chains may hinder NP aggregation necessary to achieve sufficient SERS enhancement. Recently, SERS spectra of 1,2-distearoyl-*sn*-glycero-3-phosphocholine and dimyristoyl-3-trimethylammonium-propane were obtained at $\sim 10^{-7}$ M concentration (Šimáková et al. 2012, 2013). The SERS-active systems were formed by drying a drop of (Ag NPs)/lipid on a glass slide. Drying promoted lipid adsorption as well as aggregation of Ag NPs. Comparison of SERS spectra with NRS spectra of lipids showed that the structural properties of lipids were significantly disturbed by adsorption to Ag NPs.

Different types of mimetic systems of biological membranes including vesicles (spherical phospholipid bilayers), LB monolayers, hybrid bilayers (HBLs) and tethered lipid bilayers were used in SERS investigations. LB films are monomolecular films that can be fabricated from amphiphiles at the water-air interface and transferred to a SERS solid substrate (such as island film). For SERS studies, the target molecule was treated as a dopant in a monolayer matrix formed for example by arachidic acid or phospholipids. Aroca and co-workers applied the LB technique to detect SERRS signal from a variety of chromophores such as several perylene derivatives and RH6G even in SM level in some cases (Aroca 2006). HBLs are monolayers of phospholipids incorporated into SAM of long-chain thiols such as

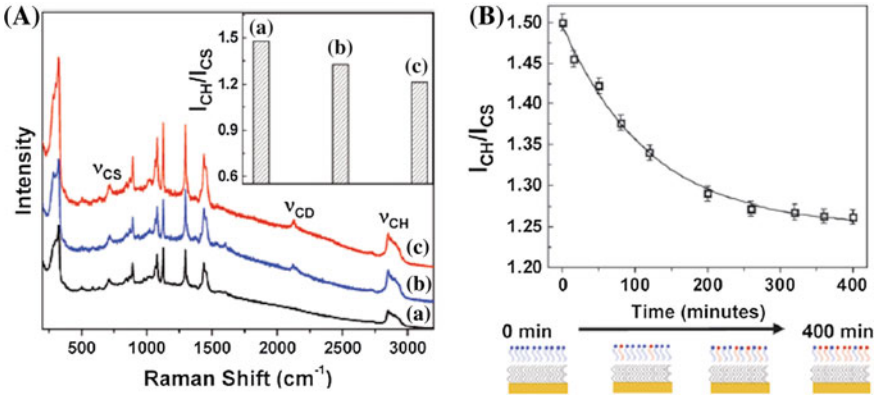

Fig. 5.16 SERS study of lipids. **A** SERS spectra of (**a**) HBL formed with DMPC, (**b**) HBL formed with DMPC incubated with d-DMPC vesicles and (**c**) a HBL formed with d-DMPC. The I_{CH}/I_{CS} ratio for the three different systems is shown in *inset*. **B** A plot of I_{CH}/I_{CS} versus time and a scheme of the plausible changes in the HBL composition (adapted with permission from Kundu et al. 2009b. Copyright 2009 The Royal Society of Chemistry)

dodecanethiol. Halas and co-workers studied the interaction of a small drug (ibuprofen) with HBL-coated Au nanoshells (Levin et al. 2008). HBLs were formed by a monolayer of lipid spread over a SAM of dodecanethiol. The interaction of ibuprofen with lipid bilayers in the gastrointestinal tract has been suggested as one of the mechanisms of observed ibuprofen side effects, such as gastrointestinal bleeding. When HBL nanoshells were incubated with ibuprofen, the changes in both SERS spectra of ibuprofen and HBL indicated that ibuprofen is partitioning into the HBL and disrupting the order of the HBL. The same group carried out SERS monitoring of in situ phospholipid transfer from unilamellar vesicles (spherical phospholipid bilayers of 85–100 nm diameter) of deuterated 1,2-dimyristoyl-*sn*-glycero-3-phosphocholine (d-DMPC) to HBL on Au nanoshell supports (Kundu et al. 2009b). Figure 5.16A compares SERS spectra of HBL formed with DMPC (spectrum a), HBL formed with DMPC incubated for 2 h with d-DMPC vesicles (spectrum b) and a HBL formed with d-DMPC (spectrum c). The SERS intensity of C–H stretching vibration at 2850 cm^{-1} was normalized to the intensity of the C–S stretching vibration at 710 cm^{-1} (I_{CH}/I_{CS}). When d-DMPC vesicles were mixed with HBL-coated nanoshells, a significant decrease in I_{CH}/I_{CS} was observed (inset of Fig. 5.16A), indicating transfer of lipids from vesicles to HBL. A plot of I_{CH}/I_{CS} versus time fitted to a first order exponential curve is shown in Fig. 5.16B together with a scheme of the plausible changes in the HBL composition. The kinetics of this transfer was characterized by a rate constant of $K = 1.3 \times 10^{-4}$ s^{-1}.

SERS has been employed to monitor incorporation of some molecules, such as medicament pirarubicin (Heywang et al. 1996) or photosensitizer hypericin (Lajos et al. 2009) inside the membranes. In order to interface lipid bilayers with solid substrates, many groups employ tethered lipid bilayers. In these systems, a lipid

molecule with a longer linking group was deposited on a surface as a SAM and then a second lipid monolayer was deposited to form a bilayer. The ordering of the lipid SAM can also be determined by SERS. Krysinski and co-workers prepared dipalmitoylphosphatidylethanolamine-mercaptopropionamine (DPPE-MPA) SAM lipid tether and studied its organization on a roughened polycrystalline gold substrate by SERS (Krysinski et al. 2001). They observed a significant difference in the conformation of the linking moiety of the SAM lipid tether monolayer in the air compared to an aqueous solution: in air, the *trans*-conformation was determined to be the dominant while in aqueous solution the *gauche* form of the tether dominated.

References

J.L. Abell, J.M. Garren, J.D. Driskell, R.A. Tripp, Y. Zhao, Label-free detection of micro-RNA hybridization using surface-enhanced Raman spectroscopy and least-squares analysis. J. Am. Chem. Soc. **134**, 12889 (2012)

R. Aroca, *Surface-Enhanced Vibrational Spectroscopy* (John Wiley & Sons, Chichester, 2006)

E. Bailo, V. Deckert, Tip-enhanced Raman spectroscopy of single RNA strands: towards a novel direct-sequencing method. Angew. Chem. Int. Ed. **47**, 1658 (2008)

K.C. Bantz, A.F. Meyer, N.J. Wittenberg, H. Im, O. Kurtulus, S.H. Lee, N.C. Lindquist, S.H. Oh, C.L. Haynes, Recent progress in SERS biosensing. Phys. Chem. Chem. Phys. **13**, 11551 (2011)

A. Barhoumi, N.J. Halas, Label-free detection of DNA hybridization using surface enhanced Raman spectroscopy. J. Am. Chem. Soc. **132**, 12792 (2010)

A. Barhoumi, D. Zhang, F. Tam, N.J. Halas, Surface-enhanced Raman spectroscopy of DNA. J. Am. Chem. Soc. **130**, 5523 (2008)

S.E.J. Bell, N.M.S. Sirimuthu, Surface-enhanced Raman spectroscopy (SERS) for sub-micromolar detection of DNA/RNA mononucleotides. J. Am. Chem. Soc. **128**, 15580 (2006)

A.R. Bizzarri, S. Cannistraro, Surface-enhanced resonance Raman spectroscopy signals from single myoglobin molecules. Appl. Spectrosc. **56**, 1531 (2002)

Y.C. Cao, R. Jin, C.A. Mirkin, Nanoparticles with Raman spectroscopic fingerprints for DNA and RNA detection. Science **297**, 1536 (2002)

Y.C. Cao, R. Jin, J.M. Nam, C.S. Thaxton, C.A. Mirkin, Raman dye-labeled nanoparticle probes for proteins. J. Am. Chem. Soc. **125**, 14676 (2003)

S. Caporali, V. Moggi-Cecchi, M. Muniz-Miranda, M. Pagliali, G. Pratesi, V. Schettino, SERS investigation of possible extraterrestrial life traces: experimental adsorption of adenine on a Martian meteorite. Meteorit. Planet. Sci. **47**, 853 (2012)

Z. Chen, S.M. Tabakman, A.P. Goodwin, M.G. Kattah, D. Daranciang, X.R. Wang, G.Y. Zhang, X.L. Li, Z. Liu, P.J. Utz, K.L. Jiang, S.S. Fan, H.J. Dai, Protein microarrays with carbon nanotubes as multicolor Raman labels. Nat. Biotechnol. **26**, 1285 (2008)

H. Chon, S. Lee, S.W. Son, C.H. Oh, J. Choo, Highly sensitive immunoassay of lung cancer marker carcinoembryonic antigen using surface-enhanced Raman scattering of hallow gold nanospheres. Anal. Chem. **81**, 3029 (2009)

G.D. Chumanov, T.M. Cotton, Surface-enhanced Raman scattering for discovering and scoring single-base differences in DNA. Proc. SPIE Biomed. Appl. Raman Spectrosc. **3608**, 204 (1999)

R.A. Copeland, S.P.A. Fodor, T.G. Spiro, Surface-enhanced Raman spectra of an active flavo enzyme: glucose oxidase and riboflavin binding protein on silver particles. J. Am. Chem. Soc. **106**, 3872 (1984)

T.M. Cotton, The applications of SERS to biological systems, in *Spectroscopy of Surfaces*, ed. by R.J.H. Clark, R.E. Hester (Wiley & Sons, Chichester, 1988), pp. 90–153

T.M. Cotton, S.G. Schultz, R.P. Van Duyne, Surface-enhanced resonance Raman scattering from cytochrome c and myoglobin adsorbed on a silver electrode. J. Am. Chem. Soc. **102**, 7960 (1980)

T.M. Cotton, J.-H. Kim, G.D. Chumanov, Application of surface-enhanced Raman spectroscopy to biological systems. J. Raman Spectrosc. **22**, 729 (1991)

Y. Cui, B. Ren, J. Yao, R. Gu, Z.Q. Tian, Multianalyte immunoassay based on surface-enhanced Raman spectroscopy. J. Raman Spectrosc. **38**, 896 (2007)

R. Das, R. Jagannathan, C. Sharan, U. Kumar, P. Poddar, Mechanistic study of surface functionalization of enzyme lysozyme synthesized Ag and Au nanoparticles using surface enhanced Raman spectroscopy. J. Phys. Chem. C **113**, 21493 (2009)

I. Delfino, A.R. Bizzarri, S. Cannistraro, Single-molecule detection of yeast cytrochrome c by surface-enhanced Raman spectroscopy. Biophys. Chem. **113**, 41 (2005)

F.T. Docherty, P.B. Monaghan, R. Keir, D. Graham, W.E. Smith, J.M. Cooper, The first SERRS multiplexing from labelled oligonucleotides in a microfluidics lab-on-a-chip. Chem. Commun. **1**, 118 (2004)

X. Dou, Y. Yamaguchi, H. Yamamoto, S. Doi, Y. Ozaki, NIR SERS detection of immune reaction on gold colloid particles without bound/free antigen separation. J. Raman Spectrosc. **29**, 739 (1998)

P. Douglas, K.M. McCarney, D. Graham, W.E. Smith, Protein–nanoparticle labelling probed by surface enhanced resonance Raman spectroscopy. Analyst **132**, 865 (2007)

V.P. Drachev, V.M. Shalaev, Biomolecule sensing with adaptive plasmonic nanostructures, in *Surface-Enhanced Raman Scattering: Physics and Applications*, vol. **103**, ed. by K. Kneipp, M. Moskovits, H. Kneipp (Springer-Verlag, Berlin Heidelberg 2006), pp. 351–366 (Top. Appl. Phys.)

V.P. Drachev, M.D. Thoreson, E.N. Khaliullin, V.J. Davisson, V.M. Shalaev, Surface-enhanced Raman difference between human insulin and insulin lispro detected with adoptive nanostructures. J. Phys. Chem. B **108**, 18046 (2004)

J.D. Driskell, J.M. Uhlenkamp, R.J. Lipert, M.D. Porter, Surface-enhanced Raman scattering immunoassays using a rotated capture substrate. Anal. Chem. **79**, 4141 (2007)

J.D. Driskell, A.G. Seto, L.P. Jones, S. Jokela, R.A. Dluhy, Y.P. Zhao, R.A. Tripp, Rapid microRNA (miRNA) detection and classification via surface-enhanced Raman spectroscopy (SERS). Biosens. Bioelectron. **24**, 917 (2008)

K. Faulds, Multiplexed SERS for DNA detection, in *Raman Spectroscopy for Nanomaterials Characterization*, ed. by C.S.S.R. Kumar (Springer, Berlin Heidelberg, 2012), pp. 353–378

K. Faulds, W.E. Smith, D. Graham, Evaluation of surface-enhanced resonance Raman scattering for quantitative DNA analysis. Anal. Chem. **76**, 412 (2004)

K. Faulds, R. Jarvis, W.E. Smith, D. Graham, R. Goodacre, Multiplexed detection of six labelled oligonucleotides using surface enhanced resonance Raman scattering (SERRS). Analyst **133**, 1505 (2008)

C. Garrido, T. Aguayo, E. Clavijo, J.S. Gómez-Jeria, M.M. Campos-Vallette, The effect of the pH on the interaction of L-arginine with colloidal silver nanoparticles. A Raman and SERS study. J. Raman Spectrosc. **44**, 1105 (2013)

J.L. Gong, Y. Liang, Y. Huang, J.W. Chen, J.H. Jiang, G.L. Shen, R.Q. Yu, Ag/SiO_2 core-shell nanoparticle-based surface-enhanced Raman probes for immunoassay of cancer marker using silica-coated magnetic nanoparticles as separation tools. Biosens. Bioelectron. **22**, 1501 (2007)

D. Graham, K. Faulds, Quantitative SERRS for DNA sequence analysis. Chem. Soc. Rev. **37**, 1042 (2008)

D. Graham, W.E. Smith, A.M.T. Linacre, C.H. Munro, N.D. Watson, P.C. White, Selective detection of deoxyribonucleic acid at ultralow concentrations by SERRS. Anal. Chem. **69**, 4703 (1997)

D. Graham, D.G. Thompson, W.E. Smith, K. Faulds, Control of enhanced Raman scattering using a DNA-based assembly process of dye-coded nanoparticles. Nat. Nanotechnol. **3**, 548 (2008)

L. Grajcar, V. Huteao, T. Huynh-Dinh, M.-H. Baron, A SERS probe for adenyl residues available for intermolecular interactions. Part II—Reactive adenyl sites in highly diluted DNA. J. Raman Spectrosc. **32**, 1037 (2001)

L. Grajcar, C. El Amri, M. Ghomi, S. Fermandjian, V. Huteau, R. Mandel, S. Lecomte, M.H. Baron, Assessment of adenyl residue reactivity within model nucleic acids by surface enhanced Raman spectroscopy. Biopolymers **82**, 6 (2006)

D.S. Grubisha, R.J. Lipert, H.Y. Park, J. Driskell, M.D. Porter, Femtomolar detection of prostate-specific antigen: an immunoassay based on surface-enhanced Raman scattering and immunogold labels. Anal. Chem. **75**, 5936 (2003)

X. Gu, Y.R. Yan, G. Jinag, J. Adkins, J. Shi, G. Jianh, S. Tian, Using a silver-enhanced microarray sandwich structure to improve SERS sensitivity for protein detection. Anal. Bioanal. Chem. **406**, 1885 (2014)

L. Guerrini, Z. Krpetic, D. van Lierop, R.A. Alvarez-Puebla, D. Graham, Direct surface-enhanced Raman scattering analysis of DNA duplexes. Angew. Chem. Int. Ed. **54**, 1144 (2015)

S. Habuchi, M. Cotlet, R. Gronheid, G. Dirix, J. Michiels, J. Vanderleyden, F.C.D. Schryver, J. Hofkens, Single-molecule surface enhanced resonance Raman spectroscopy of the enhanced green fluorescent protein. J. Am. Chem. Soc. **125**, 8446 (2003)

X.X. Han, B. Zhao, Y. Ozaki, Surface-enhanced Raman scattering for protein detection. Anal. Bioanal. Chem. **394**, 1719 (2009a)

X.X. Han, Y. Kitahama, T. Itoh, C.X. Wang, B. Zhao, Y. Ozaki, Protein-mediated sandwich strategy for surface-enhanced Raman scattering: application to versatile protein detection. Anal. Chem. **81**, 3350 (2009b)

X.X. Han, B. Huang, B. Zhao, Y. Ozaki, Label-free highly sensitive detection of proteins in aqueous solutions using surface-enhanced Raman scattering. Anal. Chem. **81**, 3329 (2009c)

X.X. Han, Y. Xie, B. Zhao, Y. Ozaki, Highly sensitive protein concentration assay over a wide range via surface-enhanced Raman scattering of coomassie brilliant blue. Anal. Chem. **82**, 4325 (2010)

C. Heywang, M. Saint-Pierre Chazalet, M. Masson, A. Garnier-Suillerot, J. Bolard, Incorporation of exogeneous molecules inside mono- and bilayers of phospholipids: influence of the mode of preparation revealed by SERRS and surface pressure studies. Langmuir **12**, 6459 (1996)

P. Hildebrandt, J.J. Feng, A. Kranich, K.H. Ly, D.F. Martín, M. Martí, D.H. Murgida, D.A. Paggi, N. Wisitruangsakul, M. Sezer, I.M. Weidinger, I. Zebger, Electron transfer of proteins at membrane models, in *Surface Enhanced Raman Spectroscopy: Analytical, Biophysical and Life Science Applications*, ed. by S. Schlücker (Wiley-WCH, Weinheim, 2011), pp. 219–240

R.E. Holt, T.M. Cotton, Surface-enhanced resonance Raman and electrochemical investigation of glucose-oxidase catalysis at a silver electrode. J. Am. Chem. Soc. **111**, 2815 (1989)

J. Hu, P.C. Zheng, J.H. Jiang, G.L. Shen, R.Q. Yu, G.K. Liu, Electrostatic interaction based approach to thrombin detection by surface-enhanced Raman spectroscopy. Anal. Chem. **81**, 87 (2009)

H. Hwang, H. Chon, J. Choo, J.K. Park, Optoelectrofluidic sandwich immunoassays for detection of human tumor marker using surface-enhanced Raman scattering. Anal. Chem. **82**, 7603 (2010)

M. Iosin, F. Toderas, P.L. Baldeck, S. Astilean, Study of protein-gold nanoparticle conjugates by fluorescence and surface-enhanced Raman scattering. J. Mol. Struct. **924–26**, 196 (2009)

N.R. Isola, D.L. Stokes, T. Vo-Dinh, Surface enhanced Raman gene probe for HIV detection. Anal. Chem. **70**, 1352 (1998)

A. Kandakkathara, I. Utkin, R. Fedosejevs, Surface-enhanced Raman scattering (SERS) detection of low concentrations of trypthophan amino acid in silver colloid. Appl. Spectrosc. **65**, 507 (2011)

K. Kneipp, Y. Wang, H. Kneipp, L.T. Perelman, I. Itzkan, R.R. Dasari, M.S. Feld, Single molecule detection using surface-enhanced Raman scattering (SERS). Phys. Rev. Lett. **78**, 1667 (1997)

E. Koglin, J.-M. Séquaris, Surface enhanced Raman scattering of biomolecules. Top. Curr. Chem. **134**, 1 (1986)

P. Krysinski, A. Zebrowska, A. Michota, J. Bukowska, L. Becucci, M. Moncelli, Tethered mono- and bilayer lipid membranes on Au and Hg. Langmuir **17**, 3852 (2001)

J. Kundu, O. Neumann, B.G. Janesko, D. Zhang, S. Lal, A. Barhoumi, G.E. Scuseria, N.J. Halas, Adenine- and adenosine monophosphate (AMP)-gold binding interactions studied by surface-enhanced Raman and infrared spectroscopies. J. Phys. Chem. C **113**, 14390 (2009a)

J. Kundu, C.S. Levin, N.J. Halas, Real-time monitoring of lipid transfer between vesicles and hybrid bilayers on Au nanoshells using surface-enhanced Raman scattering (SERS). Nanoscale **1**, 114 (2009b)

G. Lajos, D. Jancura, D.P. Miskovsky, J.V. Garcia-Ramos, S. Sanchez-Cortes, Interaction of the photosensitizer hypericin with low-density lipoproteins and phosphatidylcholine: a surface-enhanced Raman scattering and surface-enhanced fluorescence study. J. Phys. Chem. C **113**, 7147 (2009)

I.A. Larmour, K. Faulds, D. Graham, The past, present and future of enzyme measurements using surface enhanced Raman spectroscopy. Chem. Sci. **1**, 151 (2010)

C.S. Levin, J. Kundu, B.G. Janesko, G.E. Scuseria, R.M. Raphael, N.J. Halas, Interactions of ibuprofen with hybrid lipid bilayers probed by complementary surface-enhanced vibrational spectroscopies. J. Phys. Chem. B **112**, 14168 (2008)

E. Lipiec, R. Sekine, J. Bielecki, W.M. Kwiatek, B.R. Wood, Molecular characterization of DNA double strand breaks with tip-enhanced Raman scattering. Angew. Chem. Int. Ed. **53**, 169 (2014)

X.L. Liu, S.G. Huan, Y. Bu, G. Shen, R. Yu, Liposome-mediated enhancement of the sensitivity in immunoassay based on surface-enhanced Raman scattering at gold nanosphere array substrate. Talanta **75**, 797 (2008)

I.D.G. Macdonald, W.E. Smith, Orientation of cytochrome c adsorbed on a citrate-reduced silver colloid surface. Langmuir **12**, 706 (1996)

N.E. Marotta, K.R. Beavers, L.A. Bottomley, Limitations of surface enhanced Raman scattering in sensing DNA hybridization demonstrated by label-free DNA oligos as molecular rulers of distance-dependent enhancement. Anal. Chem. **85**, 1440 (2013)

C.D. McGuinness, A.M. Macmillan, J. Karolin, W.E. Smith, D. Graham, D.J.C. Pickup, D.J.S. Birch, Single molecule level detection of allophycocyanin by surface enhanced resonance Raman scattering. Analyst **132**, 633 (2007)

D.H. Murgida, P. Hildebrandt, Surface-enhanced vibrational spectroelectrochemistry: electric-field effects on redox and redox-coupled processes of heme proteins, in *Surface-enhanced Raman scattering: physics and applications*, vol. **103**, ed. by K. Kneipp, M. Moskovits, H. Kneipp (Springer-Verlag, Berlin Heidelberg 2006), pp. 313–334 (Top. Appl. Phys.)

D.H. Murgida, P. Hildebrandt, Disentangling interfacial redox processes of proteins by SERR spectroscopy. Chem. Soc. Rev. **37**, 937 (2008)

R. Narayanan, R.J. Lipert, M.D. Porter, Cetyltrimethylammonium bromide-modified spherical and cube-like gold nanoparticles as extrinsic Raman labels in surface-enhanced Raman spectroscopy based heterogeneous immunoassays. Anal. Chem. **80**, 2265 (2008)

J. Ni, R.J. Lipert, G.B. Dawson, M.D. Porter, Immunoassay readout method using extrinsic Raman labels adsorbed on immunogold colloids. Anal. Chem. **71**, 4903 (1999)

E. Papadopoulou, S.E.J. Bell, DNA reorientation on Au nanoparticles: label-free detection of hybridization by surface enhanced Raman spectroscopy. Chem. Commun. **47**, 10966 (2011a)

E. Papadopoulou, S.E.J. Bell, Label-free detection of single-base mismatches in DNA by surface-enhanced Raman spectroscopy. Angew. Chem. Int. Ed. **50**, 9058 (2011b)

E. Papadopoulou, S.E.J. Bell, Label-free detection of nanomolar unmodified single- and double-stranded DNA by using surface-enhanced Raman spectroscopy on Ag and Au colloids. Chem. Eur. J. **18**, 5394 (2012)

I. Pavel, E. McCarney, A. Elkhaled, A. Morrill, K. Plaxco, M. Moskovits, Label-free SERS detection of small proteins modified to act as bifunctional linkers. J. Phys. Chem. C **112**, 4880 (2008)

N. Pazos-Perez, R.A. Álvarez-Puebla, SERS-encoded particles, in *Raman spectroscopy for nanomaterials characterization*, ed. by C.S.S.R. Kumar (Springer, Berlin Heidelberg, 2012), pp. 33–50

M.A. Penn, D.M. Drake, J.D. Driskell, Accelerated surface-enhanced Raman spectroscopy (SERS)-based immunoassay on a gold-plated membrane. Anal. Chem. **85**, 8609 (2013)

R. Picorel, R.E. Holt, R. Heald, T.M. Cotton, M. Seibert, Stability of isolated bacterial and photosystem-II reaction center complexes on Ag electrode surfaces—a surface-enhanced resonance Raman study. J. Am. Chem. Soc. **113**, 2839 (1991)

E. Podstawka, Y. Ozaki, L.M. Proniewicz, Surface-enhanced Raman spectroscopy investigation of amino acids and their homodipeptides adsorbed on colloidal silver. Appl. Spectrosc. **58**, 570 (2004a)

E. Podstawka, Y. Ozaki, L.M. Proniewicz, Adsorption of S-S containing proteins on a colloidal surface studied by surface-enhanced Raman spectroscopy. Appl. Spectrosc. **58**, 1147 (2004b)

M.D. Porter, R.L. Lipert, L.M. Siperko, G. Wang, R. Narayanan, SERS as a bioassay platform: fundamentals, design, and applications. Chem. Soc. Rev. **37**, 1001 (2008)

E. Prado, N. Daugey, S. Plumet, L. Servant, S. Lecomte, Quantitative label-free RNA detection using surface-enhanced Raman spectroscopy. Chem. Commun. **47**, 7425 (2011)

L. Rodríguez-Lorenzo, R. de la Rica, R.A. Alvarez-Puebla, L.M. Liz-Marzán, M.M. Stevens, Plasmonic nanosensors with inverse sensitivity by means of enzyme-guided crystal growth. Nature Mat. **11**, 604 (2012)

T.E. Rohr, T. Cotton, N. Fan, P.J. Tarcha, Immunoassay employing surface-enhanced Raman spectroscopy. Anal. Biochem. **182**, 388 (1989)

G. Rusciano, A.C. De Luca, G. Pesce, A. Sasso, G. Oliviero, J. Amato, N. Borbone, S. D'Errico, V. Piccialli, G. Piccialli, L. Mayol, Label-free probing of G-quadruplex formation by surface-enhanced Raman scattering. Anal. Chem. **83**, 6849 (2011)

S. Schlücker, SERS microscopy: nanoparticle probes and biomedical applications, in *Surface Enhanced Raman Spectroscopy: Analytical, Biophysical and Life Science Applications*, ed. by S. Schlücker (Wiley-WCH, Weinheim, 2011), pp. 263–284

S. Schlücker, Surface-enhanced Raman spectroscopy: concepts and chemical applications. Angew. Chem. Int. Ed. **53**, 4756 (2014)

P. Šimáková, M. Procházka, E. Kočišová, SERS Microspectroscopy of biomolecules on dried Ag colloidal drops. Spectrosc. Int. J. **27**, 449 (2012)

P. Šimáková, M. Procházka, E. Kočišová, Sensitive Raman spectroscopy of lipids based on drop deposition using DCDR and SERS. J. Raman Spectrosc. **44**, 1479 (2013)

W.E. Smith, Practical understanding and use of surface enhanced Raman scattering/surface enhanced resonance Raman scattering in chemical and biological analysis. Chem. Soc. Rev. **37**, 955 (2008)

G. Smulevich, T.G. Spiro, Surface enhanced Raman-spectroscopic evidence that adsorption on silver particles can denature heme-proteins. J. Phys. Chem. **89**, 5168 (1985)

R. Stevenson, K. Faulds, D. Graham, Quantitative DNA analysis using surface-enhanced resonance Raman scattering, in *Surface Enhanced Raman Spectroscopy: Analytical, Biophysical and Life Science Applications*, ed. by S. Schlücker (Wiley-WCH, Weinheim, 2011), pp. 241–262

R. Treffer, R. Böhme, T. Deckert-Gaudig, K. Lau, S. Tiede, X. Lin, V. Deckert, Advances in TERS (tip-enhanced Raman scattering) for biochemical applications. Biochem. Soc. Trans. **40**, 609 (2012)

E.A. Vitol, E. Brailoiu, Z. Orynbayeva, N.J. Dun, G. Friedman, Y. Gogotsi, Surface-enhanced Raman spectroscopy as a tool for detecting Ca^{2+} mobilizing second messengers in cell extracts. Anal. Chem. **82**, 6770 (2010)

T. Vo-Dinh, D.L. Stokes, G.D. Griffin, M. Volkan, U.J. Kim, M.I. Simon, Surface-enhanced Raman scattering (SERS) method and instrumentation for genomics and biomedical analysis. J. Raman Spectrosc. **30**, 785 (1999)

T. Vo-Dinh, F. Yan, M.B. Wabuyele, Surface-enhanced Raman scattering for medical diagnostics and molecular imaging, in *Surface-Enhanced Raman Scattering: Physics and Applications*, vol. **103**, ed. by K. Kneipp, M. Moskovits, H. Kneipp (Springer-Verlag, Berlin Heidelberg 2006), pp. 409–426 (Top. Appl. Phys.)

Y. Wang, H. Wei, B. Li, W. Ren, S. Guo, S. Dong, E. Wang, SERS opens a new way in aptasensor for protein recognition with high sensitivity and selectivity. Chem. Commun. **48**, 5220 (2007)

G. Wang, H. Park, R. Lipert, M.D. Porter, Mixed monolayers on gold nanoparticle labels for multiplexed surface-enhanced Raman scattering based immunoassays. Anal. Chem. **81**, 9643 (2009)

G.F. Wang, R.J. Lipert, M. Jain, S. Kaur, S. Chakraboty, M.P. Torres, S.K. Batra, R.E. Brand, M. D. Porter, Detection of the potential pancreatic cancer marker MUC4 in serum using surface-enhanced Raman scattering. Anal. Chem. **83**, 2554 (2011)

Y. Wang, B. Yan, L. Chen, SERS tags: novel optical nanotags for bioanalysis. Chem. Rev. **113**, 1391 (2013)

Y. Wang, R. Vaidyanathan, M.J.A. Shiddiky, M. Trau, Enabling rapid and specific surface-enhanced Raman scattering immunoassay using nanoscaled surface shear forces. ACS Nano **9**, 6354 (2015)

F. Wei, D. Zhang, N.J. Halas, J.D. Hartgerink, Aromatic amino acids providing characteristics motifs in the Raman and SERS spectroscopy of peptides. J. Phys. Chem. B **112**, 9158 (2008)

H. Xu, E.J. Bjerneld, M. Käll, L. Börjesson, Spectroscopy of single hemoglobin molecules by surface enhanced Raman scattering. Phys. Rev. Lett. **83**, 4357 (1999)

L.J. Xu, C. Zong, X.S. Zheng, P. Hu, J.M. Feng, B. Ren, Label-free detection of native proteins by surface-enhanced Raman spectroscopy using iodide-modified nanoparticles. Anal. Chem. **86**, 2238 (2014)

N.R. Yaffe, E.W. Blanch, Effects and anomalies that can occur in SERS spectra of biological molecules when using a wide range of aggregating agents for hydroxylamine-reduced and citrate-reduced silver colloids. Vib. Spectrosc. **48**, 196 (2008)

D. Zhang, K.F. Domke, B. Pettinger, Tip-enhanced Raman spectroscopic studies of the hydrogen bonding between adenine and thymine adsorbed on Au(III). Chem. Phys. Chem. **11**, 1662 (2010)

Chapter 6
SERS Investigations of Cells, Viruses and Microorganisms

Abstract Spectroscopic analysis of various species distributed inside living cells or microorganisms is currently one of the main challenges for development of SERS applications. This chapter will focus on the main principles of intracellular SERS studies and SERS detection along with identification of viruses and microorganisms. Intracellular SERS detection is based on measurement of SERS signal from metallic nanoparticles or nanoaggregates delivered inside the cell. Chemical probing in cells can be obtained by intrinsic SERS spectra from bare nanoparticles. SERS tags consisting of metallic nanoparticles and RRMs enable an assignment of intrinsic SERS signatures to specific locations where the tag is targeted. The spectra are dominated by spectral features of nucleic acids and proteins. The intracellular pH can be monitored via the SERS spectrum of SERS tag containing a molecule sensitive to pH (e.g. 4-mercaptobenzoic acid). The SERS measurements on bacteria are performed on bulk material using metallic nanoparticles which are accumulated in the outer part of the bacterium walls resulting in an averaging over a lot of bacterial cells. To distinguish and group together bacteria based on their spectral fingerprints, a multivariate data analysis technique should be used.

6.1 Intracellular SERS Investigations

6.1.1 Intracellular SERS Detection Strategies

Intracellular SERS detection is based on measurement of SERS signal from metallic NPs or nanoaggregates delivered inside the cell. Figure 6.1 illustrates three major strategies for intracellular SERS applications (Kneipp 2011). Bare metallic individual NPs or aggregates are delivered into cells and intrinsic intracellular SERS spectra are measured (a). This provides molecular information from the immediate surroundings of metallic NPs. SERS tags consisting of metallic NPs and RRM are used in targeting strategy enabling an assignment of intrinsic SERS signatures to specific locations where the tag was targeted (b). A third strategy represents the use

M. Procházka, *Surface-Enhanced Raman Spectroscopy*,
Biological and Medical Physics, Biomedical Engineering,
DOI 10.1007/978-3-319-23992-7_6

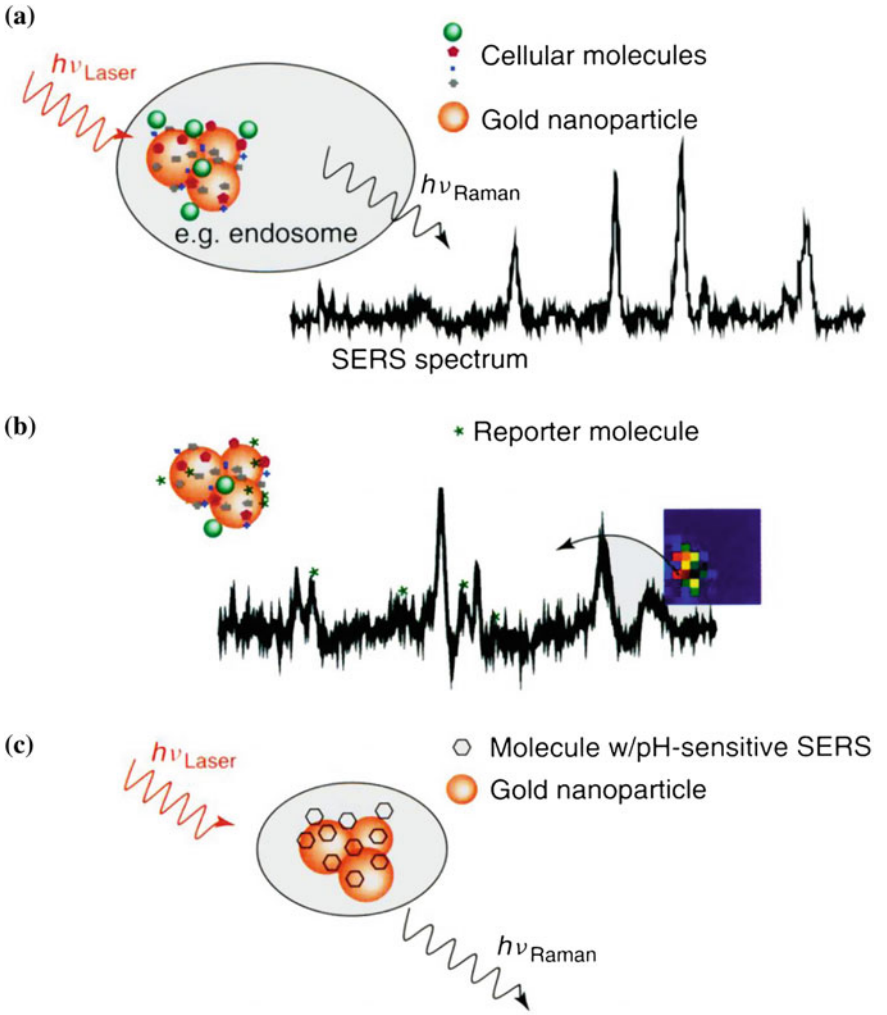

Fig. 6.1 Summary of different strategies for intracellular SERS. **a** Au NPs or aggregate provide molecular information from their immediate surroundings. **b** Hybrid SERS tag constructed from the Au NPs and RRMs that serve to identify the tag. It generates SERS signal from both the cell and RRM. **c** Au NPs with pH-sensitive RRM can serve as a pH sensor (adapted with permission from Kneipp 2011. Copyright 2011 Wiley-VCH Verlag GmbH & Co. KGaA, Weinheim)

of SERS tags which function on the basis of a signature of RRM without spectral information about cellular molecules. An example is the pH nanosensor (c). All three strategies are discussed in the following paragraphs.

6.1.2 *Delivery of the Metallic NPs Inside the Cells*

Intracellular SERS measurements require an delivery of the metallic NPs into the living cell. Most of the known applications are based on the Ag or Au NPs. Au NPs are used more often because they are inert, have minimum influence on their surroundings, are not toxic and thus they are biocompatible with cells (Boisselier and Astruc 2009). In the case of Ag NPs, their potential cytotoxicity at high concentrations should be taken into account (Bar-Ilan et al. 2009). Evidence that cells are alive after treatment with metallic NPs comes from phase contrast inspection of the cultures, showing that cells are visibly growing and that there is no evidence of cell rounding, apoptotic activity, or cell detachment from the growth surface (Xie et al. 2011). The employment of metallic NPs has both advantages and limitations. The main advantage is the small NP size (below 150 nm for isolated NPs and below 1–2 μm for aggregates) compared to cell dimensions (typically 10–20 μm). Therefore, the isolated NPs or small aggregates can be introduced into a cell with minimal damage of the cellular membrane integrity and then distributed within the cell with minimal perturbation of the subcellular environment. The principal limitations of NPs come from the difficulty to deliver them into cells and the control of their intracellular aggregation and distribution. SERS enhancement differs drastically between individual NPs and NP aggregates. SERS signal is then inhomogeneously distributed over the cell and varies due to different enhancement from different NPs clusters and also due to their heterogeneous distribution (Kneipp and Drescher 2014). TEM was used to monitor aggregation of NPs inside the immortalized rat renal proximal tubule cells. Such an approach was applied to optimize SERS signal of intracellular components measured from particular NPs aggregates (Kneipp et al. 2006). The distribution of metallic NPs inside cells can be also visualized by elemental analysis, such as laser ablation inductively coupled plasma mass spectrometry. This technique provides high sensitivity and spatial resolution enabling quantification of NPs at the single cell level (Drescher et al. 2012).

Delivery of NPs into the cells can be achieved in a number of ways depending on the type of cell line and the physicochemical parameters of the NPs such as size, shape and surface functionalization. The natural passive uptake mechanism from cell culture medium is called endocytosis. Such delivery is illustrated in Fig. 6.2a adapted from Kneipp (2006). The subcultured cell lines: NIH/3T3 fibroblasts and J774 macrophages were seeded on glass coverslips on which they were grown and Au NPs (or Au tags) were added to the culture medium for delivery. After an incubation time varying from a few minutes to several hours, the cells were washed in buffer to remove all excess NPs. Parallel samples were prepared for biological assays, electron microscopy and Raman microspectroscopy. SERS measurements were carried out while the cells were alive in a PBS solution. When the NP approaches the surface of the cell, the cellular membrane invaginates around a NP and forms a membrane vesicle called endosome. After several hours of incubation with Au NPs, numerous NP-containing endosomes were accumulated in these cell

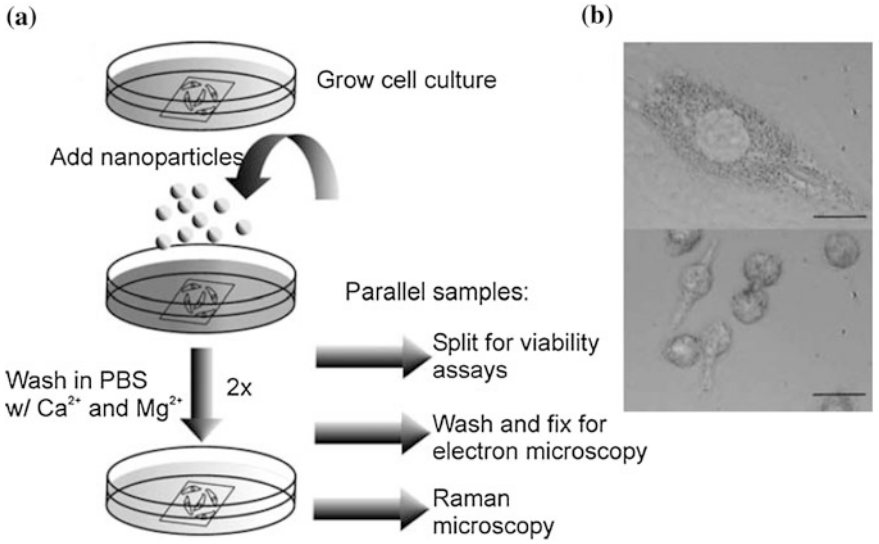

Fig. 6.2 Basic scheme of intracellular SERS experiment. **a** Scheme for the delivery of Au NPs into eukaryotic cells from the culture medium. Parallel samples were prepared for biological assays, electron microscopy and Raman microspectroscopy. **b** Cell lines NIH/3T3 (*upper panel*) and J774 (*lower panel*) after several hours of incubation with Au NPs (scale bar 20 μm) (adapted with permission from Kneipp 2006. Copyright 2006 Springer)

lines, therefore the NPs became visible as black dots in a common light microscope (Fig. 6.2b). Thus, the NPs were found mostly in endolysosomal cell structures and no NPs were present in the area of the nuclei. In order to reach other cellular organelles, the endocytosed NP should escape from the endosome. Uptake to cellular nucleus can be accomplished for NPs functionalized with specific transport proteins (Oyelere et al. 2007).

It is necessary to note that the biological system has a big influence on the physicochemical properties of delivered nanostructures, e.g. by chemical reactions taking place at the NP surface and by adsorption of molecular species from cells resulting in change of surface charge, solubility and aggregation behaviour (Drescher and Kneipp 2012). A simple transfer of nonfunctionalized NPs into cell culture medium can result in their partial aggregation and coating with proteins like BSA. This coating should then favour the internalization of the NP by living cells through endocytosis (Chourpa et al. 2008). It was found that the Ag NPs introduced into the culture medium provided little SERS effect and the spectra from interfering molecules rather than intracellular target analytes are observed (Chourpa et al. 1996). This can be overcome when the cells are placed in a PBS buffer instead of a culture medium. To stimulate the NPs internalization, the cell/colloid mixture can undergo mild centrifugation (100–200 g for 2–5 min) in a PBS buffer. After that, the excess of noninternalized NPs can be removed by additional washing with PBS (Chourpa et al. 1996).

In general, passive uptake of metallic NPs by cells has been the dominant approach for transferring NPs into the cells. However, there are three main disadvantages of the traditional passive uptake method: (i) it is time-consuming (metallic NPs have to be incubated with living cells for more than 20 h before SERS experiments), (ii) it has poor translocation efficiency and (iii) it has inherent lack of control over aggregation and/or distribution of NPs inside the cell. In some studies, microinjection (Wang et al. 2010) or electroporation (Lin et al. 2009) was used for direct uptake of NPs to the cells. The intensity of SERS from transient electroporation treatment was found to be comparable to that of passive uptake after 1 day incubation. Thus, to achieve the same number of Ag NPs into a cell, electroporation delivery is much faster and more efficient than incubation. This technique significantly shortened the time for SERS analysis of living cells. The Ag NPs are localized only in the cell cytoplasm after the electroporation delivery, which improve the data reproducibility (Lin et al. 2009). Recently, Feng and co-workers demonstrated the use of ultrasound mediated rapid transfer of Ag NPs into living cells for SERS analysis (Feng et al. 2015). To validate this method, they studied cancerous and normal human nasopharyngeal cells as models. The ultrasound treatment of cells caused cavitations, where the oscillation and collapse of cavitation bubbles were believed to mechanically break and open cells in a manner that permits them to subsequently reseal. From the TEM imaging of cells, the authors could not find any damage on the cell nucleus after ultrasound exposure and most of the cells were kept alive. Reproducible SERS spectra were successfully obtained from cancerous and normal cell lines with 1 min of ultrasound-mediated Ag NP delivery and 10 s spectral measurement time. Therefore, compared with the conventional passive uptake method, ultrasound was much faster and more efficient for SERS spectroscopy based analyses of living cells.

As an alternative to delivered NPs, intracellularly grown Au NP can be employed to obtain SERS spectra from cytoplasm and/or the nucleus of a single cell (Shamsaie et al. 2007).

6.1.3 Chemical Probing in Cells by Intrinsic SERS Spectra

Since the metallic NPs after delivery to cells are mostly present in endosomes, the majority of SERS intracellular studies provide information about the composition of endosomal structures or their local environment. SERS spectra from cellular compartments in different types of cells using Ag and Au NPs, both free and carrying RRMs, are obtained.

In the case of intrinsic intracellular SERS studies without RRMs, there is no analytically significant SERS response of intrinsic molecules (Chourpa et al. 2008). A particularly high number of NPs per cell should be used to obtain intrinsic SERS spectra. Typical SERS intrinsic spectra from cells of the immortalized rat renal proximal tubule cells are shown in Fig. 6.3 as an example (Kneipp et al. 2006). The spectra obtained after 120 min incubation with Au NPs provided the best SERS

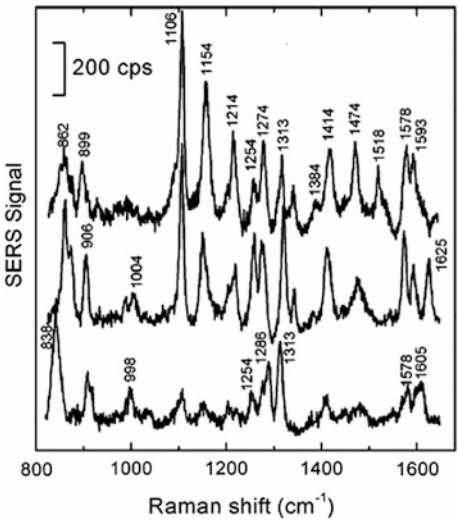

Fig. 6.3 Typical SERS spectra from cells of the immortalized rat renal proximal tubule cells after 120 min incubation with Au NPs, excited with less than 3×10^5 W cm^{-2} at 786 nm, collection time 1 s (adapted with permission from Kneipp et al. 2006. Copyright 2006 American Chemical Society)

signals probably due to the formation of small Au aggregates. The spectra are dominated by spectral features of NAs and proteins (namely aromatic amino acids like Phe) possibly due to their high affinity to metallic NPs (Kneipp et al. 2002; Tang et al. 2007; Kneipp 2006; Kneipp et al. 2006). A strong SERS signal of adenosine-like species indicates damage of the cell integrity probably due to high content of metallic NPs (Tang et al. 2007). Table 6.1 lists the positions of most of the characteristic Raman bands of typical cellular constituents and their assignment to molecular groups and/or vibrational modes (Kneipp et al. 2006). The differences between the spectral signatures indicated that the molecular composition of the endosomal vicinity of the NPs changes over time. All SERS intrinsic intracellular spectra demonstrated a very inhomogeneous chemical constitution of the cells. Moreover, SERS spectra are different for different cell lines, NPs incubation times, etc.

The cell nucleus is also a desirable target because it contains the genetic information of cells. A few studies have reported SERS experiments with metallic NPs carrying nuclear targeting sequences (such as TAT peptide) in cultured cells. For example, Oyelere and co-workers delivered Au NPs inside the nucleus of two cell lines, an epithelial cell line and an oral cancer cell line. They reported SERS spectral contributions from NA and protein components, which they assigned to the molecular constituents of the nucleus (Oyelere et al. 2007). Later, nuclear targeted SERS detection was performed by using the Au NPs conjugated with SV-40 large T-antigen nuclear localization signal peptide. Such functionalized Au NPs efficiently entered the cell nucleus after the incubation with HeLa cells. SERS spectral map provided the spatially localized chemical information of the nucleus (Xie et al. 2009).

Table 6.1 Raman frequencies and their tentative assignments from SERS spectra of the immortalized rat renal proximal tubule cells and in the mouse macrophage cell line J774

Raman shift (cm^{-1})	Tentative assignment
815	Phosphate: ν(OPO)
827, 850	Proteins, Tyr: δ(CCH) aliphatic, Tyr (ring)
862	Ribose: ν(CC), ring breathing, ν(COC)
899	Ribose-phosphate, saccharides
906	Amino acids
927	Pro: ring ν(CC)
998	Proteins: amide III
1004	Phe, ring breathing
1099	Phosphate: ν(PO_2^-), ν(CC), ν(COC), glycosidic link
1106, 1118	Proteins, ν(CN)
1133	Pro
1154	ν(CC, CN), ρ(CH_3)
1188, 1194, 1204	Nucleotides: base ν(CN), Tyr, Phe
1214, 1240, 1254	T, C, A, ring ν
1254, 1274, 1286	Proteins, lipids: amide III /δ(CH_2, CH_3)
1313	A/proteins: ring ν/γ_T(CH_2, CH_3)
1338, 1358	Proteins: γ_T(CH_2, CH_3), γ_W(CH_2, CH_3)
1384	Nucleotides, proteins, lipids, δ(CH_3) sym
1414	Amino acids, δ(CH_3) asym, ν(COO^-)
1427	A,G
1448, 1474	Lipids, proteins: δ(CH_2, CH_3)
1505, 1518, 1532, 1578	A, C, G
1548, 1563	Proteins: amide II
1582, 1593, 1605	Proteins, Phe, Tyr
1625	Nucleotides, lipids, proteins, ν(C=C) olefinic

ν stretching; *δ* deformation; *ρ* rocking; γ_T twisting; γ_W wagging; *sym* symmetrical; *asym* asymmetrical; *Pro* proline, *Tyr* tyrosine; *Phe* phenylalanine; *A* adenine; *T* thymine; *C* cytosine; *G* guanine (adapted with permission from Kneipp et al. 2006. Copyright 2006 American Chemical Society)

In fact, the possibility of obtaining molecular structural information from the target analyte inside the cell is the most important characteristic of SERS. Until now this has not been possible by any other techniques. On the other hand, the limitation of intracellular SERS spectroscopy exists due to the complex matrix of molecules present in the cell that can produce SERS. Consequently, very complicated SERS spectra are acquired from the cells. Such SERS spectra provide only general information about the types of molecules present inside the cell. Therefore, in order to obtain a specific and known SERS spectrum from cells functionalization of the SERS tags with a RRM is required.

6.1.4 Chemical Probing in Cells Using SERS Tags with RRMs

SERS tags with RRMs can provide an intense SERS signal that can be easily distinguished in a complex chemical biological object such as cells. The SERS tag is formed by Au or Ag nanostructure, such as NPs, NRs, nanoshells and others, labelled or embedded with RRM providing a strong SERS signal (Wang et al. 2013). It has been reported that successive SERS tags have been made by some reporter chromophores, i.e. Raman-active dyes, which strongly bind to Ag or Au NPs. The suitable biocompatible dye labels include RH6G, indocyanine green (ICG), CV, methylene blue (MB) and rose bengal. Thiolated labels, which are not fluorescent, such as ATP, mercaptopyridine, MBA, benzenethiol, naphtalenethiol are also employed but aromatic thiols are known to be cytotoxic for some cells (Amrolia et al. 1989). The uptake, accumulation and distribution of SERS tags inside the cells can be monitored in the course of hours and days via the SERS signal of RRM. There are generally two types of SERS tags: one without a protective layer and second one with a protective layer.

The first type of SERS tag (often called a hybrid tag) does not use a protective layer (Matschulat et al. 2010). The main advantage of such SERS tag is its multifuncionality. SERS tags can be identified by the SERS spectrum of a RRM. This spectrum can serve to determine intracellular distribution of SERS tags (Wabuyele et al. 2005). At the same time, the SERS tags provide sensitive spectral information about the cellular nanoenvironment (Matschulat et al. 2010; Kneipp et al. 2005). The possibility to obtain intrinsic SERS spectra from living cells using hybrid SERS tags has been demonstrated. Eliasson and co-workers tested RH6G as a model molecule which can be imaged together with nucleotides and amino acids of single living lymphocyte cells. The PCA enabled an identification of SERS spectra containing different chemical information and separation of the spectral contribution of RH6G from the complex cellular matrix (Eliasson et al. 2005). Kneipp and co-workers (Kneipp et al. 2005; Kneipp 2006) reported Au NPs (60 nm diameter) labelled with 1×10^{-7} M ICG complexed with albumin delivered into cells of metastatic Dunning R3327 rat prostate carcinoma line. Albumin prevents ICG aggregation and stabilizes NPs. SERS tag contains a label and at the same time enhances the Raman signal from the surrounding molecules when delivered into a cell. The presence of Au NPs in the cells was verified by the appearance of ICG SERS signal. SERS spectra of some biomolecular components (nucleobases and amino acids) were measured in various spots inside the cell. Examples of SERS spectra, photomicrograph of the cell indicating the studied area and SERS spectral maps of ICG-Au tag are shown in Fig. 6.4 (Kneipp et al. 2005). The data indicate that the SERS spectrum of ICG consists of more than 10 characteristic bands distributed over a broad frequency range. SERS spectra of cell components can be measured along with SERS signatures of the RRM (spectra b, d and e in Fig. 6.4A). The relative contributions of ICG and cell components depend on the coadsorption of both kinds of molecules. The capability to extract qualitative vibrational

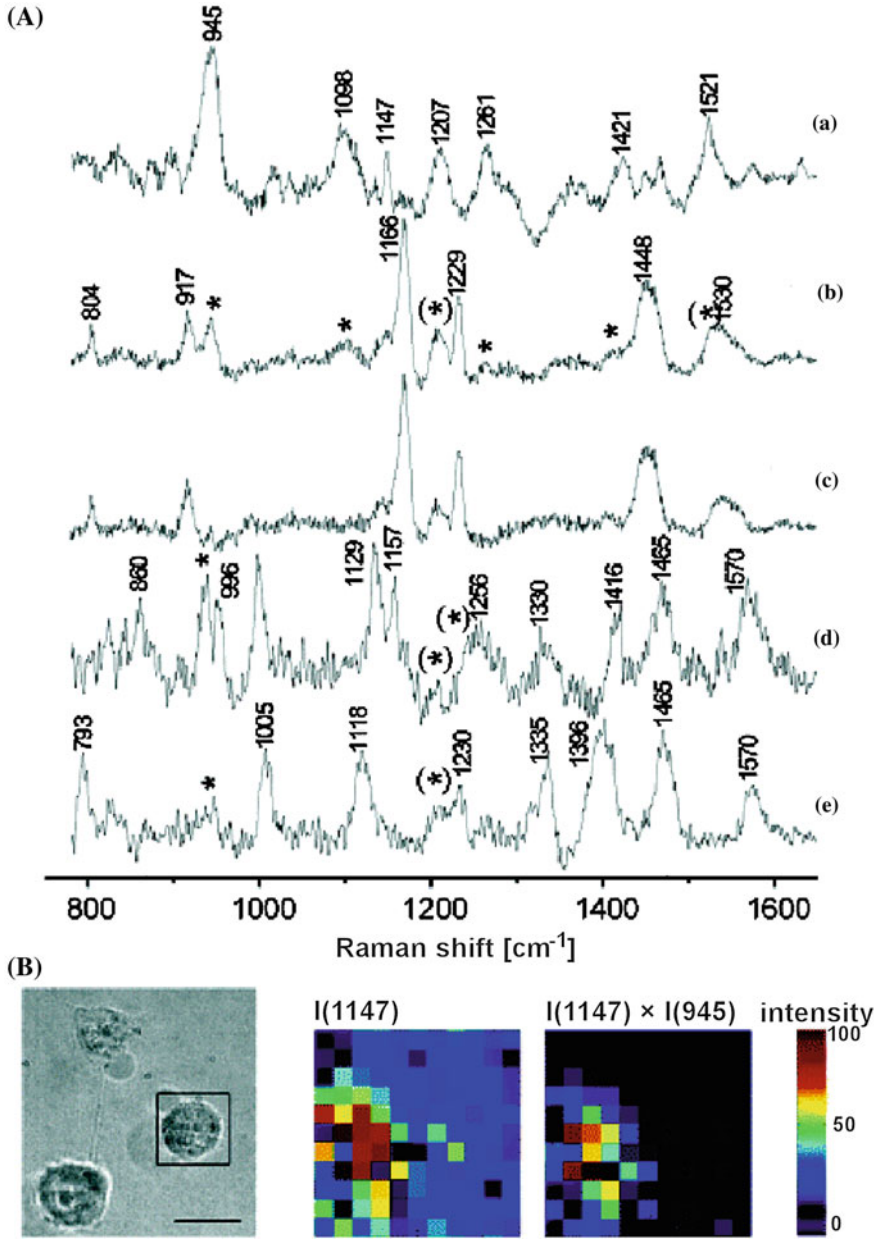

information on the cell is illustrated in spectrum c, which displays a spectrum of native cell components obtained after subtraction of the ICG spectrum (spectrum a) from spectrum b. Imaging of the RRM offers the advantage that spectral correlation methods can be used to enhance the contrast between the label and the cellular

◀ **Fig. 6.4** Intracellular SERS using RRM (ICG). **A** Examples of SERS spectra measured in single living cells incubated with the ICG-Au NPs at 830 nm excitation. ICG bands are marked with an *asterisk*, while an *asterisk* in parentheses indicates contribution of both ICG and cell. Spectrum (**a**) represents the ICG signature. Spectrum (**c**) shows the difference between spectra (**b**) and (**a**). **B** Spectral map of the ICG-Au tag in a cell based on 1147 cm^{-1} ICG line and of two ICG lines at 1147 and 945 cm^{-1}. Intensities are colour-scaled to the highest value in each area. A photomicrograph of the cell, indicating the studied area, is shown for comparison. Scale bar 20 μm (adapted with permission from Kneipp et al. 2005. Copyright 2005 American Chemical Society)

background. Figure 6.4B shows a spectral map of the ICG-Au NPs tag in a cell based on the 1147 cm^{-1} ICG SERS line and one of two ICG SERS lines at 1147 and 945 cm^{-1}. It is clear that using two bands already increased the contrast and enabled better localization of the tag. Later, the Kneipp group reported SERS tag consisting of Au NPs and 4-ATP RRM incubated with mouse fibroblast cells. After 5 days of incubation and several cell divisions, the intracellular signal intensity of 4-ATP and the amount of detected SERS spectra per cell decreased significantly since the primary vesicles were distributed over more cells. At an incubation time shorter then ~1 day, the SERS spectra were dominated by 4-ATP bands. After 1–5 days of incubation, cell-specific Raman bands were detected in addition to the 4-ATP bands. This was attributed to the replacement of particle-bound 4-ATP by cellular molecules. Since the Raman spectra showed the same 4-ATP signature after 30 min and 5 days, they assumed that 4-ATP was stable during cellular processing. Furthermore, the signal intensity increased from 30 min to 48 h of incubation, which was correlated with the NP aggregation with increasing incubation times due to multivesicular fusion (Drescher and Kneipp 2012). Recently, the SERS tags based on Au nanostars have been introduced for cellular imaging and sensing (Cao et al. 2015). The SERS tags were tested on human lung adenocarcinoma cells (A549) and alveolar type II cells (AT II) and found to present a low level of cytotoxicity and high chemical stability. NB and BSA were used as RRMs and capping materials, respectively. It was shown that endocytosis is the main channel of SERS tags internalized in cells. The Au nanostars-based tags provided a strong SERS signal. The SERS spectra clearly identified cellular components such as proteins, NAs, lipids and carbohydrates.

The second type of SERS tag is a metallic NP/RRM coated with a protective layer of polymer like polyethylenglycol (PEG) (Qian et al. 2008) or silica (SiO_2) (Wang et al. 2013). Coating helps cellular uptake, NP aggregation control and chemical stability of SERS tag. The concept of silica encapsulation of SERS tag was introduced by Mulvaney and co-workers (Mulvaney et al. 2003). Küstner and co-workers improved the sensitivity of SERS tag by using SAM of RRMs. They showed that complete SAM yields ~22× higher SERS signal in comparison with submonolayer coverage of label (Küstner et al. 2009). Tan and co-workers reported PVP coated Ag NP aggregates for SERS enhancement of RRMs in living HeLa cells (Tan et al. 2009). An advantage of coated SERS tags is physical robustness, stability and biocompatibility.

It is necessary to emphasize that SERS tag exhibits the same function as the fluorescent tag, i.e. it provides only the spectral signature of the RRM. Thus, it is an imaging instrument rather than a detection probe. The SERS tags can also increase specificity for biomolecules of interest when functionalized with target-specific molecules. The surface can be functionalized with a DNA sequence complementary to a sequence of interest or with a particular antibody in order to detect certain antigens or receptors present in a cell (Kim et al. 2006). This will provide SERS spectra of a particular RRM in a subcellular compartment when the targeted biomolecule is present. For example, Nithipatikom and co-workers applied CV-labelled Ag NPs conjugated with biotin for the localization of cellular enzymes and receptors in cells (Nithipatikom et al. 2003). For this purpose, antibodies were used to conjunct enzymes or receptors of interest with Raman labels in cells and, then, intracellular SERS was detected directly by a confocal Raman microscope. Although a spectral mapping was not carried out and the distribution of the analytes was not clear, this work showed that the Raman labels could be used for simultaneous detection of multiple components in a single cell (Nithipatikom et al. 2003). Kennedy and co-workers reported multiplex SERS imaging of receptor proteins on the surface of a single cell by using antibody-functionalized Ag NPs (Kennedy et al. 2010). The co-localization of β_2-adrenergic and caveolin-3 receptors on the cell surface was explored by using Ag NPs with different RRMs. Such SERS tags are used also at in vivo medical SERS applications (see Chap. 7).

6.1.5 Endosomal pH Monitored by SERS

Local pH plays an important role in regulation of cellular function. Many groups have used SERS sensors for sensitive determination of the local pH in cells. The intracellular pH can be monitored via the SERS spectrum of RRM as a part of SERS tag sensitive to pH. 4-MBA is an ideal candidate since it strongly binds to Au or Ag surfaces and the vibrational Raman spectrum of the protonated form (COOH, carboxylic acid) differs significantly from that of the deprotonated/ionized form (COO^-, carboxylate). The pH dependent spectra of 4-MBA adsorbed on Au nanoshells were applied in a pH sensor over the pH range of 5.8–7.6 (Bishnoi et al. 2006). Similar experiments using hollow Au nanospheres with 4-MBA extended the detectable pH range from 3.5 to 9 (Schwartzberg et al. 2006). When 4-mercaptopyridine was used, the pH range detection from Au nanoshells was between 3 to 7 (Jensen et al. 2007).

Classical metallic NPs can form a SERS tag for pH sensing. SERS studies on Ag NP clusters with 4-MBA showed the pH sensitivity in the range of 6–8 (Talley et al. 2004). Kneipp and co-workers (Kneipp et al. 2007) analysed the pH sensitive SERS of 4-MBA on aggregated Au NPs in order to determine and to image the pH values in subcellular structures in the pH range from 6.8 to 5.4. The results are shown in Fig. 6.5. The NIH/3T3 cells were incubated 4.5 h with the Au NP tag (Au NPs and 4-MBA). Numerous Au NPs have accumulated in the cell, enabling pH

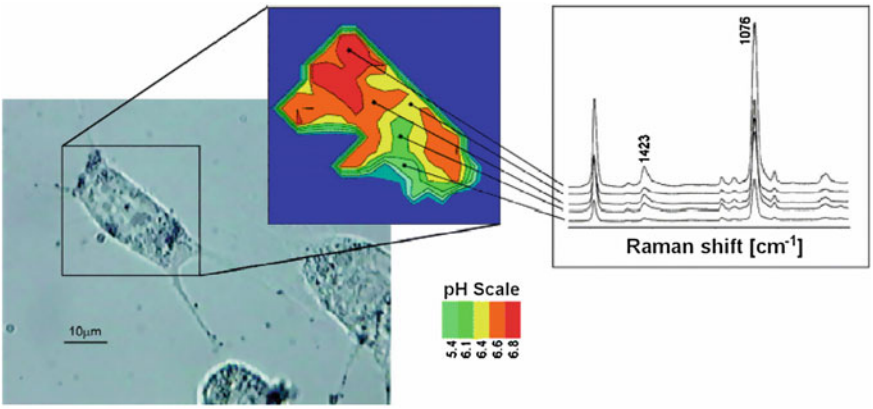

Fig. 6.5 pH SERS nanosensor. Photomicrograph of an NIH/3T3 cells incubated with Au tag (Au NPs and 4-MBA), pH map of the cell displayed as false colour plot of the ratios of the SERS lines of 4-MBA at 1423 and 1076 cm^{-1}. The values given in the colour scale bar determine the upper end value of each respective colour. Typical anti-Stokes part of SERS spectra collected in the endosomal compartments with different pH (reproduced with permission from Kneipp et al. 2007. Copyright 2007 American Chemical Society)

probing in different endosomes over the entire cell. The SERS spectra were collected in the endosomal compartments with different pH. The spectra were acquired in 1 s each using 830 nm excitation (3 mW). A pH map of the cell was constructed as false colour plot of the ratios of the SERS lines at 1423 and 1076 cm^{-1} of 4-MBA. In a second step, they could successfully prove that the concept of a SERS pH sensor can be extended to two-photon excitation using surface-enhanced hyper Raman scattering (SEHRS) of 4-MBA on nanoaggregates. Hyper Raman scattering is a two-photon excited RS process and thus results in Raman signals shifted relative to the doubled energy of the excitation laser. The rather weak effect can be greatly strengthened if it takes place in the local optical fields of metallic nanostructures. Since SEHRS follows different selection rules, it results in a different spectral signature compared to RS and SERS. Particularly for biological applications, the pH sensor based on two-photon excitation benefits from excitation at longer wavelengths in the NIR. Most important, SEHRS spectra of 4-MBA exhibit a spectral signature suited for measurements and differentiation of pH values between 8 and 2. The extended response range of the SEHRS pH sensor enabled probing of a variety of subcellular compartments including those of extreme pH, e.g. very acidic lysosomes, without the use of multiple probes.

Many SERS pH sensors required high laser power ($\sim$10 mW) and long collection time (about 10 s) and thus they were not suitable for scanning living cells. Moskovits and co-workers showed pH dependence of SERS spectra using 4-MBA-functionalized NP clusters and mapped local pH in HeLa cells (Pallaoro et al. 2010). Ag clusters were linked with bifunctional hexamethylenediamine molecules and encapsulated by PVP to prevent aggregation. The SERS-active

clusters were also coated by dye-labelled streptavidin and BSA to track the distribution of Ag NP clusters in cells and correlate the fluorescence and SERS pH maps. The 4-MBA molecules infused through the polymer coat into junctions between NPs and facilitated measurement of pH values inside HeLa cells using a relatively low laser power (1.1 mW) and a short integration time (250 ms).

Drescher and Kneipp developed the mobile pH sensor based on 4-MBA-coated Au NP for 3T3 mouse fibroblast cells at ~2 μm subendosomal resolution (Drescher and Kneipp 2012). Vo-Dinh and co-workers used Ag-coated submicron sized fibre-optic probe functionalized with 4-MBA as pH sensor (Scaffidi et al. 2009). The probe was physically inserted into a live cell using a micromanipulator. The intracellular pH value was determined by comparison of SERS intensity of 4-MBA bands with a calibration curve obtained from standard pH solutions ranging from pH 6.0 to 7.5. Han and co-workers developed Si NWs endoscope for intracellular pH detection based on SERS (Han et al. 2013). The endoscope was fabricated by first depositing uniform, densely packed Ag NPs on Si NW and subsequently functionalizing them with pH-sensitive 4-MBA molecules. SERS spectra of 4-MBA were collected on a single NW using 785 nm excitation which is less hazardous for living cell. As tested in the cell culture medium, this endoscope provided a high-resolution and sensitive response to local pH changes over the wide pH range of 4.0−9.0. It also exhibited high reproducibility, good reversibility and at least 1 week stability in an aqueous environment. The authors suggested that their Si NW endoscope can be inserted into living cell and used as a in vivo intracellular pH sensor.

6.1.6 Intracellular SERS Using Tip-like Substrates

The introduction of NPs in selected cellular regions can be ensured by a commercially available femtotip needle as small as 0.7/0.5 μm (Femtotip II, Eppendorf Ga, Hamburg, Germany) but the final intracellular distribution of NPs remains uncontrollable (Chourpa et al. 2008). An alternative approach is the employment of metal-coated tips or nanopipettes in SERS cellular study. Gessner and co-workers (Gessner et al. 2002, 2004a) developed an etched Ag or Au coated SERS fibre probe to perform highly spatial resolution micro-Raman measurements on different biological samples. A glass tip of ~200 μm or glass capillary ~100−500 nm in the case of nanopipettes was covered by metallic NPs and inserted into the cell. SERS spectra were measured from cellular components in contact with the tip. Composition of essential oils inside the glandular trichomes was identified by glass nanotips (Gessner et al. 2002).

SERS-active nanopipettes were fabricated for in situ chemical sensing of living HeLa cells (Vitol et al. 2009). A glass pipette was coated with a poly-L-lysine polymer layer which contains positive NH_2– functional groups. Then the nanopipette was coated with negatively charged Au NPs. Inset of Fig. 6.6 shows SEM image of the nanopipette tip covered with Au NPs. The nanopipette was inserted into a cell following a standard procedure used in cell biology for interrogating

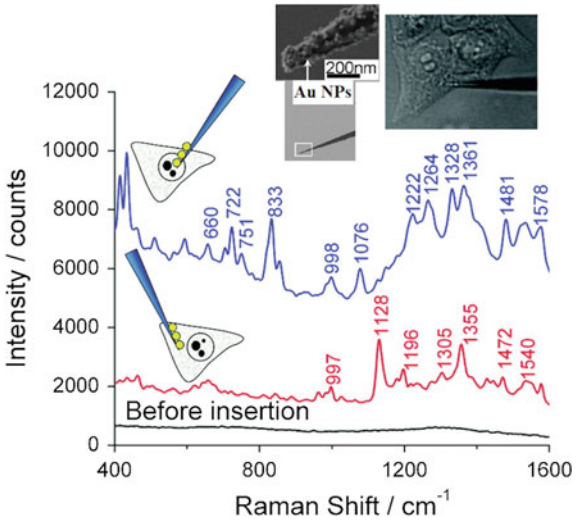

Fig. 6.6 Nanopipette for SERS intracellular studies. SERS spectra from the cell nucleus (*upper* spectrum) and cytoplasm (*middle* spectrum). The *bottom* spectrum (*black line*) was collected from the nanopipette tip before insertion; 785 nm excitation was used. The spectra are offset for clarity. *Inset* SEM image of the nanopipette tip covered with Au NPs and their insertion to HeLa cell (adapted with permission from Vitol et al. 2009. Copyright 2009 American Chemical Society)

adherent cell cultures with glass pipettes. A commercial micromanipulator was applied to ensure precise control over the nanopipette movement. The nanopipette was positioned above a Petri dish with adherent HeLa cells and then directed toward the cells at a 45° angle. This was continuously monitored under the Raman microscope with a 50× long working distance objective. The nanopipette insertion did not cause fatal damage to a cell. During the Raman spectra acquisition, the excitation laser was always focused on the nanopipette tip. The SERS spectra were collected from the nanopipette tip inserted in the cell nucleus or cytoplasm. The spectra are shown in Fig. 6.6. SERS spectra from the cell nucleus (upper spectrum) and cytoplasm (middle spectrum) indicate distinctly different features. The cytoplasmic SERS spectrum is dominated by spectral features of proteins and amino acids (mostly Phe). The nuclear spectrum contains also strong DNA bands. The SERS nanopipette provided well reproducible data. This tip-like substrate could be used for in situ intracellular SERS detection either within the cell nucleus or cytoplasm.

6.1.7 Experimental Aspects of Intracellular SERS Studies

In the intracellular studies lateral resolution and detection sensitivity are two major parameters influencing the vibration information obtained. The lateral resolution is

related to the size, number, amount and heterogeneity of the studied biological object. Detection sensitivity is related to the acquisition time, sample integrity, time resolution and in vivo applicability. An advantage of SERS microspectroscopy is that spectral information from complex biological objects can be obtained rapidly and with a high lateral resolution. It can serve for example to analyse small morphological structures inside the cells with resolution of optical confocal microscope. The accumulation time at a particular measuring position can be shortened to 1 s or less, which gives a possibility for spectral mapping over the cells. SERS spectra can be, however, obtained only from the molecules in the close vicinity of an enhancing metallic nanostructure. The maximum lateral resolution is in this case not limited by the excitation wavelength but only by the metallic nanostructure providing SERS enhancement. In vivo SERS applications are conducted with individual SERS tags positioned at discrete locations in the biological object. SERS-labelled tags are often used providing higher sensitivity and specificity.

The intracellular SERS signals show the high degree of variability with both NPs and tip-like substrates because of the dynamic nature of analyte close to the metal surface. The variability concerns both intensities and positions of spectral bands. For the same molecule, different adsorption orientations and different types of adsorption sites can result in quite different spectra. The equilibrium of the adsorbed/replaced species on the metal surface within a given cell compartment could change with time. Moreover, in case of cells, another analytes could compete for adsorption on the SERS tag. The inserted NPs and small NP clusters are inhomogeneously distributed over the cell which changes the SERS enhancement. In case of nanotips, the slight variation of the tip distance from the target spot can also affect the SERS measurement. Therefore, qualitatively and quantitatively different SERS spectra are observed from the same intracellular SERS study (Tang et al. 2007). In these cases, multivariate statistical signal analysis such as PCA should be used for discriminating between stable and unstable spectral information (Chourpa et al. 2008). PCA is a multivariate data analysis technique (Jolliffe 1986) that is widely applied in spectroscopy for facilitating data interpretation by reducing its dimensionality and calculating the degree of correlation (similarity) between the spectra.

6.2 Detection and Identification of Viruses and Microorganisms

6.2.1 Detection and Identification of Viruses

Viruses can be identified and classified by using SERS spectroscopy after adsorption on Ag NPs (Bao et al. 2001) or solid metal surfaces (Alexander 2008). Obtained SERS spectra contain spectral information about capsid (protein shell) of the virus due to Raman bands of amino acids containing COOH–, NH_2– and

SH– groups (Bao et al. 2001). Insect nuclear polyhedrosis virus (Bao et al. 2001), parapoxviruses (Alexander 2008) and respiratory syncytial virus (Shanmukh et al. 2008) were studied. Higher sensitivity and selectivity were obtained by a combination of AFM and SERS in a study of nm-sized feline caliciviruses (Porter et al. 2006) and by TERS in the case of single tobacco mosaic virus at a molecular level (Cialla et al. 2009).

6.2.2 Detection and Identification of Bacteria

Bacteria are important biological systems and their association with disease, infection and, recently, bioterror threats, makes their detection of prime interest. Naturally, efforts were made to develop methods of detection based on the vibrational spectroscopy, owing to its high inherent specificity. SERS represents a promising tool for identification and classification of bacteria in clinical microbiology (see Sect. 7.2) or detection of biological warfare agents (see Sect. 4.4).

Most of the measurements on bacteria were performed on bulk material using Ag NPs (mostly citrate-reduced ones) aggregated by NaCl. Although in early studies metallic NPs were prepared in situ in bacterial suspension (Efrima and Bronk 1998), the majority of SERS bacterial studies were carried out on metallic NPs mixed with it (Zeiri and Efrima 2005; Jarvis et al. 2006a; Sengupta et al. 2006; Jarvis and Goodacre 2008; Premasiri et al. 2014). In both cases, metallic NPs are accumulated in the outer part of a bacterium wall resulting in an averaging over a lot of bacterial cells, which increases the SERS intensity. The main problem encountered with this approach is that when a low numerical aperture objective lens is used, the illumination volume will often not be sufficient to encompass a whole bacterial cell with NPs. This causes a highly irreproducible single point spectral response. The disadvantage of using aggregated Ag NPs as SERS-active substrate is poor reproducibility of SERS spectra. Therefore, Jarvis and Goodacre firstly reported a simple method of averaging SERS spectra after acquiring signal of multiple bacteria (Jarvis and Goodacre 2004). While each spectrum took 10 s to collect, to acquire reproducible data, 50 spectra were collected within the spectral acquisition times $\sim$8 min per bacterium. Thus, the main drawback of this approach was that it is time-consuming. Further studies have compromised to some extent on maximum SERS enhancements by using a higher numerical aperture objective lens (Jarvis et al. 2006b) or Raman instrument coupled to an electron microscope (Jarvis et al. 2004). This provides an increased collection volume to obtain an average SERS profile directly from a sample. Later, Cheng and co-workers developed an integrated dielectrophoretic microfluidic platform that can filter, focus, sort and trap heterogeneous bioparticle and identified two gastrointestinal bacteria, *Escherichia coli Nissle* and *Lactobacillus*, by SERS on a single chip (Cheng et al. 2007). This platform provided a significant contribution to the effort to miniaturize the multi-target bacterium detection.

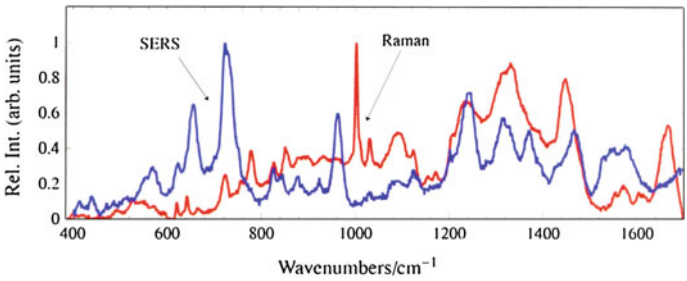

Fig. 6.7 Comparison of typical SERS and NRS spectra of the same *Escherichia coli* strain. Spectra were excited at 785 nm and normalized to the maximum band intensity (reproduced with permission from Premasiri et al. 2014. Copyright 2014 John Wiley & Sons, Ltd)

It was found that the SERS spectra of bacteria significantly differ from the NRS spectra of the identical bacterial cells. For example, the typical SERS and NRS spectra of a strain *E. coli* are compared in Fig. 6.7 (Premasiri et al. 2014). NRS is dominated by molecular species in the cell cytoplasm while only molecules at the outer layers of less than $\sim$10 nm will contribute the SERS. Premasiri and co-workers introduced detail assignment of typical Raman bands observed in SERS spectra of bacteria (Premasiri et al. 2005). It is anticipated that vibrational bands of proteins, phospholipids, NAs and polysaccharides will contribute to these spectra. The features at $\sim$735, 965, 1030 and 1080 cm^{-1} arising from the lipid layer components of the cell walls and membranes. Amide I, II and III vibrations, associated with protein backbone and carboxylic stretches, are expected in the 1220–1660 cm^{-1} region and probably dominate the SERS vibrational signature in this region. The positions and relative intensities vary, however, for each particular bacterium type which can serve for their identification (Premasiri et al. 2005). One aspect of bacterial SERS is that if experimental parameters (type of Ag NPs, excitation wavelength) are altered, the spectra are entirely different despite the fact that the cells have very similar surface chemistries (Jarvis and Goodacre 2008).

To distinguish and to group bacteria based on their spectral fingerprints, a multivariate data analysis technique such as PCA should be used (Jarvis et al. 2004). However, PCA is often insufficient to separate closely related bacterial classes based on their complex spectral profiles and therefore supervised analysis should be applied as predictive models. This involves proposing a priori class structure from which a determinative model is derived. One popular supervised method is discriminant function analysis (DFA) (Manly 1994), which maximizes the within-group to between-group ratio (Fisher ratio) to differentiate between classes (groups). For the identification of large numbers of different bacteria, it is often necessary to inspect more than just the first 2 or 3 discriminant functions. Jarvis and co-workers (Jarvis and Goodacre 2004; Jarvis et al. 2006a) reduced this problem by constructing a dendrogram based on DFA output using hierarchical cluster analysis (HCA). One example of such approach applied on set of a 7 clinical

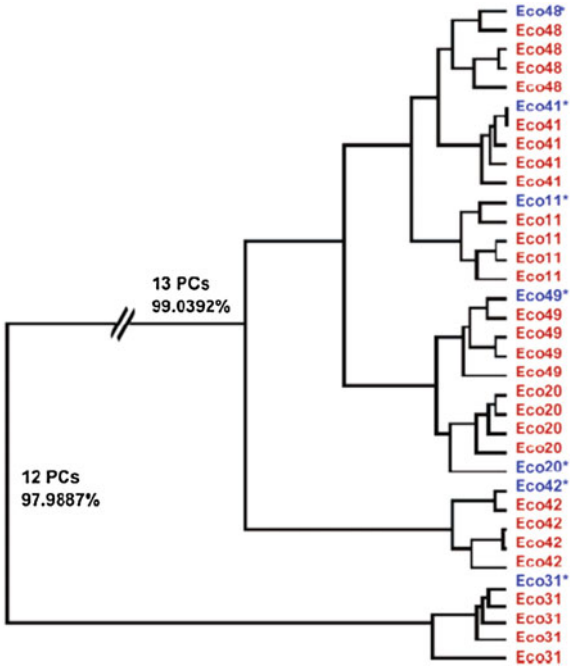

Fig. 6.8 Discrimination of 7 clinical isolates of *E. coli* bacteria from UTIs using PCA-HCA analysis of their SERS spectra. The composite dendrogram generated by HCA using the combined PC-DFA space from the training and validation replicates (adapted with permission from Jarvis and Goodacre 2004. Copyright 2004 American Chemical Society)

isolates of *E. coli* from a urinary tract infection (UTI) is illustrated in Fig. 6.8. The dendrogram showed correct groupings including discrimination to strain level for a sample group of *E. coli*, which was validated by projection of test spectra into DFA and HCA space. The entries in red represent the training data and those marked with an asterisk in blue, the validation data. It can be seen that the projected SERS spectra (marked with an asterisk) fall within the training data applied to construct the dendrogram. Isolate C31 is considerably different from the other isolates, therefore C31 was extracted and the remaining data analysed again (Jarvis and Goodacre 2004). Later, the barcode methodology was developed (Patel et al. 2008) resulting in significantly enhanced diagnostic specificity (see Sect. 7.2.3).

Recently, Ag NPs synthesized in situ on the bacterium wall were reported for label-free SERS discrimination between live and dead bacteria (Zhou et al. 2015). The suspensions containing Gram-negative *E. coli* bacteria as well as Ag NPs provided strong SERS signals of live bacteria when generated selectively on the particle surface. In contrast to that, almost no SERS signals were detected from suspensions containing Ag NP and dead bacteria. The authors demonstrated quantification of different percentages of dead bacteria both in bulk liquid and on glass surfaces by SERS mapping on a single cell basis. Moreover, they successfully applied their method to distinguish between wild type strains and antibiotic resistant mutant strains of bacteria. Therefore, this SERS approach is a promising tool for a rapid, culture free analysis of the efficiency of antibiotics against a specific Gram-negative microorganism.

6.2.3 Detection and Identification of Yeasts

Yeast cells are considered to be one of the most extensive model eukaryotic systems for various fields of life sciences. The cell walls of yeasts are interesting to study due to their sensitivity toward different biological functions.

Metal-coated microparticles trapped by optical tweezers were used as SERS substrates for a pioneer study of yeast cells (Gessner et al. 2004b). The particular configuration consisted of two lasers which made trapping independent from the Raman excitation laser and allowed a separate adjustment of the trapping and excitation wavelengths. SERS spectra of trapped yeast cells *Rhodoturula mucilaginosa* have been recorded. Although these cells exhibit a filament-like shape, the gradient forces of the trapping laser could align the cells into the direction of the beam axis of the laser and hold them. The two bands observed in the SERS spectra were assigned to β-carotene. When the optical gradient trap was blocked, the cells did not stay long enough in the laser focus and the recording of SERS spectra failed.

Later, living yeast cells (*Saccharomyces cerevisiae* strain W303-1A) were studied using Ag NP aggregates (Sujith et al. 2009). The cell wall of a single living yeast cell has been imaged by use of a Raman microspectroscope. The SERS spectra were found to be different from the NRS spectra of yeast cells. They originated mainly from mannoproteins which form the outer layer of the yeast cell walls. The SERS spectra measured from different Ag aggregates were also different which was attributed to a variation in the interaction of Ag NPs with nitrogen and oxygen atoms in proteins (Sujith et al. 2009). The similar study was carried out on yeast cells incubated with SHINs (Li and Tian 2014). SERS (or SHINERS) spectra of yeast cells were similar to SERS spectra of mannoproteins. Some other peaks attributed to amide, protein backbone and amino acids related to bioactivity of living cells were also observed.

References

T.A. Alexander, Development of methodology based on commercialised SERS-active substrates for rapid discrimination of Poxviridae virions. Anal. Chem. **80**, 2817 (2008)

P. Amrolia, S.G. Sullivan, A. Stern, R. Munday, Toxicity of aromatic thiols in the human red blood-cell. J. Appl. Toxicol. **9**, 113 (1989)

P.D. Bao, T.Q. Huang, X.M. Liu, T.Q. Wu, Surface-enhanced Raman spectroscopy of insect nuclear polyhedrosis viruses. J. Raman Spectrosc. **32**, 227 (2001)

O. Bar-Ilan, R.M. Albrecht, V.E. Fako, D.Y. Furgeson, Toxicity assessments of multisized gold and silver nanoparticles in zebrafish embryos. Small **5**, 1897 (2009)

S.W. Bishnoi, C.J. Rozell, C.S. Levin, M.K. Gheith, B.R. Johnson, D.H. Johnson, N.J. Halas, All-optical nanoscale pH meter. Nano Lett. **6**, 1687 (2006)

E. Boisselier, D. Astruc, Gold nanoparticles in nanomedicine: preparations, imaging, diagnostics, therapies and toxicity. Chem. Soc. Rev. **38**, 1759 (2009)

X.W. Cao, C.W. Shi, W.B. Lu, H. Zhao, M. Wang, W. Tong, J. Dong, X.D. Han, W.P. Qian, Synthesis of Au nanostars and their application as surface enhanced Raman scattering-activity tags inside living cells. J. Nanosci. Nanotechnol. **15**, 4829 (2015)

I.F. Cheng, H.C. Chang, D. Hou, H.C. Chang, An integrated dielectrophoretic chip for continuous bioparticle filtering, focusing, sorting, trapping, and detecting. Biomicrofluidics **1**, 021503 (2007)

I. Chourpa, H. Morjani, J.F. Riou, M. Manfait, Intracellular molecular interactions of antitumor drug amsacrine (m-AMSA) as revealed by surface-enhanced Raman spectroscopy. FEBS Lett. **397**, 61 (1996)

I. Chourpa, F.H. Lei, P. Dubois, M. Manfait, G.D. Sockalingum, Intracellular applications of analytical SERS spectroscopy and multispectral imaging. Chem. Soc. Rev. **37**, 993 (2008)

D. Cialla, T. Deckert-Gaudig, C. Budich, M. Laue, R. Moller, D. Naumann, V. Deckert, J. Popp, Raman to the limit: tip-enhanced Raman spectroscopic investigations of a single tobacco mosaic virus. J. Raman Spectrosc. **40**, 240 (2009)

D. Drescher, J. Kneipp, Nanomaterials in complex biological systems: insights from Raman spectroscopy. Chem. Soc. Rev. **41**, 5780 (2012)

D. Drescher, C. Giesen, H. Traub, U. Panne, J. Kneipp, N. Jakubowski, Quantitative imaging of gold and silver nanoparticles in single eukaryotic cells by laser ablation ICP-MS. Anal. Chem. **84**, 9684 (2012)

S. Efrima, B.V. Bronk, Silver colloids impregnating or coating bacteria. J. Phys. Chem. B **102**, 5947 (1998)

C. Eliasson, A. Lorén, J. Engelbrektsson, M. Josefson, J. Abrahamsson, K. Abrahamsson, Surface-enhanced Raman scattering imaging of single living lymphocytes with multivariate evaluation. Spectrochim. Acta A **61**, 755 (2005)

S. Feng. Z. Li, G. Chen, D. Lin, S. Huang, Z. Huang, Y. Li, J. Lin, R. Chen, H. Zeng, Ultrasound-mediated method for rapid delivery of nanoparticles into cells for intracellular surface-enhanced Raman spectroscopy and cancer cell screening. Nanotechnology **26**, 065101 (2015)

R. Gessner, P. Rösch, W. Kiefer, J. Popp, Raman spectroscopy investigation of biological materials by use of etched and silver coated glass fiber tips. Biopolymers **67**, 327 (2002)

R. Gessner, P. Rösch, R. Petry, M. Schmitt, M.A. Strehle, W. Kiefer, J. Popp, The application of a SERS fiber probe for the investigation of sensitive biological samples. Analyst **129**, 1193 (2004a)

R. Gessner, C. Winter, P. Rösch, M. Schmitt, R. Petry, W. Kiefer, N. Lankers, J. Popp, Identification of biotic and abiotic particles by using a combination of optical tweezers and in situ Raman spectroscopy. Chem. Phys. Chem. **5**, 1159 (2004b)

X.M. Han, H. Wang, X.M. Ou, X.H. Zhang, Silicon nanowire-based surface enhanced Raman spectroscopy endoscope for intracellular pH detection. ACS Appl. Mater. Inter. **5**, 5811 (2013)

R.M. Jarvis, R. Goodacre, Discrimination of bacteria using surface-enhanced Raman spectroscopy. Anal. Chem. **76**, 40 (2004)

R.M. Jarvis, R. Goodacre, Characterisation and identification of bacteria using SERS. Chem. Soc. Rev. **37**, 931 (2008)

R.M. Jarvis, A. Brooker, R. Goodacre, Surface-enhanced Raman spectroscopy for bacterial discrimination utilizing a scanning electron microscope with a Raman spectroscopy interface. Anal. Chem. **76**, 5198 (2004)

R.M. Jarvis, A. Brooker, R. Goodacre, Surface-enhanced Raman scattering for the rapid discrimination of bacteria. Faraday Discuss. **132**, 281 (2006a)

R. Jarvis, S. Clarke, R. Goodacre, Rapid analysis of microbiological systems using SERS, in *Surface-enhanced Raman scattering: physics and applications,* vol. **103**, ed. by K. Kneipp, M. Moskovits, H. Kneipp (Springer Berlin Heidelberg 2006b), pp. 397–408 (Top. Appl. Phys.)

R.A. Jensen, J. Sherin, S.R. Emory, Single nanoparticle based optical pH probe. Appl. Spectrosc. **61**, 832 (2007)

I.T. Jolliffe, *Principal Component Analysis* (Springer New York, Heidelberg, 1986)

D.C. Kennedy, K.A. Hoop, L.L. Tay, J.P. Pezacki, Development of nanoparticle probes for multiplex SERS imaging of cell surface proteins. Nanoscale **2**, 1413 (2010)

J.H. Kim, J.S. Kim, H. Choi, S.M. Lee, B.H. Jun, K.N. Yu, E. Kuk, Y.K. Kim, D.H. Jeong, M.H. Cho, Y.S. Lee, Nanoparticle probes with surface enhanced Raman spectroscopic tags for cellular cancer targeting. Anal. Chem. **78**, 6967 (2006)

J. Kneipp, Nanosensors based on SERS for applications in living cells, in *Surface-enhanced Raman scattering: physics and applications,* vol. **103**, ed. by K. Kneipp, M. Moskovits, H. Kneipp (Springer Berlin Heidelberg 2006), pp. 335–350 (Top. Appl. Phys.)

J. Kneipp, 1-P and 2-P excited SERS as intracellular probe, in *Surface enhanced Raman spectroscopy: analytical, biophysical and life science applications*, ed. by S. Schlücker (Wiley-WCH, Weinheim, 2011), pp. 285–304

J. Kneipp, D. Drescher, SERS in cells: from concepts to practical applications, in *Frontiers of surface-enhanced Raman scattering: single nanoparticles and single cells*, ed. by Y. Ozaki, K. Kneipp, R. Aroca (John Wiley & Sons, Chichester, 2014), pp. 285–308

J. Kneipp, H. Kneipp, W.L. Rice, K. Kneipp, Optical tags for biological applications based on surface-enhanced Raman scattering from indocyanine green on gold nanoparticles. Anal. Chem. **77**, 2381 (2005)

J. Kneipp, H. Kneipp, M. McLaughlin, D. Brown, K. Kneipp, In vivo molecular probing of cellular compartments with gold nanoparticles and nanoaggregates. Nano Lett. **6**, 2225 (2006)

J. Kneipp, H. Kneipp, B. Wittig, K. Kneipp, One- and two-photon excited optical pH probing for cells using surface-enhanced Raman and hyper-Raman nanosensors. Nano Lett. **7**, 2819 (2007)

K. Kneipp, A.S. Haka, H. Kneipp, K. Badizadegan, N. Yoshizawa, C. Boone, K.E. Shafer-Peltier, J.T. Motz, R.R. Dasari, M.S. Feld, Surface-enhanced Raman spectroscopy in single living cells using gold nanoparticles. Appl. Spectrosc. **56**, 150 (2002)

B. Küstner, M. Gellner, M. Schütz, F. Schöppler, A. Marx, P. Ströbel, P. Adam, C. Schmuck, S. Schlücker, SERS labels for red laser excitation: Silica-encapsulated SAMs on tunable gold/silver nanoshells. Angew. Chem. Int. Ed. **48**, 1950 (2009)

J.F. Li, Z.Q. Tian, Shell-isolated nanoparticle-enhanced Raman spectroscopy (SHINERS), in *Frontiers of surface-enhanced Raman scattering: single nanoparticles and single cells*, ed. by Y. Ozaki, K. Kneipp, R. Aroca (John Wiley & Sons, Chichester, 2014), pp. 163–192

J. Lin, R. Chen, S. Feng, Y. Li, Z. Huang, S. Xie, Y. Yu, M. Cheng, H. Zeng, Rapid delivery of silver nanoparticles into living cells by electroporation for surface-enhanced Raman spectroscopy. Biosens. Bioelectron. **25**, 388 (2009)

B.F.J. Manly, *Multivariate Statistical Met.: A Primer* (Chapman & Hall/CRC, New York 1994)

A. Matschulat, D. Drescher, J. Kneipp, Surface-enhanced Raman scattering hybrid nanoprobe multiplexing and imaging in biological systems. ACS Nano **4**, 3259 (2010)

S.P. Mulvaney, M.D. Musick, C.D. Keating, M.J. Natan, Glass-coated, analyte-tagged nanoparticles: a new tagging system based on detection with surface-enhanced Raman scattering. Langmuir **19**, 4784 (2003)

K. Nithipatikom, M.J. McCoy, S.R. Hawi, K. Nakamoto, F. Adar, W.B. Campbell, Characterization and applications of Raman labels for confocal Raman microspectroscopic detection of cellular proteins in single cells. Anal. Biochem. **322**, 198 (2003)

A.K. Oyelere, P.C. Chen, X. Huang, I.H. El-Sayed, M.A. El-Sayed, Peptide-conjugated gold nanorods for nuclear targeting. Bioconjugate Chem. **18**, 1490 (2007)

A. Pallaoro, G.B. Braun, N.O. Reich, M. Moskovits, Mapping local pH in live cells using encapsulated fluorescent SERS nanotags. Small **6**, 618 (2010)

I.S. Patel, W.R. Premasiri, D.T. Moir, L.D. Ziegler, Barcoding bacterial cells: a SERS-based methodology for pathogen identification. J. Raman Spectrosc. **39**, 1660 (2008)

M.D. Porter, J.D. Driskell, K.M. Kwarta, R.J. Lipert, J.D. Neill, J.F. Ridpath, Detection of viruses: atomic force microscopy and surface enhanced Raman spectroscopy, in *New diagnostic technology: applications in animal health and biological controls, developments in biological controls*, ed. by P. Vannier, D. Espeseth (Basel, Karger Postfach, 2006), pp. 31–39

W.E. Premasiri, D.T. Moir, M.S. Klempner, N. Krieger, G. Jones II, L.D. Ziegler, Characterization of the surface enhanced Raman scattering (SERS) of bacteria. J. Phys. Chem. B **109**, 312 (2005)

W.R. Premasiri, P. Lemler, Y. Chen, Y. Gebregziabher, L.D. Ziegler, SERS analysis of bacteria, human blood, and cancer cells: a metabolomic and diagnostic tool, in *Frontiers of surface-enhanced Raman scattering: Single nanoparticles and single cells*, ed. by Y. Ozaki, K. Kneipp, R. Aroca (John Wiley & Sons, Chichester, 2014), pp. 257–283

X. Qian, X.H. Peng, D.O. Ansari, Q. Yin-Goen, G.Z. Chen, D.M. Shin, L. Yang, A.N. Young, M. D. Wang, S. Nie, In vivo tumor targeting and spectroscopic detection with surface-enhanced Raman nanoparticle tags. Nat. Biotechnol. **26**, 83 (2008)

J.P. Scaffidi, M.K. Gregas, V. Seewaldt, T. Vo-Dinh, SERS-based plasmonic nanobiosensing in single living cells. Anal. Bioanal. Chem. **393**, 1135 (2009)

A.M. Schwartzberg, T.Y. Oshiro, J.Z. Zhang, T. Huser, C.E. Talley, Improving nanoprobes using surface-enhanced Raman scattering from 30-nm hollow gold particles. Anal. Chem. **78**, 4732 (2006)

A. Sengupta, M. Mujacic, E.J. Davis, Detection of bacteria by surface-enhanced Raman spectroscopy. Anal. Bioanal. Chem. **386**, 1379 (2006)

A. Shamsaie, M. Jonczyk, J. Sturgis, J.P. Robinson, J. Irudayaraj, Intracellularly grown gold nanoparticles as potential surface-enhanced Raman scattering probes. J. Biomed. Opt. **12**, 020502 (2007)

S. Shanmukh, L. Jones, Y.P. Zhao, J.D. Driskell, R.A. Tripp, R.A. Dluhy, Identification and classification of respiratory syncytial virus (RSV) strains by surface-enhanced Raman spectroscopy and multivariate statistical techniques. Anal. Bioanal. Chem. **390**, 1551 (2008)

A. Sujith, T. Itoh, H. Abe, K. Yoshida, M.S. Kiran, V. Biju, M. Ishikawa, Imaging the cell wall of living single yeast cells using surface-enhanced Raman spectroscopy. Anal. Bioanal. Chem. **394**, 1803 (2009)

C.E. Talley, L. Jusinski, C.W. Hollars, S.M. Lane, T. Huser, Intracellular pH sensors based on surface-enhanced Raman scattering. Anal. Chem. **76**, 7064 (2004)

X.B. Tan, Z.Y. Wang, J. Yang, C.Y. Song, R.H. Zhang, Y.P. Cui, Polyvinylpyrrolidone-(PVP-)coated silver aggregates for high performance surface-enhanced Raman scattering in living cells. Nanotechnology **20**, 445102 (2009)

H.W. Tang, X.B. Yang, J. Kirkham, D.A. Smith, Probing intrinsic and extrinsic components in single osteosarcoma cells by near-infrared surface-enhanced Raman scattering. Anal. Chem. **79**, 3646 (2007)

E.A. Vitol, Z. Orynbayeva, M.J. Bouchard, J. Azizkhan-Clifford, G. Friedman, Y. Gogotsi, In situ intracellular spectroscopy with surface enhanced Raman spectroscopy (SERS)-enabled nanopipettes. ACS Nano **3**, 3529 (2009)

M.B. Wabuyele, F. Yan, G.D. Griffin, T. Vo-Dinh, Hyperspectral surface-enhanced Raman imaging of labeled silver nanoparticles in single cells. Rev. Sci. Instrum. **76**, 063710 (2005)

Y. Wang, J.L. Seebald, D.P. Szeto, J. Irudayaraj, Biocompatibility and biodistribution of surface-enhanced Raman scattering nanoprobes in zebrafish embryos: in vivo and multiplex imaging. ACS Nano **4**, 4039 (2010)

Y. Wang, B. Yan, L. Chen, SERS tags: novel optical nanotags for bioanalysis. Chem. Rev. **113**, 1391 (2013)

W. Xie, L. Wang, Y.Y. Zhang, L. Su, A.G. Shen, J.Q. Tan, J.M. Hu, Nuclear targeted nanoprobe for single living cell detection by surface-enhanced Raman scattering. Bioconjugate Chem. **20**, 768 (2009)

W. Xie, L. Su, A. Shen, A. Materny, J. Hu, Application of surface-enhanced Raman scattering in cell analysis. J. Raman Spectrosc. **42**, 1248 (2011)

L. Zeiri, S. Efrima, Surface-enhanced Raman spectroscopy of bacteria: the effect of excitation wavelength and chemical modification of the colloidal milieu. J. Raman Spectrosc. **36**, 667 (2005)

H. Zhou, D. Yang, N.P. Ivleva, N.E. Mircescu, S. Schubert, R. Niessner, A. Wieser, C. Haisch, Label-free *in situ* discrimination of live and dead bacteria by surface-enhanced Raman scattering. Anal. Chem. **87**, 6553 (2015)

Chapter 7
Medical Applications of SERS

Abstract The expanding need for noninvasive diagnostics and nondestructive structural analysis led to great progress in SERS medical applications. In this chapter, selected medical in vitro, ex vivo and in vivo applications of SERS from the past decade will be summarized. It involves both intrinsic and extrinsic (SERS tags) detection schemes. In vitro applications include primarily detection of infectious pathogens and cancer diagnostics. In the case of pathogen sensing, the bacterial or viral contamination is detected via their building blocks such as DNA and proteins using hybridization or immunoassays concepts. Cancer diagnostics includes SERS analysis of proteins, nucleic acids, circulating tumour cells, immunophenotyping of cancer cells as well as the detection of various tumour biomarkers produced by cancer cells. The advantages of SERS are the rapid screening, capability of multiplexing and high sensitivity. Glucose monitoring of diabetes will be demonstrated in both in vitro and in vivo conditions. The possibility of introducing metallic NPs or rationally designed NP tags into living cells or living organisms enables many medical applications. Among them in vitro medical therapy, drug release and theranostics along with ex vivo tissue diagnostics and histology will be described. Concerning in vivo applications, Raman imaging for tumour targeting and monitoring of drug release will be primarily highlighted. Finally, clinical SERS applications as guided intraoperative imaging for tumour resection and endoscope-based imaging will be introduced.

7.1 Glucose Sensing In Vitro

The increasing worldwide prevalence of *diabetes mellitus*, which is a major epidemic of this century, requires frequent monitoring of glucose levels of potential patients. Therefore, development of minimally invasive and biologically compatible methods for quantitative glucose detection is needed. SERS is a promising technique for this purpose due to high speed and sufficient sensitivity. In order to be a practicable glucose detection method, SERS must also prove to be accurate and

M. Procházka, *Surface-Enhanced Raman Spectroscopy*,
Biological and Medical Physics, Biomedical Engineering,
DOI 10.1007/978-3-319-23992-7_7

reliable in the clinically relevant concentration range and in complex biological fluids. Glucose concentration over 100 mg dl^{-1} in blood is indicative of a prediabetic conditions and concentration higher than 126 mg dl^{-1} (7.0 mM) generally results in a diagnosis of diabetes. SERS is sensitive enough for this concentration range. Moreover, SERS is compatible with aqueous solutions and Raman spectral characteristics can avoid possible interference of other molecular species. A large challenge, however, is the poor adsorption of glucose to bare silver or gold substrates.

Specific analytical label-free SERS biosensor for glucose was designed by using of suitable functionalized Ag FON or Au FON substrates (described in Sect. 3.4.4) by the Van Duyne group (Haynes et al. 2005; Yonzon et al. 2006). The diameter of used nanospheres and the thickness of metal layer were optimized for a particular excitation wavelength. The substrates were functionalized with SAMs and an additional alumina layer of about 1 nm thickness. Implementing a partition layer between metal surface and analyte has three advantages for Ag surface: (i) protection it from oxidation; (ii) improvement of its stability and (iii) tailoring it by choosing appropriate SAMs to selectively bind analyte of interest. The SAMs of decanethiol (DT) on Ag FON substrate (Shafer-Peltier et al. 2003) functioned as a partition layer that concentrates glucose near the Ag FON surface enabling it to be detected at concentrations lower than 5 mM. To further improve the performance of partition layer glucose sensors, a mixed SAM monolayer of DT and mercaptohexanol (DT/MH), was formed on an Ag FON and employed for real-time sensing (Lyandres et al. 2005). The DT/MH monolayer was shown to be stable for 10 days and was used as a partition layer for quantitative analysis of glucose with less calibration error than previous SAMs. Moreover, this sensing strategy was successfully applied for real-time detection of physiological glucose concentrations (0–450 mg dl^{-1}) in bovine plasma. In a flow cell setup, the authors demonstrated glucose sensing and departitioning with time constants of 25 and 28 s, respectively (Lyandres et al. 2005). Later, accurate glucose detection was possible over a larger concentration range (10–800 mg dl^{-1}, 0.5–44 mM), making this sensing strategy applicable to a more diverse set of diabetes patients (Stuart et al. 2005).

The novel glucose biosensor using (Ag@Au NPs)/(graphene oxide) nanostructures functionalized with mercaptophenylboronic acid has been reported (Gupta et al. 2013). The assay was based on the ability of glucose to form a bidentate glucose-boronic complex while most of the other physiologically relevant carbohydrates bind to boronic acid as monodentate complexes. The biosensor was successfully applied for the determination of glucose in blood samples. The concentration of glucose was determined to be 1.970 mM with high precision from measurements repeated six times (Gupta et al. 2013). The same approach was applied to determine glucose concentration in urine samples (Kong et al. 2013). The scheme of sensor is depicted in Fig. 7.1. Sensor was formed by a sandwich assay in conjunction with a metal carbonyl probe. Two carbohydrate receptors were used; the first (primary) receptor was 4-mercaptophenylboronic acid anchored onto a SERS substrate and the second (secondary) receptor was a 4-mercaptophenylboronic acid–triosmium carbonyl cluster conjugate (Os–BA). Glucose was first captured by the

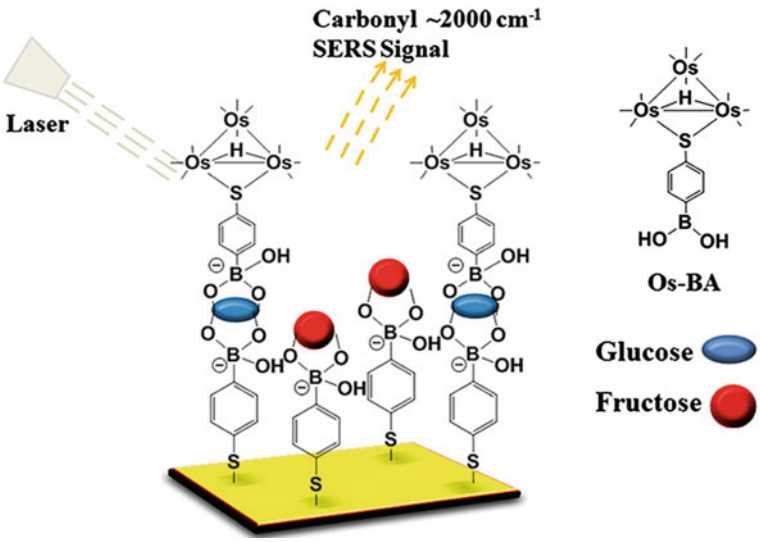

Fig. 7.1 Glucose sensor. A glucose molecule brings 4-mercaptophenylboronic acid-triosmium carbonyl cluster conjugate (Os–BA) to the substrate via formation of a bidentate complex. The *short lines* extending from Os represent carbonyl (CO) ligands (adapted with permission from Kong et al. 2013. Copyright 2013 American Chemical Society)

primary carbohydrate receptor and then labelled with the Os–BA. In this way, it was possible to selectively quantify the concentration of glucose via the SERS band of CO stretching vibration of the metal carbonyl $\sim$2000 cm^{-1} which lies far from possible interference with spectral bands of other biomolecules. Os–BA possesses a much greater affinity for glucose than for fructose and galactose. The SERS-active substrate in this study was bimetallic Ag/Au FONs. In a pilot experiment, the concentration of glucose in the urine sample was determined to be 5.1 mM, which was in agreement with the amount of added glucose (5.0 mM), but LOD was even less (0.1 mM). In comparison to other glucose detection methods, this assay exhibited several advantages: (i) no prior purification of the sample was needed, (ii) an extremely low sample volume was required and (iii) it showed very high specificity for glucose.

7.2 Pathogen Sensing In Vitro

The rapid screening of pathogens remains an issue in food safety, public health assurance and diagnosis of infectious diseases. The bacterial or viral contamination is detected via their building blocks such as DNA and proteins. Routine analyses of pathogens typically involve time-consuming (several days) biochemical characterization of cultured bacteria taken from contaminated sources. Advances in SERS

analysis using SERS tags offer possibilities for rapid screening and detection. SERS analyses include pathogen NA identification via NA hybridization scheme, immunoassays detecting specific protein pathogen biomarkers and direct diagnosis of bacteraemia as well as UTI from body fluids.

7.2.1 Pathogen Sensing Using NA Hybridization

The main approach of pathogen sensing is identification of pathogen NA sequence. Owing to the small content of DNA in cells and its structural complexity, its analysis requires denaturation (heat), fragmentation (restriction endonucleases), separation (electrophoresis), amplification (PCR) and detection (quantitative PCR or microarray techniques). The advantages of SERS are the capability of multiplexing and high sensitivity. The detection scheme is based on hybridization which was described in Sect. 5.2.2. Synthetic oligonucleotides labelled with dye form SERS probes to proper identification of pathogen sequence complementary to the probe. The PCR can be used to simultaneously amplify the specific target DNA sequences enabling amplification of sensitivity of pathogens (Isola et al. 1998).

First SERS gene probe based on hybridization of labelled target sequence has been developed for the selective detection of human immunodeficiency virus (HIV) on Ag islands as SERS-active surface (Vo-Dinh et al. 1994). The effectiveness of such detection scheme was later improved by PCR amplification (Isola et al. 1998). The primer labelled with cresyl fast violet was used for PCR amplification of the 93-base pair target sequence (HIV *gag* gene). The capture probe sequence was bound to PS and hybridized with the total PCR product. Only the amplified target sequence hybridized with the capture probe sequence provided SERRS signal of cresyl fast violet (Isola et al. 1998). Later, a subattomolar HIV-1 DNA detection assay based on multilayer metal-molecule-metal nanojunctions was developed (Hu et al. 2010). First, label-free target DNA facilitated the precipitation of "detection unit I" on the substrate through forming a sandwiched structure based on the capture probe. It results in the first level amplification of the target. Following that, the binding site on "detection probe I" was further recognized by "detection unit II". These two complementary probes served as bricks to build up the metal-molecule-metal nanojunctions between Au NPs that not only created SERS "hot spots" between Au NPs, but also obviously decreased the distance between Au NPs and Raman labels. Therefore, the SERS signal of the tag molecules on these detection probes was significantly enhanced. Such a platform was able to detect a HIV-1 DNA sequence at concentration as low as 10^{-19} M with the specificity of single base mismatch discrimination (Hu et al. 2010). In a multiplex assay (depicted in Sect. 5.2.5), six commercially available dyes—Cy3, Cy3.5, Cy5, TAMRA, texas red and RH6G—were conjugated to different oligonucleotide sequences specific for six different targets including several viruses (Cao et al. 2002). For hybridization, the target DNA and the Au SERS probes were first sequentially added to the chip functionalized with the corresponding capture

sequence. Next, SERRS enhancement for detection of the hybridization event was performed by the reduction of silver ions with hydroquinone. Such sandwich system allowed SERS detection of specific sequences, effectively discriminating between single nucleotides of Hepatitis A, Hepatitis B, HIV, Ebola and Variola viruses. Sufficient correlation between the oligonucleotide sequence and the corresponding SERRS spectrum of the dye attached to it was excellent and LOD of 20 fM was obtained.

An experimental setup to detect dengue (the most common mosquito-borne global disease) virus sequences by SERS on-a-chip was invented. A microfluidic SERS assay was based on synthetic DNA sequences that mimic viral dengue serotypes and TAMRA-labelled targets. The complementary capture probes were immobilized on Au NPs and the SERS measurement was performed within the optofluidic SERS-chip (Huh et al. 2009). Marotta and co-workers reported a label-free detection of DNA hybridization using short oligonucleotides (less than 9 base pairs) for the analysis of the respiratory syncytial virus responsible for lower respiratory tract infections (Marotta et al. 2013). An assay consisted of an array of 5′-thiolated ssDNA oligonucleotides immobilized on the Ag NR surface. It served as capture probes for the detection of synthetic RNA sequences coding for a genetic mutation in the influenza PB1-F2 protein (Negri and Dluhy 2013). Hybridization of the DNA probes to their complementary RNA sequences was detected using SERS. HCA procedure was able to distinguish with 100 % accuracy the spectra of the complementary DNA probe–RNA target from the spectra of the immobilized DNA probes alone, or the DNA probes incubated with complementary RNA sequences, which are not complementary. LOD of such immunoassay was about 10 nM which is 10× lower than standard ELISA.

Molecular sentinel (MS) is a very interesting concept of SERS-based DNA detection (Wabuyele and Vo-Dinh 2005). Figure 7.2 shows the principle of the MS detection strategy. The MS consists of a DNA probe sequence that has a SERS label at one end and a metallic NP attached to the other end via a thiol group. The middle section of DNA probe sequence contains a sequence complementary to the target sequence to be detected and two arms that have complementary sequences in order to form a hairpin loop configuration under normal conditions. The hairpin loop configuration is designed so that the SERS label is in contact or in proximity (<1 nm) to the metallic NP, which induces a strong SE(R)RS signal of the label. SERS signal from the label is detected when the probe is in the closed hairpin state. Hybridization with complementary sequence causes the hairpin opening and thus separation of the label and the metallic NP, which leads to decrease of SERS signal. This concept does not need the target sequences to be labelled.

To demonstrate the feasibility of the MS as a SERS diagnostic tool, the Vo-Dinh group introduced GeneAmplimer HIV-1 control reagents having *gag*-specific primers SK38 and SK39 to amplify a 115-bp HIV-1 *gag* fragment (Wabuyele and Vo-Dinh 2005). The PCR amplicons of retroviral DNA template were hybridized with the SERS nanoprobe—SK 19 MS—incorporating a partial sequence for the HIV-1 *gag* gene and detected using the SERS MS approach. Later, the same group reported SERS MS to detect the human radical S-adenosyl methionine domain

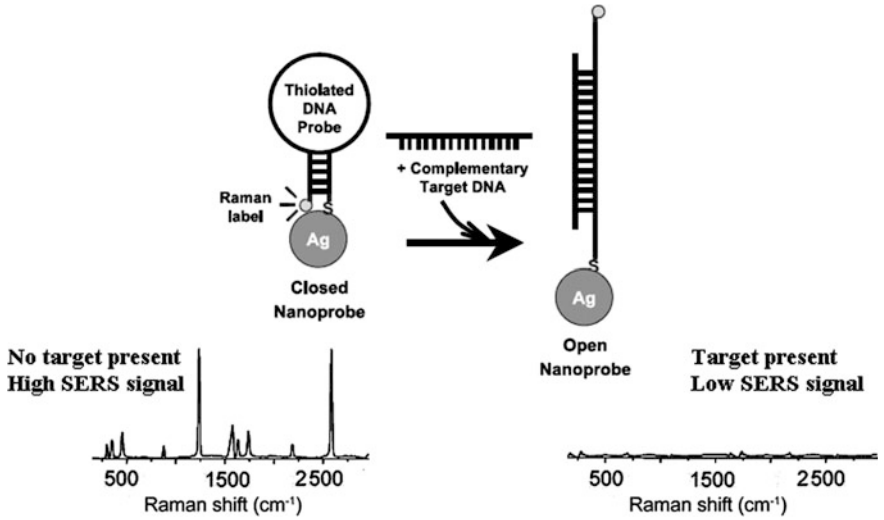

Fig. 7.2 Signalling concept of SERS molecular sentinels (MS). Strong SERS signal is observed when the MS nanoprobe is in the hairpin closed conformation (which is in the absence of target DNA). SERS signal is diminished in the presence of the target DNA which causes opening of MS (adapted with permission from Wabuyele et al. 2010. Copyright 2010 Springer)

containing 2 (RSAD2) RNA target (Wang et al. 2013a). The human RSAD2 gene has recently emerged as a novel host-response biomarker for diagnosis of respiratory infections. The results showed that the RSAD2 MS nanoprobes exhibited high specificity and could detect as low as 1 nM target sequences. The human samples were used in their preliminary tests and the authors suggested the system could be further developed into a portable lab-on-a-chip device. It could measure multiple genome-derived markers for rapid diagnosis of infectious diseases caused by viruses at the point of care. Recently, LOD 2.67 aM for the RNA genetic marker associated with influenza virus was reported (Pang et al. 2014). The assay consisted of an array of Raman label tagged hairpin-DNA (MS reporter) immobilized on metallic FON SERS substrate. The sensing process only required a single hybridization step and post-hybridization washing as well as PCR amplification steps were not necessary.

Concerning bacterial pathogens, a triplex scheme was successfully applied to detect three mixed oligonucleotide probe sequences of different *Escherichia coli* bacterium variants. This was the first multiplex SERRS detection using oligonucleotides labelled with 3 different dyes in a microfluidic system (Docherty et al. 2004). Later, the multiplex system consisting of the oligonucleotides labelled with 5 different dyes (at concentration 1.82×10^{-9} M) was applied in situ (Faulds et al. 2007). Moreover, two different excitation wavelengths enabled to optimize the resonance of a particular dye and consequently to maximize its SERRS signal. The same group reported multiplexed detection of several *Escherichia coli* strains by

using 5 different dye labels and multivariate analysis to better distinguish between the SERS signals of five labels. The ability to discriminate the presence or the absence of a particular label in the mixture was achieved with sensitivity, specificity, accuracy and precision between 0.98 and 1 (Faulds et al. 2008). MacAskill and co-workers developed an easy SERRS assay to monitor simultaneously three DNA sequences from methicillin-resistant bacterium *Staphylococcus aureus,* common hospital contamination (MacAskill et al. 2009). The principle is that ssDNA is adsorbed more readily to Ag NPs treated by spermine to overcome electrostatic repulsion than dsDNA. Possible hybridization event is taking place before adsorption to Ag NPs. If only nontarget DNA was present, the dye-labelled DNA was free to be adsorbed on the Ag NPs and provided a strong SERRS signal. The presence of target DNA allowed the hybridization and formation of dsDNA which cannot be adsorbed onto the Ag surface resulting in a reduction of the SERRS signal.

A positive homogeneous assay, very similar to MS designed by Wabuyele and Vo-Dinh (Wabuyele and Vo-Dinh 2005), was developed by van Lierop and co-workers (van Lierop et al. 2011). The assay utilizes specifically designed self-complementary primers labelled with a SERS-active dye. In contrast to MS, the high SERS signal of dye is obtained in the presence of target DNA which opened the primer through preferential binding, resulting in a region of labelled ssDNA remaining free to adsorb onto the NP. On the other hand, SERS signal is diminished in the absence of target DNA when the primer stayed closed. Highly intense SERS signals were obtained after addition of genomic DNA from *Staphylococcus epidermis* demonstrating the possibility for the detection of multiple targets in clinical samples (van Lierop et al. 2011). Later, the same group improved SERS assay using PCR and enzyme digestion to generate dye-labelled ssDNA and to detect *Staphylococcus aureus* pathogens (van Lierop et al. 2013).

Harper and co-workers employed a combination of TaqMan assay in which signal is generated through enzymatic probe cleavage and SERS to detect DNA of a *Staphylococcus aureus* (Harper et al. 2012). TaqMan assay is based on the 5′-to 3′-exonuclease activity of the thermostable enzyme *Thermus aquaticus* (Taq) polymerase to simultaneously amplify the template and digest the TaqMan probe. The LOD of DNA of a *Staphylococcus aureus* was lower than for conventional fluorescence detection and clinically relevant samples were detected with high specificity. Graham and co-workers introduced another sandwich hybridization assay based on oligonucleotide-NPs conjugates with enhanced stability for the assembly-based detection of *mecA* gene of *Staphylococcus aureus* (Graham et al. 2011). In typical experiment, Au NP or Ag NP conjugates functionalized with two different, noncomplementary oligonucleotides, hybridized upon addition of target oligonucleotide. The molecular recognition event and the formation of structured NP assemblies caused a visual colour change in the NP suspension.

Kang and co-workers developed a Au NP-on-wire SERS sensor for multiplex pathogen DNA detection (Kang et al. 2010). The sensor is illustrated in Fig. 7.3. Au NWs (150 nm diameter) were functionalized with thiolated captured sequences on the Si substrate and incubated with target sequences. Then, such functionalized Au

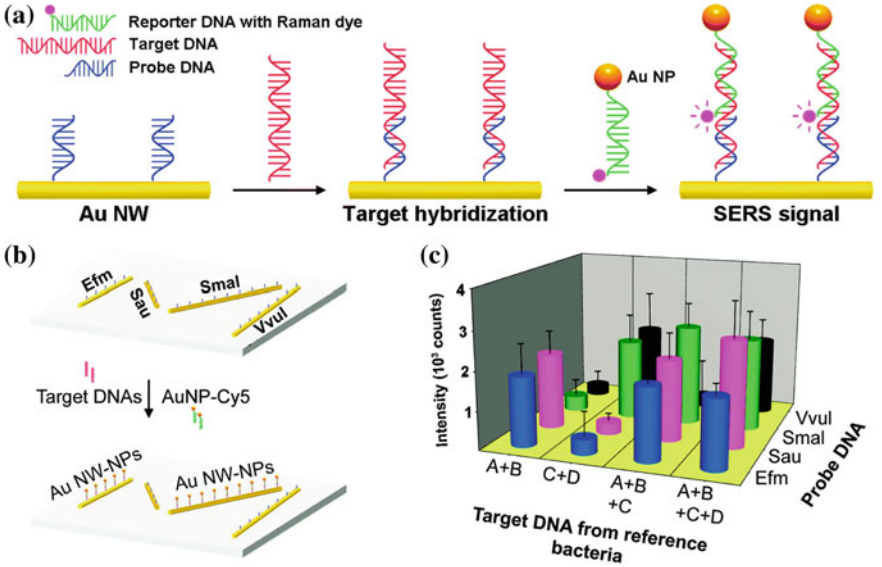

Fig. 7.3 Au NP-on-wire SERS sensor for multiplexed pathogen DNA detection. **a** Scheme of the target DNA detection. **b** Scheme of multiplex approach for detection of DNA extracted from four bacteria. **c** SERS intensities of the RRM when sample contains different kinds of target DNA. *A* Efm: *Enterococcus faecium*; *B* Sau: *Staphylococcus aureus*; *C* Smal: *Stenotrophomonas maltophilia*; *D* Vvul: *Vibrio vulnificus* (adapted with permission from Kang et al. 2010. Copyright 2010 American Chemical Society)

NWs were immersed into a suspension of the reporter DNA-functionalized Au NPs to form Au particle-on-wire structure via sandwich hybridization of probe-target-reporter sequences (Fig. 7.3a). Thus, SERS "hot spots" were created at the gaps between the Au NW and the Au NPs. Strong SERS signals from RRM (Cy5) on the reporter sequences were observed only when the complementary target sequences were added, indicating a high specificity to DNA sequences. A multiplexed pathogen DNA detection platform was constructed by Au NWs attached to different probe sequences, respectively, on a single Si substrate. Four different Au NWs were first functionalized with probe DNA corresponding to the four targets. These NWs were then hybridized with the target DNA, followed by incubation with reporter DNAs with Cy5 at 5′-terminus and Au NP at 3′-terminus (Fig. 7.3b). Identification of DNA sequences extracted from four pathogenic strains, *Enterococcus faecium, Staphylococcus aureus, Stenotrophomonas maltophilia* and *Vibrio vulnificus* (responsible for severe human diseases like sepsis or gastroenteritis) was possible with very low LOD (10 pM). Figure 7.3c shows SERS intensities of 1580 cm^{-1} band (corresponding to the RRM—Cy5) when the sample contains two, three and four kinds of target DNAs of concentrations 10^{-8} M each.

Hybrid MNPs for the enrichment of the target molecules and consequently for the increased detection sensitivity were also employed in pathogen DNA detection in a hybridization scheme. For example, the *omp*A gene of *Chlamydia trachomatis* which is a sexually transmitted bacterium, was detected using a SERS assay based on MNPs (Dougan et al. 2011). Spermine hydrochloride served to promote adsorption of oligonucleotides on the NP surface. A sandwich-hybridization was performed with a magnetic bead immobilized capture probe, the target DNA and terminal phosphate/TAMRA-modified reporter probe. Strelau and co-workers reported a novel approach for the sequence specific detection of DNA using MNPs to amplify PCR products (Strelau et al. 2011). To achieve fast and efficient binding, the hybridization procedure was performed in solution. A streptavidin-modified MNPs, biotin-labelled capture DNAs and probe oligonucleotides carrying a RRM were used. SERS substrate was generated by enzyme-induced growth of Ag NPs and the SERS label attached to the probe DNA was detected. To further purify and enrich the DNA strands of interest, MNPs served for their separation. The system was applied to detect PCR products amplified from DNA of specific agents of epizootic diseases. Sequences of the bacterium *Mycoplasma mycoides* subspecies *mycoides* small colony type (causing contagious bovine pleuropneumonia) were used as PCR targets. To demonstrate the multiplex capability of SERS, the simultaneous detection of three different PCR products labelled with three dyes (Cy3, FAM and TAMRA) was performed (Strelau et al. 2011). MNPs also served in sandwich hybridization assays of synthetic target DNA of the West Nile virus producing West Nile fever and encephalitis (Zhang et al. 2011). The Au NPs and iron MNPs were employed for capturing the target DNA, instead of flat solid substrates commonly used in conventional SERS assays for DNA detection. Figure 7.4 shows the detection method for the West Nile virus target DNA. DSNB served as both the RRM and the linker for the reporter sequence. The hybridization reactions were incubated for a short period. Hybridized complex was formed by a capture substrate, a target oligonucleotide and a SERS label. After the hybridization event, an external magnet served to concentrate hybridized complexes within the focus of laser beam for SERS measurement. This approach reached a LOD 10 pM for West Nile virus target DNA.

7.2.2 Pathogen Sensing Using Immunoassays

Immunoassay platforms, where metallic NPs are functionalized with antibodies or aptamers that recognize target biomolecules on the surface of the pathogen, represent another approach to detect pathogens. The main principles of immunoassays have been explained in Sect. 5.3.3.

Knauer and co-workers reported the label-free SERS detection of *Legionella pneumophila* and *Salmonella typhimurium* cells in water (Knauer et al. 2010). The total assay time was only 65 min. The bacterial suspension was incubated on a glass chip containing the respective antibodies. After the cells were captured and

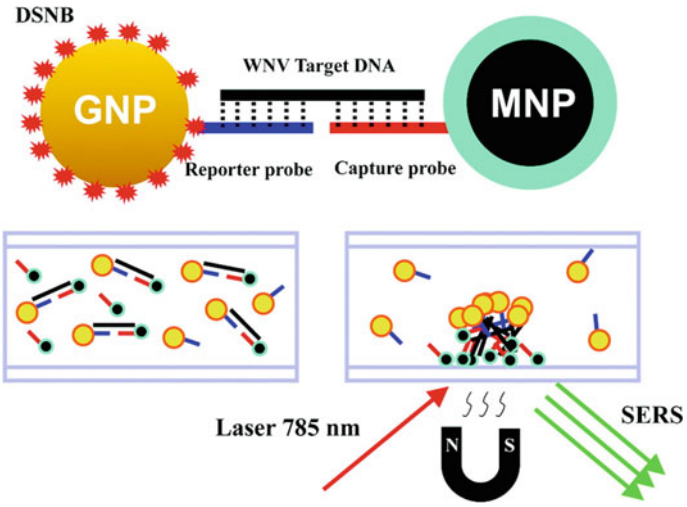

Fig. 7.4 SERS detection of West Nile virus target DNA using MNPs as capture substrates. DSNB served as both the RRM and the linker for the reporter sequence, *GNP* gold nanoparticle, *MNP* magnetic nanoparticle, *WNV* West Nile virus. The hybridization complex was separated and concentrated within the focus beam of the laser by magnetic pull-down and detected by SERS (reproduced with permission from Zhang et al. 2011. Copyright 2011 American Chemical Society)

immobilized on the glass chip, the chip was placed on a polycarbonate tray which was filled with Ag colloid. Sodium azide served for specific agglomeration of the Ag NPs at the bacterial cell wall resulting in a significant SERS signal enhancement. Reliable identification of the bacteria was possible by means of their fingerprint spectra containing mostly strong peaks of amide I, II and III of peptides. Concentrations between 10^6 and 10^9 cells per ml were examined for *Salmonella typhimurium* and between 10^8 and 10^9 cells per ml for *Legionella pneumophila*. SERS spectra obtained from several cells of the same colony provided good reproducibility. In other studies, immunoassays based on labelled SERS tags were employed. Au NPs coated with anti-protein A and RRM (5,5′-dithiobis-2-nitrobenzoic acid) were used for identification of *Staphylococcus aureus* via specific binding of functionalized SERS tag to the bacterial surface antigen. LOD of 1 pg ml^{-1} of protein A was achieved this way (Lin et al. 2008). Similarly, 500 *Mycobacterium avium* subspecies *paratuberculosis* per ml were detected in milk (Yakes et al. 2008). The simultaneous detection of three different bacteria was realized by using Au, Ag and Ag/Au nanoshell NPs immobilized with anti-*Salmonella typhimurium* aptamers, anti-*Staphylococcus aureus* and anti-*Escherichia coli* O157:H7 antibodies, respectively, and unique RRMs (Ravindranath et al. 2011). Here, a microfiltration step was applied to consolidate a highly selective and specific detection platform with total detection time under 45 min and LOD ranging between 10^2 and 10^3 colony forming units per ml.

The possibility of separation and detection of multiple pathogens in a food matrix by using magnetic SERS tags has also been reported (Wang et al. 2011a). In this work, pathogens were first immunomagnetically captured with MNPs and then pathogen-specific SERS tags were functionalized with corresponding antibodies to allow the formation of a sandwich assay. The detection of multiple pathogens in selected food matrices was achieved by changing the RRM on the SERS tags. *Salmonella enterica* serovar *Typhimurium* and *Staphylococcus aureus* were chosen to demonstrate the possibility of multiple pathogens detection. The lowest cell concentration detected in a spinach solution was 10^3 colony forming units per ml. The results of a blind test in peanut butter validated that this LOD was achieved with high specificity.

7.2.3 Direct Bacterial Identification in Human Body Fluids

Bacteraemia, the presence of bacteria in the patient's blood, resulting from severe infections in the body, surgical wounds, or contaminated implanted devices may lead to a sepsis. Its onset is very fast. The current standard testing methods in hospitals are based on cultivation bacteria. However, this procedure normally takes up to 3 days. Therefore, the big advantage of SERS is the speed of identification. Effort is made to improve SERS detection of pathogens in human body fluids using portable Raman microscopes, robust metallic substrates and by a simplification of sample preparations (Premasiri et al. 2012b, 2014).

The SERS diagnostics based on direct analysis of blood samples requires a detail SERS study of whole blood. SERS spectra of whole human blood, plasma and red blood cells were reported for the first time by Premasiri et al. (2012a). They used small aggregates (2−15 NPs) of monodispersed Au NPs (80 nm diameter) covering the outer layer of $\sim$1 mm^2 SiO_2 substrate. The freshly drawn blood sample was refrigerated (8 °C) prior to SERS measurements. For SERS experiment, the blood sample ($\sim$1 µl) was placed on the Au substrate to form only a thin film. The SERS spectra of fresh whole human blood and fresh plasma, observed $\sim$1 h after being drawn are compared in Fig. 7.5, spectrum b and c, respectively. The spectra look very similar showing strong vibrational bands at 490, 639, 895, 1134, 1362, 1569 and 1649 cm^{-1}. The NRS spectrum of dried whole blood (spectrum a) is very different. The authors concluded that the NRS spectrum of whole blood shows exclusively the spectral features of haemoglobin while SERS spectrum is due to blood components other than haemoglobin. Moreover, the SERS spectra of the same blood sample stored at 8 °C undergo significant evolution as a function of storage time over a period of 24 h. For example, new vibrational bands at 724, 965, 1070, 1332, 1365 and 1453 cm^{-1} appeared and increased in relative importance as a function of whole blood storage time. All the changes were attributed to hypoxanthine and SERS spectrum of whole blood stored for $\sim$24 h was essentially that of hypoxanthine.

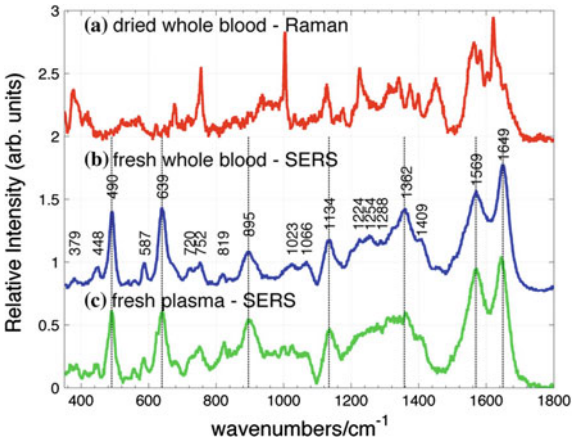

Fig. 7.5 Raman spectra of whole blood samples. **a** NRS spectrum of dried whole blood, **b** SERS spectrum of fresh whole blood, **c** SERS spectrum of fresh plasma. 785 nm excitation wavelength (reproduced with permission from Premasiri et al. 2012a. Copyright 2012 American Chemical Society)

In practice, the problem of diagnosis of pathogen bacteria from a blood sample is that the relative concentration of bacterial cells (only 10^3 per ml) in the infected blood of patients is much smaller than of blood cells (10^9 per ml). Premasiri and co-workers developed an automated selective lyses, centrifugation and micro-evaporation procedure to achieve the required enrichment $\sim 10^5$ of bacterial cells to observe their SERS spectra. It allows acquisition of SERS spectra in 100 nl volumes of infected blood (Premasiri et al. 2014). Since only relatively subtle distinctions are often observed between the SERS spectra of samples containing various pathogens, the empirical algorithm based on the SERS intensity or particular bands does not provide a sufficient diagnostic sensitivity and specificity. Therefore, the PCA approach was applied to determine the reproducibility and specificity of the diagnosis derived from SERS spectra (Patel et al. 2008). The PCA procedure involves removing the high frequency noise by Fourier filtering and conversion of SERS spectrum into a barcode, which is of "ones" or "zeros" based on the sign of the second derivative of the spectrum as a function of Raman frequency. The best clustering results derived from the SERS bacterial spectra are consistently obtained when second-derivative-based barcodes are used as input vectors for the PCA treatment. When barcodes are assigned on the basis of the sign of the second derivative, i.e. 1 for upward curvature (positive second derivatives) and 0 for downward curvature (negative second derivatives), each species is represented by a frequency-dependent binary fingerprint. A threshold for zero, usually set at about 10 % of the maximum value of the second derivative, is used to determine a minimum value for a 0 bit assignment for this barcode. This threshold helps discriminate against residual noise components. Such second-derivative barcodes for the two closely related *Bacillus* bacteria (*Bacillus antracis Sterne* and *Bacillus thuringiensis*) are shown in Fig. 7.6a as an example. The barcodes were the

inputs for the PCA analysis. Figure 7.6b shows barcode PCA plots for four *Bacillus* bacteria spiked and recovered from human blood. Black lines are equidistant to the mean of each cluster (Premasiri et al. 2014). The barcode methodology resulted in significantly enhanced diagnostic specificity.

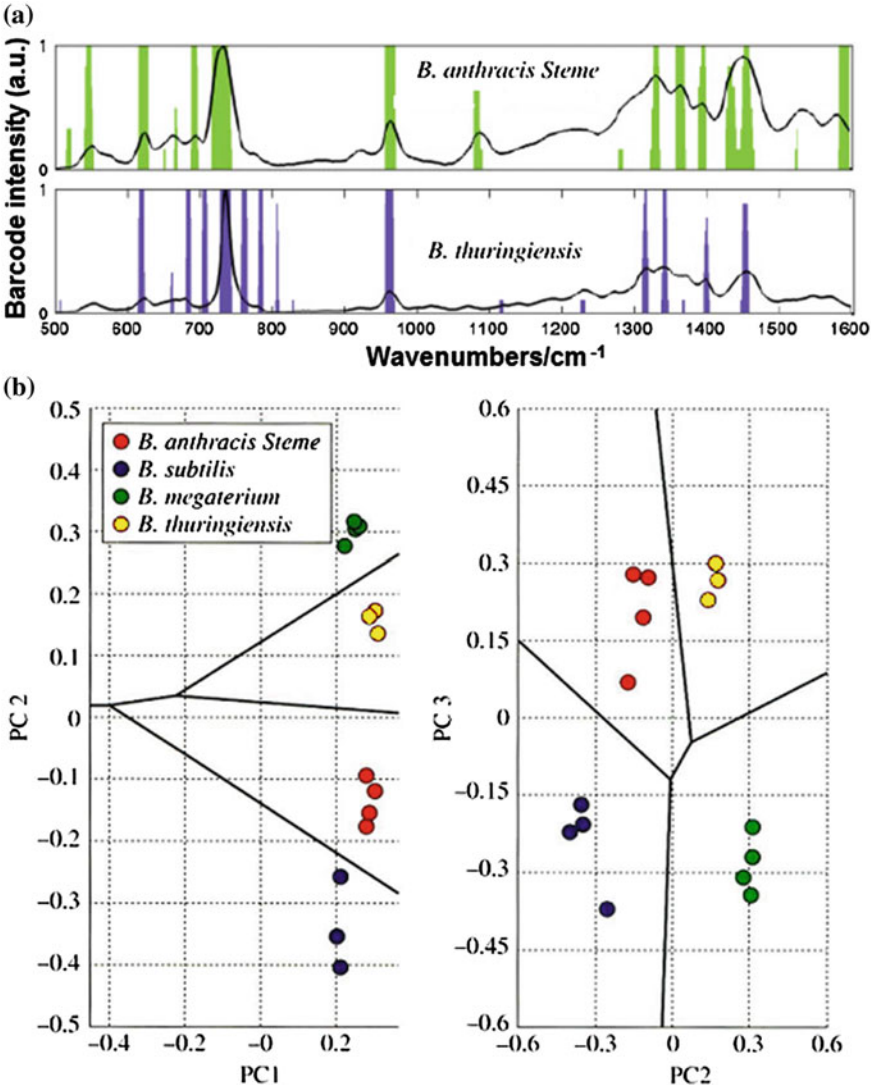

Fig. 7.6 Pathogen bacteria SERS detection from blood samples. **a** Second-derivative barcodes for the two closely related *Bacillus* bacteria. **b** Barcode-based PCA analysis of four *Bacillus* bacteria spiked and recovered from human blood. *Black lines* are equidistant to the mean of each cluster (**a** adapted with permission from Patel et al. 2008, **b** adapted with permission from Premasiri et al. 2014. Copyright 2008, 2014 John Wiley & Sons, Ltd)

The first SERS analysis of clinical bacterial isolates associated with UTI was reported by employing aggregated citrate-reduced Ag NPs (Jarvis and Goodacre 2004). To acquire reproducible data, 50 spectra were collected making the spectral acquisition time ~8 min per bacterium. The multivariate statistical techniques were applied in order to group these organisms based on their spectral fingerprints. The results are shown in Fig. 6.8. The disadvantage was that all isolates were cultivated for 16 h and evidently more rapid analysis is required (Jarvis and Goodacre 2004). Recently, Premasiri and co-workers reported faster and direct analysis from urine samples obtained from patients (Premasiri et al. 2014). The sample preparation did not need any cultivation step. It was also easier in comparison to blood samples because the concentration of pathogen bacteria in urine is much higher than in blood and urine is a less complex body fluid than blood. Routine centrifugation and filtration led to 10^3–10^4 enrichment of bacterial concentration, which corresponds to clinically relevant concentrations and the typical threshold for antibiotic treatment. The SERS spectra of three different *Escherichia coli* strains that were spiked into urine at this minimal diagnostic level were analysed by SERS barcode procedure and PCA. After analysis, distinct clusters were obtained for the bacterial cells, demonstrating that specific spectral signatures can be identified. This test took about 40 min to perform thus it is very promising for rapid and low-cost UTI diagnosis.

7.3 SERS Cancer Diagnostics In Vitro

Reliable methods for cancer diagnosis and prognosis are a tremendous challenge for modern medicine. Detection of earlier stages of cancer is especially desirable because it reduces the risk of metastasis and gives a better chance for successful and efficient treatment. Owing to the progressive increase in human deaths resulting from cancer, a major effort is being made to develop noninvasive, effective and fast cancer detection. The sensitivity, speed and ease of use, together with strategies to achieve specificity make SERS an analytical approach that could be successful for real-time cancer diagnostics. It includes the SERS analysis of proteins, NAs, circulating tumour cells (CTCs), immunophenotyping of cancer cells as well as the detection of various tumour biomarkers such as cell surface markers or those produced by cancer cells.

There are potentially more than 150 biomarkers found in serum for the detection of various types of cancers. Examples are PSA or epidermal growth factor (EGF). Pancreatic cancer (PC) is one of the most lethal cancers and has a very poor prognosis because of the lack of a reliable tumour marker for early diagnosis. The most prevalent markers are mucin-type glycoproteins (MUC), which express elevated concentrations in PC patients. Mucins have emerged in recent years as useful markers for the early detection and predicting prognosis and response to therapy in several solid tumours because the expression of various mucin backbones and associated carbohydrate epitopes is altered during the initiation and progression of

various cancers, including PC. For most applications, single biomarkers are unlikely to provide the necessary sensitivity and specificity owing to the substantial heterogeneity among cancers. It is unrealistic to expect that a single biomarker will bring information about tissue type and malignant transformation throughout the various stages of tumour development and progression. Therefore, panels of biomarkers are needed, but before such panels can be employed in clinical practice, each biomarker must be discovered and validated individually (Phan et al. 2009).

7.3.1 Cancer Diagnostics Using NA Hybridization

The cancer susceptibility genes in DNA are associated with genetically predisposed cancer development. They can be detected in DNA isolated from patient's cells through SERS hybridization assays using labels. In the first model experiment of Allain and Vo-Dinh, the breast cancer susceptibility genes *BRCA1* nucleotide capture sequence (23-mer) labelled with rhodamine B was detected (Allain and Vo-Dinh 2002). Ag islands serving as SERS-active substrate were etched to form a microwell platform and subsequently modified with a monolayer of mercaptoundecanoic acid. The complementary probe was covalently bound to the Ag surfaces using a succinimidylester intermediate. In a hybridization experiment, the Ag surface coated with the immobilized capture oligonucleotides was used and the SERS spectra of the blank and the hybridized DNA were collected (Allain and Vo-Dinh 2002). Later, the hybridization probe was employed to oligonucleotides fragments labelled with cresyl fast violet containing a breast cancer sequence (Pal et al. 2006). The detection of a DNA sequence of the *Ki-67* gene, a critical breast cancer biomarker, on the triangular-shaped NWs substrate demonstrated the potential of the MS strategy for SERS-based DNA detection (Wang and Vo-Dinh 2009). Here, 150 μl of sample was spread over the entire chip area of 1.5 × 1.5 cm^2. SERS signal was acquired only from 15 pl fraction of the sample, which corresponds to 15 aM. For practical clinical applications, it would be desirable to have detection sensitivity in the range of 0.5–1.5 aM. Therefore, for clinical utilization, the authors stress the necessity of improving the sensitivity of the MS by an order of 10–30 times by the optimization of several fabrication parameters, such as probe surface density and chip size (Wang and Vo-Dinh 2009). DNA sensing using MS was further refined by development of a repeatable and reproducible MS-on-a-chip platform formed by triangular-shaped nanowire arrays having controlled gap (<10 nm) nanostructures over an entire 6 inch wafer (Wang et al. 2013b). Sun and co-workers designed the hybridization approach with the sensitivity close to 1 fM by using the Au NPs. The assay was able to detect alternative sequences in the gene splicing profile of the *BRCA1* gene linked to the malignant transformation of tumours in breast cancer (Sun et al. 2008). Later, the same group reported an advanced gene expression assay for *BRCA1* gene. It involved the isolation of RNA from breast cancer cell lines followed by a translation into complementary DNA

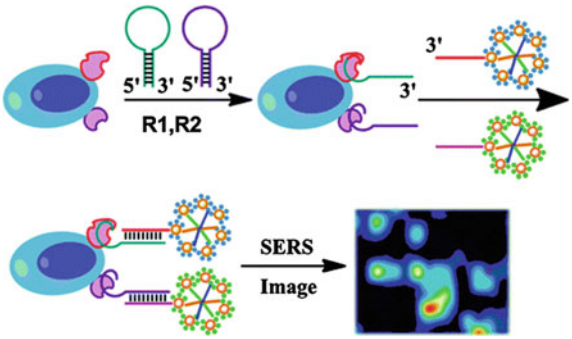

Fig. 7.7 Schematic diagram for simultaneous detection of two biomarkers on the cancer cell surface based on self-assembly of branched DNA–Au nanoaggregates (adapted with permission from Li et al. 2014. Copyright 2014 The Royal Society of Chemistry)

and sensitive quantification of the expression levels of splice junction, skipping exon 9 and 10, of the *BRCA1* gene (Sun and Irudayaraj 2009).

Recently, Li and co-workers applied aptamer-based recognition for simultaneous detection and imaging of two human breast cancer biomarkers MUC1 and nucleolin overexpressed on the MCF-7 cell surface (Li et al. 2014). The scheme of this experiment is shown in Fig. 7.7. Two hairpin-structured recognition probes (R1 and R2) composed of a target-specific aptamer sequence at the 5'-terminus and a linker segment at the 3′-terminus for connecting with the Raman probe. In the presence of target cancer cells, the aptamer can specifically recognize the biomarkers on the cell surface and undergo a conformational alteration, leading to stem separation. Following this, the (Au aggregates)/DNA hybridized with the opened stem and served as Raman probes for SERS measurement and imaging. To prepare the Raman probe, the hairpin DNA and barcode DNA modified by Raman dye label were simultaneously immobilized on the surface of Au NPs to form hairpin DNA-barcode-Au nanoaggregates, in which each Au NP can be loaded with a large number of Raman dye molecules. This proposed method possesses several advantages. First, by using DNA-gold nanoaggregates as Raman probes, the SERS signal can be significantly enhanced and the distribution of biomarkers can be readily visualized by SERS imaging. Second, this method permits simultaneous determination of two or more biomarkers on the cell surface. Third, as the aptamer sequence in the recognition probe can be easily replaced by other aptamers, the design can be conveniently used for detection of diverse ranges of biological targets.

Cancer diagnostics often needs a discrimination of genomic mutations in DNA sequences or special NA structures (miRNA) which can cause various diseases including cancer. SERS technique is very promising for mutation and single nucleotide polymorphisms detection because of the possibility of spatial multiplexing at array format linked with a portable biosensor device. Mahajan and co-workers reported such SERS-based approach using Au substrates prepared by

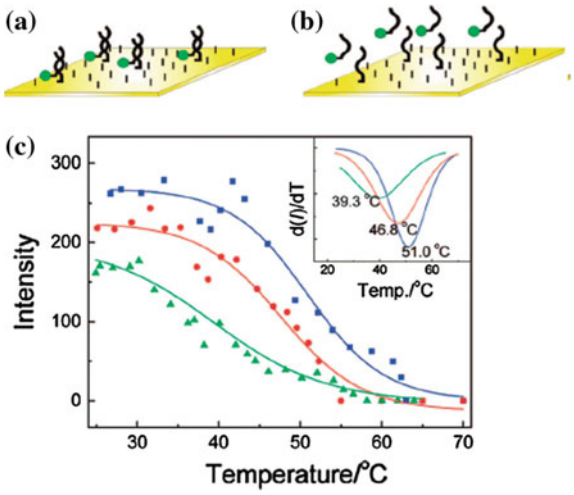

Fig. 7.8 SERS-based approach for discriminating mutations in DNA. **a** Labelled target sequences hybridized to capture oligonucleotides immobilized on the sphere segment void Au surface (label is marked by *green*). **c** Melting curves obtained from thermally induced dehybridization (**b**) of three different target sequences wild type without mutation (*squares*, *blue curve*), single point mutant (*circles*, *red curve*) and triple mutant (*triangles*, *green curve*). The first derivatives of the sigmoidal fits of the intensity curves are shown in the *inset* (adapted with permission from Mahajan et al. 2008. Copyright 2008 American Chemical Society)

electrodeposition around a close packed monolayer template (Mahajan et al. 2008). Their experiment is illustrated in Fig. 7.8. Disulphide-modified oligonucleotides were first immobilized on the sphere segment void Au surface to capture the corresponding target strand. Second, the Au surface was incubated with MH so as to cover the rest of the surface and thus avoid nonspecific binding. The target sequences were labelled with SERRS-active label and hybridized to the capture strand. SERRS label should be located near the Au surface to obtain a strong SERRS signal (Fig. 7.8a). Temperature and potential ramp were applied to the surface to obtain melting curves (Fig. 7.8b). The melting curves as a result of thermally induced dehybridization are shown in Fig. 7.8c. The SERRS intensity of the label was plotted against temperature for three different target sequences: wild type (no mutation), single point mutant and triple mutant (triple deletion). The wild type displayed the highest melting temperature (51 °C). It is because the target sequence matched perfectly the capture sequence. The melting temperatures of the single point mutant and the triple mutant were lower (46.8 and 39.3 °C, respectively) indicating a worse fit because of the mutation (Mahajan et al. 2008). In other experiment, the MS was applied to detect the single nucleotide polymorphisms at codon 504 of the *BRCA1* gene (Wabuyele et al. 2010). Hybridization with target DNA opened the hairpin and physically separated the Raman label (5-carboxy-tetramethylrhodamine) from the metallic NP. This reduced the plasmonic effect and quenched the SERS signal of the label. A linear relationship was

observed over low concentrations of target DNA (0–2 μmol l^{-1}) and reproducibility for the assay was <2 %.

Driskell and Tripp reported a label-free SERS detection of miRNAs based on affinity for an unmodified Ag NR array substrate (Driskell and Tripp 2010). MiRNAs are small noncoding RNA molecules that regulate eukaryotic gene expression and can serve as biomarkers of human cancers. The applicability of SERS for miRNA analysis was demonstrated using Ag NRs and the pathogenic relevant human miRNAs. The results indicated that miRNA sequences could be accurately discriminated and quantified even in multicomponent mixtures (Driskell and Tripp 2010). Later, highly reproducible Ag NRs were used to obtain SERS spectra of clinically relevant miRNA sequence in hybridization event. Straightforward LS analysis applied on SERS spectra enabled SERS quantitative determination of the relative ratios of the four nucleotide components: adenine, cytosine, guanine and thymine/uracyl (Abell et al. 2012).

7.3.2 Cancer Diagnostics Using Immunoassays

Sandwich immunoassays (described in Sect. 5.3.3) allowing specific detection of protein biomarkers are routinely used in clinical cancer diagnostics. Porter and co-workers developed immunoassays for SERS detection of PSA (Grubisha et al. 2003; Park et al. 2006; Porter et al. 2008). The assay for measuring PSA in human serum comprised a bifurcated fibre optical bundle for coupling the laser source to the Raman probe head, which focused the light onto the sample area and from the probe head to the Raman spectrometer. DSNB already activated for subsequent bioconjugation served as a RRM. DSNB was synthesized from the corresponding biscarboxylic acid using standard N-hydroxysuccinimide ester chemistry. The addition of DSNB disulfide to the Au NPs (32 nm diameter) led to the formation of a SAM monolayer on the metal surface. The DSNB ester terminus could subsequently react with the antibody by forming the corresponding amide. Such immunoassays showed LOD of PSA in human serum about 1 pg ml^{-1} (30 fM) with variation of signal less than 10 % from a different spot of the sample. It is necessary to mention that conventional assays have LOD of PSA about 100 pg ml^{-1} or above (Ferguson et al. 1996). The detection of PSA at a concentration 10 pg ml^{-1} and less helps patient relapse to be noticed months or even years quicker.

A SERS sandwich immunoassay has been applied successfully for quantitative measurements of MUC4 levels in the serum of patients with PC (Wang et al. 2011b). First, an Au-coated glass slide was functionalized with capture antibody through coupling with dithiobis-(succinimidyl propionate) ligands on the Au surface. Second, SERS tag was formed by a mixed thiol monolayer composed of dithiobis-(succinimidylpropionate) and RRM (4-NBT) on Au NP, followed by conjugation with the detection 8G7 antibody (Fig. 7.9a). This assay used the same anti-MUC4 antibody (8G7) for both capture and detection since it targets repeating epitopes (part of the antigen that is recognized by the antibody) of the MUC4

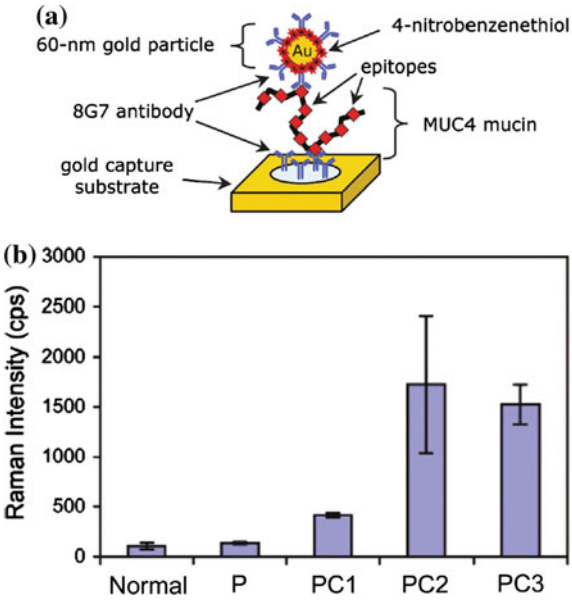

Fig. 7.9 Detection of MUC4 biomarker of pancreatic cancer using a SERS tag. **a** A schematic representation of the detection array. **b** SERS detection of MUC4 in pooled sera from normal individuals and patients with pancreatitis (P) or pancreatic cancer (PC1, PC2 and PC3). Each pool includes sera from 10 individuals (adapted with permission from Wang et al. 2011b. Copyright 2011 American Chemical Society)

molecules. In a typical immunoassay experiment, capture substrate was exposed to the sample solution for 8 h in a humidity chamber. After rinsing with buffer, captured MUC4 antigens were labelled by exposition to the functionalized NPs for 16 h. The substrates were then rinsed and dried with a stream of nitrogen and analysed by SERS. Concentration-dependent assay for MUC4 in the PBS buffer was performed. The analyte concentration was quantified using the peak intensity of 4-NBT at $\sim$1336 cm^{-1}. Based on these results, the SERS-based assay was applied to detect MUC4 in the serum of PC patients. Five sets of pooled serum samples were analysed after a 20× dilution in PBS: one pool from healthy individuals (normal), one pool from patients with acute pancreatitis (P) and three pools from PC patients (PC1, PC2, PC3). The results show that sera of patients with PC produce significantly higher SERS response for MUC4 compared to sera from healthy subjects (Fig. 7.9b). Later, they refined their diagnosis by using two relevant and well established markers for PC: serum carbohydrate antigen 19-9 (CA 19-9) and matrix metalloproteinase-7 (MMP-7). The LODs using the SERS platform were determined to be 2.28 pg ml^{-1} (matrix metalloproteinase-7) and 34.5 pg ml^{-1} (carbohydrate antigen 19-9) from spiked serum which is 29× and 14× lower for carbohydrate antigen 19-9 and matrix metalloproteinase-7 in comparison to ELISA technique, respectively (Granger et al. 2013). A novel SERS-based sandwich immunoassay using DNA aptamers, silica-encapsulated hollow gold nanospheres and a gold-patterned microarray was developed for sensitive detection of vascular EGF angiogenesis protein markers (Ko et al. 2013). Target specific DNA aptamers that fold into a G-quadruplex structure were used as a target recognition

unit instead of vascular EGF antibodies. The detection sensitivity was improved by 2 or 3 orders of magnitude over the conventional ELISA method.

The antibody-based recognition of two important cancer biomarkers, CEA and AFP, has been reported. In this experiment, a duplex SERS tag was created by coupling two antibodies against the cancer biomarkers on magnetic beads and both biomarkers were detected simultaneously in blood serum using a single excitation wavelength (Chon et al. 2011). Au patterned microarray was used as a matrix for the immuno-based detection of angiogenin which has an important role in tumour angiogenesis (Lee et al. 2011a). Park and co-workers reported the identification of HER2-positive breast cancer cell lines using antibody-conjugated Au NRs (Park et al. 2009). The Epstein-Barr virus-associated expression of latent membrane protein 1, a tumour marker for nasopharyngeal carcinoma, was also detected (Chen et al. 2012d). Immunoassay consisted of Au/Ag core-shell NPs coated with antibody specific to latent membrane protein 1 and 4-MBA as a RRM. Latent membrane protein 1 was detected in paraffin-embedded nasopharyngeal carcinoma tissues of patients that were positive for Epstein-Barr virus and healthy volunteers. The authors reported excellent accuracy of SERS: 97.1 % of the cancer patients were tested positive for the virus encoded protein, whereas only 64.7 % of the protein was detectable when a conventional immunohistochemical staining technique was applied (Chen et al. 2012d). A human p65 tumour suppressor and the cyclin-dependent kinase inhibitor p21cip (both proteins which are presented in elevated concentration in tumour cells) were detected in a multiplex SERS immunoassay based on antibody-functionalized Au/Ag NRs (Wu et al. 2013).

It has been found that breast cancer cells expressing the CD44 antigen and not the CD24 antigen exhibited enhanced invasive properties. The two cell surface markers C24 and C44 were detected by SERS in three human breast cancer cell (MCF-7, MDA-MB-231, MDA-MB-468) populations (Lee et al. 2011b). Au NPs functionalized with antibodies specific to CD24 or CD44 and different DNA sequences were used to target these two surface markers. Au NPs conjugated with corresponding complementary DNA sequences and RRMs were employed to form a network structure around the pointer NPs that can be detected by SERS. Fixed cancer cells were first incubated with pointer NPs to localize the NPs at corresponding membrane marker sites due to the antibody-antigen recognition. Then, the NPs were added to form the hybridization network structure at the corresponding marker sites targeted by the pointer particles. SERS mapping of two different RRMs, 4-mercaptopyridine (characteristic peak at 1094 cm^{-1}) and 4,6-dimethyl-2-pyrimidinethiol (characteristic peak at 569 cm^{-1}), representing CD44 and CD24, respectively, was conducted to determine the distribution of corresponding surface markers on selected cancer cells. The results indicated that MDA-MB-231 cells express the CD44 antigen and not the CD24 antigen (Lee et al. 2011b). Similarly, the selective targeting of chronic lymphocytic leukaemia was done using Ag NPs conjugated with anti-CD19 antibodies (MacLaughlin et al. 2013).

7.3.3 Direct Cancer Diagnostics from Blood Plasma

7.3.3.1 Cancer Diagnostics from SERS Spectra of Blood Samples

The direct SERS cancer diagnostics using blood plasma was discovered by the Chen group (Chen et al. 2012a). The procedure involved a mixing of crude blood or pretreated/purified blood samples with hydroxylamine-reduced Ag NPs, followed by SERS measurement and spectral analysis. Since the SERS from Ag NPs was often not reproducible, a drop of (Ag NP)/blood mixture was transferred onto an aluminium plate and SERS spectra were acquired using a confocal Raman microspectrometer. For each sample, three spectra were collected from different spot within the sample to obtain a mean spectrum. All these steps were completed within less than 3 h after the blood was drawn. SERS spectra were treated by PCA algorithms. It was found that, a combination of PCA and linear discriminate analysis (LDA) provided the best results. PCA was used for simplifying complex data sets and determining the key principal components in multidimensional data sets that best explained the spectral differences. LDA generated a diagnostic algorithm using the PC scores for the most significant PCs (Chen et al. 2012a). For example, the integration of the SERS spectral bands (at 1310–1430 and 1560–1700 cm^{-1} regions) achieved a sensitivity of only 70 and 83.3 % and a specificity of 76 and 78 %, respectively. However, the PCA-LDA algorithms yielded a diagnostic sensitivity of 96.7 % and a specificity of 92 % for separating cervical cancerous samples from normal samples (Feng et al. 2013).

The first report on SERS analysis of blood plasma for cancer diagnostics was nasopharyngeal cancer detection with diagnostic sensitivity 90.7 %, specificity 100 % and accuracy 95.4 % on a set of 33 normal subject and 43 nasopharyngeal cancer patient blood plasma samples (Feng et al. 2010; Chen et al. 2012a). Another SERS cancer diagnostics using Ag NPs reported by the Chen group involved a cervical (Feng et al. 2013), colorectal (Lin et al. 2011a) and esophageal (Li et al. 2013) cancer. Figure 7.10a compares the mean SERS spectrum for the cervical cancer plasma samples (blue curve, n = 60) with that of the normal plasma (red curve, n = 50). The peak positions and tentative assignment of major vibrational bands observed in blood plasma samples are listed in Table 7.1. The intensities of SERS bands at 1445 and 1580 cm^{-1} assigned to the CH_2 bending mode of collagen or phospholipids and amino acid Phe, respectively, are lower in healthy plasma than in cancer plasma. On the other hand, a decrease of signal intensities of SERS bands of Arg (496 cm^{-1}), Tyr (638 cm^{-1}), serine (813 cm^{-1}), galactosamine (888 cm^{-1}) and mannose (1135 cm^{-1}), reflects a tumour's vigorous metabolism. The peak at $\sim$1338 cm^{-1} of CH vibration of NA bases exhibits higher signal in the cancer samples indicating that there is an increase in the relative amount of NAs in the blood of cancer patient. Therefore, an abnormal NA metabolism (observed as circulating plasma DNA) of cancer cells (Gormally et al. 2007) can be used as biomarker for monitoring cancer occurrence in blood plasma samples. These spectral changes are typical for blood samples from all types of cancer patients

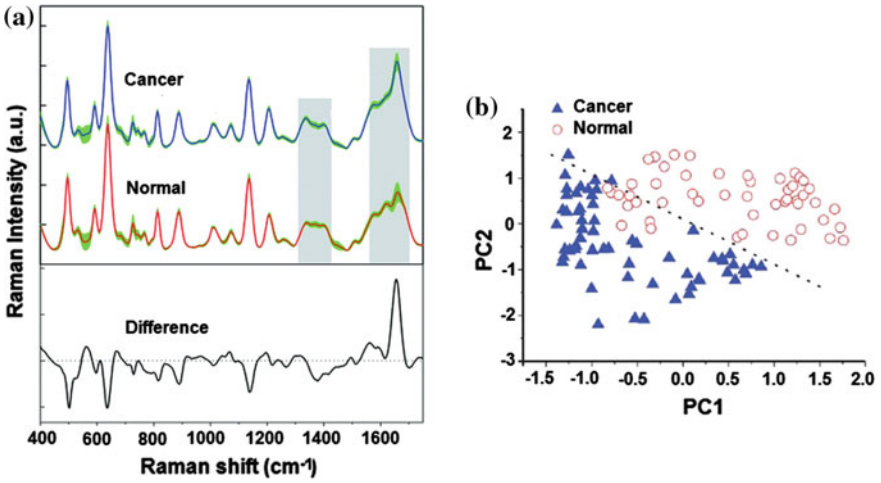

Fig. 7.10 Cervical cancer SERS detection from blood plasma. **a** Comparison of the mean spectrum for the cervical cancer plasma samples (*blue curve*, n = 60) versus that of the normal plasma (*red curve*, n = 50) samples. The *green shaded* areas represent the standard deviations of the means. *Black bottom* spectrum is the difference spectrum. **b** Plot of the first principal component (PC1) versus the second principal component (PC2) for the normal group versus the cervical cancer group. The *dotted line* as a diagnostic algorithm separates the two groups (adapted with permission from Feng et al. 2013. Copyright 2013 The Royal Society of Chemistry)

Table 7.1 The peak positions and tentative assignment of major vibrational bands observed in blood plasma samples, ν—stretching mode, δ—bending mode

Peak position (cm^{-1})	Vibrational mode	Major assignment
496	ν(S–S)	L-Arg
534		Cholesterol ester
638	ν(C–S)	Tyr
813	ν(C–C–O)	L-Serine
888	δ(C–O–H)	D-Galactosamine
1135	ν(C–N)	D-Mannose
1338		Adenine
1400	$\delta(CH_2)$	Collagen, phospholipids
1578	δ(C=C)	Phe
1655	ν(C=O)	Amide I

Reproduced with permission from Feng et al. 2013. Copyright 2013 The Royal Society of Chemistry

investigated up to now. PCA analysis showed that normal and cancer groups can be clearly separated (Fig. 7.10b).

Although the first results obtained for nasopharyngeal (Feng et al. 2010) and gastric (Feng et al. 2011) cancer were very promising, in both cases, the data points

for the normal as well as cancer patients were slightly overlapped preventing a clear separation of the two groups. To further improve the cancer detection using blood plasma, the Chen group introduced pretreatment and purification of blood plasma samples before SERS analysis (Lin et al. 2011b; Chen et al. 2012a). First, the purified plasma proteins (albumin and globulin) were separated from blood plasma by membrane electrophoresis, eluted and mixed with Ag NPs. Second, the SERS spectra were measured and analysed by PCA-LDA. Using these steps, the interferences of other native plasma constituents and exogenous substances were minimized and reliable spectral signatures were obtained. Thus, the gastric cancer group (31 patients) and the normal group (33 healthy volunteers) were completely discriminated with both diagnostic sensitivity and specificity of 100 % (Lin et al. 2011b; Chen et al. 2012a).

Recently, it was found that cancer can be detected by changes of molecular compositions and structures of human OxyHb (the common type of haemoglobin) in blood. SERS monitoring of such changes was applied to liver cancer investigations and diagnostic sensitivity 95.0 % and specificity of 85.7 % were achieved (Liu et al. 2013a). To improve reproducibility, Liu and co-workers developed Ag nanofilms from polyvinylalcohol-protected Ag NPs by electrostatic SAMs to obtain highly reproducible SERS spectra of human serum from 20 healthy donors. The major spectral features were reproducible but some spectral differences have been seen among spectra reflecting the diversity of the individuals (Liu et al. 2011). Later, a label-free serum RNA analysis enabled the detection of colorectal cancer by using 3D Ag nanofilm as a SERS-active substrate with sensitivity of 89 % and a specificity of 95.6 % (Chen et al. 2012b).

7.3.3.2 Detection of CTCs

Malignant cells are disseminating from a solid tumour and circulate in the bloodstream of patients manifesting a metastasis. The detection/identification of CTCs is therefore a promising cancer diagnostic approach. However, direct identification of CTCs is difficult since their concentration in blood is very low (only 1–10^3 CTCs per ml) compared to blood cells (10^9 per ml). Both capture sensitivity and specificity are critical for the detection of CTCs. SERS tags can be used to identify cancer cells in biological samples via specific membrane cancer marker binding.

SERS was successfully applied for the detection of CTCs in human blood. Sha and co-workers employed commercial SERS tags (Nanoplex biotags, Oxonica Inc.) comprised one or more Au NPs with a submonolayer of RRMs and protective silica coating (Sha et al. 2008). Magnetic beads functionalized with anti-epithelial cell adhesion molecule (EpCAM) antibodies immobilized on the surface served to capture of breast cancer SK-BR-3 cells spiked in human blood. Subsequently, the captured EpCAM-overexpressing cancer cells were detected with SERS tags. Scheme of the immunocomplex formed by SERS tag and magnetic bead conjugates

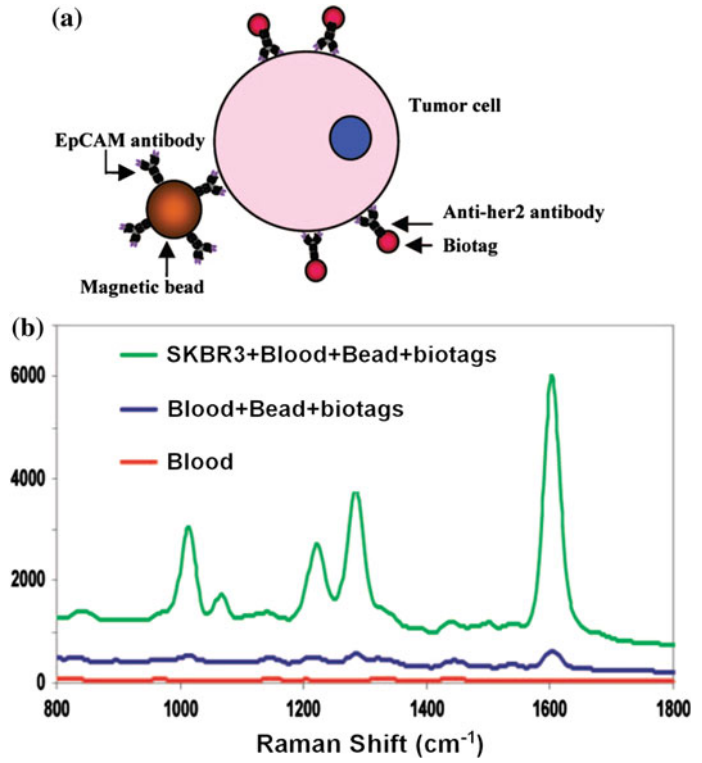

Fig. 7.11 Direct SERS detection of CTCs in blood. **a** Scheme of immunocomplex formed by Nanoplex biotags and magnetic bead conjugates binding to the model tumour cell. **b** Detection of breast cancer SK-BR-3 cells spiked into whole blood. SERS spectra of whole blood and of beads and biotag reagents in blood without and with SK-BR-3 cells spike (adapted with permission from Sha et al. 2008. Copyright 2008 American Chemical Society)

binding to the model tumour cell is illustrated in Fig. 7.11a. In contrast to other optical detection methods, near-IR excitation permitted the use of SERS tags in biological matrices such as whole blood. SK-BR-3 cells were spiked directly into whole blood prior to a short incubation of 30 min with magnetic bead-EpCAM and SERS tag-her2 conjugates. A magnet served to concentrate the magnetic beads along with captured cells to a specific position on the side of the tube where the SERS signal was collected. The results are shown in Fig. 7.11b. No SERS signal was detected from whole blood. In the absence of SK-BR-3 cells, a low background signal was observed when magnetic beads and SERS tags were added to whole blood. However, a strong SERS signal was detected when SK-BR-3 cells were spiked into whole blood, indicating that a signal can be directly acquired in whole blood without washing or additional handling steps. The detection limit was less

than 10 cells per ml with 99.7 % confidence in buffer solution. For the blood test, the cancer cells were spiked directly into whole blood prior to the incubation with capture particles and SERS labels. After magnetic enrichment, the SERS signal was obtained directly in whole blood without washing or other handling steps. The LOD in blood was about 50 cells per ml. This sensitive, simple and rapid assay platform requires no sample preparation and thus is promising for rapid clinical diagnosis and even real-time monitoring of the therapy progress.

Wang and co-workers successfully identified CTCs in the peripheral blood from patients with squamous cell carcinoma of the head and neck (Wang et al. 2011c). They employed Au NPs with RRM and functionalized with thiolated PEG layer to stabilize the NPs and minimize nonspecific interaction with blood cells. 15 % of PEG molecules have carboxyl functional groups for conjugation with N-terminus of EGF peptide. Detection limit was in the range of 5–50 tumour cells per ml of blood (Wang et al. 2011c). To achieve detection of CTCs with higher sensitivity and specificity, Shi and co-workers proposed a combination of magnetic enrichment and multiplex detection of CTCs by using targeted MNPs and SERS tags (Shi et al. 2014). SERS commercial tags (S440 and S420, Oxonica Materials Inc.) composed of a Au core (60 nm diameter) and a RRM adsorbed onto it. The NPs were conjugated with folate to target folate receptors of cancer cells. Both Au NPs and MNPs were targeted to folate receptor overexpressed on many cancer cells but absent on most normal blood cells. The results showed that only cells targeted with both SERS NPs and MNPs exhibit an increasing SERS signal due to magnetic accumulation of CTCs. Thus, the SERS signal increase correlates with CTCs detection. Free NPs or CTCs targeted with only SERS NPs or only MNPs did not exhibit this optical increase. The authors demonstrated SERS imaging system with 1 pM sensitivity and 2.5 mm penetration depth. A magnetic trapping system was able to effectively trap cells at flow velocities ranging from 0.2 to 12 cm s^{-1}. In addition, discrete SERS signals were detected in the magnetic trapping zone from a mixture of flowing dual-NP labelled HeLa cells and PBS buffer or rat blood indicative of single cell trapping events. Recently, Nima and co-workers presented a scheme for the multiplex detection of CTCs in whole human blood using tunable, silver-decorated, Au NRs as SERS multispectral contrast agents (Nima et al. 2014). Au NRs were functionalized with four RRMs and four antibodies breast cancer markers–anti-EpCAM, anti-IGF-1, receptor β, anti-CD44, anti-Keratin18, as well as leukocyte-specific marker anti-CD45. More than two orders of magnitude of SERS signal enhancement was observed from these hybrid nanosystems compared to conventional Au NRs.

7.3.4 Direct Cancer Diagnostics from Urine and Saliva

Recently, the Chen group presented a simple and noninvasive SERS diagnostics of cancer from urine and saliva using hydroxylamine-reduced Ag NPs (Huang et al. 2014; Feng et al. 2015). First, the impurities in the urine and saliva were removed

by centrifugation and the samples were then frozen to avoid degradation. In the case of saliva, the proteins were separated from saliva by membrane purification. Second, the samples were mixed with the Ag NPs and deposited on a piece of a rectangular aluminium plate. Urine SERS spectra were measured on esophagus cancer patients (n = 56) and healthy volunteers (n = 36) for control analysis (Huang et al. 2014). The prominent urine SERS peaks located at around 527, 656, 725, 807, 889, 959, 1002, 1138, 1209, 1342, 1376, 1465 and 1597 cm^{-1} can be visually observed in both normal and cancer urine, with the strongest signals at 725, 889, 1002 and 1138 cm^{-1}. A comparison of SERS spectra of the cancer urine with respect to the normal urine revealed a remarkable difference in spectral intensities: the normalized intensities of SERS peaks at 725 and 1465 cm^{-1} were higher for cancer than for healthy urine. Moreover, SERS peaks at 527, 889, 1002 and 1138 cm^{-1} were less intense for cancer than for healthy urine samples. These spectral differences were assigned to decrease in the relative content of urea and an increase in the percentage of uric acid in the urine of esophagus cancer patients compared to that of healthy subjects. The diagnostic algorithms utilizing a PCA-LDA method achieved a diagnostic sensitivity of 89.3 % and specificity of 83.3 % for separating esophagus cancer samples from normal urine samples.

Later, the saliva samples were used to demonstrate a capability for detecting benign and malignant breast tumours (Feng et al. 2015). A total of 97 SERS spectra from purified saliva proteins were acquired from samples obtained from three groups: 33 healthy subjects, 33 patients with benign breast tumours and 31 patients with malignant breast tumours. Comparison of the SERS intensities of the six prominent SERS peaks of saliva proteins (1004, 1049, 1176, 1265, 1340 and 1684 cm^{-1}) indicated significant differences between normal and breast tumour saliva samples. In contrast to the normal saliva protein samples, the benign and malignant breast tumour saliva proteins exhibited lower intensities at 1049 and 1176 cm^{-1}, but they showed much increased SERS signals at 1004, 1340 and 1684 cm^{-1}. In addition, the unusual SERS intensities associated with the different degrees of diagnostic utility were applied for discriminating between the three saliva protein groups (normal, benign breast tumour and malignant breast tumour). In particular, the malignant breast tumour samples showed greater intensities of SERS peaks at 1265 and 1684 cm^{-1} and much decreased signals at 1004, 1176 and 1340 cm^{-1} when compared with benign breast tumour saliva proteins. Multiclass partial LS discriminant analysis was utilized to analyse and classify the saliva protein SERS spectra from healthy subjects, benign breast tumour patients and malignant breast tumour patients, yielding diagnostic sensitivities of 75.75, 72.73 and 74.19 %, as well as specificities of 93.75, 81.25 and 86.36 %, respectively. These results demonstrated that saliva protein SERS analysis combined with discriminant analysis has good potential for the noninvasive and label-free detection of breast cancer.

7.4 SERS In Vitro Diagnostics of Other Diseases

In addition to pathogen's sensing and cancer diagnostics, SERS was applied to diagnostics of other diseases. This paragraph will introduce some examples.

The blood serum from type II diabetes, diabetics with complication and healthy volunteers was analysed by SERS (Han et al. 2009). The PCA successfully separated the diabetic patients from healthy volunteers with a sensitivity of 95 %, however, type II diabetes and diabetic complication groups were undistinguishable (Han et al. 2009). Recently, the Chen group first employed SERS to detect OxyHb variation in type II diabetic development (Lin et al. 2014). Label-free SERS spectra obtained from blood samples of 49 diabetic patients and 40 healthy volunteers using Ag NPs are compared in Fig. 7.12a. Differences in normalized spectral intensity between diabetic and normal OxyHb are clearly shown in their corresponding difference spectrum (bottom in Fig. 7.12b). The most obvious spectral differences (intensities and positions) can be found in the peaks at 478, 1212, 1312,

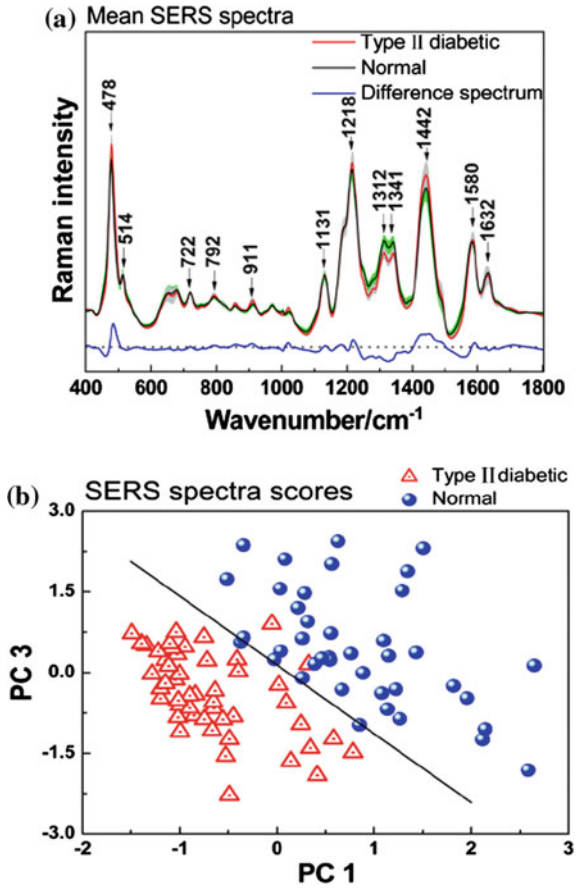

Fig. 7.12 Label-free SERS detection of type II diabetes. **a** Comparison of the mean SERS spectra of normal (*black line*, n = 40) and type II diabetic OxyHb (*red line*, n = 49). The *shaded areas* indicate the respective standard deviations. *Blue* spectrum is the difference spectrum. **b** Scatter plots of the PCA scores from the first principal component (PC1) and the third principal component (PC3) for the normal group (*blue circle*) versus the diabetic group (*red triangle*) (reproduced with permission from Lin et al. 2014. Copyright 2014 John Wiley & Sons, Ltd)

1341 and 1442 cm^{-1}. These changes were assigned to specific structural changes of OxyHb molecule in diabetes, including haem transformation and globin variation. To use OxyHb SERS spectra for discriminating diabetic from healthy patients, multivariate statistical methods based on PCA-LDA were performed on the measured SERS spectra. Scatter plots of the PCA scores from the first principal component (PC1) and the third principal component (PC3) for the normal group (blue circle) versus the diabetic group (red triangle) are shown in Fig. 7.12b. The solid line as a diagnostic algorithm by LDA separates the two groups with a sensitivity of 95.9 % (47/49), a specificity of 95.0 % (38/40) and an accuracy of 95.5 % (85/89).

In recent years, the infertility rate in married couples has been as high as 10–15 %, with male infertility comprising the majority of cases. Routine semen analysis based on microscopy and specialized software programs includes examination of such sperm parameters as concentration, motility and vitality. However, this method is only approximative and subjective. It is known that semen consists of a cellular part and noncellular part. The noncellular part (seminal plasma) has been found to be related to spermatozoa (mature male germ cells) function. Analysis of seminal plasma can predict sperm quality and has the potential to assess male fertility. SERS analysis and differentiation of seminal plasma was for the first time reported (Chen et al. 2012c). In this work, 61 semen samples (24 normal and 37 abnormal) were used. The spermatozoa were removed from sperm samples by centrifugation to obtain the seminal plasma. A pipette tip was applied to create a mixture containing the seminal plasma and the hydroxylamine-reduced Ag NPs in 1:1 proportions. Then, the mixture was transferred to a rectangular aluminium plate for SERS measurements. For the normal and abnormal seminal plasma, the SERS peaks at 649, 720, 809, 954, 1132, 1220, 1445 and 1584 cm^{-1} can be clearly identified. However, the SERS peaks at 649, 720 and 954 and 1584 cm^{-1} were more intense in the normal group than those in abnormal group and the peaks at 809 and 1132 cm^{-1} were more intense in the abnormal group. Distinctive SERS features and intensity differences between normal and abnormal seminal plasma could reflect molecular changes associated with the process of sperm abnormality. For example, the band at 649 cm^{-1} was attributed to the guanine ring breathing mode indicating higher content of guanine in the normal group than in the abnormal group. The relative SERS peak intensity at 720 cm^{-1} due to coenzyme A was found to be lower in the abnormal group than in the normal group. The peak at 954 cm^{-1}, which can be attributed to the spermine phosphate hexahydrate, was more intense in the normal group than that in the abnormal group. The diagnostic performance in differentiating abnormal seminal plasma (n = 37) from normal seminal plasma (n = 24) was evaluated. A PCA-LDA analysis of results obtained for different laser polarizations demonstrated different diagnostic sensitivities and specificities, among which, left-handed circularly polarized laser excitation showed the best diagnostic result (95.8 % sensitivity and 64.9 % specificity).

Buoyant silica bubbles were employed as capture substrates in a cholera SERS immunoassay (Schmit et al. 2012). Silica bubbles were silanized and then functionalized with an anti-cholera toxin antibody. Au NPs were used as SERS

substrates. The freshly prepared NPs (50 nm diameter) were labelled with 1,2-bis (2-pyridyl)ethylene coated with a silica shell and then incubated with the anti-cholera toxin antibody solution to allow antibodies to adsorb on the silica-coated Au NPs. After that, recombinant β subunit cholera toxin antigen was incubated with the capture bubbles and functionalized Au NPs. Buoyancy could pull the immunocomplexes from the sample solution to a compact monolayer of bubbles on the surface of the sample. Following the incubation, the entire reaction suspension was transferred to a polished aluminium surface where the bubbles were allowed to rise to the surface for about 5 min. SERS was collected from the monolayer of the bubbles on top of the sample volume. The detection limit of this assay for the β subunit of the cholera toxin in a buffer was 1100 ng.

Chon and co-workers developed a fast and sensitive SERS-based competitive immunoassay using SERS tags and magnetic capture beads for the early diagnosis of acute myocardial infarction (Chon et al. 2014). In this novel assay technique, free target antigens and antigen-conjugated tags based on hollow gold nanospheres reacted competitively with monoclonal antibodies on magnetic capture beads. The simultaneous quantification of dual acute myocardial infarction biomarkers in patient serum, namely, cTnI and CK-MB, was successfully achieved within a single excitation wavelength. This SERS-based competitive immunoassay has multiple advantages including a quick assay time (less than 15 min), an easy assay procedure (using magnetic beads), small sample consumption (minimum of 10 ml) and simultaneous dual marker detection using reliable, sharp and easily distinguishable SERS peaks.

Many neurological diseases are caused by the aggregation of specific types of proteins inside and/or outside of cells causing a kind of fibrosis. Diseases such as Alzheimer's, Parkinson's, Creutzfeldt−Jakob's, Huntington's, as well as prion diseases and amyotrophic lateral sclerosis, are being diagnosed by identifying protein aggregation (Kopito 2000). β-amyloid peptide, which is a small molecule that forms brain plaques and Alzheimer's disease, has been detected and characterized using a nanofluidic SERS device (Chou et al. 2008; Choi et al. 2012). This nanofluidic device was fabricated from PDMS microchannels by using photolithography to create nanochannels. Parkinson's and Alzheimer's diseases are also characterized by a form of abnormal enzyme activity. In the study of Stevenson and co-workers, Au NPs were incorporated by cell populations along the colourless substrate, where upon internalisation it was enzymatically transformed by β-galactosidase enzymes to 5,5′-dibromo-4,4′-dichloroindigo (Stevenson et al. 2013). This transformation was characterized by the appearance of a peak in the SERS spectra at 598 cm^{-1} and a blue colour which was indicative of the turnover of the substrate by the enzyme. The conversion was specific to the enzyme as confirmed when known enzyme inhibitors were introduced and the corresponding reduction in the measured SERS signal was observed. High resolution analysis of single cells and cell populations suggested that enzyme action was localized in specific cellular compartments which were proposed to be endosomes. The authors expressed a desire to quantify enzyme levels within these compartments, particularly in

response to different disease stimuli and states (Stevenson et al. 2013). Recently, Guerrini and co-workers reported SERS platform for detection of amyloid oligomers on metallorganic-decorated plasmonic beads. Here, the detection is based on the sensing properties of hybrid Au-decorated PS beads that are engineered with an effective metallorganic Raman chemoreceptor, composed of Al^{3+} ions coordinated to 4-MBA (Guerrini et al. 2015). The thiol group of 4-MBA bound the Au surface via Au–S covalent bonds, whereas the carboxylic groups of 4-MBA chelated the Al^{3+} ions forming a coordination complex and offering effective adsorption sites for oligomer interaction. The SERS platform was tested on oligomers formed from the N-terminal domain of the *Escherichia coli* protein HypF. The 4-MBA-Al^{3+} chemoreceptor decorating Au-PS beads experienced mechanical deformations of its phenyl ring upon complexation with HypF-N oligomer species, which are registered in their SERS spectrum and served for their quantitative detection. The plot of the SERS intensity values versus oligomer concentration demonstrated a linear correlation ($r^2 > 0.98$) and LOD of 0.1 μM, which corresponded to less than 6 pmol in the analysed sample volume (60 μl).

A highly sensitive immunoassay in a microfluidic system for Hepatitis B virus antigen from human blood was developed (Kaminska et al. 2015). The Au nanoflowers labelled with fuchsin as RRM formed a sandwich structure with the antigen and the antibody immobilized on the Au/Ag coated GaN support served as SERS-active substrate. They showed that if the microchannels are fabricated by such support it provides more sensitivity in comparison to the microchannels made from PDMS. In clinical practice, the presence of Hepatitis B virus antigen is monitored in whole blood, serum or plasma. In this study, the authors demonstrated that their SERS-based immunoassay could be used for the detection of Hepatitis B virus antigen in human serum or plasma samples. Quantitative analysis was performed by plotting the SERS intensity of the fuchsin marker band at 1178 cm^{-1} versus the concentration of the antigen. The LOD for Hepatitis B virus antigen was estimated to be ~40 times lower than the LOD of the ELISA. RSD of this method was less than 10 %.

Lactic acid is a simple and effective indicator for estimating physiological functions. The normal physiological range is about 0.55–1.67 mM in clinical diagnostics. Lactate is an important indicator of potential mortality in intensive care patients. To demonstrate multianalyte sensing capabilities with partition layer-modified substrates, the Van Duyne group prepared Ag FONs with DT/MH mixed SAMs to detect both glucose and lactate (Shah et al. 2007). They reported quantitative analysis of lactate in the concentration range of 10–240 mg dl^{-1}. Sequential injection of lactate and glucose into a flow cell was used to demonstrate the capability of the sensor to discriminate between the two analytes. Hsu and Chiang applied Ag NPs for rapid and quantitative SERS detection of lactic acid in human serum. The sensitivity of detection is about 10^{-5} M at a 50 s acquisition time (Hsu and Chiang 2010).

Creatinine is an endogenous degradation product of muscle metabolism and its serum or urine concentration can be the primary indicator in establishing renal function. The SERS spectra of creatinine from human serum down to 0.1 μg ml^{-1}

concentration were obtained using Ag NPs within 200 s acquisition time (Stosch et al. 2005). (Ag NP)/(Graphene oxide) hybrid structures were employed to intrinsic detection of folic acid (vitamin B related to many diseases including heart attacks, congenital malformation and mental devolution) in serum (Ren et al. 2011). The modification of graphene oxide with positively charged poly(diallyldimethyl ammoniumchloride) was employed for the electrostatic self-assembly of the negatively charged Ag NPs onto graphene. The folic acid was bound to the positively charged hybrid surface via electrostatic interaction, which provided a SERS signal. The LOD for folic acid was 9 nM and the calibration curve showed a good linear relation in the concentration range from 9 to 180 nM.

7.5 SERS-Based Medical Therapy and Theranostics In Vitro

One of the efficient therapeutic procedures is a photodynamic therapy (PDT), which combines the use of light at appropriate wavelengths with a photoactive drug (photosensitizer) to produce highly toxic reactive oxygen species. Theranostics is a new technology, which combines diagnostics and therapy. Such a combination can increase the specificity and efficacy of therapeutics, resulting in improved outcomes and reduced side effects. SERS-based theranostics incorporates SERS as the diagnostic imaging modality, which offers easy multiplexing and does not suffer from photobleaching (Vo-Dinh et al. 2015). To achieve efficient cellular damage via PDT, it is necessary to deliver the appropriate light dose and photosensitizer concentration at the site of interest. In order to better understand drug delivery, precise observation of drug release and delivery is required. The analytical interest is related to detection and distribution of anticancer agents inside cancer cells and their cytotoxic activity after photothermal treatment. Anticancer agents are highly cytotoxic and thus cannot be accumulated in the cells at concentrations higher than nanomolar. Therefore, SERS because of its high sensitivity is a suitable technique for this purpose. The strong absorption and efficient heat conversion of metallic nanostructures suggest that they can be highly promising plasmonic photothermal therapeutic (PPTT) agents (Link and El-Sayed 2000). Metallic nanostructures, predominantly Au ones, in many different forms (i.e. NPs, NRs and nanostars), have been utilized for the destruction of cancerous cells. SERS macroscopic imaging can help to localize the nanostructures inside the cells.

Chourpa and co-workers recorded simultaneously the fluorescence emission and SERRS spectra of the anticancer drug mitoxantrone over the cell (Chourpa et al. 2008). The spectra confirmed the presence of small Ag NP aggregates when they contain fluorescence background superimposed with SERRS signal of mitoxantrone, noticeable due to the most intense band at $\sim 1300\ cm^{-1}$. A semiquantitative analysis of the intracellular spectra was used to deconvolute into a proportional addition of characteristic fluorescence and SERRS spectra. The deconvolution coefficients

served to generate specific fluorescence and SERRS maps that could be superimposed with the white light image of the cell. Analysis of such SERRS/fluorescence multispectral maps provided multiple information about the drug molecular contacts in a given subcellular compartment (Chourpa et al. 2008). Kang and co-workers presented SERS/fluorescence imaging spectroscopy approach to monitor in real-time the uptake and release of anticancer drug doxorubicin (DOX) from Au NPs at a single cell level (Kang et al. 2013). Their study is illustrated in Fig. 7.13. The DOX molecules were conjugated to Au NPs via a hydrazone linker, which is sensitive on local pH. Following PEGylation, arginylglycylaspartic and nuclear localizing signal peptides were conjugated to the NP surface to increase internalization of the Au NPs as well as selectively deliver it to the cell nucleus. When DOX

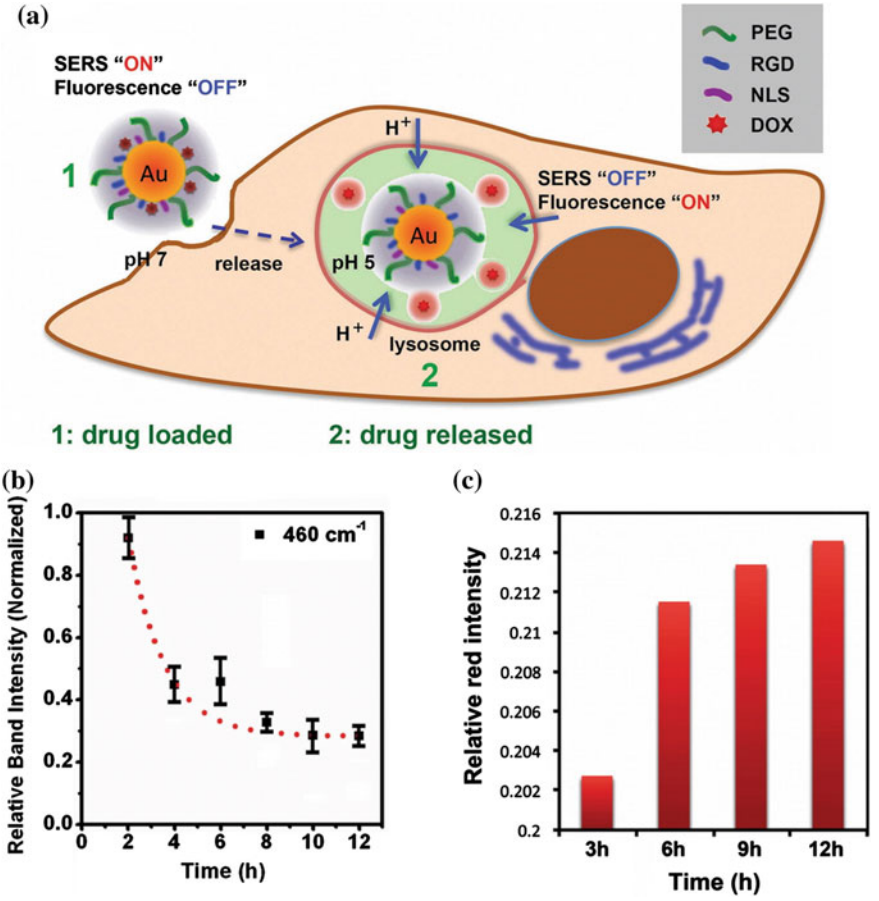

Fig. 7.13 pH-triggered DOX release tracking in acidic lysosomes. Schematic diagram of experiment (**a**), real-time monitoring of the DOX release from Au NPs in HSC-3 cells by SERS spectra (**b**) and fluorescence (**c**) (adapted with permission from Kang et al. 2013. Copyright 2013 The Royal Society of Chemistry)

was bound to the Au NPs, its SERS spectrum could be observed, while the fluorescence was quenched. When the DOX-loaded Au NPs were internalized by the cells, the hydrazone bond was cleaved at the acidic pH of the lysosomes causing the release of DOX molecules from Au NPs. Consequently, SERS signal of DOX significantly decreased and fluorescence of free DOX molecules appeared (Fig. 7.13a). In order to monitor the release dynamics of DOX in real-time, human oral squamous carcinoma (HSC-3) cells were incubated with DOX(0.2 nM)/(Au NP) and both Raman and fluorescence signals were recorded at different instants of drug treatment. The intensity of the 460 cm^{-1} DOX band was found to decrease continuously at 4 h of DOX/(Au NP) incubation until it completely disappeared after 12 h of treatment (Fig. 7.13b). Figure 7.13c shows the relative intensity of the DOX red fluorescence at different times. The red fluorescence intensity increased in cells over time indicating the continuous release of DOX molecules from Au NPs via hydrazone bond breakage induced by the slightly acidic pH microenvironment of the lysosomes (pH 5.0). Both SERS and fluorescence data indicated that the DOX release from the Au NPs was time-dependent.

Song and co-workers reported a theranostics strategy based on plasmonic vesicles assembled from Au NPs for targeted drug delivery, which can be tracked by SERS spectroscopy (Song et al. 2012). The SERS tag contains the RRM, mixed brushes of hydrophilic PEG and pH-sensitive hydrophobic copolymers of PMMA and 4-vinylpyridine to allow drug release, HER2 antibodies for cancer cell targeting and encapsulated DOX. To prove this concept, the study was performed with breast cancer cells overexpressing EGF receptor 2 (HER2). The vesicle-coated cancer cells displayed a strong SERS signal of the RRM that gradually decreased with time caused by acidic driven disruption of the vesicles and a drug release.

The release of a dye/drug from Au nanocages formed by Au nanocubes was also monitored by SERS (Tian et al. 2013). Nanocages with an edge length of $\sim$73 nm and wall thickness of $\sim$6 nm were produced by galvanic replacement of Ag nanocubes by Au. The surface of the Au NPs was first modified by PEG to improve the biostability and reduce nonspecific binding of proteins. Second, arginylglycylaspartic and nuclear localizing signal peptides were conjugated to the Au NP surface to increase their internalization as well as selectively deliver the Au NPs about the cell nucleus. Nile red and DOX were used as the model cargo and loaded into the nanocages together with 1-tetradecanol. Phase change of 1-tetradecanol can be controlled by a temperature, which can serve to ensure the release of the drug in response to an external stimulus. The phase change of 1-tetradecanol is used for encapsulating drugs at lower temperature. After the loading with drugs, SERS spectra were recorded from the plasmonically active nanocages. The encapsulated molecules can be released along with the melted 1-tetradecanol through diffusion after raising the local temperature by thermal or ultrasonic means. During the drug release experiment, the 785 nm laser induced photothermal effect led to melting of 1-tetradecanol and it resulted in the release of the drug from the nanocages. The release of nile red and DOX from the nanocages was monitored by SERS when

decrease of the SERS intensity with increasing laser exposure time was observed. Importantly, 1-tetradecanol has a melting point at 38–39 °C which is only slightly higher than the normal human body temperature.

Investigation of the molecular changes of cancer cells with drugs treatment is crucial for the design of new anticancer drugs and the development of novel diagnostic strategies. The local pH inside glioma U-87 MG cancer cells was monitored after PDT treatment by 6-methyl-1,3,8-trihydroxyanthraquinone (emodin) drug (Bálint et al. 2011). The cellular pH was determined by the real-time measurement of the SERS from a pH-sensitive probe 4-MBA that is embedded in the cell. The SERS tag was a micrometre-sized silica bead covered by nanosized Ag NPs with 4-MBA as RRM. Visible excitation at different light dosages was used to activate the drug. The results indicate cell maintenance of internal pH and cell death at low and high light dosage, respectively (Bálint et al. 2011). Recently, to analyse the detailed effects of targeting ligands on cell nuclei, in situ SERS detection was performed by the Raman platform with the assistance of dark-field and fluorescence microscopes to simultaneously locate Au NRs and small molecules (Liang et al. 2015). Here, human gastric carcinoma (SGC-7901) cell nuclei were treated with two model drugs, DNA binder (Hoechst33342) and DOX. Nuclear targeting nanoprobes with an assembly structure of thiol-modified PEG and nuclear localizing signal peptides around Au NRs were prepared to achieve the amplified SERS signals of biomolecules in the cell nuclei. Through the analysing of SERS spectra measured from the cell nucleus, they found that both drugs can cause the obvious changes of DNA and proteins.

The combination of SERS tag and PDT drug carrier into a single platform is also promising for theranostic applications. Lu and co-workers reported SERS monitoring of PDT on prostate cancer cells by using popcorn-like Au NPs (Lu et al. 2010). Spherical Au NPs were prepared by citrate-reduction and then ascorbic acid was added as a reducing agent in the presence of CTAB as a shape-templating surfactant and Au nanopopcorns were formed. For selective sensing, therapy and monitoring of therapy progress, Au nanopopcorn NPs were conjugated with multiple targets specific for membrane PSA: anti-PSA antibody and RH6G attached to A9 RNA anti-PSA aptamers. RH6G-modified RNA aptamers covalently attached to the surface have a dual function as targeting molecules and Raman dye-carrying vehicles. RH6G modification on the RNA aptamer was used as a RRM for SERS measurement. Photothermal treatment of the human prostate cancer (LNCaP) cells was performed with 785 nm laser radiation. SERS detection was carried out by using 670 nm excitation wavelength. The decrease of the SERS intensity was attributed to the breaking of the S–Au bond between the Au NPs and the RH6G-modified A9 RNA aptamer caused by the strong photothermal effect. This change was not observed when the target cells were absent: in this case no aggregates were formed and the LSPR at 580 nm could not be excited by the NIR laser radiation (Lu et al. 2010). Beqa and co-workers introduced an aptamer-conjugated hybrid nanomaterial (Au popcorn-like NPs attached to carbon nanotubes) as a probe for targeted diagnosis and PDT of human breast cancer cells (SK-BR-3), even at level of 10 cells per ml (Beqa et al. 2011). The results showed

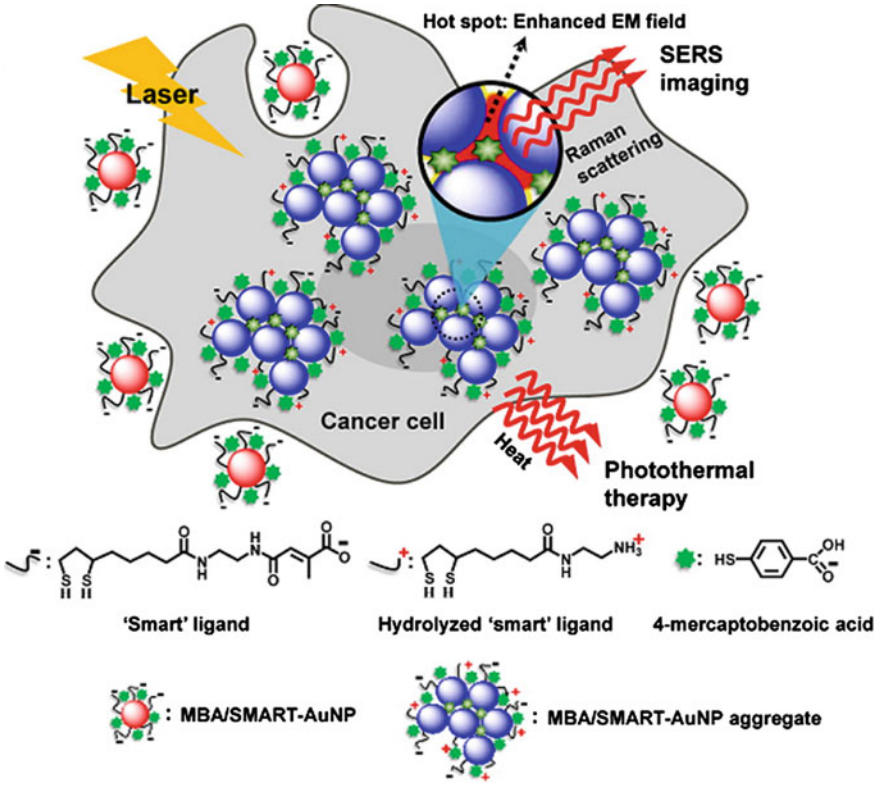

Fig. 7.14 Schematic illustration of the working mechanism of 4-MBA/(SMART-Au NPs) in a cancer cell. See text for details (reproduced with permission from Jung et al. 2013. Copyright 2013 American Chemical Society)

significant SERS enhancement with the addition of SK-BR-3 cells because the nanoprobes were highly specific to HER2, which promotes the growth of cancer cells. HER2 expressed in the SK-BR-3 breast cancer cells. This approach distinguishes between the different breast cancer cell lines.

Jung and co-workers prepared "SMART" Au NP tags for simultaneous Raman imaging/diagnosis and photothermal therapy (Jung et al. 2013). Schematic illustration of the working mechanism in a cancer cells is shown in Fig. 7.14. The "SMART" Au spherical NPs (10 nm diameter) were covered with surface molecules that contain hydrolysis-susceptible citraconic amide units ("smart" ligands) and pH sensitive RRM (4-MBA). The NP surfaces were engineered to have both positive and negative charges which induce rapid aggregation of the NPs by electrostatic interactions under mildly acidic conditions. Upon internalization by the cell, 4-MBA/(Au NPs) aggregated as the result of pH-sensitive surface charge on the NPs. The aggregates served as SERS imaging tags providing strong SERS signal due to the existence of "hot spots". The aggregation shifted the LSPR to the

NIR region due to the appearance of coupled plasmon modes. This shift was successively used for selective and deep-tissue-penetrating photothermal therapy. In therapeutical experiment, B16 F10 cancer (mouse melanoma) cells were coincubated with 4-MBA (40 nM)/(SMART-Au NPs) for 12 h. Control cells were prepared using 4-MBA (40 nM)/(Au NPs) without "smart" ligands or with no Au NPs. SERS spectra were acquired from the cells using a microscope system with 785 nm laser excitation. The 4-MBA/(SMART-Au NPs) sample showed the distinct SERS peaks, while the 4-MBA/(Au NPs) without "smart" ligands and no Au NP control samples showed no detectable signal. Representative spots in the 4-MBA/(SMART-Au NPs) sample and the control samples were irradiated for 10 min by the same 785 nm laser with a 19.5 W cm^{-2} power density. For the 4-MBA/(SMART-Au NPs) sample spots, distortion in the cellular morphology was observed which is indicative of the cell mortality. No noticeable changes were found for the control 4-MBA/(Au NPs) without "smart" ligands and no Au NP samples under identical laser irradiation. The experiment was repeated with higher NP concentration (100 nM) and longer incubation time (24 h). The theranostic Au NPs are cancer-specific because they aggregate rapidly and accumulate selectively in cancerous cells.

The Vo-Dinh group reported the combination of SERS detection and PDT in a silica-coated gold nanostars platform (Fales et al. 2011). The SERS tag was formed by Au nanostar labelled with a 3,3′-diethylthiatricarbocyanine (DTTC) as RRM. The Au nanostars have a higher plasmonic effect than Au spherical NPs under the red excitation conditions. DTTC has strong absorption in NIR region providing strong SERRS signal with 785 nm excitation. The silica shell of SERS tag was then loaded with a fluorescent PDT photosensitizer (MB) that could be activated at 633 nm. The 785 nm wavelength of light falls outside of the absorption band of MB, thus preventing any unwanted activation of the photosensitizer. Thus, SERRS detection could be performed at 785 nm and PDT at 633 nm, with no interference between the two modalities. Upon excitation at 785 nm, SERRS was observed from the NIR Raman dye on the nanostar surface. Excitation at 633 nm generated fluorescence (and singlet oxygen) from the MB. PDT on BT549 breast cancer cells after incubation with MB-loaded particles and light exposure was clearly observed. The same light exposure was performed on cells treated with silica-coated nanostars that did not contain MB, showing no evidence of any photothermal effects (Fales et al. 2011). The theranostic nanoplatform was further functionalized with a cell-penetrating peptide (TAT), which increased intracellular accumulation of SERS tags (Fales et al. 2013). In this case, the Au nanostars were labelled with a dye to match the 633 nm excitation and protoporphyrin IX was encapsulated in the silica shell as the PDT photosensitizer. After activation using UV light, the greater number of SERS tags per cell provided SERS spectra for Raman imaging and PDT effect. In contrast, without TAT, not enough SERS tags were delivered into the cells to allow Raman imaging (Fales et al. 2013). The limitation of this approach is the necessity of using two excitation wavelengths (one for SERS imaging and one for PDT) and the difficulty to discern the fate of two components (RRM and photosensitizer) in a biologically complex environment.

Recently, Farhadi and co-workers proposed a novel approach which enables obtaining the spectroscopic SERS information during light irradiation for PDT. Here, Pd-pyrolipid photosensitizers that are essentially not fluorescent were employed. Pd-pyrolipid theranostic NPs, when excited by same excitation wavelength (638 nm), simultaneously were both PDT active and emitted a strong SERS signal (Farhadi et al. 2015). A unique multifunctional theranostic SERS tags were developed with gold nanostars for SERS, magnetic resonance imaging (MRI), computed tomography (CT), two-photon luminescence (TPL) imaging and PPTT. The synthesized gold nanostars were tagged with a RRM (4-MBA) and linked with an MRI contrast agent Gd^{3+} (Liu et al. 2013b). These tags have LOD of 2 pM (SERS), 10 pM (MRI) and 100 pM (CT). Tumour phantom experiment demonstrated the potential of multifunctional nanoprobe for future in vivo applications. The photothermal ablation was performed under 850 nm excitation proved cell death following irradiation whereas cells in the area which was not irradiated remained alive.

Noh and co-workers employed Au/Ag hollow nanoshells (HNSs) and Au NRs as multifunctional therapeutic agents for effective, targeted, photothermally induced drug delivery under NIR light (Noh et al. 2015). Au/Ag HNSs and Au NRs showed similar photothermal efficiency under optimized NIR laser power. SERS tag was formed by PEGylated HNSs conjugated with antibodies against the EGF receptor (EGFR) and with the antitumour drug DOX for lung cancer treatment. The targeting of such SERS tag was confirmed by light scattering images of human lung carcinoma A549 cells and DOX release from the HNSs was evaluated under low pH and NIR-irradiated conditions. Multifunctional SERS tags induced photothermal ablation of the targeted lung cancer cells and rapid DOX release following irradiation with NIR laser. Furthermore, the authors evaluated the effectiveness of HNS/EGFR/DOX tags for drug delivery by comparing two drug delivery methods: receptor-mediated endocytosis and cell-surface targeting. Accumulation of the SERS tags on the cell surfaces by targeting EGFR turned out to be more effective for lung cancer treatments than its uptake. The results suggest a new and optimal method of NIR-induced drug release via the accumulation of targeted SERS tags on cancer cell membranes.

7.6 SERS Ex Vivo: Tissue Diagnostics and Histology

Detection and localization of prognostic markers in tissues were applied for cancer diagnostics. For example, PSA can be used for identification of tumours tissues from patients undergoing prostatectomy. In 2006, this approach was first reported by Schlücker and co-workers using SERS tags formed by Au/Ag nanoshells containing aromatic RRMs and a PSA antibody (Schlücker et al. 2006). SERS from the RRM was detected in the epithelium (PSA positive) of the incubated prostate tissue section. Stroma and lumen (PSA negative) locations served as controls.

Unique composite organic-inorganic NP (COIN) served as a part of SERS tags for PSA localization in the prostate tissue (Sun et al. 2007). COIN is a nanocluster formed by Ag NPs aggregated by organic analyte in the presence of an inorganic RRM. Ag COIN provides higher SERS enhancement and the possibility to use a broader range of RRMs in respect to gold. PSA in tissue samples from the human prostate was detected ex vivo using the Ag COINs encapsulated by BSA layer and functionalized with PSA antibodies (AbPSA). The schema of a direct binding assay is shown in Fig. 7.15a. Two different COINs, one conjugated with acridine orange and one conjugated with basic fuchsin as RRMs, were selected for multiplex tissue analysis. The major components of the SERS spectrum determined from LS analysis are signals from (basic fuchsin)/AbPSA (blue), (acridine orange)/AbPSA (red) and tissue autofluorescence (grey) (Fig. 7.15b). The best fit spectrum is indicated in black and the small error shown is typical of this kind of duplex

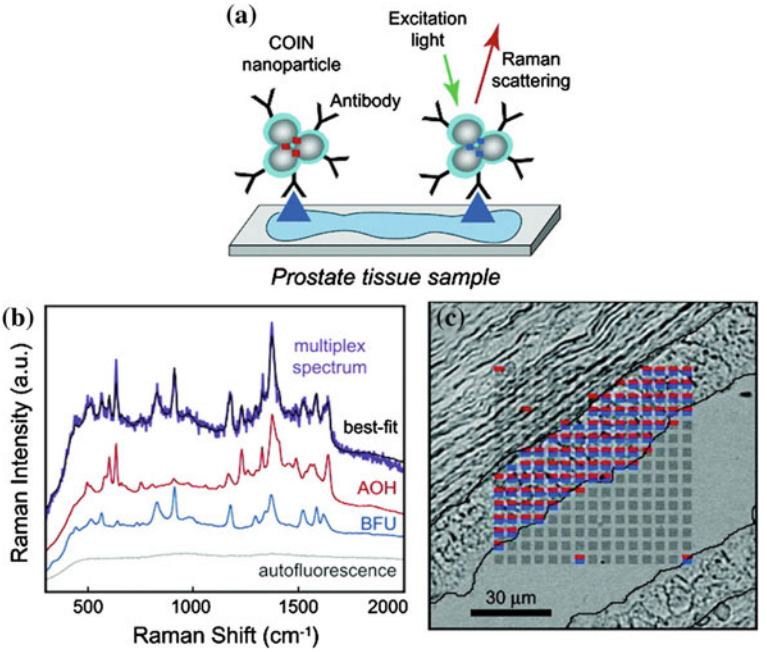

Fig. 7.15 Simultaneous two-COIN staining in the direct PSA detection assay in tissue. **a** Schematic representation of a direct binding assay. **b** Spectral fitting in duplex COIN experiments on tissue. The upper set of spectra are the measured spectrum from a single point in the epithelium (*purple*) and the best-fit spectrum (*black*) found from LS regression using reference spectra. The major fitting components are the two conjugated COINs: (acridine orange)/AbPSA (*red*), (basic fuchsin)/AbPSA (*blue*) and the tissue autofluorescence (*grey*). **c** PSA expression patterns reported by two COINs in a simultaneous duplex measurement. In each pixel, colour represents PSA-positive classification based on (basic fuchsin)/AbPSA (*blue*) and (acridine orange)/AbPSA (*red*) and *grey* represents PSA-negative classification (adapted with permission from Sun et al. 2007. Copyright 2007 American Chemical Society)

experiment. The unique peaks from each of the two COINs are easily visible in the raw spectrum acquired from the epithelium (Fig. 7.15b, purple spectrum), indicating the presence of both types of COIN at individual spots in the raster. The PSA expression pattern reported for each COIN is shown in Fig. 7.15c, where red and blue indicate classification as PSA positive by (acridine orange)/AbPSA and (basic fuchsin)/AbPSA, respectively, and grey represents classification as PSA negative. Both COINs were detected in almost all spots of the epithelium where tumour is expected. High sensitivity and specificity were achieved in the case of the combination of COINs with two RRMs. Because of COIN's high signal intensity, the tissue binding assay can be conducted using a low concentration ($\sim$30 pM) of COIN-antibody conjugate without the need for secondary amplification and the Raman data can be collected using a relatively low power laser (0.3 mW) and very short signal acquisition times (0.1 s). The single step staining procedure was significantly shorter than traditional immunohistochemistry because steps such as incubation with secondary antibodies, enzymatic colour development time and endogenous biotin blocking are all eliminated (Sun et al. 2007). For multiplex analysis, appropriate mathematical procedures for signal decomposition were employed (Lutz et al. 2008).

Schlücker and co-workers used hydrophilically stabilized Au nanostars with PEG-modified aryl thiols as RRMs for immuno-SERS microscopy on prostate tissue (Schütz et al. 2011). The advantage of Au nanostars is a higher SERS enhancement with the red excitation than for Au spherical NPs. RRMs yielded a complete SAM on the Au nanostar surface. Benign prostate tissue sections were incubated with the antibody-functionalized nanostars. The signature of the SERS label ($\sim$1340 cm^{-1}) was only observed in the basal epithelium, but not in the stroma/connective tissue or lumen (Schütz et al. 2011).

Stone and co-workers reported surface-enhanced spatially offset Raman spectroscopy for detecting NPs deeply in tissue (Stone et al. 2010). Ag NPs labelled with RRMs were injected into the centre of fresh porcine tissue. SERS spectra from these Ag NPs were obtained by spatially offset Raman spectroscopy from a depth of 4.5–5 cm. Later, the same group improved this approach for multiplexed detection and imaging using four different commercial SERS probes (Stone et al. 2011). Each NP suspension was injected into one of the corners of a 10 mm square, from where multiplexed spatially offset Raman spectroscopy imaging of the NPs was obtained according to the characteristic bands of each RRM.

7.7 SERS Medical Applications In Vivo

7.7.1 In Vivo Glucose Sensor

Glucose sensor described above (see Sect. 7.1) was designed even for in vivo transcutaneous glucose sensing on rat models (Stuart et al. 2006). The principle of the sensor is illustrated in Fig. 7.16. Ag FON with mixed SAMs of DT/MH was

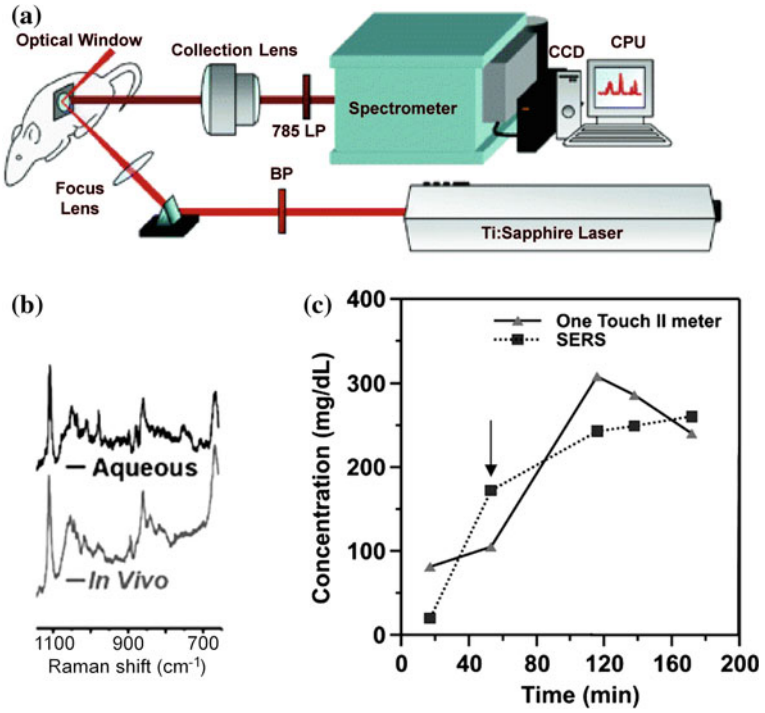

Fig. 7.16 In vivo glucose SERS sensor. **a** Scheme of instrumental apparatus. **b** Typical in vivo spectrum compared to a typical ex vivo spectrum. **c** Time course of the in vivo glucose measurement, *triangles* are measurements made using blood glucometer (One Touch II) and *squares* are measurements made using the SERS sensor. Glucose infusion was started at 60 min, as marked by the *arrow* (adapted with permission from Stuart et al. 2006. Copyright 2006 American Chemical Society)

subcutaneously implanted in a rat so that the glucose concentration of the interstitial fluid could be measured optically through an optical window in the rat's body (Fig. 7.16a). Figure 7.16b shows a typical in vivo spectrum compared to a typical ex vivo spectrum obtained using the same surface and within the same experimental conditions (785 nm excitation, laser power 50 mW, acquisition time 2 min). Figure 7.16c depicts the glucose concentration variation in the rat measured using SERS and the blood glucometer (One Touch II) with respect to time. Both the standard glucometer and the SERS-based measurements effectively tracked the change in glucose concentration. A sharp rise in glucose concentration was detected by both techniques 60 min after the start of the glucose infusion. Moreover, the results demonstrated that glucose binds reversibly to the SERS-active surface and the changes in its concentration as rapidly as 30 s can be tracked. The glucose concentration was monitored in the interstitial fluid of six separate rats. The sensor was able to perform accurately over lower glucose concentrations for 17 days after subcutaneous implantation.

7.7.2 *In Vivo Imaging and Tumour Targeting*

In the last 5–8 years, there has been a progression in the number of studies reporting on in vivo and the clinical use of the SERS spectroscopy (Zavaleta et al. 2011).

The first noninvasive SERS image using a living mouse was reported by Qian and co-workers in 2008 (Qian et al. 2008). Later, Keren and co-workers showed the first SERS image of a whole organ (liver) in a living mouse (Keren et al. 2008). SERS tags, commercial glass-coated Au NPs (Nano-plex Biotags) functionalized with RRM, were injected into the tail vein of a mouse. The mouse was anesthetized on a microscopic table equipped with a horizontal translation stage. This allowed a raster scanning and Raman imaging. SERS images acquired 2 h after injection revealed a bright liver, the primary organ responsible for the natural uptake (because of the reticuloendothelial cells) and excretion of the NPs. This in vivo approach demonstrated ultrasensitive picomolar detection of SERS tags. The maximum depth of penetration for Raman microscope was evaluated by using a tissue mimicking phantom, where a maximum depth of 5.5 mm was observed by using SERS NPs in low (1.3 nM) concentration. Later, Charan and co-workers imaged *Caenorhabditis elegans*—a small, transparent and well characterized nematode—by using bare Ag NPs. SERS signal came preferentially from the lipids and their environment (Charan et al. 2011). This signal was imaged by selecting the spectral range of the CH stretching modes of lipids as an integral signal for imaging. This is one of the very few examples, where intrinsic SERS signatures from the tissue or a cell have been used for whole body Raman imaging. Wang and co-workers monitored the distribution of Au NPs in zebrafish embryos (Wang et al. 2010a). Au NPs were labelled with two different RRMs: 4-MBA and mercaptopyridine. The labelled Au NP tags were microinjected into the one cell stage. SERS spectra were collected from the various regions of the embryos and in different stages of their development.

The first in vivo SERS tumour targeting was reported in previously mentioned work of Qian and co-workers (Qian et al. 2008). Figure 7.17 illustrates this experiment. Single chain variable fragment (scFv) antibodies were conjugated to the Au NPs through heterofunctional thiolated PEG (HS–PEG–COOH) (Fig. 7.17b). It served to recognize the EGFR, which is overexpressed in many types of malignant tumours. Au NPs with core size of 60–80 nm diameter and RRM were components of the SERS tag. The SERS tags were injected into subcutaneous and deep muscular sites in nude mouse (Fig. 7.17a) bearing human head and neck squamous cell carcinoma (Tu686) tumour. A healthy nude mouse received 50 µl of the SERS NP tags (1 nM) by subcutaneous (1–2 mm under the skin) or muscular ($\sim$1 cm under the skin) injection. The subcutaneous spectrum was acquired in 3 s, the muscular spectrum in 21 s and the control spectrum (obtained in an area away from the injection site) also in 21 s. The reference spectrum was acquired from the SERS tags in PBS solution in 0.1 s. The RRM was malachite green with spectral signatures at 427, 525, 727, 798, 913, 1169, 1362, 1581 and 1613 cm^{-1} (Fig. 7.17c). These features were distinct from the Raman signal of animal skin.

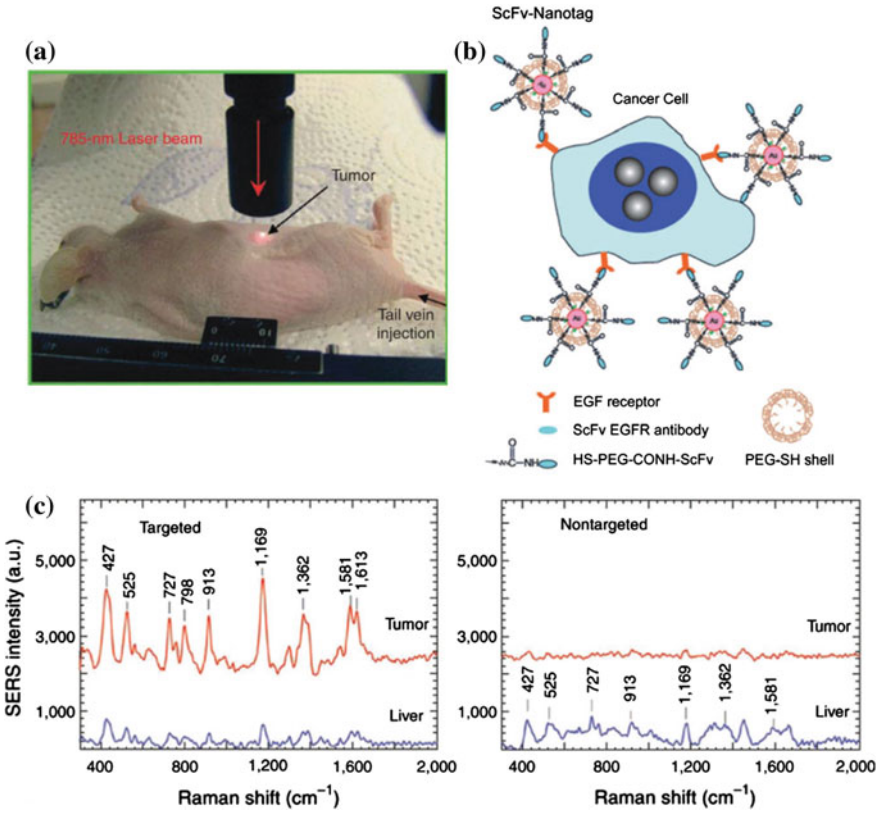

Fig. 7.17 In vivo SERS imaging and cancer targeting. **a** Experimental setup for SERS imaging of tumour of living mouse. **b** Detection scheme and structure of SERS tag for cancer targeting. **c** SERS spectra obtained from the tumour (*red*) and liver (*blue*) by using targeted NPs and nontargeted NPs. The spectra were background subtracted and shifted for better visualization. The RRM is malachite green (adapted with permission from Qian et al. 2008. Copyright 2008 Nature Publishing Group)

In vivo SERS spectra were obtained with a 785 nm excitation (laser power 20 mW). This excitation ensured the minimal optical absorption of water and haemoglobin. SERS signals from approximately 1–2 cm depth in the tissue were acquired. The SERS spectra obtained using targeted NPs demonstrated specific recognition of EGFR-positive tumour sites (Fig. 7.17c) with some nonspecific distribution into liver and spleen, but not into the brain, muscle or other major organs. On the other hand, control experiment using nontargeted NPs proved no SERS signal in tumour region.

The SWNTs were also tested as tumour targeting nanostructures (Keren et al. 2008; Zavaleta et al. 2008). SWNTs have a very small diameter of $\sim$3 nm and a length of 200 nm. Moreover, the high aspect ratio of the carbon structure of SWNTs is ideal for bioconjugation. SWNTs provide intense and inherent Raman peak

(G-band at $\sim$1593 cm^{-1}) which can be tracked in whole body by noninvasive Raman imaging. The results clearly demonstrated that it is possible to examine the distribution and localization of SWNTs in tumour of living mice 24 h after the injection.

The first multiplex imaging of ten different SERS tags upon subcutaneous injection in ten separate areas of a living mouse was reported by Zavaleta et al. (2009). Each SERS tag (Oxonica Materials, Mountain View, CA) consisted of a unique RRM layer adsorbed onto a Au core (60 nm diameter) coated with silica, making the entire diameter of the NP $\sim$120 nm (Fig. 7.18a). 10 separate

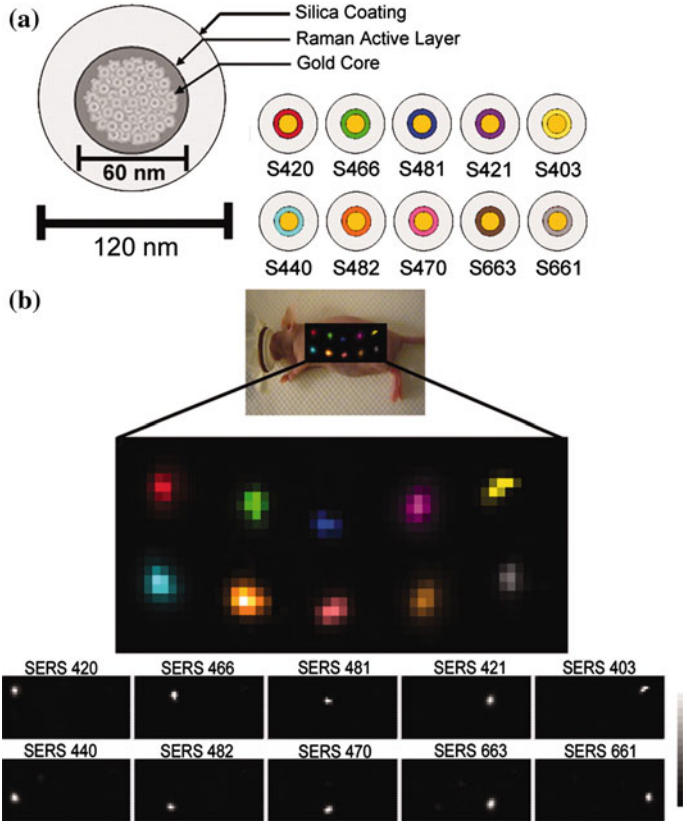

Fig. 7.18 Multiplex in vivo SERS detection using ten different SERS tags. **a** Schematic representation of a SERS tag. To simplify nomenclature, each type of SERS tag is given a three-digit suffix (e.g. S-420) instead of the formal name of the adsorbed RRM. **b** Map of 10 different SERS particles injected in a nude mouse. Arbitrary colours have been assigned to each unique SERS tag batch injected. *Panels below* depict separate channels associated with each of the injected SERS tag. S420, S466, S481, S421, S403, S440, S482, S470, S663 and S661, respectively). Greyscale bar on the *right* depicts the Raman intensity, where *white* represents the maximum intensity and *black* represents no intensity (adapted with permission from Zavaleta et al. 2009. Copyright 2009 The National Academy of Sciences of the USA)

subcutaneous injections of each SERS tag to a nude mouse were carried out and then the entire area of interest was mapped with a Raman microscope. The map was then analysed with postprocessing software, where preassigned reference spectra of each SERS tag were used to determine the best spectral fit with their corresponding SERS tag. The software then separated out intensity maps into various channels showing where in the map each SERS tag was detected. The resulting image showed all 10 injections correctly separated out into their corresponding spectral channel with minimal overlap among the channels (Fig. 7.18b). These results demonstrated a great potential for multiplexed imaging in living subjects. It can be particularly useful when multiple biomarkers associated with a specific disease should be detected.

Dinish and co-workers reported the targeted multiplex detection of intrinsic cancer biomarkers in MDA-MB-231 breast cancer cell line and in a murine xenograft model (Dinish et al. 2014). Three biocompatible SERS tags were constructed with Au NPs and three RRMs: Cy5, malachite green isothiocyanate and RH6G. The SERS tags were further conjugated with antibodies against EGFR, CD44 and TGF beta receptor II cancer biomarkers. EGFR is the cell's surface receptor for members of the EGFR family of extracellular protein ligands. It is a prognostic marker in many types of cancers including breast cancer. CD44 is a major cell surface adhesion molecule and is a receptor for the glycosaminoglycan, hyaluronan. It plays an important role in tumour growth and metastasis. Down regulation of TGF beta receptor II is a key step in breast carcinogenesis. In the case of in vitro experiment with cancer cells, SERS spectra from the cells showed the fingerprint Raman peak from each SERS tag bound to corresponding biomarker on the cell surface: 1120 cm^{-1} of Cy5, 1175 cm^{-1} of malachite green isothiocyanate and 1650 cm^{-1} of RH6G. SERS intensity map image demonstrated the expression and relative distribution of the cancer biomarkers on the cell surface bound to the antibody conjugated SERS tags, Cy5, malachite green isothiocyanate and RH6G respectively. In vivo multiplex detection was carried out by injecting 200 μl of the three bioconjugated SERS tags into the centre of the tumour on a subcutaneous MDA-MB-231 breast cancer xenograft mouse model. Xenograft is a surgical graft of tissue from one species to an unlike species. The results showed that intratumourally injected SERS tags specifically targeted the three biomarkers. SERS spectra of RRMs exhibited maximum signal at 6 h and no detectable signal at 72 h. However, SERS tags without antibodies showed no detectable signal after 6 h. This difference could be due to the specific binding of the bioconjugated SERS tags to the receptors on the cell surface.

The major problem of in vivo SERS detection/imaging comes from the limited penetration depth (in the range of few mm) of biological objects. This can be partly solved using NIR-IR excitation (typically 785 nm) where optical penetration in tissue is maximized. Therefore, employing NIR-IR resonance excitation of both metallic nanostructure and RRM in SERS tag can substantially enhance the SERS signal and thus increase sensitivity. The most common RRMs such as CV and R6G are more efficient in the visible region. Small Ag NPs and Au NPs have also limited LSPR in NIR-IR region. Thus, the new SERS tags with spectral properties in the

NIR-IR range are definitely required for in vivo SERS applications. The Au NRs or Au nanostars (Rodríguez-Lorenzo et al. 2011) were found to be suitable nanostructures providing high SERS enhancement in NIR-IR. Au NRs coated with PEG polymers and various RRMs were presented as an efficient platform for multiplex in vivo SERS detection within NIR-IR excitation (Qian et al. 2011; von Maltzahn et al. 2009; Jokerst et al. 2012). Au NRs were found to be highly stable, to be detectable down to femtomolar concentrations and to have low baseline cytotoxicity (von Maltzahn et al. 2009).

Concerning RRMs, Samanta and co-workers synthesized a series of tricarbocyanine derivatives with NIR absorption properties and ultrasensitive SERS in vivo cancer detection (Samanta et al. 2011). Their SERS efficiency was compared with those of Au NPs (60 nm diameter). Among them, CyNAMLA-381, which displayed about 12× higher sensitivity than the standard DTTC, was chosen as the best RRM (Fig. 7.19). SERS tags with this RRM and BSA and glutaraldehyde protective layer were used for in vivo cancer detection. The SERS tag was functionalized with HER2-recognition antibodies (anti-HER2 monoclonal antibody or scFv anti-HER2 antibody). Such SERS tags were injected into nude mice bearing xenografts generated from SK-BR-3 cells. After 5 h, SERS spectra from the tumour site perfectly resembled the SERS spectra of the tag (Samanta et al. 2011). The same group later developed the SERS tags with two new NIR RRMs—Cy7LA and Cy7.5LA—as a partner with recently synthesized CyNAMLA-381 for multiplexing (Maiti et al. 2012). These SERS tags possess excellent SERS signal stability over a period of 1 month. As a proof of concept for multiplex targeted in vivo detection, they successfully demonstrated the simultaneous sensing of cancer in a living mouse using these three bioconjugated SERS tags.

Recently, a new class of ultra sensitive, NIR RRMs—2-thienyl-substituted chalcogenopyrylium dye—was synthesized (Harmsen et al. 2015b). The 2-thienyl

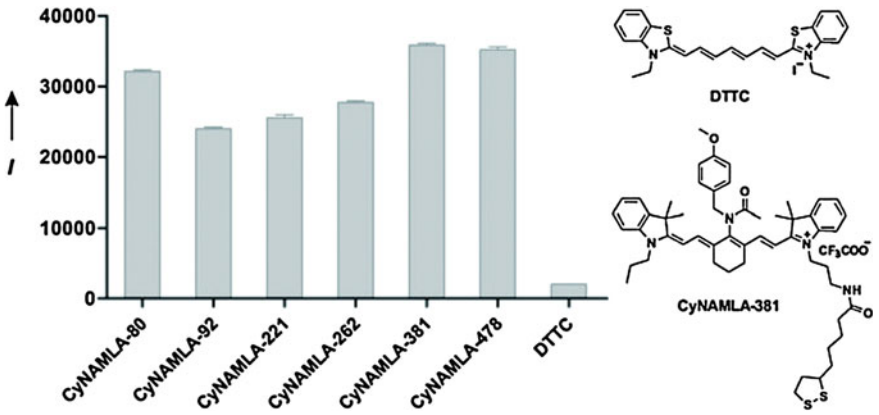

Fig. 7.19 SERS intensity of selected BSA-encapsulated-tricarbocyanine derivatives on 60 nm Au NPs recorded using 785 nm excitation (reproduced with permission from Samanta et al. 2011. Copyright 2011 Wiley-VCH Verlag GmbH & Co. KGaA, Weinheim)

group is not only part of the dye chromophore, but also can be rigorously coplanar with the rest of the chromophore. This allows the dye molecules to be in close proximity to the NP surface creating higher SERS. Thus, when adsorbed onto Au NPs, these dyes produce biocompatible SERS tags with unprecedented LOD about 100 aM. Ex vivo multiplexed Raman imaging of the tumour showed that the SERRS signals from two different EGFR-targeted SERS tags were more intense for the tumour site than for the surrounding tissue. It was a proof of selective localization of SERS tags at the tumour site. The low LOD in combination with the high resolution of Raman imaging enabled highly sensitive and specific real-time tumour targeting, as a result of the fingerprint spectra of the different SERS tags. This can offer multiplexed disease marker detection in vivo (Harmsen et al. 2015b). Similarly, SERS tags operating with 1280 nm excitation were constructed from RRMs selected from a library of 14 chalcogenopyrylium dyes containing phenyl, 2-thienyl and 2-selenophenyl substituents and of hollow Au HNSs (Bedics et al. 2015). These SERS tags are unique as they have multiple chalcogen atoms available which allow them to adsorb strongly onto the surface of the Au HNSs thus producing exceptional SERS signals at this long excitation wavelength. LODs about pM were obtained and individual RRMs of the library were identified by PCA and classified according to their unique structure and SERS signature.

Another issue of SERS tags for in vivo biomedical applications is that it requires efficient uptake of SERS tags, long circulation times and high stability. To date, silication of a dye-adsorbed NP has been most effective in retaining in vivo SERS tag stability and biocompatibility (Wang et al. 2013c). Current silication methods depend on high dye-metal affinities, which can be limited by unfavourable electrostatic interactions. Sulphur-containing dyes with affinities to gold are available, but scaling up the silication process can also often lead to size variation, aggregation and uncontrollable dye incorporation. The silica layer also approximately doubles the size of the metallic core that limits the synthesis of SERS NPs of the smaller size necessary for a variety of biomedical applications. This can be overcome if hydrophilic polymers surface coatings are employed. The synthesis of these SERS tags includes treating dye-adhered metallic NPs with thiolated-PEG or analogous polymers. However, competition for vacant binding sites can limit signal intensities and/or polymer grafting densities (Wang et al. 2013c). Iacono and co-workers reported a new hydrophilic NIR dye-loaded poly(N-(2-hydroxypropyl) methacrylamides) polymer and their application for Au NPs-based SERS imaging of lymph nodes (Iacono et al. 2014). The integration of various SERS RRMs into a biocompatible polymeric surface coating allowed for controlled dye incorporation, high colloidal stability and optimized in vivo circulation times. This technique led to the synthesis of very small (<20 nm) SERS tags but depending on their size, the NPs can emit both SERS and fluorescence. Au NPs covered by poly(N-(2-hydroxypropyl)methacrylamides) polymer showed longer in vivo signal stability in a 24 h period compared to coated particles assembled with noncovalent gold-dithioester chelate interactions.

Dong and co-workers reported the use of acupuncture needles as a carrier of SERS-active NPs (Dong et al. 2011). The SERS-active needles were fabricated

from commercial stainless-steel acupuncture needles of 0.2 mm in diameter. They were first incubated with 3-mercaptopropyltriethoxysilane and then the SERS-active NPs, comprising a thin Au shell coated on a dielectric core, were assembled on the needle surface. When the needle was inserted into the body, interstitial fluids would diffuse into the gaps between the attached NPs. Then, the needle was pulled out and analytes in the fluids were taken out for SERS measurement. The ability of in vivo SERS detection was assessed by using 6-mercaptopurine (6-MP). Its aqueous solution was injected into the ear vein of anesthetized New Zealand rabbit. Then, two SERS-active needles were inserted into the other ear vein and *vastus lateralis* tendon (removed with scissors) to detect the drug concentration in the blood and muscles, respectively. SERS measurement was carried out immediately after the needle was pulled out. The results indicated that the concentration of free 6-MP in the body decreased after injection and the concentration of 6-MP in the blood is higher than that in muscles.

7.7.3 Clinical Utility of SERS

7.7.3.1 Surgery Guidance of Brain Tumours

Delineation of tumour margins is very important for better treatment of patients with tumours. Surgery remains a mainstay in the treatment of brain tumours, in particular glioblastoma multiforme. Incomplete tumour resections lead to tumour recurrence at 80−90 % patients (Oh et al. 2011). Different imaging techniques are currently being utilized to better visualize tumour margins. 3D imaging with high spatial resolution (photoacoustic) in combination with SERS imaging of Au NRs was used for detection and resection guidance of ovarian cancer in living mice (Jokerst et al. 2012). The same group proposed multimodal probe based on a single imaging agent, whole brain tumour localization by MRI, 3D imaging with high spatial resolution (photoacoustic) and high-resolution surface imaging of tumour margins by SERS (Kircher et al. 2012). Here, the SERS tags containing a 60 nm Au core modified with the RRM (*trans*-1,2-bis(4-pyridyl)-ethylene) and a protective silica shell were injected in glioblastoma-bearing mice. The SERS signal helped in identifying microscopic tumour and its resection in vivo. Since the NPs did not carry any tumour targeting molecule, the authors speculated that the NPs would enter the extravascular space by diffusion through the disrupted blood-brain barrier and accumulate in cells within the brain tumour because of enhanced permeability and retention effect.

Harmsen and co-workers presented the precise visualization of the full tumour extent in transgenic mouse models of breast cancer, sarcoma, pancreatic ductal adenocarcinoma and prostate cancer (Harmsen et al. 2015a). Their SERRS tag has the following features: (i) star-shaped Au core (75 nm diameter) demonstrating a LSPR in the NIR region, (ii) a RRM that is in resonance with the detection laser (785 nm) and (iii) a biocompatible encapsulation method that allows efficient

loading of the resonant RRM at the Au surface. The Au nanostars were coated with silica in the presence of the resonant RRM IR-780 perchlorate without the need for any surface primers. SERRS nanostars generated photostable SERRS signal with a LOD of 1.5 fM in solution under conditions that are close to those required for clinical translation (100 mW laser power, 1.5 s acquisition time, 5× objective). They showed also a high degree of batch-to-batch consistency with minimal variation in SERRS signal intensity (±4.5 % coefficient of variation) (Harmsen et al. 2015a). Bifunctional NPs comprising a superparamagnetic material and a plasmonic metal were also used in both MRI and SERS (Yigit et al. 2011). The bifunctional Au/iron NPs embedded with the RRM DTTC and PEG protective shell were injected into the muscle of a living mouse for in vivo MRI and SERS detection. SERS detection was performed directly in the injection area. Both spectra from the living mouse and excised muscle tissue (excised after in vivo detection) showed the same spectral feature as the DTTC SERS spectrum obtained in solution (Harmsen et al. 2015a).

However, MRI is costly and a time-consuming method. Moreover, it was found that the assessment of tumour borders by MRI was often incongruent with the actual tumour borders due to the brain shift during surgery. To overcome this limitation, Karabeber and co-workers developed an intraoperative tumour detection method that could be applied clinically in the near future (Karabeber et al. 2014). It combines static SERS imaging and real-time SERS NP detection using a hand-held Raman scanner during surgery. This was accomplished in a genetic mouse model that closely mimics the pathology of human glioblastoma multiforme. The SERS tags formed by Au core, RRM (4,4′-dipyridyl) and silica shell were allowed to circulate for 24 h in the mouse to ensure that they accumulated in the tumours. Tumour tissue was detected in situ with the hand-held Raman scanner using 785 nm laser line as excitation. Figure 7.20 shows the residual brain tumour before resection (a) and subsequently resected (b) and corresponding SERS spectra (c). SERS signal of RRM was observed only in the case of a tumour present while no SERS signal appeared in normal tissue. The presence of SERS tags within the resected specimen was proved by TEM. Immunohistochemical staining for the tumour marker Olig-2 confirmed that the resected tissue indeed represented microscopic glioblastoma multiform cancer spread. Importantly, the hand-held scanner was able to identify in 10 mice small tumour spots that were not detected on the Raman images. This is attributable to the flexibility of angulating hand-held scanner to probe any area in the operating bed, even those located at the lateral margins underneath overlying normal brain tissue. Therefore, SERS-guided surgery using a hand-held Raman scanner represents a highly translatable approach to facilitate the resection of brain tumours and potentially other cancer types. It also provides the capability of scanning the operative bed from any desired angle in order to examine every aspect of the tumour bed. One of the limitations of this approach is that it was performed on brains that had been fixed in paraformaldehyde and is therefore not fully representative of the actual surgical environment. Another potential limitation

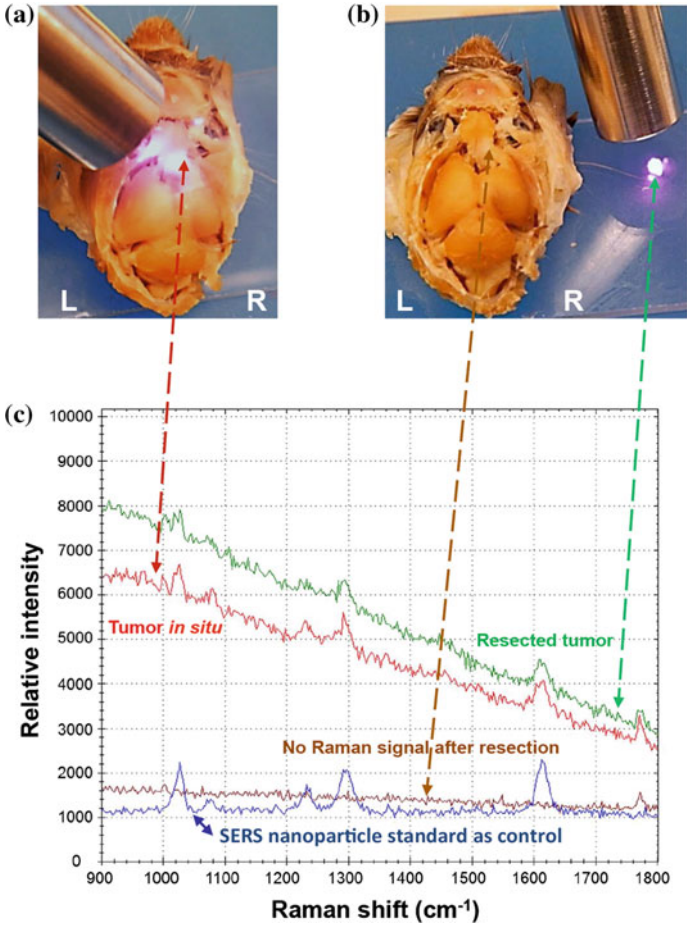

Fig. 7.20 In situ SERS-NP-guided surgery of brain tumour using hand-held Raman scanner. The tumour tissue before resection (**a**), after resection (**b**) and corresponding SERS signal coming from SERS tags (**c**) (adapted with permission from Karabeber et al. 2014. Copyright 2014 American Chemical Society)

of the technique is that depth penetration with conventional Raman spectroscopy imaging techniques is in the order of few mm.

7.7.3.2 Endoscopic Imaging Using SERS

Endoscopic imaging is an invaluable diagnostic tool allowing minimally invasive access to tissues deep within the body. It has played a key role in screening colon cancer and is credited with preventing deaths through the detection and removal of precancerous polyps. Because of limited depth of penetration associated with most

optical techniques, endoscopic approach in attempting to translate Raman spectroscopy to clinical use was tested. In 2000, Shim and co-workers reported the first in vivo Raman spectroscopy of human gastrointestinal tissues measured during a routine clinical endoscopy (Shim et al. 2000). This was achieved by using a NIR fibre-optic Raman probe that was passed through the endoscope instrument channel and placed in contact with the tissue surface. Thus far, it was possible to evaluate intrinsic tissue signals using contact endoscopic Raman probes. However, another strategy currently being developed could exploit ultrasensitive detection of using endoscopic SERS molecular imaging agents to diagnose cancer in vivo (Zavaleta et al. 2011). SERS-endoscopic strategy for colon cancer detection involves three basic steps: (i) topical administration of tumour-targeted SERS-active NPs to a particular area of interest during endoscopy followed by washing of the unbound NPs, (ii) utilization of Raman endoscopic device as it is deployed through the working channel of a commercial endoscope to detect and quantify the presence of the bound targeted NPs relative to internal controls and (iii) interpretation of results in real-time to determine what pathological conditions exist based on SERS signal associated with tumour-targeted NPs (Zavaleta et al. 2011). Several groups have developed a fibre-based, noncontact Raman endoscope to interrogate SERS NPs as contrast agents (Mohs et al. 2010; McVeigh et al. 2012; Zavaleta et al. 2013; Wang et al. 2014).

Zavaleta and co-workers reported first SERS-based multiplexing using commercial SERS tags (Cabot Security Systems) consisting of 10 different RRMs adsorbed onto a Au core (60 nm diameter) and then coated with silica (Zavaleta et al. 2013; Garai et al. 2013). The Raman endoscopic device was equipped with a flexible fibre bundle with a centrally located single-mode fibre for illumination at 785 nm and an additional 36 surrounding multimode fibres for light collection. Characterization of the Raman instrument was performed with SERS tags on excised human tissue samples and it has shown unsurpassed sensitivity and multiplexing capabilities, detecting 326 fM concentration of NPs and unmixing 10 variations of colocalized SERS tags. Another unique feature of this noncontact Raman endoscope is that it has been designed for efficient use over a wide range of working distances from 1 to 10 mm.

As a point-detection device, images could only be created on-the-bench by physically moving the sample, which is not a viable approach for in vivo imaging of large, complex surfaces. Recently, Garai and co-workers reported the design and in vivo application of a miniature, noncontact, opto-electro-mechanical Raman endoscopic device (Garai et al. 2015). The concept is illustrated in Fig. 7.21. The device was designed such that it can be inserted through the accessory channel of a clinical endoscope. As the endoscope was being retracted in the gastrointestinal tract, the device simultaneously scanned the lumen and the collected SERS signal from SERS tags was analysed (Fig. 7.21a). Figure 7.21b shows a scheme of the distal end of the device. A brushless DC motor that rotates a mirror caused the collimated beam to sweep 360°, enabling luminal imaging of the colon wall. The device was not required to be in contact with the tissue, which was enabled through the use of the collimated illumination beam. A custom, miniature, concentrically

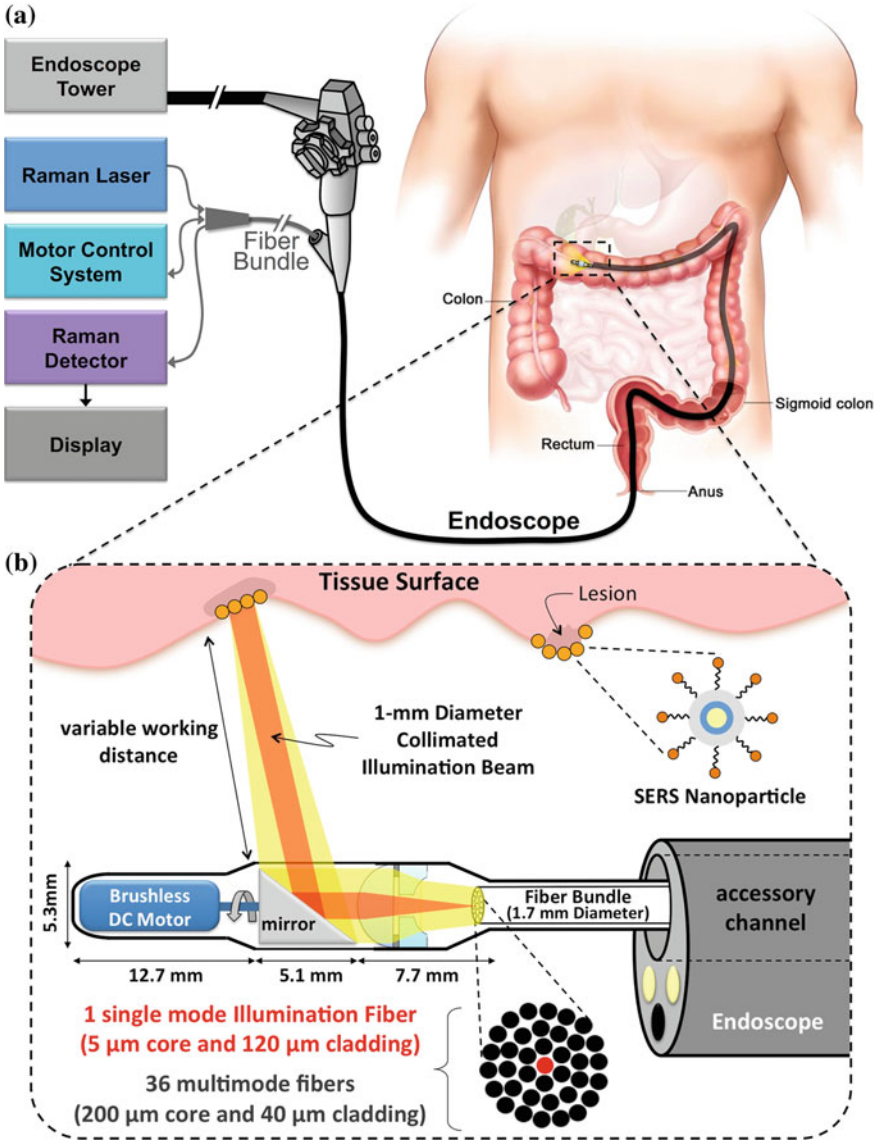

Fig. 7.21 Endoscopic SERS molecular imaging. **a** The scheme of the basic concept. **b** Expanded scheme of the distal end of the device. See text for details (adapted from Garai et al. 2015. Copyright 2015 Garai et al.)

segmented, air-spaced doublet lens having a nonreciprocal optical path consists of a plano-convex lens and an adjacent plano-concave lens with a central hole. The doublet lens increased collection efficiency at longer, clinically relevant working distances. This device enabled rapid scanning of topologically complex luminal

surfaces of hollow organs (e.g. colon and esophagus) and produced quantitative images of the relative concentrations of present SERS tags. This approach can also provide multiplexed information via a panel of SERS tags. Human studies demonstrated the speed and simplicity of this technique. A male patient undergoing routine colonoscopy screening consented to participate in the study. A signal was acquired over 30 s and no intrinsic Raman signal from the tissue was detected. Therefore, this new screening strategy has the potential to improve diagnosis and to guide therapy by enabling sensitive quantitative molecular detection of small and otherwise hardly detected lesions in the context of white light endoscopy.

7.7.4 *Intracellular SERS Monitoring of Drug Release In Vivo*

Thiopurine analogues represent potential antileukaemic and antineoplastic drugs for the treatment of many cancer diseases. Ock and co-workers employed label-free SERS and live cell imaging techniques to in vitro and in vivo study of uptake and release of thiopurine drugs (Ock et al. 2012). The main principle of this study is illustrated in Fig. 7.22. 6-MP and 6-thioguanine (6-TG) adsorbed on the surface of Au NPs were replaced by glutathione monoester (GSH–OEt) as an intracellular external stimulus (Fig. 7.22a). The release of a portion of 6-MP or 6-TG molecules from the Au NPs was proved by a decrease of their SERS signal. A tripeptide with a methyl group instead of a thiol group was used as an inactive GSH derivative in a negative control experiment. In vivo SERS studies were carried out by subcutaneous injection of 6-TG modified Au NPs in living nude mice. The SERS intensity of 6-TG decreased upon GSH–OEt injection, whereas the control tripeptide did not show a significant influence (Fig. 7.22b). A live cell imaging technique provided a nanomolar range release of thiopurine from Au NP surfaces after the injection of external glutathione.

Conde and co-workers developed Au NP conjugates labelled with a RRM and the commercial antibody-drug conjugate Cetuximab (Erbitux®) for targeted detection and treatment of tumours in vivo (Conde et al. 2014). Mice models were implanted with cancerous cells to generate xenografts and the mice were then treated with nanostructures via tail injection, while the tumours were located in the right leg. The conjugates were successfully translocated to the tumour site and resulted in a reduction of further tumour development by the inhibition of cellular division. Active targeting of the tumour was monitored via SERS and large SERS signals were observed in mice treated with the drug conjugates whilst minimal signals were observed from those treated with drug-free nanostructures. The authors reported that the signals measured from drug labelled NPs at the xenograft were 4.5× higher than those of the drug-free system as measured from a key identification peak at 508 cm^{-1}.

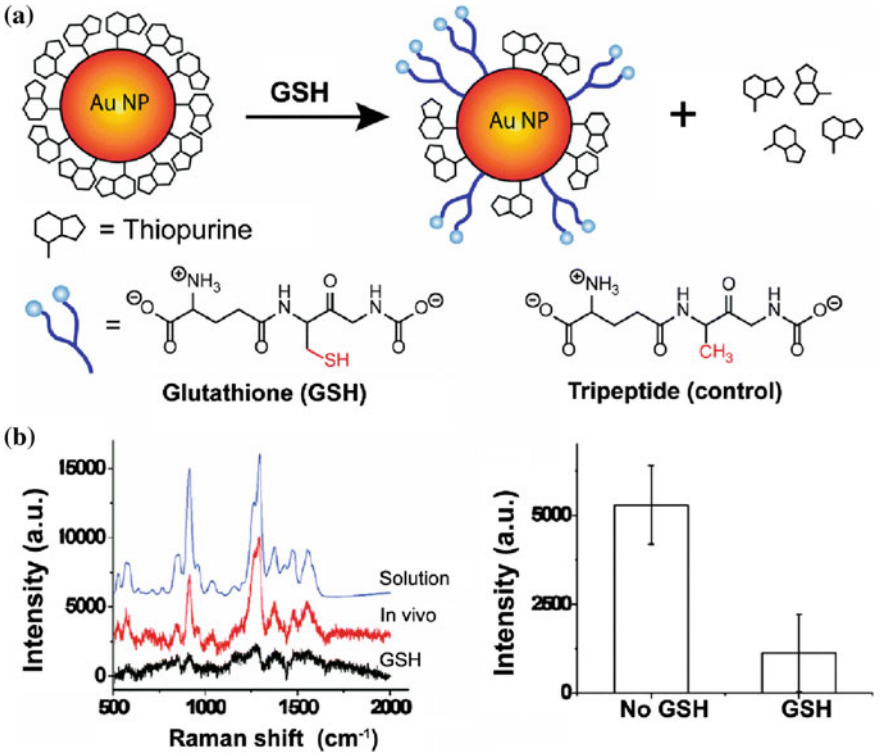

Fig. 7.22 SERS study of uptake and release of thiopurine drugs. **a** GSH-mediated release of thiopurines adsorbed on Au NPs. **b** In vivo SERS spectra of 6-TG adsorbed on Au NPs after treatment of GSH and the corresponding stick diagram of results obtained with and without GSH treatment (adapted with permission from Ock et al. 2012. Copyright 2012 American Chemical Society)

The expression of adhesion molecules such as intercellular adhesion molecule 1 (ICAM-1) by endothelial cells is crucial during acute inflammation. In vivo SERS detection of (ICAM-1) expression on endothelial cells was reported by using SERS tags injected into live mice (McQueenie et al. 2012). SERS tags consist of Au NPs with RRMs encapsulated with a silica shell and then conjugated to anti-ICAM-1 antibody to target ICAM-1 expressed in mice. ICAM-1 expression was induced by local lipopolysaccharide injection in the ear of mice. Approximately 24 h after the intradermal local lipopolysaccharide injections, an intravenous injection of the SERS labels was performed. SERS spectra were measured 30 min after the injection of the SERS tags. SERS spectra recorded from the ears of mice injected with anti-ICAM-1 NPs reproduced spectral features corresponding to the neat SERS tag. The authors also demonstrated that SERS tags provide higher detection sensitivity for ICAM-1 in comparison with a conventional fluorescence probe and offer improvements in terms of depth resolution and signal-to-noise ratio.

7.7.5 *Toxicity Issue*

The long-term toxicity of metallic NPs inside the human body is not fully explored. Toxicity studies of developing systems, organisms or individual differentiating cells provide particular challenges for in vivo SERS applications. The biocompatibility of Ag NPs is not as good as that of Au NPs because of silver's oxidative nature, which drives genotoxic and cytotoxic outcomes (AshaRani et al. 2009). The biocompatibility of metallic NPs is dependent on several factors, including metal type, shape, size and capping materials. In general, ultrasmall Au nanoclusters have greater cytotoxic effects due to their strong endocytosis effectiveness and binding ability to B-form DNA (Jiang et al. 2008). However, the Au NPs about 30–100 nm diameter that are commonly used as SERS substrates cause no noticeable toxicity at concentrations up to 100 mM (Jiang et al. 2008).

Generally, it is necessary to use the lowest possible concentration of Au NPs. This can be achieved only at optimal sensitivity conditions such as using RRMs and SERS tags providing maximal SERS signal in NIR IR. The biocompatibility of PEGylated Raman-active Au NPs was investigated using human cells. No cytotoxicity occurred in either HeLa (human cervical cancer cells) or HepG2 (human liver cancer cells) cell lines in the acute setting (Thakor et al. 2011a). Physical redistribution of NPs in time can change their cytotoxicity with developmental stage. After prolonged exposures (48 h) at relatively high concentrations (1000 NPs per cell), a minimal amount of cytotoxicity was seen in both cell lines because of increases in cellular oxidative stress (Thakor et al. 2011a). Surface coating is also a key factor that determines the biocompatibility of NPs. The biocompatibility of cytotoxic NPs can be greatly increased by using proper coating materials. For example, reduced cytotoxicity was reported after the removal (Wang et al. 2010b) or replacement (Boca and Astilean 2010) of toxic surfactants from metallic nanostructures (e.g. Au NRs) with amino groups or polymers that stabilize the particles while minimizing their toxic effects. Silica-coating which is often used to stabilize the SERS tag also reduces the toxicity of Au NPs and favours them for in vivo applications (Thakor et al. 2011b).

References

J.L. Abell, J.M. Garren, J.D. Driskell, R.A. Tripp, Y. Zhao, Label-free detection of micro-RNA hybridization using surface-enhanced Raman spectroscopy and least-squares analysis. J. Am. Chem. Soc. **134**, 12889 (2012)

L.R. Allain, T. Vo-Dinh, Surface-enhanced Raman scattering detection of the breast cancer susceptibility gene BRCA1 using a silver-coated microarray platform. Anal. Chim. Acta **469**, 149 (2002)

P.V. AshaRani, G. Low Kah Mun, M.P. Hande, S. Valiyaveettil, Cytotoxicity and genotoxicity of silver nanoparticles in human cells. ACS Nano **3**, 279 (2009)

Š. Bálint, S. Rao, M. Marro, P. Miškovský, D. Petrov, Monitoring of local pH in photodynamic therapy-treated live cancer cells using surface-enhanced Raman scattering probes. J. Raman Spectrosc. **42**, 1215 (2011)

M.A. Bedics, H. Kearns, J.M. Cox, S. Mabbott, F. Ali, N.C. Shand, K. Faulds, J.B. Benedict, D. Graham, M.R. Detty, Extreme red shifted SERS nanotags. Chem. Sci. **6**, 2302 (2015)

L. Beqa, Z. Fan, A.K. Singh, D. Senapati, P.C. Ray, Gold nano-popcorn attached SWCNT hybrid nanomaterial for targeted diagnosis and photothermal therapy of human breast cancer cells. ACS Appl. Mater. Interfaces **3**, 3316 (2011)

S.C. Boca, S. Astilean, Detoxification of gold nanorods by conjugation with thiolated poly (ethylene glycol) and their assessment as SERS-active carriers of Raman tags. Nanotechnology **21**, 235601 (2010)

Y.C. Cao, R. Jin, C.A. Mirkin, Nanoparticles with Raman spectroscopic fingerprints for DNA and RNA detection. Science **297**, 1536 (2002)

S. Charan, F.C. Chien, N. Singh, C.W. Kuo, P. Chen, Development of lipid targeting Raman probes for in vivo imaging of caenorhabditis elegant. Chem.–Eur. J **17**, 5165 (2011)

R. Chen, J. Lin, S. Feng, Z. Huang, G. Chen, J. Wang, Y. Li, H. Zeng, Applications of SERS spectroscopy for blood analysis, in *Applications of Raman Spectroscopy to Biology—From Basic Studies To Disease Diagnosis*, ed. by M. Ghomi (IOS Press, Amsterdam, 2012a), pp. 72–105

Y. Chen, G. Chen, S. Feng, J. Pan, X. Zheng, Y. Su, Y. Chen, Z. Huang, X. Lin, F. Lan, R. Chen, H. Zeng, Label-free serum ribonucleic acid analysis for colorectal cancer detection by surface-enhanced Raman spectroscopy and multivariate analysis. J. Biomed. Opt. **17**, 067003 (2012b)

X. Chen, Z. Huang, S. Feng, J. Chen, L. Wang, P. Lu, H. Zeng, R. Chen, Analysis and differentiation of seminal plasma via polarized SERS spectroscopy. Int. J. Nanomed. **7**, 6115 (2012c)

Y. Chen, X. Zheng, G. Chen, C. He, W. Zhu, S. Feng, G. Xi, R. Chen, F. Lan, H. Zeng, Immunoassay for LMP1 in nasopharyngeal tissue based on surface-enhanced Raman scattering. Int. J. Nanomed. **7**, 73 (2012d)

I. Choi, Y. Huh, D. Erickson, Ultra-sensitive, label-free probing of the conformational characteristics of amyloid beta aggregates with a SERS active nanofluidic device. Microfluid. Nanofluid. **12**, 663 (2012)

H. Chon, S. Lee, S.Y. Yoon, S.I. Chang, D.W. Lim, J. Choo, Simultaneous immunoassay for the detection of two lung cancer markers using functionalized SERS nanoprobes. Chem. Commun. **47**, 12515 (2011)

H. Chon, S. Lee, S.Y. Yoon, E.K. Lee, S.I. Chang, J. Choo, SERS-based competitive immunoassay of troponin I and CK-MB markers for early diagnosis of acute myocardial infarction. Chem. Commun. **50**, 1058 (2014)

I.H. Chou, M. Benford, H.T. Beier, G.L. Cote, M. Wang, N. Jing, J. Kameoka, T.A. Good, Nanofluidic biosensing for beta-amyloid detection using surface enhanced Raman spectroscopy. Nano Lett. **8**, 1729 (2008)

I. Chourpa, F.H. Lei, P. Dubois, M. Manfait, G.D. Sockalingum, Intracellular applications of analytical SERS spectroscopy and multispectral imaging. Chem. Soc. Rev. **37**, 993 (2008)

J. Conde, C. Bao, D. Cui, P.V. Baptista, F. Tian, Antibody-drug gold nanoantennas with Raman spectroscopic fingerprints for in vivo tumour theranostics. J. Control. Release **183**, 87 (2014)

U.S. Dinish, G. Balasundaram, Y.T. Chang, M. Olivo, Actively targeted in vivo multiplex detection of intrinsic cancer biomarkers using biocompatible SERS nanotags. Sci. Rep. **4**, 4075 (2014)

F.T. Docherty, P.B. Monaghan, R. Keir, D. Graham, W.E. Smith, J.M. Cooper, The first SERRS multiplexing from labelled oligonucleotides in a microfluidics lab-on-a-chip. Chem. Commun. **1**, 118 (2004)

J. Dong, Q.F. Chen, C.H. Rong, D.Y. Li, Y.Y. Rao, Minimally invasive surface-enhanced Raman scattering detection with depth profiles based on a surface-enhanced Raman scattering-active acupuncture needle. Anal. Chem. **83**, 6191 (2011)

J.A. Dougan, D. MacRae, D. Graham, K. Faulds, DNA detection using enzymatic signal production and SERS. Chem. Commun. **47**, 4649 (2011)

J.D. Driskell, R.A. Tripp, Label-free SERS detection of microRNA based on affinity for an unmodified silver nanorod array substrate. Chem. Commun. **46**, 3298 (2010)
A.M. Fales, H.T. Yuan, Vo-Dinh, Silica-coated gold nanostars for combined surface-enhanced Raman scattering (SERS) detection and singlet-oxygen generation: a potential nanoplatform for theranostics. Langmuir **27**, 12186 (2011)
A.M. Fales, H.T. Yuan, Vo-Dinh, Cell-penetrating peptide enhanced intracellular Raman imaging and photodynamic therapy. Mol. Pharmaceutics **10**, 2291 (2013)
A. Farhadi, A. Roxin, B.C. Wilson, G. Zheng, Nano-enabled SERS reporting photosensitizers. Theranostics **5**, 469 (2015)
K. Faulds, F. McKenzie, W.E. Smith, D. Graham, Quantitative simultaneous multianalyte detection of DNA by dual-wavelength surface-enhanced resonance Raman scattering. Angew. Chem. Int. Ed. **46**, 1829 (2007)
K. Faulds, R. Jarvis, W.E. Smith, D. Graham, R. Goodacre, Multiplexed detection of six labelled oligonucleotides using surface enhanced resonance Raman scattering (SERRS). Analyst **133**, 1505 (2008)
S. Feng, R. Chen, J. Lin, J. Pan, G. Chen, Y. Li, M. Cheng, Z. Huang, J. Chen, H. Zheng, Nasopharyngeal cancer detection based on blood plasma surface-enhanced Raman spectroscopy and multivariate analysis. Biosens. Bioelectron. **25**, 2414 (2010)
S.Y. Feng, R. Chen, J.Q. Lin, J. Pan, Y. Wu, Y.Z. Li, J. Chen, H. Zeng, Gastric cancer detection based on blood plasma surface-enhanced Raman spectroscopy excited by polarized laser light, Biosens. Bioelectron. **26**, 3167 (2011)
S. Feng, D. Lin, J. Lin, B. Li, Z. Huang, G. Chen, W. Zhang, L. Wang, J. Pan, R. Chen, H. Zeng, Blood plasma surface-enhanced Raman spectroscopy for non-invasive optical detection of cervical cancer. Analyst **138**, 3967 (2013)
S. Feng, S. Huang, D. Lin, G. Chen, Y. Xu, Y. Li, Z. Huang, J. Pan, R. Chen, H. Zeng, Surface-enhanced Raman spectroscopy of saliva proteins for the noninvasive differentiation of benign and malignant breast tumors. Int. J. Nanomed. **10**, 537 (2015)
R.A. Ferguson, H. Yu, M. Kalyvas, S. Zammit, E.P. Diamandis, Ultrasensitive detection of prostate-specific antigen by a time-resolved immunofluorometric assay and the immulite(R) immunochemiluminescent third-generation assay: Potential applications in prostate and breast cancers. Clin. Chem. **42**, 675 (1996)
E. Garai, S. Sensarn, C.L. Zavaleta, D. Van de Sompel, N.O. Loewke, M.J. Mandella, S.S. Gambhir, C.H. Contag, High-sensitivity, real-time, ratiometric imaging of surface-enhanced Raman scattering nanoparticles with a clinically translatable Raman endoscope device. J. Biomed. Opt. **18**, 096008 (2013)
E. Garai, S. Sensarn, C.L. Zavaleta, N.O. Loewke, S. Rogalla, M.J. Mandella, S.A. Felt, S. Friedland, J.T.C. Liu, S.S. Gambhir, C.H. Contag, A real-time clinical endoscopic system for intraluminal, multiplexed imaging of surface-enhanced Raman scattering nanoparticles. PLoS ONE **10**, e0123185 (2015)
E. Gormally, E. Caboux, P. Vineis, P. Hainaut, Circulating free DNA in plasma or serum as biomarker of carcinogenesis: Practical aspects and biological significance. Mutat. Res. Rev. Mutat. **635**, 105 (2007)
D. Graham, R. Stevenson, D.G. Thompson, L. Barrett, C. Dalton, K. Faulds, Combining functionalised nanoparticles and SERS for the detection of DNA relating to disease. Faraday Discuss. **149**, 291 (2011)
J.H. Granger, M.C. Granger, M.A. Firpo, S.J. Mulvihill, M.D. Porter, Toward development of a surface-enhanced Raman scattering (SERS)-based cancer diagnostic immunoassay panel. Analyst **138**, 410 (2013)
D.S. Grubisha, R.J. Lipert, H.Y. Park, J. Driskell, M.D. Porter, Femtomolar detection of prostate-specific antigen: an immunoassay based on surface-enhanced Raman scattering and immunogold labels. Anal. Chem. **75**, 5936 (2003)
L. Guerrini, R. Arenal, B. Mannini, F. Chiti, R. Pini, P. Matteini, R.A. Alvarez-Puebla, SERS detection of amyloid oligomers on metallorganic-decorated plasmonic beads. ACS Appl. Mater. Interfaces **7**, 9420 (2015)

V.K. Gupta, N. Atar, M.L. Yola, M. Eryilmaz, H. Torul, U. Tamer, I.H. Boyaci, Z. Üstündag, A novel glucose biosensor platform based on Ag@AuNPs modified graphene oxide nanocomposite and SERS application. J. Colloid Interf. Sci. **406**, 231 (2013)

H. Han, X. Yan, R. Dong, G. Ban, K. Li, Analysis of serum type II diabetes mellitus and diabetic complication using surface-enhanced Raman spectra (SERS). Appl. Phys. B **94**, 667 (2009)

S. Harmsen, R. Huang, M.A. Wall, H. Karabeber, J.M. Samii, M. Spaliviero, J.R. White, S. Monette, R. O'Connor, K.L. Pitter, S.A. Sastra, M. Saborowski, E.C. Holland, S. Singer, K. P. Olive, S.W. Lowe, R.G. Blasberg, M.F. Kircher, Surface-enhanced resonance Raman scattering nanostars for high-precision cancer imaging. Sci. Transl. Med. **7**, 271ra7 (2015a)

S. Harmsen, M.A. Bedics, M.A. Wall, R. Huang, M.R. Detty, M.F. Kircher, Rational design of a chalcogenopyrylium-based surface-enhanced resonance Raman scattering nanoprobe with attomolar sensitivity. Nat. Commun. **6**, 6570 (2015b)

M.M. Harper, B. Robertson, A. Ricketts, K. Faulds, Specific detection of DNA through coupling of a TaqMan assay with surface enhanced Raman scattering (SERS). Chem. Commun. **48**, 9412 (2012)

C.L. Haynes, C.R. Yonzon, X. Zhang, R.P. Van Duyne, Surface-enhanced Raman sensors: early history and the development of sensors for quantitative biowarfare agents and glucose detection. J. Raman Spectrosc. **36**, 471 (2005)

P.H. Hsu, H.K. Chiang, Surface-enhanced Raman spectroscopy for quantitative measurement of lactic acid at physiological concentration in human serum. J. Raman Spectrosc. **41**, 1610 (2010)

J. Hu, P.C. Zheng, J.H. Jiang, G.L. Shen, R.Q. Yu, G.K. Liu, Sub-attomolar HIV-1 DNA detection using surface-enhanced Raman spectroscopy. Analyst **135**, 1084 (2010)

S. Huang, L. Wang, W. Chen, S. Feng, J. Lin, Z. Huang, G. Chen, B. Li, R. Chen, Potential of non-invasive esophagus cancer detection based on urine surface-enhanced Raman spectroscopy. Laser Phys. Lett. **11**, 115604 (2014)

Y.S. Huh, A.J. Chung, B. Cordovez, D. Erickson, Enhanced on-chip SERS based biomolecular detection using electrokinetically active microwells. Lab. Chip **9**, 433 (2009)

P. Iacono, H. Karabeber, M.F. Kircher, A "schizophotonic" all-in-one nanoparticle coating for multiplexed SE(R)RS biomedical imaging. Angew. Chem. Int. Ed. **53**, 11756 (2014)

N.R. Isola, D.L. Stokes, T. Vo-Dinh, Surface enhanced Raman gene probe for HIV detection. Anal. Chem. **70**, 1352 (1998)

R.M. Jarvis, R. Goodacre, Discrimination of bacteria using surface-enhanced Raman spectroscopy. Anal. Chem. **76**, 40 (2004)

W. Jiang, B.Y.S. Kim, J.T. Rutka, W.C.W. Chan, Nanoparticle-mediated cellular response is size-dependent. Nat. Nanotechnol. **3**, 145 (2008)

J.V. Jokerst, A.J. Cole, D. Van de Sompel, S.S. Gambhir, Gold nanorods for ovarian cancer detection with photoacoustic imaging and resection guidance via Raman imaging in living mice. ACS Nano **6**, 10366 (2012)

S. Jung, J. Nam, S. Hwang, J. Park, J. Hur, K. Im, N. Park, S. Kim, Theragnostic pH-sensitive gold nanoparticles for the selective surface enhanced Raman scattering and photothermal cancer therapy. Anal. Chem. **85**, 7674 (2013)

A. Kaminska, E. Witkowska, K. Winkler, I. Dziecielewski, J.L. Weyher, J. Waluk, Detection of hepatitis B virus antigen from human blood: SERS immunoassay in a microfluidic system. Biosens. Bioelectron. **66**, 461 (2015)

T. Kang, S.M. Yoo, I. Yoon, S.Y. Lee, B. Kim, Patterned multiplex pathogen DNA detection by Au particle-on-wire SERS sensor. Nano Lett. **10**, 1189 (2010)

B. Kang, M.M. Afifi, L.A. Austin, M.A. El-Sayed, Exploiting the nanoparticle plasmon effect: observing drug delivery dynamics in single cells via Raman/fluorescence imaging spectroscopy. ACS Nano **7**, 7420 (2013)

H. Karabeber, R. Huang, P. Iacono, J.M. Samii, K. Pitter, E.C. Holland, M.F. Kircher, Guiding brain tumor resection using surface-enhanced Raman scattering nanoparticles and hand-held Raman scanner. ACS Nano **8**, 9755 (2014)

S. Keren, C.L. Zavaleta, Z. Cheng, A. de la Zerda, O. Gheysens, S.S. Gambhir, Noninvasive molecular imaging of small living subjects using Raman spectroscopy. Proc. Natl. Acad. Sci. **105**, 5844 (2008)

M.F. Kircher, A. de la Zerda, J.V. Jokerst, C.L. Zavaleta, P.J. Kempen, E. Mittra, K. Pittner, R.M. Huang, C. Campos, F. Habte, R. Sinclair, C.W. Brennan, I.K. Mellinghoff, E.C. Holland, S.S. Gambhir, A brain tumor molecular imaging strategy using a new triple-modality MRI-photoacoustic-Raman nanoparticle. Nat. Med. **18**, 829 (2012)

M. Knauer, N.P. Ivleva, X.J. Liu, R. Niessner, C. Haisch, Surface-enhanced Raman scattering-based label-free microarray readout for the detection of microorganisms. Anal. Chem. **82**, 2766 (2010)

J. Ko, S. Lee, E.K. Lee, S.I. Chang, L. Chen, S.Y. Yoon, J. Choo, SERS-based immunoassay of tumor marker VEGF using DNA aptamers and silica-encapsulated hollow gold nanospheres. Phys. Chem. Chem. Phys. **15**, 5379 (2013)

K.V. Kong, Z. Lam, W.K.O. Lau, W.K. Leong, M. Olivo, A transition metal carbonyl probe for use in a highly specific and sensitive SERS-based assay for glucose. J. Am. Chem. Soc. **135**, 18028 (2013)

R.R. Kopito, Aggresomes, inclusion bodies and protein aggregation. Trends Cell Biol. **10**, 524 (2000)

M. Lee, S. Lee, J.H. Lee, H.W. Lim, G.H. Seong, E.K. Lee, S.I. Chang, C.H. Oh, J. Choo, Highly reproducible immunoassay of cancer markers on a gold-patterned microarray chip using surface-enhanced Raman scattering imaging. Biosens. Bioelectron. **26**, 2135 (2011a)

K. Lee, V.P. Drachev, J. Irudayaraj, DNA-gold nanoparticle reversible networks grown on cell surface marker sites: application in diagnostics. ACS Nano **5**, 2109 (2011b)

S.X. Li, Q.Y. Zeng, L.F. Li, Y.J. Zhang, M.M. Wan, Z.M. Liu, H.L. Xiong, Z.Y. Guo, S.H. Liu, Study of support vector machine and serum surface-enhanced Raman spectroscopy for noninvasive esophageal cancer detection. J. Biomed. Opt. **18**, 027008 (2013)

Y. Li, X. Qi, C. Lei, Q. Yue, S. Zhang, Simultaneous SERS detection and imaging of two biomarkers on the cancer cell surface by self-assembly of branched DNA–gold nanoaggregates. Chem. Commun. **50**, 9907 (2014)

L.J. Liang, D.S. Huang, H.L. Wang, H.B. Li, S.P. Xu, Y.X. Chang, H. Li, Y.W. Yang, C.Y. Liang, W.Q. Xu, In situ surface-snhanced Raman scattering spectroscopy exploring molecular changes of drug-treated cancer cell nucleus. Anal. Chem. **87**, 2504 (2015)

C.C. Lin, Y.M. Yang, Y.F. Chen, T.S. Yang, H.C. Chang, A new protein A assay based on Raman reporter labeled immunogold nanoparticles. Biosens. Bioelectron. **24**, 178 (2008)

D. Lin, S. Feng, J. Pan, Y. Chen, J. Lin, G. Chen, S. Xie, H. Zeng, R. Chen, Colorectal cancer detection by gold nanoparticle based surface-enhanced Raman spectroscopy of blood serum and statistical analysis. Opt. Express **19**, 13565 (2011a)

J. Lin, R. Chen, S. Feng, J. Pan, Y. Li, G. Chen, M. Cheng, Z. Huang, Y. Yu, H. Zeng, A novel blood plasma analysis technique combining membrane electrophoresis with silver nanoparticle based SERS spectroscopy for potential applications in non-invasive cancer detection. Nanomed. Nanotechnol. **7**, 655 (2011b)

J. Lin, Z. Huang, S. Feng, J. Lin, N. Liu, J. Wang, L. Li, Y. Zeng, B. Li, H. Zeng, R. Chen, Label-free optical detection of type II diabetes based on surface-enhanced Raman spectroscopy and multivariate analysis. J. Raman Spectrosc. **45**, 884 (2014)

S. Link, M.A. El-Sayed, Shape and size dependence of radiative, non-radiative and photothermal properties of gold nanocrystals. Int. Rev. Phys. Chem. **19**, 409 (2000)

R. Liu, X. Zi, Y. Kang, M. Si, Y. Wu, Surface-enhanced Raman scattering study of human serum on PVA-Ag nanofilm prepared by using electrostatic self-assembly. J. Raman Spectrosc. **42**, 137 (2011)

R.M. Liu, Y. Xiong, W.Y. Tang, Y. Guo, X.H. Yan, M.Z. Si, Near-infrared surface-enhanced Raman spectroscopy (NIR-SERS) studies on oxyheamoglobin (OxyHb) of liver cancer based on PVA-Ag nanofilm. J. Raman Spectrosc. **44**, 362 (2013a)

Y. Liu, Z. Chang, H. Yuan, A.M. Fales, T. Vo-Dinh, Quintuple-modality (SERS-MRI-CT-TPL-PTT) plasmonic nanoprobe for theranostics. Nanoscale **5**, 12126 (2013b)

W.T. Lu, A.K. Singh, S.A. Khan, D. Senapati, H.T. Yu, P.C. Ray, Gold nano-popcorn-based targeted diagnosis, nanotherapy treatment, and in situ monitoring of photothermal therapy response of prostate cancer cells using surface-enhanced Raman spectroscopy. J. Am. Chem. Soc. **132**, 18103 (2010)

B. Lutz, C.E. Dentinger, L. Nguyen, L. Sun, J. Zhang, A. Allen, S. Chan, B.S. Knudsen, Spectral analysis of multiplex Raman probe signature. ACS Nano **2**, 2306 (2008)

O. Lyandres, N.C. Shah, C.R. Yonzon, J.T. Walsh, M.R. Glucksberg, R.P. Van Duyne, Real-time glucose sensing by surface-enhanced Raman spectroscopy in bovine plasma facilitated by a mixed decanethiol/mercaptohexanol partition layer. Anal. Chem. **77**, 6134 (2005)

A. MacAskill, D. Crawford, D. Graham, K. Faulds, DNA sequence detection using surface-enhanced resonance Raman spectroscopy in a homogeneous multiplexed assay. Anal. Chem. **81**, 8134 (2009)

C.M. MacLaughlin, N. Mullaithilaga, G. Yang, S.Y. Ip, C. Wang, G.C. Walker, Surface-enhanced Raman scattering dye-labeled au nanoparticles for triplexed detection of leukemia and lymphoma cells and sers flow cytometry. Langmuir **29**, 1908 (2013)

S. Mahajan, J. Richardson, T. Brown, P.N. Bartlett, SERS-melting: a new method for discriminating mutations in DNA sequences. J. Am. Chem. Soc. **130**, 15589 (2008)

K.K. Maiti, U.S. Dinish, A. Samanta, M. Vendrell, K.S. Soh, S.J. Park, M. Olivo, Y.T. Chang, Multiplex targeted in vivo cancer detection using sensitive near-infrared SERS nanotags. Nano Today **7**, 85 (2012)

N.E. Marotta, K.R. Beavers, L.A. Bottomley, Limitations of surface enhanced Raman scattering in sensing DNA hybridization demonstrated by label-free DNA oligos as molecular rulers of distance-dependent enhancement. Anal. Chem. **85**, 1440 (2013)

R. McQueenie, R. Stevenson, R. Benson, N. MacRitchie, I. McInnes, P. Maffia, K. Faulds, D. Graham, J. Brewer, P. Garside, Detection of inflammation in vivo by surface-enhanced Raman scattering provides higher sensitivity than conventional fluorescence imaging. Anal. Chem. **84**, 5968 (2012)

P.Z. McVeigh, R.J. Mallia, I. Veillieux, B.C. Wilson, Development of widefield SERS imaging endoscope. Proc. SPIE **8217**, 821704 (2012)

A.M. Mohs, M.C. Mancini, S. Singhal, J.M. Provenzale, B. Leyland-Jones, M.D. Wang, S.M. Nie, Hand-held spectroscopic device for in vivo and intraoperative tumor detection: contrast enhancement, detection sensitivity, and tissue penetration. Anal. Chem. **82**, 9058 (2010)

P. Negri, R.A. Dluhy, Detection of genetic markers related to high pathogenicity in influenza by SERS. Analyst **138**, 4877 (2013)

Z.A. Nima, M. Mahmood, Y. Xu, T. Mustafa, F. Watanabe, D.A. Nedosekin, M.A. Juratli, T. Fahmi, E.I. Galanzha, J.P. Nolan, A.G. Basnakian, V.P. Zharov, A.S. Biris, Circulating tumor cell identification by functionalized silver-gold nanorods with multicolor, super-enhanced SERS and photothermal resonances. Sci. Rep. **4**, 4752 (2014)

M.S. Noh, S. Lee, H. Kang, J.K. Yang, H. Lee, D. Hwang, J.W. Lee, S. Jeong, Y. Jang, B.H. Jun, D.H. Jeong, S.K. Kim, Y.S. Lee, M.H. Cho, Target-specific near-IR induced drug release and photothermal therapy with accumulated Au/Ag hollow nanoshells on pulmonary cancer cell membranes. Biomaterials **45**, 81 (2015)

K. Ock, W.I. Jeon, E.O. Ganbold, M. Kim, J. Park, J.H. Seo, K. Cho, S.W. Joo, S.Y. Lee, Real-time monitoring of glutathione-triggered thipurine anticancer drug release in live cells investigated by surface-enhanced Raman scattering. Anal. Chem. **84**, 2172 (2012)

J. Oh, A. Sahgal, P. Sanghera, M.N. Tsao, P. Davey, K. Lam, S. Symons, R. Aviv, J.R. Perry, Glioblastoma: patterns of recurrence and efficacy of salvage treatments. Can. J. Neurol. Sci. **38**, 621 (2011)

A. Pal, N.R. Isola, J.P. Alarie, D.L. Stokes, T. Vo-Dinh, Synthesis and characterization of SERRS gene probe for BRCA-1 (breast cancer). Faraday Discuss. **132**, 293 (2006)

W. Pang, J. Wang, R. Xiao, S. Wang, SERS molecular sentinel for the RNA genetic marker of PB1-F2 protein in highly pathogenic avian influenza (HPAI) virus. Biosens. Bioelectron. **61**, 460 (2014)

H.Y. Park, J.D. Driskell, K.M. Kwarta, R.J. Lipert, M.D. Porter, C. Schoen, J.D. Neill, J.F. Ridpath, Ultrasensitive immunoassays based on surface-enhanced Raman scattering by immunogold labels, in *Surface-Enhanced Raman Scattering: Physics and Applications,* vol. **103**, ed. by K. Kneipp, M. Moskovits, H. Kneipp (Springer, Berlin Heidelberg 2006), pp. 427–446 (Top. Appl. Phys.)

H. Park, S. Lee, L. Chen, E.K. Lee, S.Y. Shin, Y.H. Lee, S.W. Son, C.H. Oh, J.M. Song, S.H. Kang, J. Choo, SERS imaging of HER2-overexpressed MCF7 cells using antibody-conjugated gold nanorods. Phys. Chem. Chem. Phys. **11**, 7444 (2009)

I.S. Patel, W.R. Premasiri, D.T. Moir, L.D. Ziegler, Barcoding bacterial cells: a SERS-based methodology for pathogen identification. J. Raman Spectrosc. **39**, 1660 (2008)

J.H. Phan, R.A. Moffitt, T.H. Stokes, J. Liu, A.N. Young, S. Nie, M.D. Wang, Convergence of biomarkers, bioinformatics and nanotechnology for individualized cancer treatment. Trends Biotechnol. **27**, 350 (2009)

M.D. Porter, R.L. Lipert, L.M. Siperko, G. Wang, R. Narayanan, SERS as a bioassay platform: fundamentals, design and applications. Chem. Soc. Rev. **37**, 1001 (2008)

W.R. Premasiri, J.C. Lee, L.D. Ziegler, Surface-enhanced Raman scattering of whole human blood, blood plasma, and red blood cells: cellular processes and bioanalytical sensing. J. Phys. Chem. B **116**, 9376 (2012a)

W.R. Premasiri, A.F. Sauer-Budge, J.C. Lee, C.M. Klapperich, L.D. Ziegler, Rapid bacterial diagnostics via surface-enhanced Raman microscopy. Spectroscopy **27**, s8 (2012b)

W.R. Premasiri, P. Lemler, Y. Chen, Y. Gebregziabher, L.D. Ziegler, SERS analysis of bacteria, human blood and cancer cells: a metabolomic and siagnostic tool, in *Frontiers of Surface-Enhanced Raman Scattering: Single Nanoparticles and Single Cells*, ed. by Y. Ozaki, K. Kneipp, R. Aroca (Wiley, Chichester, 2014), pp. 257–283

X.M. Qian, X.H. Peng, D.O. Ansari, Q. Yin-Goen, G.Z. Chen, D.M. Shin, L. Yang, A.N. Young, M.D. Wang, S.M. Nie, In vivo tumor targeting and spectroscopic detection with surface-enhanced Raman nanoparticle tags. Nat. Biotechnol. **26**, 83 (2008)

J. Qian, L. Jiang, F. Cai, D. Wang, S. He, Fluorescence-surface enhanced Raman scattering co-functionalized gold nanorods as near-infrared probes for purely optical in vivo imaging. Biomaterials **32**, 1601 (2011)

S.P. Ravindranath, Y. Wang, J. Irudayaraj, SERS driven cross-platform based multiplex pathogen detection. Sensor Actuat. B Chem. **152**, 183 (2011)

W. Ren, Y.X. Fang, E.K. Wang, A binary functional substrate for enrichment and ultrasensitive SERS spectroscopic detection of folic acid using graphene oxide/Ag nanoparticle hybrids. ACS Nano **5**, 6425 (2011)

L. Rodríguez-Lorenzo, Z. Krpetic, S. Barbosa, R.A. Alvarez-Puebla, L.M. Liz-Marzán, I.A. Prior, M. Brust, Intracellular mapping with SERS-encoded gold nanostars. Integr. Biol. **3**, 922 (2011)

A. Samanta, K.K. Maiti, K.S. Soh, X.J. Liao, M. Vendrell, U.S. Dinish, S.W. Yun, R. Bhuvaneswari, H. Kim, S. Rautela, J.H. Chung, M. Olivo, Y.T. Chang, Ultrasensitive near-infrared Raman reporters for SERS-based in vivo cancer detection. Angew. Chem. Int. Ed. Engl. **50**, 6089 (2011)

S. Schlücker, B. Küstner, A. Punge, R. Bonfig, A. Marx, P. Ströbel, Immuno-Raman microspectroscopy: In situ detection of antigens in tissue specimens by surface-enhanced Raman scattering. J. Raman Spectrosc. **37**, 719 (2006)

V.L. Schmit, R. Martoglio, K.T. Carron, Lab-on-a-bubble surface enhanced Raman indirect immunoassay for cholera. Anal. Chem. **84**, 4233 (2012)

M. Schütz, D. Steinigeweg, M. Salehi, K. Kömpe, S. Schlücker, Hydrophilically stabilized gold nanostars as SERS labels for tissue imaging of the tumor suppressor p63 by immuno-SERS microscopy. Chem. Commun. **47**, 4216 (2011)

M.Y. Sha, H. Xu, M.J. Natan, R. Cromer, Surface-enhanced Raman scattering tags for rapid and homogeneous detection of circulating tumor cells in the presence of human whole blood. J. Am. Chem. Soc. **130**, 17214 (2008)

K.E. Shafer-Peltier, C.L. Haynes, M.R. Glucksberg, R.P. Van Duyne, Toward a glucose biosensor based on surface-enhanced Raman scattering. J. Am. Chem. Soc. **125**, 588 (2003)

N.C. Shah, O. Lyandres, J.T. Walsh, M.R. Glucksberg, R.P. Van Duyne, Lactate and sequential lactate-glucose sensing using surface-enhanced Raman spectroscopy. Anal. Chem. **79**, 6927 (2007)

W. Shi, R.J. Paproski, R. Moore, R. Zemp, Detection of circulating tumor cells using targeted surface-enhanced Raman scattering nanoparticles and magnetic enrichment. J. Biomed. Opt. **19**, 056014 (2014)

M.G. Shim, L.M. Song, N.E. Marcon, B.C. Wilson, In vivo near infrared Raman spectroscopy: demonstration of feasibility during clinical gastrointestinal endoscopy. Photochem. Photobiol. **72**, 146 (2000)

J. Song, J. Zhou, H. Duan, Self-assembled plasmonic vesicles of SERS-encoded amphiphilic gold nanoparticles for cancer cell targeting and traceable intracellular drug delivery. J. Am. Chem. Soc. **134**, 13458 (2012)

R. Stevenson, S. McAughtrie, L. Senior, R.J. Stokes, H. McGachy, L. Tetley, P. Nativo, J.M. Brewer, J. Alexander, K. Faulds, D. Graham, Analysis of intracellular enzyme activity by surface enhanced Raman scattering. Analyst **138**, 6331 (2013)

N. Stone, K. Faulds, D. Graham, P. Matousek, Prospects of deep Raman spectroscopy for noninvasive detection of conjugated surface enhanced resonance raman scattering nanoparticles buried within 25 mm of mammalian tissue. Anal. Chem. **82**, 3969 (2010)

N. Stone, M. Kerssens, G.R. Lloyd, K. Faulds, D. Graham, P. Matousek, Surface enhanced spatially offset Raman spectroscopic (SESORS) imaging—the next dimension. Chem. Sci. **2**, 776 (2011)

R. Stosch, A. Henrion, D. Schiel, B. Guttler, Surface-enhanced Raman scattering based approach for quantiative determination of creatinine in human serum. Anal. Chem. **77**, 7386 (2005)

K.K. Strelau, A. Brinker, C. Schnee, K. Weber, R. Möller, J. Popp, Detection of PCR products amplified from DNA of epizootic pathogens using magnetic nanoparticles and SERS. J. Raman Spectrosc. **42**, 243 (2011)

D.A. Stuart, C.R. Yonzon, X.Y. Zhang, O. Lyandres, N.C. Shah, M.R. Glucksberg, J.T. Walsh, R. P. Van Duyne, Glucose sensing using near-infrared surface-enhanced Raman spectroscopy: gold surfaces, 10-day stability, and improved accuracy. Anal. Chem. **77**, 4013 (2005)

D.A. Stuart, J.M. Yuen, N. Shah, O. Lyandres, C.R. Yonzon, M.R. Glucksberg, J.T. Walsh, R. P. Van Duyne, In vivo glucose measurement by surface-enhanced Raman spectroscopy. Anal. Chem. **78**, 7211 (2006)

L. Sun, J. Irudayaraj, Quantitative surface-enhanced Raman for gene expression estimation. Biophys. J. **96**, 4709 (2009)

L. Sun, K.B. Sung, C. Dentinger, B. Lutz, L. Nguyen, J. Zhang, H. Qin, M. Yamakawa, M. Cao, Y. Lu, A.J. Chmura, J. Zhu, X. Su, A.A. Berlin, S. Chan, B. Knudsen, Composite organic-inorganic nanoparticles as Raman labels for tissue analysis. Nano Lett. **7**, 351 (2007)

L. Sun, C. Yu, J. Irudayaraj, Raman multiplexers for alternative gene splicing. Anal. Chem. **80**, 3342 (2008)

A.S. Thakor, R. Paulmurugan, P. Kempen, C. Zavaleta, R. Sinclair, T.F. Massoud, S.S. Gambhir, Oxidative stress mediates the effects of Raman-active gold nanoparticles in human cells. Small **7**, 126 (2011a)

A.S. Thakor, R. Luong, R. Paulmurugan, F.I. Lin, P.Kempen, C. Zavaleta, P. Chu, T.F. Massoud, R. Sinclair, S.S. Gambhir, The fate and toxicity of Raman active silica-gold nanoparticles in mice. Sci. Transl. Med. **3**, 79ra33 (2011b)

L.M. Tian, N. Gandra, S. Singamaneni, Monitoring controlled release of payload from gold nanocages using surface enhanced Raman scattering. ASC Nano **7**, 4252 (2013)

D. van Lierop, K. Faulds, D. Graham, Separation free DNA detection using surface enhanced Raman scattering. Anal. Chem. **83**, 5817 (2011)

D. van Lierop, I.A. Larmour, K. Faulds, D. Graham, SERS primers and their mode of action for pathogen DNA detection. Anal. Chem. **85**, 1408 (2013)

T. Vo-Dinh, K. Houck, D.L. Stokes, Surface-enhanced Raman gene probes. Anal. Chem. **66**, 3379 (1994)

T. Vo-Dinh, Y. Liu, A.M. Fales, H. Ngo, H.N. Wang, J.K. Register, H. Yuan, S.J. Norton, G.D. Griffin, SERS nanosensors and nanoreporters: golden opportunities in biomedical applications. WIREs Nanomed. Nanobiotechnol. **7**, 17 (2015)

G. von Maltzahn, A. Centrone, J.H. Park, R. Ramanathan, M.J. Sailor, T.A. Hatton, S. Bhatia, SERS-coded gold nanorods as a multifunctional platform for densely multiplexed near-infrared imaging and photothermal heating. Adv. Mater. **21**, 3175 (2009)

M.B. Wabuyele, T. Vo-Dinh, Detection of human immunodeficiency virus type 1 DNA sequence using plasmonic nanoprobes. Anal. Chem. **77**, 7810 (2005)

M.B. Wabuyele, F. Yan, T. Vo-Dinh, Plasmonics nanoprobes: detection of single-nucleotide polymorphisms in the breast cancer BRCA1 gene. Anal. Bioanal. Chem. **398**, 729 (2010)

H.N. Wang, T. Vo-Dinh, Multiplex detection of breast cancer biomarkers using plasmonic molecular sentinel nanoprobes. Nanotechnology **20**, 065101 (2009)

Y.L. Wang, J.L. Seebald, D.P. Szeto, J. Irudayaraj, Biocompatibility and biodistribution of surface-enhanced Raman scattering nanoprobes in zebrafish embryos: in vivo and multiplex imaging. ACS Nano **4**, 4039 (2010a)

Z.Y. Wang, S.F. Zong, J. Yang, C.Y. Song, J. Li, Y.P. Cui, One-step functionalized gold nanorods as intracellular probe with improved SERS performance and reduced cytotoxicity. Biosens. Bioelectron. **26**, 241 (2010b)

Y.L. Wang, S. Ravindranath, J. Irudayaraj, Separation and detection of multiple pathogens in a food matrix by magnetic SERS nanoprobes. Anal. Bioanal. Chem. **399**, 1271 (2011a)

G. Wang, R.J. Lipert, M. Jain, S. Kaur, S. Chakraboty, M.P. Torres, S.K. Batra, R.E. Brand, M.D. Porter, Detection of the potential pancreatic cancer marker MUC4 in serum using surface-enhanced Raman scattering. Anal. Chem. **83**, 2554 (2011b)

X. Wang, X. Qian, J.J. Beitler, Z.G. Chen, F.R. Khuri, M.M. Lewis, H.J.C. Shin, S. Nie, D.M. Shin, Detection of circulating tumor cells in human peripheral blood using surface-enhanced Raman scattering nanoparticles. Cancer Res. **71**, 1526 (2011c)

H.N. Wang, A.M. Fales, A.K. Zaas, C.W. Woods, T. Burke, G.S. Ginsburg, T. Vo-Dinh, Surface-enhanced Raman scattering molecular sentinel nanoprobes for viral infection diagnostics. Anal. Chim. Acta **786**, 153 (2013a)

H.N. Wang, A. Dhawan, Y. Du, D. Batchelor, D.N. Leonard, V. Misra, T. Vo-Dinh, Molecular sentinel-on-chip for SERS-based biosensing. Phys. Chem. Chem. Phys. **15**, 6008 (2013b)

Y. Wang, B. Yan, L.X. Chen, SERS tags: novel optical nanoprobes for bioanalysis. Chem. Rev. **113**, 1391 (2013c)

Y. Wang, A. Khan, S.Y. Leigh, D.N. Wang, Y. Chen, D. Meza, J.T.C. Liu, Comprehensive spectral endoscopy of topically applied SERS nanoparticles in the rat esofagus. Biomed. Opt. Express **5**, 2883 (2014)

L. Wu, Z.Y. Wang, S.F. Zong, H. Chen, C.L. Wang, S.H. Xu, Y.P. Cui, Simultaneous evaluation of p53 and p21 expression level for early cancer diagnosis using SERS technique. Analyst **138**, 3450 (2013)

B.J. Yakes, R.J. Lipert, J.P. Bannantine, M.D. Porter, Detection of Mycobacterium avium subsp paratuberculosis by a sonicate immunoassay based on surface-enhanced Raman scattering. Clin. Vaccine Immunol. **15**, 227 (2008)

M.V. Yigit, L.Y. Zhu, M.A. Ifediba, Y. Zhang, K. Carr, A. Moore, Z. Medarova, Noninvasive MRI-SERS imaging in living mice using an innately bimodal nanomaterial. ACS Nano **5**, 1056 (2011)

C.R. Yonzon, O. Lyandres, N.C. Shah, J.A. Dieringer, R.P. Van Duyne, Glucose sensing with surface-enhanced Raman spectroscopy, in *Surface-Enhanced Raman Scattering: Physics and Applications*, vol. **103** ed. by K. Kneipp, M. Moskovits, H. Kneipp (Springer-Verlag, Berlin Heidelberg 2006), pp. 367–379 (Top. Appl. Phys.)

C. Zavaleta, A. de la Zerda, Z. Liu, S. Keren, Z. Cheng, M. Schipper, X. Chen, H. Dai, S.S. Gambhir, Noninvasive Raman spectroscopy in living mice for evaluation of tumor targeting with carbon nanotubes. Nano Lett. **8**, 2800 (2008)

C.L. Zavaleta, B.R. Smith, I. Walton, W. Doering, G. Davis, B. Shojaei, M.J. Natan, S.S. Gambhir, Multiplexed imaging of surface enhanced Raman scattering nanotags in living mice using noninvasive Raman spectroscopy. P. Natl. Acad. Sci. USA **106**, 13511 (2009)

C.L. Zavaleta, M.F. Kircher, S.S. Gambhir, Raman's "effect" on molecular imaging. J. Nucl. Med. **52**, 1839 (2011)

C.L. Zavaleta, E. Garai, J.T.C. Liu, S. Sensarn, M.J. Mandella, D. Van de Sompel, S. Friedland, J. Van Dam, C.H. Contag, S.S. Gambhir, A Raman-based endoscopic strategy for multiplexed molecular imaging. P. Natl. Acad. Sci. USA **110**, E2288 (2013)

H. Zhang, M.H. Harpster, H.J. Park, P.A. Johnson, Surface-enhanced Raman scattering detection of DNA derived from the West Nile virus genome using magnetic capture of Raman-active gold nanoparticles. Anal. Chem. **83**, 254 (2011)

Chapter 8
Conclusions and Outlook

About 40 years after its discovery, SERS spectroscopy has become a fully grown spectroscopic technique and the number of applications in the chemical, material, and in particular in life sciences has been rapidly increasing over the last few decades. SERS spectroscopy is based on the enormous enhancement of a Raman signal from molecules on or close to a suitable metallic (primarily silver and gold) nanostructure. Two enhancement mechanisms contribute to the total enhancement: the electromagnetic one based on resonance excitation of surface plasmons in the metal and the chemical (or molecular) one increasing the polarizability of the molecule. The electromagnetic mechanism has been identified theoretically and experimentally as the dominant one. The molecular enhancement mechanism is often explained by charge-transfer between the molecule and the metal surface, however, the theoretical aspects of the molecular enhancement mechanism are still not fully understood.

The employed SERS substrate plays a key role in any SERS application. Since the discovery of SERS, a broad variety of metallic substrates have been prepared and employed as an enhancing medium. Nowadays, the SERS substrates can be classified in three basic categories: (i) NPs in suspension, (ii) NPs assembled and immobilized on solid substrates (bottom-up approach) and (iii) nanostructures built directly on solid substrate (top-down approach). First of all, physical top-down preparation techniques of high precision, such as nanolithography, have been developed extensively during the last decade. Solid planar 2-dimensional SERS substrates providing impressive stability and spectral reproducibility can be reliably fabricated this way. On the other hand, rapid, easy and low-cost fabrication of large area commercial SERS substrates still remains a challenge.

Reproducibility and sensitivity provided by SERS substrates represent a major preoccupation of researchers interested in developing practical quantitative SERS methods. Unfortunately, the conflict between reproducibility and sensitivity of SERS measurements still seems to be unresolvable due to poor spectral reproducibility of metallic nanostructures with high SERS enhancement. The aggregates of metallic NPs, for instance, can provide extremely high SERS enhancement enabling even detection of single molecules but in this case spectral reproducibility is poor. Regardless of this drawback, the possibility of introducing individual or small aggregates of metallic NPs or rationally designed NP tags into living

M. Procházka, *Surface-Enhanced Raman Spectroscopy*,
Biological and Medical Physics, Biomedical Engineering,
DOI 10.1007/978-3-319-23992-7_8

cells/organisms enables many in vitro and in vivo medical applications with sufficient sensitivity. Although silver generally gives higher SERS enhancement than gold, gold NPs are primarily used in in vivo applications because of the better stability and biocompatibility when compared with the silver NPs.

In contrast to NPs, highly ordered nanostructures reduce the maximum enhancement for the sake of gaining reproducibility. Therefore, SERS can be applied to real analytical problems when the balance between reproducibility and enhancement is optimized. In practice, quantitative SERS measurements are the result of considerable effort in optimizing an enhancing substrate and experimental conditions. Synthesis of monodisperse and stabilized metallic NPs or nanostructures with highly efficient SERS activity will definitely help to this optimization. Also rationally designed 3-dimensional superstructures or hybrid nanostructures comprising of two or more materials seem to be promising for positive results. More close collaborations between theoreticians and experimentalists are much needed in this field.

SERS spectroscopy has two main advantages over ordinary spectroscopic techniques. First, SERS provides intense Raman signals (enhancement about 10^4–10^{11}) and thus, SERS sensitivity is often better than that of other spectroscopic techniques, such as fluorescence. During the last decade, the SM-SERS has demonstrated the possibility of measuring SERS spectra of individual molecules through the bianalyte approach. The key issue of the SM event is to ensure that the molecule of interest is present in spatially highly localized regions exhibiting extreme field enhancement ("hot spot"). Unfortunately up to now, SM-SERS spectra were obtained only from few dyes and nonresonant molecules. Furthermore, the reproducibility of SERS spectra selectively acquired from "hot spot" sites is poor. Therefore, for a typical quantitative (bio)analytical SERS experiment it is more desirable to average many more enhancement sites. It ensures smaller but still sufficiently high enhancements and, most importantly, better spectral reproducibility. The second advantage of SERS is that it enables identification of analytes through their specific molecular fingerprint information as observed in the SERS spectra. Raman spectra also have narrow bands, which avoid possible spectral overlap in multiplex detection schemes. Taking into account both high sensitivity and molecular fingerprinting, SERS is a very useful technique for molecular diagnostics. However, a basic understanding of the applied experimental approaches as well as of the theoretical aspects of SERS is absolutely necessary for a correct interpretation of SERS spectra.

Generally, SERS detection can be accomplished by two basic schemes: (i) intrinsic (often called label-free) and (ii) extrinsic (using labels). In an intrinsic detection scheme, the SERS spectrum of the analyte is directly obtained and it can serve to identify the analyte and to determine its concentration. Nevertheless, SERS is highly molecular specific technique and label-free SERS detection is usually limited to molecules with surface-seeking groups to ensure their easy adsorption onto the enhancing surface. Unfortunately, many molecules do not have any surface-seeking group. Chemists have brought creative ideas about ways to detect the analytes without surface-seeking groups. Chemical anchors ensure the analyte

will be attached to the enhancing surface. Alternative concept is based on host-guest chemistry between analyte and the metallic surface.

The problem of detecting molecules without surface-seeking groups or providing only weak SERS effect can also be solved by extrinsic detection based on labelling of a target molecule. The label should have a high affinity for the metallic surface as well as provide high SERS signal. The SERS spectrum obtained by this indirect approach is the spectrum of the label without any chemical or structural information about the target molecule itself. The SE(R)RS spectra of labels provide strong and fingerprint spectra. Hence, extrinsic detection is more sensitive and reliable than label-free detection, especially for biomolecules in a complex biological system. For example, while intrinsic SERS spectra of oligonucleotides are difficult to obtain, SERS detection limits for labelled oligonucleotides in extrinsic approach can be about 10^{-11}–10^{-12} M. Such sensitivity is about three orders of magnitude better than this provided by standard fluorescence technique.

An alternative to the labelling of target analyte, SERS tags formed by attaching a reporter (RRM) to the metallic NPs can be used, thereby providing again only SERS signal of the RRM. SERS tags have been synthesized by combining different types of metallic nanomaterials, RRMs and functional moieties. For example, the surface of SERS tags can be further functionalized with a biorecognition element such as an antibody to give the SERS tags with a specific binding feature (such as cancer biomarkers). When MNPs—hybrid NPs with magnetic core and Au or Ag shell—are used, the magnetic field accumulates the target molecules in the measuring spot and thus significantly improves detection sensitivity.

A number of studies during the last few decades indicates that SERS is a feasible analytical technique for detection and identification of analytes in biologically relevant samples. SERS bioanalytical applications include detection of pharmaceuticals, drugs (including nicotine and cocaine), pollutants and pesticides, food contaminants and food additives (e.g. melamine, food colourants) and biowarfare agents (e.g. anthrax). SERS provides sufficient sensitivity of target analytes in real complex matrix (human body fluids, food, drinks, etc.). From the analytical point of view, the key parameters of SERS sensors are the sensitivity (limitation of detection referred to as LOD), specificity (or selectivity) and spectral reproducibility enabling precise quantification of analyte of interest. The LOD as well as accuracy of SERS analysis are comparable and in some cases even better than those provided by standard analytic techniques (such as HPLC). The SERS approach is often simple and rapid (timescale of minutes) prescan method, which can be easily implemented for a field application and for preliminary testing of real complex samples. Better separation of target analytes from complex matrices can be achieved through either integration with separation techniques, or functionalization of the SERS substrates with selective capture agents. Combining SERS with lab-on-a-chip platforms and microfluidic devices need further development to become a flexible analytical technique with respect to sensitivity, reliability, sample throughput and mobility. It is also challenging to interpret the SERS spectra of very complex mixtures. Multivariate/chemometric analysis, such as PCA, may certainly be very useful in

completing this task. In situ spectral measurements can be potentially realized using the portable Raman spectrometers.

SERS biomolecular applications primarily include the studies of NAs, proteins, membranes and their components. Both detection schemes—direct (intrinsic) and extrinsic—are employed. In general, the SERS spectra of biomolecules depend on various parameters like their distance and orientation towards the metal surface. The interaction of some biomolecules, such as NAs and proteins, with a metal surface can cause a distortion of its conformation or structure. In the case of NA detection, hybridization of a labelled SERS probe to its complementary target provides to its unambiguous molecular recognition. For protein detection, SERS immunoassay platforms are employed to detect the target antigens or antibodies (typically small proteins) through specific antibody-antigen binding. SERS tags with biorecognition element such as an antibody are used in SERS extrinsic immunoassay experiments to increase their sensitivity. Detection of microorganisms is a SERS application in which SERS-active substrates could be employed for rapid detection, identification, and classification of microorganisms in complex mixtures such as pathogens (viruses, bacteria, yeast, fungi, and protozoa). In the case of pathogen sensing, the bacterial or viral contamination is detected via their building blocks such as DNA and proteins.

In the context of cancer diagnostics, SERS-based assays made great strides towards the immunophenotyping of cancer cells and the detection of various tumour biomarkers or metastasis. The advantages of SERS such as the rapid screening, capability of multiplexing and high sensitivity are unquestionable. SERS could result in the accurate and sensitive detection of cancer at an early stage. The assays require a small sample volume (a few microlitres) and have extremely low detection limits (up to femtomolar level). Biocompatible SERS tags enables easy and fast spectral imaging of cancer cells and tissues. A considerable amount of research is focused on developing SERS tags for either molecular multiplexed detection or bioimaging at the level of living animals. NIR excitation is more suitable for medical in vivo studies because of low background fluorescence, minimal radiation damage and deep tissue penetration in this region. Employing NIR resonance excitation of both metallic nanostructure and RRM in a SERS tag can substantially enhance the detection sensitivity in medical applications. For this purpose, Au nanorods, nanostars, nanoshells and many RRMs with absorption in the NIR region are currently being tested as components of the SERS tags. However, a number of opportunities for refinement of SERS tags especially in medical in vivo applications, still remains. For example, to synthesize SERS tags with higher sensitivity and reproducibility, it is necessary to fabricate high-performance, single NP-based SERS substrates, precisely control the placement of interparticle “hot spots”, and generate ultrasmall tags for single-molecule labelling and subcellular imaging. Moreover, the biocompatibility, toxicity, and long-term stability of SERS tags introduced in living biological systems should be also taken into account.

Also, SERS tags provide an excellent theranostic platform combining diagnostics (SERS imaging) and therapy (controlled drug release, photodynamic or

photothermal therapy). The emerging integration of SERS tags with complementary imaging methods (such as magnetic resonance) are advancing the SERS as a clinical utility. Recent examples are hand-held SERS guided intraoperative imaging for tumour resection and endoscope-based imaging. Besides injected NPs, SERS-active needles have demonstrated their potential for in vivo applications. The encouraging combination of SERS with spatially offset Raman spectroscopy makes possible to acquire SERS spectra from tissues even milimetres to centimetres deep.

Finally, it is evident that SERS should be considered from a wider perspective and comparing the performance of SERS with other techniques can always be useful. For example, fluorescence microscopy and spectroscopy are extremely sensitive and widely used techniques in many areas of the life sciences. Further development and expanding of other surface-enhanced spectroscopic techniques such as surface-enhanced infrared absorption (SEIRA), surface-enhanced fluorescence (SEF) and tip-enhanced Raman scattering (TERS) are also highly desirable. It is highly appreciable so that these techniques will help to refine information obtained by SERS in many bioanalytical, biomolecular and medical studies.

Index

Symbol
β-amyloid, 177, 178

A
Aggregation, 31–34, 48, 63, 96, 104, 118, 127, 130
Amino acid, 104–110, 132–134, 141, 169
Anthrax, 86
Antibody-antigen, 109, 110, 116, 168
Aptamer, 48, 71, 112, 158, 164, 167, 182
Azorubine, 85

B
Bacteria, 86, 142–144, 154–162
Barcode, 144, 160–164
Bianalytical SERS, 28
Biomolecules, 17, 93–120
Blood, 150, 159–162, 169–173, 175, 178, 188
Bottom-up technique, 30, 34, 39, 85
Breast cancer, 117, 163, 164, 168, 171–174, 181–184

C
Cancer diagnostics, 162–174, 179–185, 190–202
Carbon nanotubes, 113
CCD, 17
Cell, 127–140
Charge-transfer, 25
Chemical mechanism, 25
Cholera, 176
Cocaine, 73–76
Coffee-ring effect, 65
COINs, 186, 187
Colloidal lithography, 39, 44
Colloids, 29–34, 63, 67–73, 96, 104, 108, 130, 158
Commercial substrates, 47
Creatinine, 178, 179
Circulated tumours cells (CTCs), 162, 171–173
Cytotoxicity, 129, 136, 202

D
Deformation vibrations, 14
Diabetes, 149, 150, 175, 176
Dimer, 26, 27, 49, 71–72, 75
Dipicolinic acid (DPA), 68, 69, 86, 87
Dipole moment, 21
DNA, 35, 97–104, 152–158, 163–166
Dopamine (DA), 71, 72
Doxorubicin (DOX), 180–182, 185
Drugs, 72–76, 179–182, 185, 200, 201

E
Enhancement factor (EF), 26, 27
Epidermal growth factor (EGF), 118, 162, 167, 168, 173, 181, 185, 189–192
Electrochemical deposition, 40, 46
Electron beam lithography, 37
EM enhancement, 23
EM mechanism, 22
Endoscopic imaging, 197, 198
Etching, 37, 38, 41–43
Excitation profiles, 25
Extrinsic detection, 94, 100–103, 108

F
Fibre optics, 17
Film over nanospheres (FONs), 39–43, 66, 85, 86, 150, 151, 154, 178, 187
Fluorescence, 8, 10, 12, 18, 32, 48, 51–53, 62, 80, 95, 101, 139, 155, 179–182, 184, 186, 194, 201
Fluorescent dye, 94–95, 100, 108, 184
Food colourants, 84
Food contaminants and food additives, 77–82

M. Procházka, *Surface-Enhanced Raman Spectroscopy*,
Biological and Medical Physics, Biomedical Engineering,
DOI 10.1007/978-3-319-23992-7

G
Glucose, 149–151, 178, 187, 188

H
Hepatitis, 153, 178
Herbicide, 63, 79
Heroin, 74, 75
Histology, 185–187
HIV, 152, 153
Hollow Au NPs, 83, 84, 114, 115, 137, 167, 177
Host-guest approach, 78
Hot spot, 27, 28, 34, 47, 77, 107
Hybridization, 91, 98–100, 102–104, 152–158, 163–166

I
Immunoassay, 63, 94, 109–118, 157–159, 166–168, 176–178
Internal standard, 65–68, 83–85
Interparticle coupling, 34
Intracellular SERS, 127–140
Intrinsic detection, 96–100, 104–107
Ion beam lithography, 37

J
Jablonski diagram, 8

K
Klarite, 47, 82, 83

L
Labelling, 19, 48, 95, 108–111, 116
Lab-on-a-chip, 63, 64, 68, 154
Lactic acid, 178
Limit of detection, 68
Lipids, 118, 120, 133
Lithography, 37–39, 44, 63, 75

M
Magnetic NPs (MNPs), 73, 74, 114, 115, 157–159, 173, 215
Melamine, 67, 82–84
Membranes, 118, 119
Microfluidic, 63–65, 68, 142, 153, 154, 178
MiRNA, 164, 166
Molecular polarizability, 11, 14, 15, 21, 24
Molecular sentinel, 153, 154, 163
Molecular vibrations, 12
Myocardial infarction, 177

N
Nanoimprint lithography, 39
Nanopillars, 47
Nanopipettes, 139
Nanorods (NRs), 31, 32, 36, 43, 46, 71, 75, 79–81, 97, 166, 168, 173, 182, 185, 193, 195
Nanoshells, 32, 97, 99, 105, 117, 119, 137, 158, 185
Nanosphere lithography, 39
Nanostars, 31, 114, 136, 184, 187, 193, 196
Nanowires (NWs), 46, 139, 156, 163
Needles, 19, 76, 194
Nicotine, 66–68, 73
Nucleic acid (NA), 95, 100, 102, 136

P
Pancreatic cancer (PC), 162, 166
Pathogen, 151–161
Pesticide, 77–81
pH nanosensor, 128, 137, 139
Pharmaceuticals, 70, 71
Photodynamic therapy (PDT), 179, 182–185
Photothermal therapy (PTT), 179, 181–185
Plasmon resonance, 22, 23, 26, 27, 31–34, 40, 48, 114, 182, 192
Plasticizers, 81
Polarized Raman, 12
Pollutants, 77–81
Polymerase chain reaction (PCR), 103, 152, 157
Principal component analysis (PCA), 70, 76, 82, 134, 141, 143, 144, 160–162, 169–176, 194
Prostate cancer, 111, 134, 182, 186, 195
Prostate-specific antigen (PSA), 111, 114, 162, 166, 182, 185–187
Proteins, 104–109, 133
Pyramidal arrays, 42

Q
Quantitative SERS, 61–65

R
Raman bands, 17, 18
Raman cross-section, 12
Raman effect, 7
Raman experiment, 15
Raman reporter molecule (RRM), 70, 95, 109, 110, 112, 134, 137, 192–196

Raman scattering, 8
Raman spectrometers, 16
Raman spectrum, 9, 10, 15
Raman tensor, 14
Relative standard deviation, 65
Reproducibility, 34, 61, 62
Resonance Raman, 10, 26
RNA, 95–100, 153, 154, 163, 164, 166, 171, 182

S
Saliva, 71, 174
Selection rules, 14, 24, 49
Semishell, 41, 49
Sensitivity, 61, 62, 68
SERS enhancement, 22
SERS mechanisms, 21
SERS substrate, 30–48
SERS tag, 33, 94, 95, 103, 109–117, 127, 128, 133–137, 141, 152, 158, 159, 166–168, 171–173, 177, 181, 182, 184–186, 189–195, 196–198, 201, 202
SERS uncertainty principle, 63
SERRS, 26
Shell-isolated NP, 33, 51, 80, 145
Silver enhanced step, 112, 113
Silver staining, 107, 108
Single-molecule (SM) SERS, 27–30, 98
Soft lithography, 38
Specificity, 68, 70
Stokes shift, 10
Stretching vibrations, 13
Sudan I dye, 85
Surface-enhanced fluorescence (SEF), 52, 53
Surface-enhanced infrared absorption (SEIRA), 51
Surface complex, 49
Surface plasmons, 22, 31
Surgery guidance, 195

T
Template techniques, 39
Theranostics, 179–181
Tip-enhanced Raman (TERS), 50, 100
Top-down technique, 37
Transition metal, 24
Tumour targeting, 189–196

U
Uptake, 72, 74, 129–131, 134, 136, 180, 185, 189, 194, 200, 201
UTI, 144, 162
Urine, 173–174

V
Vapour deposition, 36, 39
Vibrational modes, 13, 17, 18
Viruses, 103, 141, 142, 152–154

W
Western-SERS, 108, 109

Y
Yeast, 145